Development of closures of Scalar Dissipation Rate for Large Eddy Simulation of turbulent premixed combustion using Direct Numerical Simulation data

Yuan Gao

School of Mechanical and Systems Engineering

Newcastle University

A thesis submitted for the degree of

Doctor of Philosophy

March 2016

To my family

Declaration

- I declare that this thesis is my own work and that I have correctly I have correctly acknowledged the work of others. This submission is in accordance with University and School guidance on good academic conduct.
- I certify that no part of the material offered has been previously submitted by me for a degree or other qualification in this or any other University.
- I confirm that the word length is within the prescribed range as advised by my school and faculty.
- I confirm that this thesis does not contain collaborative work.

Yuan Gao

March 2016

Acknowledgements

I would like to express my deep gratitude to Professor Nilanjan Chakraborty for his invaluable expertise, advice and guidance over the course of this work. I am grateful to Dr. John Appleby and Dr. David Swailes for their encouragement and help during difficult periods. I want to express my sincere gratitude to Professor Markus Klein, Professor N. Swaminathan, Dr. Hemanth Kolla, Dr. Thomas Dunstan and Dr. Yuki Minamoto for their technical advice during collaboration.

Thanks are due to the Engineering and Physical Sciences Research Council (EPSRC) and School of Mechanical and Systems Engineering of Newcastle University for the generous financial support throughout the course of this PhD. Additionally, I am grateful to the Combustion Institute for the travel grants, which have allowed me to attend and present parts of this work.

Special thanks to my parents for the consistent support, I will always be indebted to them. Finally, I would like to thank Jing Qu for the consistent companion and support throughout the period.

Abstract

In turbulent premixed combustion, the mean reaction rate can be modelled based on scalar dissipation rate (SDR) in the context of both Reynolds Averaged Navier-Stockes (RANS) and Large Eddy Simulations (LES) simulations. The SDR, which characterises the mixing rate of the unburnt reactants and hot burnt products, itself requires modelling as well. The SDR based reaction rate closure has been studied extensively in the context of RANS. However, modelling of SDR and SDR based reaction rate closure are yet to be addressed in the context of LES for turbulent premixed combustion. There are two major approaches for SDR based reaction rate modelling, which are algebraic closure and SDR transport equation based closure respectively. Several Direct Numerical Simulation (DNS) databases, part of which were generated by this study, have been explicitly filtered using a Gaussian filter for both *a-priori* analysis of Favre filtered SDR and filtered SDR transport equation and *a-posteriori* assessment of the SDR based reaction rate closure.

In the *a-priori* DNS analysis, a three-dimensional DNS database of freely propagating statistically planar flames for a range of different heat release parameter, global Lewis number and turbulent Reynolds number has been LES filtered using a Gaussian filter. An existing SDR based reaction rate closure for RANS simulations has been extended for LES and a satisfactory performance of this LES closure is observed for a range of filter widths, covering both laboratories scale to practical scales.

When the generation and destruction of the scalar gradient are at equilibrium, it is viable for an algebraic SDR model in the context of LES. *A-priori* DNS assessment of algebraic SDR closures based on passive scalar mixing model and a power-law has been conducted, which have been found unsuitable for the reactive turbulent flows of premixed flames.

Subsequently, a new algebraic model of Favre-filtered SDR has been proposed by extending a popular algebraic model of RANS averaged SDR into the context of LES. The performances of the newly proposed algebraic closure were assessed with respect to Favre-filtered SDR directly extracted from the DNS datasets. It has been found that the newly proposed SDR model for LES predicts both local and volume-averaged behaviours of SDR satisfactorily. However, when the generation and destruction of the scalar gradient are not at equilibrium, the Favre-filtered SDR transport equation need to be modelled for both RANS and LES. The statistical behaviours of the SDR transport equation have been studied for different global Lewis number, turbulent Reynolds number and heat release parameter at different filter widths. Based on the scaling analysis of all the unclosed terms in the Favre-filtered SDR transport equation, models are proposed for those terms in the context of LES and their performances have been assessed with respect to their corresponding values obtained from explicitly filtered DNS data. These newly proposed models are found to satisfactorily predict both the qualitative and quantitative behaviours of these unclosed terms for a range of different values of filter widths, heat release parameter, global Lewis number and turbulent Reynolds number.

The newly proposed algebraic closure and transport equation based closure of Favre-filtered SDR in the context of LES, which were proposed based on simple chemistry DNS database, are assessed by a v-flame detail chemistry DNS database as *a-posteriori* assessment. The algebraic model is found to capture both qualitative and quantitative behaviours of SDR with reaction progress variable defined based on both deficient reactants and products. The models of the unclosed terms of SDR transport equation are found to capture the behaviours of the explicitly filtered terms of the detail chemistry DNS database in an order-of-magnitude sense. Further improvement is required in order

to address the effects of diffusivity gradient, the gradients of reaction rate and molecular dissipation of SDR.

Contents

List of Journal Publications

1. Gao Y, Minamoto Y, Tanahashi M, Chakraborty N. A priori assessment of scalar dissipation rate closure for Large Eddy Simulations of turbulent premixed combustion using a detailed chemistry Direct Numerical Simulation database. Combustion Science and Technology 2016. In Press.

2. Gao Y, Chakraborty N. "Modeling of Lewis Number Dependence of Scalar Dissipation Rate Transport for Large Eddy Simulations of Turbulent premixed Combustion". *Numerical Heat Transfer A: Applications* 2015, In press.

3. Gao Y, Chakraborty N, Swaminathan N. "Dynamic closure of scalar dissipation rate for Large Eddy Simulations of turbulent premixed combustion: A Direct Numerical Simulations analysis". *Flow, Turbulence and Combustion* 2015,
DOI: 10.1007/s10494-015-9631-3.

4. Gao Y, Chakraborty N, Dunstan TD, Swaminathan N. "Assessment of Reynolds Averaged Navier Stokes modelling of Scalar Dissipation Rate transport in turbulent oblique premixed flames". *Combustion Science and Technology* 2015. In Press.

5. Gao Y, Klein M, Chakraborty N. "Assessment of sub-grid scalar flux modelling in premixed flames for Large Eddy Simulations: A-*priori* Direct Numerical Simulation analysis". *European Journal of Mechanics - B/Fluids* 2015, **52**, 2015, 97–108.

6. Gao Y, Chakraborty N, Klein M. "Assessment of the performances of sub-grid scalar flux models for premixed flames with different global Lewis numbers: A Direct Numerical Simulation analysis". *International Journal of Heat and Fluid Flow* 2015, **52**, 28-39.

7. Gao Y, Chakraborty N, Swaminathan N. " Scalar Dissipation Rate Transport and Its Modelling for Large Eddy Simulations of Turbulent Premixed Combustion ". *Combustion Science and Technology* 2015, **187**(3), 362-383.

8. Gao Y, Chakraborty N, Swaminathan N. "Algebraic Closure of Scalar Dissipation Rate for Large Eddy Simulations of Turbulent Premixed Combustion". *Combustion Science and Technology* 2014, **186**(10-11), 1309-1337.

9. Gao Y, Chakraborty N, Swaminathan N. "Scalar Dissipation Rate Transport in the Context of Large Eddy Simulations for Turbulent Premixed Flames with Non-Unity Lewis Number". *Flow, Turbulence and Combustion.* 2014, **93**(3), 461-486.

10. Gao Y, Chakraborty N, Swaminathan N. "Local Strain Rate and Curvature Dependences of Scalar Dissipation Rate Transport in Turbulent Premixed Flames: A Direct Numerical Simulation Analysis". *Journal of Combustion* 2014, 1-29.

11. Ma T, Gao Y, Kempf AM, Chakraborty N. “Validation and Implementation of algebraic LES modelling of Scalar Dissipation Rate for reaction rate closure in turbulent premixed combustion”. *Combustion and Flame* 2014,**161**(12), 3134-3153.

12. Butz D, Gao Y, Kempf AM, Chakraborty N. “Large Eddy Simulations of a turbulent premixed swirl flame using an algebraic Scalar Dissipation Rate closure”. *Combustion and Flame* 2015, **162**(9), 3180-3196.

13. Langella I, Gao Y, Chakraborty N, Swaminathan N. “Assessment of Dynamic Closure for Premixed Combustion LES”. *Combustion Theory and Modelling* 2015.
DOI: 10.1080/13647830.2015.1080387

14. Katragadda M, Gao Y, Chakraborty N. “Modelling of the Strain Rate Contribution to the Flame Surface Density Transport for Non-Unity Lewis Number Flames in Large Eddy Simulations”. *Combustion Science and Technology*2014, **186**(10-11).

15. Klein M, Chakraborty N, Gao Y. Scale similarity based models and their application to subgrid scale scalar flux modelling in the context of turbulent premixed flames. International Journal of Heat and Fluid Flow 2016, 57, 91-108.

List of Conference Publications

1. Gao H, Kolla H, Chakraborty N, Chen JH, Swaminathan N. "A comparison of scalar dissipation rate transport between simple and detailed chemistry based Direct Numerical Simulations." In: *9th Mediterranean Combustion Symposium*. 2015, Rhodes, Greece. In Press.

2. Klein M, Kasten C, Gao Y, Chakraborty N. "A-priori assessment of sub-grid scale stress tensor closures for turbulent premixed combustion." In: *7th European Combustion Meeting*. 2015, Budapest, Hungary.

3. Klein M, Kasten C, Gao Y, Chakraborty N, Pfitzner M. "Analysis of the combined modelling of subgrid transport and filtered flame propagation for premixed turbulent combustion." In: *9th Mediterranean Combustion Symposium*. 2015, Rhodes, Greece. In Press.

4. Klein M, Chakraborty N, Gao Y. "Applications of scale similarity based models to subgrid scale scalar flux modelling in the context of turbulent premixed flames" In: *9th International Symposium on Turbulence and Shear Flow Phenomena (TSFP-9)*. 2015, Melbourne, Australia: University of Melbourne. In Press.

5. Gao Y, Langella I, Chakraborty N, Swaminathan N. "Effects of sub–grid velocity fluctuation closure on LES modelling of Scalar Dissipation Rate" In: *Joint meeting of the British Scandinavian-Nordic Sections of the Combustion Institute*. 2014, Cambridge, UK.

6. Gao Y, Chakraborty N, Swaminathan N. "Scalar dissipation rate transport and its modelling for Large Eddy Simulations of turbulent premixed combustion: A-priori Direct Numerical Simulation analysis" In: *SPEIC14 – Towards Sustainable Combustion Symposium*. 2014, Lisboa, Portugal.

7. Gao Y, Chakraborty N, Swaminathan N. "Algebraic closure of Scalar Dissipation Rate for Large Eddy Simulations of turbulent premixed combustion" In: *24th International Colloquium on the Dynamics of Explosions and Reactive Systems*. 2013, Taipei, Taiwan.

8. Katragadda M, Gao Y, Chakraborty N. "Modelling of the strain rate contribution to the FSD transport for non-unity Lewis number flames in LES" In: *24th International Colloquium on the Dynamics of Explosions and Reactive Systems*. 2013, Taipei, Taiwan.

9. Gao Y, Chakraborty N, Swaminathan N. "Scalar dissipation rate transport in the context of LES for turbulent premixed flames with non-unity Lewis number" In: *8th Mediterranean Combustion Symposium. 2013*, Izmir, Turkey: Combustion Institute and the International Centre for Heat and Mass Transfer (ICHMT).

10. Gao Y, Chakraborty N, Swaminathan N. "Scalar Dissipation Rate Transport in the Context of LES of Premixed Turbulent Flames: A DNS Analysis" In: *6th European Combustion Meeting (ECM)*. 2013, Lund University, Sweden.

11. Chakraborty N, Kolla H, Gao Y, Swaminathan N, Chen JH. "Statistical behaviours of scalar dissipation rate transport equation terms for turbulent premixed flames in the context of Large Eddy Simulations" In: *14th SIAM Numerical Combustion conference*. 2013, San Antonio, USA.

12. Gao Y, Chakraborty N. "Effects of curvature and tangential strain rate on scalar dissipation rate transport of turbulent premixed flames in the thin reaction zone regime" In: *34th International Combustion Symposium*. 2012, Warsaw, Poland.

List of Figures

List of Tables

Nomenclature

Latin Symbols

a	Sonic speed
a_T	Flame stretch due to fluid flow
$A(x, y, t)$	Elemental area factor
c	Reaction progress variable
c^*	Progress variable defining flame surface
C	Model constant
C_{EBU}	EBU model constant
C_P	Specific heat at constant pressure
C_V	Specific heat at constant volume
C_{mean}	Resolved curved component of laminar propagation term
C_{sg}	Sub-grid propagation curvature term
C_t	Reynolds averaged propagation curvature term
D	Progress variable diffusivity
Da	Damköhler number
$E(\kappa)$	Turbulent energy spectrum
f	General function denoting primitive variables
$f_i(x_i - x_i')$	LES filtering function for i^{th} variable
G	Field equation variable
$G(r)$	LES filtering function
h	Specific enthalpy
h_f	Enthalpy of formation
I_0	Flame speed modification factor
k	Sub-grid scale kinetic energy
k_m	Mean curvature of the flame
K_r	NSCBC reflection constant
K_Σ	Algebraic FSD model parameter
Ka	Karlovitz number
L	Integral length scale

L_t	Turbulent integral scale
L_y	BML model integral length scale
Le	Lewis number
$\dot{m}$	Mass flow rate to fine structures in EBU-type model
Ma	Mach number
$\vec{M}$	Flamelet model for surface averaged normal
n_{ij}	Model for flame orientation factor
$\vec{N}$	Local flame normal direction
N_c	Instantaneous Scalar Dissipation Rate
$\widetilde{N_c}$	Favre filtered Scalar Dissipation Rate
p	Pressure
p_∞	Far field pressure
P_{mean}	Resolved planar component of laminar propagation term
Pr	Prandtl number
$P(c)$	Probability density function of reaction progress variable
q	Flame speed model parameter
$Q_i(Z;\vec{x},t)$	First conditional moment of the reactive scalars
R	Ideal gas constant
Re	Reynolds number
Re_t	Turbulent Reynolds number
s	Specific entropy
$\dot{S}$	Total rate of flame stretch
Sc	Schmidt number
S_d	Local flame displacement speed
S_L	Laminar flame speed
S_T	Turbulent flame speed
t	Time
T	Temperature
T_{ad}	Adiabatic flame temperature
T_0	Reactant temperature

u_i	i^{th} component of fluid velocity
u_{mean}	Mean inflow velocity
$\bar{u}_P, \bar{u}_R$	Conditional reactant, product velocity averages
u'	Root mean square fluctuation velocity
V	Volume
w	Local flame propagation velocity
$\dot{w}$	Chemical reaction rate
x_i	i^{th} Cartesian co-ordinate
y	Cartesian co-ordinate
Y_O, Y_F	Oxidiser and fuel mass fraction
Z	Mixture fraction

Greek Symbols

$\alpha = 1 - \vec{M}.\vec{M}$	Flamelet orientation or resolution factor
α_T	Thermal diffusivity
β	Sub-grid propagation-curvature model parameter
γ	Ratio of specific heats C_P / C_V
γ_f	Volume fraction of fine structures in EBU-type models
$\delta(c - c^*)$	Fine-grained function for progress variable at a flame surface
δ_L	Laminar flame thickness
δt	Computational time step interval
δx	Computational grid node spacing
Δ	LES filter width
Δh	Enthalpy change in reaction
ε	Dissipation rate of turbulent kinetic energy
η	Kolmogorov length scale
$\vec{\kappa}$	Wave number vector
κ	Wave number magnitude
λ_i	Characteristic wave velocity
μ	Dynamic viscosity
ν	Kinematic viscosity

ν_t	LES kinematic eddy viscosity
Ξ	Flame wrinkling factor
Ξ_V	Flame wrinkling factor based on SDR
ρ	Density
ρ_0	Reactant density
Σ	Flame surface density (FSD)
Σ_{sg}	Sub-grid scale FSD
τ	Heat release parameter
τ_{ij}	Viscous stress
τ_{ij}^{sg}	Sub-grid stress
τ_η	Kolmogorov eddy turnover time
τ_c	Chemical time scale
τ_M	Time scale for sub-grid mixing in EBU type models
τ_t	Turbulent time scale

Accents

$\overline{g}$	LES filtered value of g
g'	Sub-grid fluctuation of g or root mean square fluctuation in RANS or in LES
$\widetilde{g}$	Favre LES filtered value of g
g''	Favre sub-grid scale fluctuation of g
$\hat{g}$	Fourier transform or test level filtered value of g
$\breve{g}$	Fourier transform of g in x_1 direction
$\langle g \rangle$	Reynolds average of g

A.3. Acronyms

BML	Bray-Moss,-Libby
CFD	Computational Fluid Dynamics
CFM	Coherent Flamelet Model

CMC	Conditional Moment Closure
DNS	Direct Numerical Simulation
EBU	Eddy Break Up
EDC	Eddy Dissipation Concept
FSD	Flame Surface Density
LES	Large Eddy Simulation
NSCBC	Navier Stokes Characteristic Boundary Condition
PDF	Probability Density Function
RANS	Reynolds Averaged Navier Stokes
SDR	Scalar Dissipation Rate

Chapter 1. Introduction

1.1 Background

Since fire was discovered and utilised by the ancestor of human being, from the flaring torches to space rockets, the development of the applications based on combustion underpins the civilisation of the human race. As intensive heat is released by consuming combustible materials, where chemical energy converts to heat, combustion can be utilised as energy providing tool but can also be a cause for destruction depending on interaction of heat and mass transfer, fluid dynamics and chemistry, and therefore remains one of most complex and challenging areas of thermo-fluid research. Although improved understanding of combustion process improves energy utilisation and reduces pollutant emission, the understanding of combustion is yet to be complete and still an active research topic.

The statistical and predicted world energy consumption by fuel type from 1990 to 2040 is shown in Figure 1. The total world energy consumption will increase by 56% from 524 quadrillion British thermal units (Btu) in 2010 to 820 quadrillion Btu in 2040, where almost 80 percent will still rely on burning fossil fuels (U.S. Energy Information Administration, 2013), despite the facts that the fastest-growing energy sources are renewable energy and nuclear power with 2.5% increase per year.

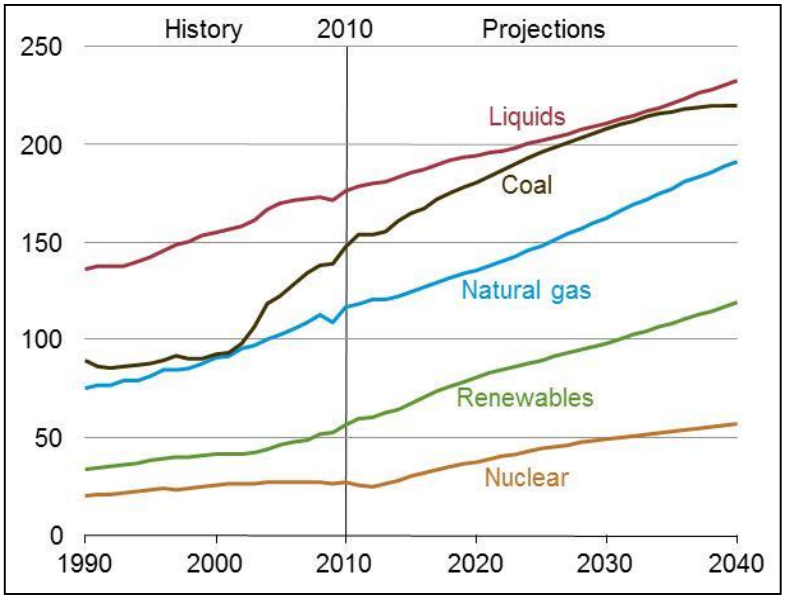

Figure 1.1: World Energy Consumption by Fuel Type 1990-2040. (Quadrillion Btu)

Among the fossil fuels, natural gas is expected to have the fastest growing rate of 1.7% per year, including the growth of tight gas, shale gas and coalbed methane. The consuming of coal is expected to exceed petroleum and other liquid fuels before 2030 mainly due to China's growing usage of the coal and the moderated consumption of liquid fuel due to the high oil price.

Considering the fast development on the combustible renewable energy such as biofuels, combustion will remain active as the main energy source in the foreseeable future. However, the next generation of combustors, such as gas turbines, airplane jet engines and automotive internal combustion engines, are required to be more energy efficient and more environmental friendly.

There are a few perspectives to characterise the combustion process, which can be based on the degree of mixing of reactants, the flow type and the flame stability. A popular way to categorise combustion is based on the degree of mixing the fuel and oxidisers before the reactants entering the reaction zone (Poinsot, 2004), which has characterised combustion into premixed, non-premixed and stratified/partially premixed flames. The fuel and oxidizer are assumed to be homogeneously mixed before combustion process in premixed combustion, whereas the fuel and oxidizer are separated from each other until they meet in the reaction zone of the non-premixed flame.

In premixed combustion, the flame preheats the cold reactants up to the required flammable temperature such that the combustion process is triggered continuously with the flame propagating towards reactants. Since, it is fairly simple to keep the mixture composition of premixed combustion as fuel lean, the emission of the pollutants such as NOx can be controlled by restricting the maximum temperature of the burnt products. As fuel and oxidizer are fully homogeneously mixed, the efficiency of premixed combustion is high as well. The above advantages of premixed combustion make it promising to design the next generation of combustors based on premixed combustion.

Based on the Reynolds number of the flow, the flames can be categorised into laminar flame and turbulent flames respectively. For premixed flames, the burning rate is enhanced by the flame area generation and the flame-brush thickens with increasing turbulent level. In reality, most combustion process of engines takes place in turbulent environment, where the flame brush exhibits considerable quantitative and qualitative differences in comparison to the

laminar premixed flames. However, the physical understanding of turbulent premixed combustion is not complete and experimental and numerical investigations of premixed turbulent combustion is an active area of research.

Computational Fluid Dynamics (CFD), emerging in 1970s, has consistently served as an increasingly important tool for both academic research and industrial design of the combustors. There are three main simulation methodologies for turbulent flows which can be categorised into Direct Numerical Simulation (DNS), Large Eddy Simulation (LES) and Reynolds Averaged Navier-Stokes Simulation (RANS). DNS resolves turbulent flows both temporally and spatially, whereas other two simulating techniques (i.e. RANS and LES) only partially resolve time and length scales and the flame structure remains fully unresolved for turbulent reacting flows. The highest resolution is achieved in DNS, while RANS requires the lowest computational cost. RANS has been widely adopted in industry already for the designing of the combustors. LES, which is increasingly becoming a promising industrial tool, requires more powerful computers and higher resolution than RANS. Instantaneous governing equations are solved in DNS while averaged and filtered transport equations are solved respectively in RANS and LES. Therefore, the unclosed terms of the averaged/filtered governing transport equations in RANS and LES require modelling. The recent development of High Performance Computing (HPC) equips CFD simulations with higher computational power than ever, which make it possible to investigate some of the unresolved problems as well as to extend simulations towards much higher resolutions. A central challenge of simulating premixed turbulent reacting flow is the modelling of chemical reaction rate which depends on temperature exponentially according to the Arrhenius law. It has been found by Bray (1980) that the mean reaction rate is closely related to another quantity of central importance, which is scalar dissipation rate (SDR). The SDR characterises the mixing process of unburnt reactants and burnt products across the flame surface. SDR based reaction rate modelling for RANS has been investigated extensively in the recent past. However, the modelling of reaction rate based on SDR is yet to be addressed in the context of LES, which is expected to become a leading tool in industrial designing of the combustors in the near future. Therefore, the current work is aimed to address the SDR based reaction rate closure for LES using *a-priori* DNS analysis of turbulent premixed flames. Based on fundamental investigation of turbulent premixed combustion, a novel methodology will be developed for LES modelling through SDR based reaction rate closure in this analysis. The models proposed in this analysis will be further assessed with respect to the explicitly filtered DNS results.

1.2 Simulation Techniques for Turbulent Combustion

In order to explain the difference between DNS, LES and RANS from a quantitative perspective, the schematic diagram of turbulent energy spectrum is shown in Fig. 1. 2 where κ denotes the wavenumber magnitude which is inversely proportional to the length scale of turbulent eddies and $E(\kappa)$ denotes the turbulent kinetic energy content associated with the wavenumber magnitude κ while η, l, Δ and Δx represent the Kolmogorov length scale, integral length scale, LES filter size and the grid size of the chosen simulation technique respectively.

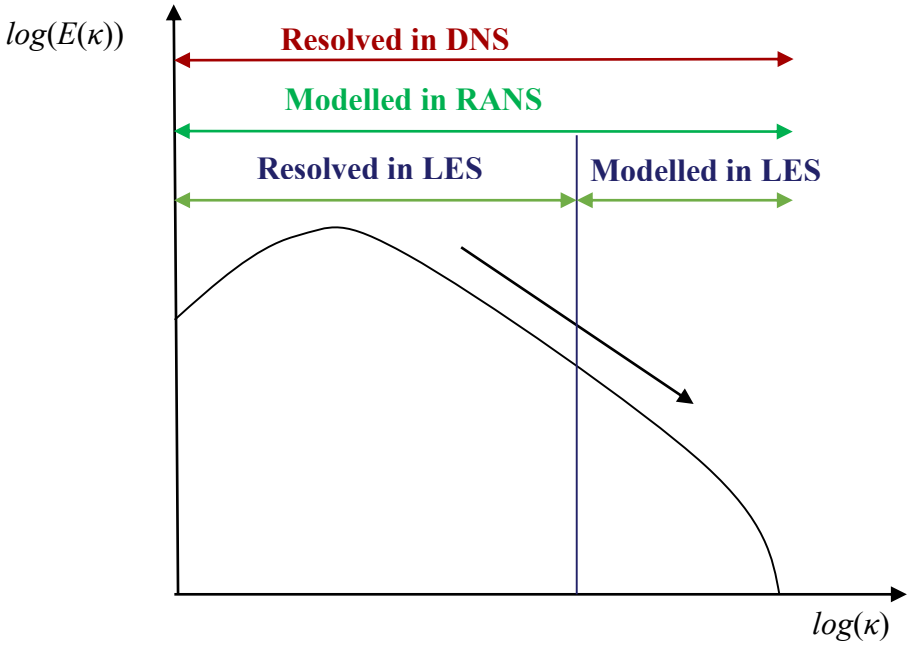

Figure 1.2: A schematic of turbulent energy spectrum ($E(\kappa)$) with wave number (κ) showing the capabilities of different simulation techniques on a log-log format .

It is demonstrated by Fig. 1. 2 that the grid size of DNS is of the same order as Kolmogorov length η therefore the most of the energy spectrum is resolved in DNS with only the viscous dissipation of kinetic energy is not resolved in DNS. The grid spacing in RANS is of the order of the integral length scale and thus a major part of turbulent kinetic energy spectrum is unresolved and need modelling. The grid/filter size of LES Δ falls between the integral length l and Kolmogorov length η, a typical filter size of LES Δ usually ensures that up to 80% of the total kinetic energy is resolved on the computational mesh (Pope, 2000).

1.2.1 Direct Numerical Simulation

Direct numerical simulation (DNS) provides the highest resolution for simulating turbulent combustion, where the transport equation of mass, momentum, energy and species are discretised directly and solved numerically without any physical approximation of the turbulent flow. All the scales of turbulent motion are resolved both temporally and spatially in DNS and henceforth the detailed information on flame structure, the heat release rate, mixing process across the flame brush can be obtained from a DNS database. Considering the large spectral range of turbulence and the complexity of chemical reaction involved in the combustion process, it is not surprising that DNS relies heavily on the computational power. Despite the significant development of high performance computing (HPC) in the recent decade, the DNS is still restricted in a relatively small domain size (e.g. a few cm^3) involving simple configurations (e.g. planar flame, v-shape flame etc.), while the combustors in industrial applications involve complex geometries with much larger scales (e.g. a few m^3). The computational cost of non-reacting flow DNS can be shown to be proportional to the power of 11/4 of turbulent Reynold number (i.e. $\sim Re_t^{11/4}$) which has restricted the simulated flow field in DNS to moderate values of turbulent Reynolds number. In addition, the flame thickness is often of the same order of the Kolmogorov scale, which is commonly taken as the smallest scale turbulent motion, henceforth in order to resolved the flame structure, the grid size in DNS of the turbulent reacting flow is often limited to microns. Therefore, DNS is mainly adopted by academic research for improved understanding of the fundamental physical processes in the turbulent reacting flows.

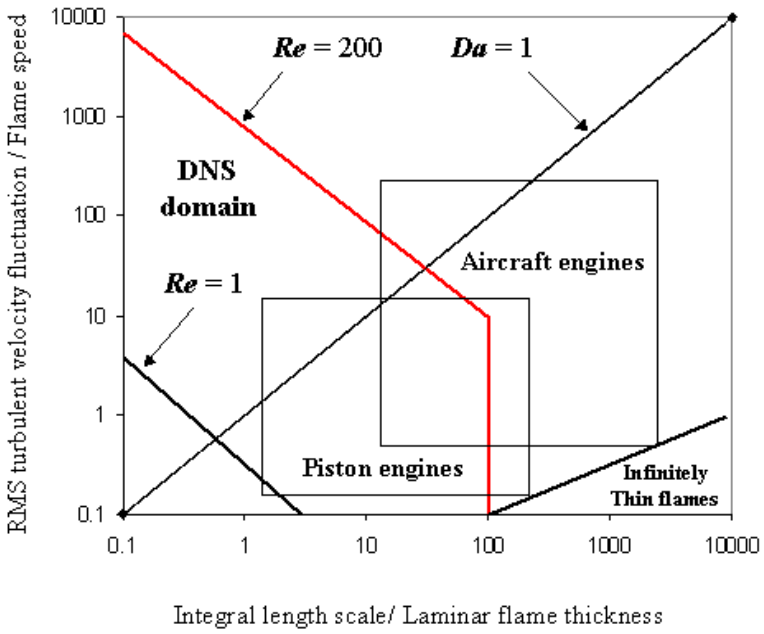

Figure 1.3: DNS domain is shown with the thick red line in relation to engineering applications in reciprocating engines and aircraft engines on the combustion diagram according to Poinsot and Veynante (2001).

The utilisation of DNS as a simulation technique for turbulent reacting flows emerged in early 1990s (Rutland and Ferziger, 1991; Poinsot *et al*., 1991; Baum *et al*., 1994) when turbulent flames were simulated in two-dimensional canonical configurations using simplified or complex chemistry, and the three dimensional information of turbulent vortices were compromised. Later in 1990s, a few three dimensional DNS were carried out for turbulent flow of moderate Reynolds number for single step (Trouve and Poinsot, 1994; Rutland and Cant, 1994; Cant, 1999), two steps (Swaminathan and Bilger, 1997) and complex chemistry (Tanahashi *et al*., 1999, 2000). The geometric configurations of DNS were mostly restricted by the computational power to canonical statistical planar flames (Poinsot *et al*., 1991; Trouve and Poinsot, 1994; Swaminathan and Bilger, 1997; Cant, 1999; Tanahashi *et al*., 2000; Grout, 2007; Shim et al., 2011; Chakraborty et al., 2004, 2010, 2013), where statistically planar the premixed flames moves for propagating towards the unburnt gas. Recently, a few attempts have been made to simulate turbulent premixed flames in more complicated geometry such as V-shape flame, swirl burner, Bunsen flames and lifted flames (Mizobuchi *et al*., 2002; Domingo *et al*., 2005; Richardson *et al*., 2010; Dunstan *et al*., 2012; Minamoto *et al*., 2011b; Tanaka *et al*., 2011). Figure 3 presents the boundary of DNS on combustion diagram regime according to Poinsot and Veynante (2013), which shows that the majority of the parameter range for combustors in piston engines can be accessed through DNS but only relatively small portion of the parameter range corresponding to aircraft jet engines can be simulated using DNS. It can be

expected that with the advancement of the High Performance Computing, DNS of realistic combustors will be possible in the near future (Chen *et al*., 2011; Moureau *et al*., 2011).

1.2.3 Reynolds Averaged Navier-Stokes Simulation

Reynolds averaged Navier-Stokes (RANS) simulation is the most widely adopted computational technique for the analysis of turbulent combustion, especially when the calculation of the instantaneous flow field is not computationally affordable. In RANS the mean values of all the quantities are obtained. The instantaneous transport equations are simulated after Reynolds averaging (i.e. directly calculating mean values) or Favre averaging (i.e. density weighted averaging) operation, where the unclosed terms, such as Reynolds stresses, turbulent fluxes of heat and species and reaction rate terms, created by the Reynolds/Favre averaging operations require models to close the transport equations. The Reynolds stresses are often closed by the k-ε model where k is the turbulent kinetic energy and ε denotes its dissipation rate. However, the ability of k-ε model in capturing the effects of buoyancy, strain, changing density (which is often the case in reacting flow) and pressure gradient is questionable. It is worth noting that this k-ε model was proposed originally for non-reacting flows, therefore, either modification to the k-ε model or a new model is required to address the effects induced by heat release due to exothermic chemical reaction. The gradient hypothesis is usually adopted to close turbulent fluxes of heat and species in non-reacting flow, which has been found to be invalid under certain conditions in premixed turbulent combustion (Bray et al.,1985). Modelling of the turbulent fluxes for turbulent premixed flames have been attempted recently (Veynante et al., 1997; Chakraborty and Cant, 2009) to capture both gradient and counter-gradient transport. A central challenge for RANS is the modelling of chemical reaction rate term, which contains an exponential function of temperature according to the Arrhenius law. However, the physical scales of the chemical reactions are limited to a very thin region (i.e. of the order of flame thickness), which is fully unresolved in RANS, therefore mean reaction rate term is modelled using various different approaches instead of expanding the term according to Taylor expansion. The relatively low computational cost of RANS makes it possible to carry out simulation involving practical geometries within a realistic period of time. Thus RANS is still the standard simulation technique in industry.

1.2.3 Large Eddy Simulation

Large eddy simulation (LES) uses a coarser level of spatial resolution than DNS. The resolution of LES is determined by the filter width Δ, which is between Kolmogorov length scale η and integral length scale l (see Fig. 1.2). however, the physical processes associated with length

scales smaller than the LES filter width (i.e. sub-grid processes) still need to be modelled. Therefore, the accuracy of LES heavily relies on both the grid size Δ and the behaviour of the sub-grid closures. In practice, the grid size Δ tends to be much larger than flame thickness such that the turbulent micro mixing and chemical reaction rate, occur in small scales, are often unresolved in LES. This brings a possible approach to model the unclosed terms in LES by adopting similar modelling methodologies used in RANS (Poinsot and Veynante, 2004). However, the resolution of LES is required to be much higher than RANS to resolve large scale turbulent flow physics. In addition, LES is inherently three-dimensional and unsteady and unlike RANS the assumption regarding axisymmetric, symmetric boundary do not remain valid for LES. Therefore the computational cost of LES is much higher than RANS for a given configuration and simulation parameters. Due to the advancement of high performance computing, LES is beginning to be adopted by industry for simulation of engineering problems involving large scale unsteadiness. LES is expected to be the main CFD tool in industry in the near future, but robust SGS models of turbulent combustion in the context of LES are needed.

1.3 Aim of the present work

The scalar dissipation rate (SDR) is a quantity of central importance in turbulent premixed combustion, which characterises the micro mixing of reactants and hot burnt products in scale of the same order of the flame thickness are thus cannot be fully resolved in LES and RANS. It has been found by Bray (1980) that SDR of reaction progress variable in RANS holds a proportional relation with the mean reaction rate for turbulent premixed flames for high Damköhler number combustion. Extensive research has been directed on SDR based reaction rate closure in RANS for turbulent premixed flames, while relatively limited effort has been made to the SDR based filtered reaction rate closure in the context of LES. Nethertheless, the statistical behaviours of Favre-filtered SDR and its transport are yet to be analysed in the open literature. Therefore, the purpose of this project is listed below:

- To analyse instantaneous scalar dissipation rate and its transport equation for turbulent premixed flames based on a well-documented DNS database.
- To investigate the effects of heat release parameter, turbulent Reynolds number and Lewis number *Le*, on the statistical behaviours of SDR and its transport.
- To investigate the statistical behaviour of SDR and its transport for different filter widths.
- To propose an algebraic closure of SDR based on the scaling analysis and statistical analysis of filtered SDR and its transport equation.

- To propose LES closures of the unclosed terms in filtered SDR transport equation for LES so that it remains valid for a large range of filter widths for flames with different values of τ, Le and Re_t.

- To compare the performances of SDR closures based on simple chemistry DNS database for explicitly filtered detailed chemistry DNS database.

1.4 Thesis outline

The current state of research on turbulent premixed combustion modelling will be reviewed in Chapter 2. The SDR approach in reaction rate closure for turbulent premixed combustion will be reviewed along with a brief review of other modelling approaches in the context of LES for turbulent premixed flames in Chapter 2. The mathematical background of basic concepts of laminar and turbulent premixed combustion are provided in Chapter 3. The details related to the DNS databases used in the current work will be presented in Chapter 4. The development of the SDR based reaction rate closure for LES is discussed based on *a-priori* DNS analysis in Chapter 5. In Chapter 6, the development of both static and dynamic algebraic closures of SDR for turbulent premixed flames in the context of LES based on *a-priori* DNS analysis is discussed. The statistical behaviour, statistical analysis and the modelling of the unclosed terms in explicitly filtered SDR transport equation will be presented in Chapter 7. Both algebraic SDR closure and transport equation based SDR closures developed in Chapters 6 and 7 based on *a-priori* analysis of simple chemistry DNS database will be assessed in the context of detailed chemistry and transport in Chapter 8. A brief conclusion of the present research and the future research directions will be discussed in the final chapter (Chapter 9).

Chapter 2. Literature Review

2.1 Flamelet approaches in turbulent premixed combustion

2.1.1 The regimes of turbulent premixed combustion

The wrinkling effects of turbulence on turbulent premixed flame were firstly described by Damköhler (1940) who suggested that combustion chemistry mostly takes place in thin, highly-wrinkled reaction interface which is not significantly disturbed by turbulent eddies as the scales of the cascading turbulent eddies are much larger than the flame scales. The laminar premixed flame structure is usually divided into three layers, which denotes the processes of homogeneous reactants, intensive chemical reaction and oxidisation of the products and intermediates respectively. The relatively small scale of the flame thickness and the fast chemical reaction result in a chemical time scale which is smaller than the large turbulent time scale (Bray, 1980). Therefore, these thin interfaces are reasonably assumed to be only wrinkled by the turbulent eddies but they maintain their quasi-laminar flame structure. These thin interfaces, separating products from mixed reactants, are termed as flamelets, which maintains laminar flame structure, but are only wrinkled and strained by the turbulent motion. A non-dimensional number which characterises the ratio between large eddy turn over time scale τ_t to the chemical time scale τ_c is known as the Damköhler number *Da* which is defined as:

$$Da = \frac{\tau_t}{\tau_c} = \frac{l/u'}{\delta_Z/S_L} \tag{2.1}$$

where l is the integral length, u' is the turbulent root mean square (RMS) velocity, S_L is unstrained laminar burning velocity and $\delta_Z \equiv \alpha_T/S_L$ is known as the Zel'dovich flame thickness and α_T denotes the unburnt gas thermal diffusivity. The flamelet assumption holds for $Da \gg 1$, where the chemical time scale is too small for the integral turbulence to affect the inner flame structure. For small values of *Da* the chemical reaction requires longer time than turbulent mixing and thus the inner flame structure is continuously destroyed and reformed by the generation (consumption) of products (reactants) and the

mixing of them. The above regime is known as 'perfectly/well stirred reactor' (Libby & Williams, 1980), where the mixing is fast and chemistry is slow. The Klimov-Williams criterion (Klimov, 1963; Williams, 1976) suggested only $Da \gg 1$ solely was not sufficient to characterise different regimes of premixed flames and suggested another non-dimensional number to characterise the effects of smallest eddies on the premixed flames. This non-dimensional number is known as Karlovitz number *Ka*, which is defined as:

$$Ka = \frac{\tau_c}{\tau_\eta} = \frac{\delta_z / S_L}{u'/\eta} \tag{2.2}$$

where τ_η is the Kolmogorov time scale and η is the Kolmogorov length scale. where Re_t is the turbulent Reynolds number which is defined as:

$$\mathrm{Re}_t = \frac{u'l}{\nu} = \left(\frac{u'}{S_L}\right)\left(\frac{l}{\delta_Z}\right) \sim Da^2 Ka^2 \tag{2.3}$$

It is possible to recast eq. (2.2) as:

$$Ka = \left(\frac{l}{\delta_z}\right)^{-\frac{1}{2}} \left(\frac{u'}{S_L}\right)^{\frac{3}{2}} = \left(\frac{\delta_z}{\eta}\right)^2 \tag{2.4}$$

Using the relation between the integral length l and Kolmogorov length scale η:

$$\frac{l}{\eta} = Re_t^{3/4} \tag{2.5}$$

Under the condition of $Ka < 1$, the chemical scale is smaller than all turbulent scales with flame is thinner than the smallest eddy in turbulence, where flamelets hold an inner structure close to laminar flames but are wrinkled by the turbulence. Based on the ratio between turbulent motion u' and the unstrained laminar burning velocity S_L, the above regime can be further characterised into two sub-regimes:

- $u' < S_L$: the flame propagates faster than turbulent velocity fluctuation and thus turbulence can hardly wrinkle the flame front in this 'wrinkled flamelet regime'.
- $u' > S_L$: the turbulent velocity fluctuation exceeds the laminar burning velocity and turbulent eddies start to corrugate the flame front in this 'corrugated flamelet regime'.

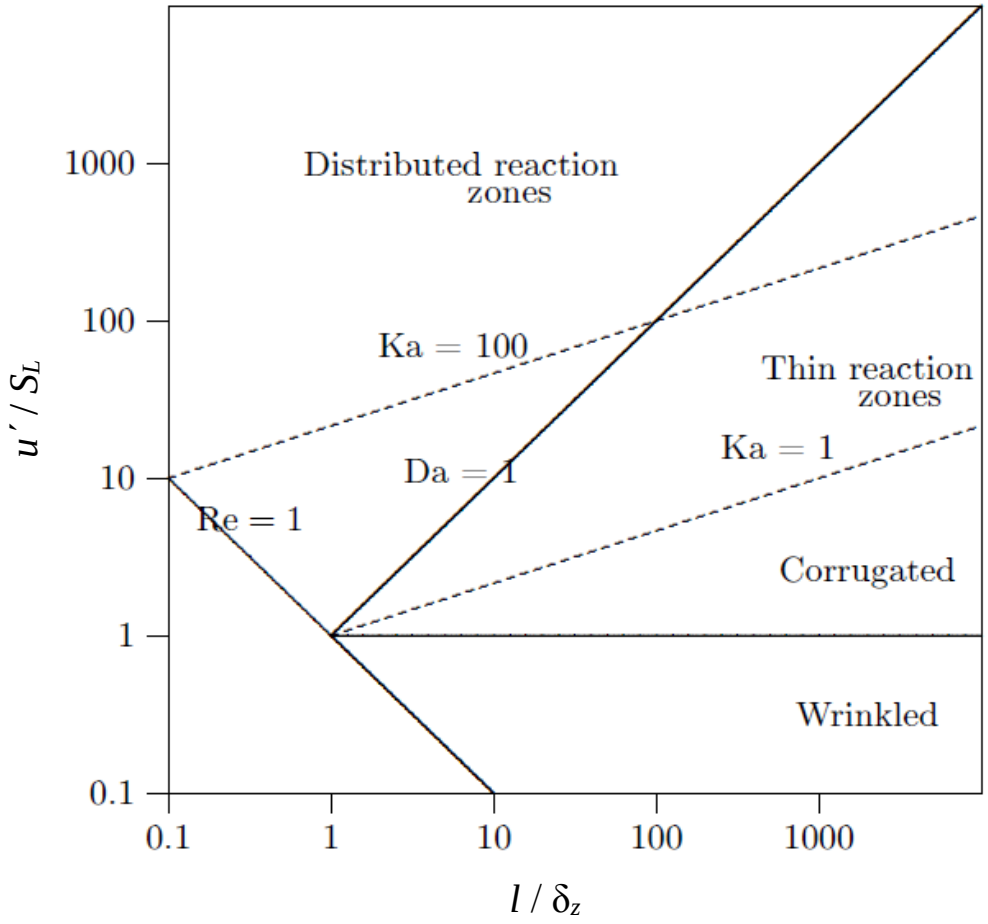

Figure 2.1: Regime diagram for turbulent premixed combustion (Peters, 2000).

The modified regime diagram by Peters (2000) is shown in Figure 2.1 where the above two regimes are explicitly denoted. Peters (2000) defined a second Karlovitz number Ka_r in terms of reaction zone thickness δ_r (which is typically one order magnitude smaller than the flame thickness, i.e. $\delta_r \sim \delta_z/10$) as:

$$Ka_r = \frac{\delta_r^2}{\eta^2} \tag{2.7}$$

when $\delta_r = \eta$, $Ka_r = 1$ and $Ka = \frac{\delta_z^2}{\eta^2} = \frac{\delta_z^2}{\delta_r^2} \sim 100$ represents a critical value of Ka, based on which two more regimes are defined:

- When $Ka_r < 1 < Ka$ where $\delta_r < \eta < \delta_z$, the eddies of Kolmogorov scales are able to enter the preheat zone and penetrate the flame structure resulting in a thickened flame. However, the reaction zone remains beyond the reach of the turbulent eddies and maintains a quasi-laminar structure. This regime is denoted as 'thin

reaction zone regime' (Peters, 2000) or 'thickened-wrinkled flame regime' (Poinsot and Veynante, 2001).

- When $Ka_r > 1$ where $\eta < \delta_r < \delta_z$, small eddies are able to penetrate into both the pre-heat zone and the reaction zone with possibility of causing local extinction resulting in pockets of reactants surrounded by flame like surface. This regime is denoted as 'the broken reaction zones regime' (Peters, 2000).

In premixed turbulent combustion, the scalar field can be represented by a reaction progress variable *c* to characteristic the development of the turbulent premixed flames based on reactant mass fraction Y_R (or product mass fraction Y_P or temperature *T*) as follows:

$$c = \frac{Y_{R0} - Y_R}{Y_{R0} - Y_{R\infty}} \tag{2.8}$$

where Y_{R0} , $Y_{R\infty}$ denotes reactant mass fraction in fresh gas and burnt products respectively. The reactant progress variable *c* increases from 0 in the unburnt reactants monotonically up to 1.0 in the fully burnt products. The reaction rate of reaction progress variable in the context of one-step Arrhenius chemistry can be expressed by the following relation in terms of mixture density ρ, reaction progress variable *c* and instantaneous temperature $\hat{T}$ as:

$$\dot{w} = f(\rho, c, T) = B^* \rho (1-c) \exp\left[\frac{-E}{R_0 \hat{T}}\right] \tag{2.9}$$

where B^* is the pre-exponential factor and *E* is the activation energy. The single step Arrhenius law of normalised form of chemical reaction $\dot{w}$ reads:

$$\dot{w} = \rho B (1-c) \exp\left[\frac{-\beta(1-T)}{1-\alpha(1-T)}\right] \quad \text{with} \quad B = \frac{B^* l}{\rho_0 u_0} \exp\left(-\frac{\beta}{\alpha}\right) \tag{2.10}$$

where

- $T = \dfrac{\hat{T} - T_0}{T_{ad} - T_0}$ is the normalised temperature with T_{ad} denoting the adiabatic temperature
- $\beta = \dfrac{E(T_{ad} - T_0)}{R_0 T_{ad}^2}$ is Zel'dovich number which is typically taken as $\beta = 6.0$,
- $\alpha = 1 - \dfrac{T_0}{T_{ad}} = \dfrac{\tau}{1+\tau}$ is closely related to heat release parameter τ.

The exponential function poses a major challenge to model the mean/filtered reaction rate in the context of RANS and LES.

2.1.2 Bray-Moss-Libby Model

This is one of the most well-established flamelet models of turbulent premixed combustion, usually referred to under the initials of the three contributors, Bray, Moss and Libby. The Bray-Moss-Libby (BML) model was initially proposed in 1977 (Bray and Moss, 1977), which has been subsequently improved (Bray, 1980; Bray et al. 1985, Bray et al., 1989). Combining the statistical approach by using the presumed probability density function (pdf) of progress variable, this model provides a thermochemical closure for turbulent premixed combustion in the context of RANS. The scalar field is assumed to be a unique function of reaction progress variable *c*. Regarding perfect gas and unity Lewis number, usual assumptions were made to maintain the simplicity of the mathematical framework. The pdf of *c* at a given location *x* has been expressed in the following manner:

$$\overbrace{p(c,x,t)}^{pdf} = \overbrace{\alpha(x,t)\delta(c)}^{fresh\ gases} + \overbrace{\gamma(x,t)f(c,x)}^{burning\ gases} + \overbrace{\beta(x,t)\delta(1-c)}^{burnt\ gases} \tag{2.11}$$

where the α, β and γ denote respectively the probability of finding unburned gases, burned gases and reacting gases, inherently summing up to unity (i.e. $\alpha + \beta + \gamma = 1$). The normalisation of pdf yields one more condition:

$$\int_0^1 f(c,x)dc = 1 \text{ with } f(0,x) = f(1,x) = 0 \tag{2.12}$$

Based on the pdf according to eq. (2.11) the mean value of a quantity Q can be easily shown as:

$$\begin{aligned}\overline{Q(x,t)} &= \int_0^1 Q(c,x,t)\,p(c,x,t)dc \\ &= \alpha(x,t)Q(0,\mathrm{x},\mathrm{t}) + \beta(x,t)Q(1,x,t) + \gamma(x,t)\int_0^1 Q(c,x,t)\,f(c,x,t)dc\end{aligned} \tag{2.13}$$

The flamelet assumption of large Reynolds and Damköhler numbers is applied in BML model where the flame front is so thin that the probability to find burning mixtures is mathematically small compared with the probability of finding fresh gases or burnt products. Therefore eq. (2.11) can be further reduced by neglecting the intermittency weight $\gamma(x,t) \sim O(1/Da)$ as:

$$p(c,x,t) \approx \alpha(x,t)\delta(c) + \beta(x,t)\delta(1\text{-}c) \tag{2.14}$$

It worth noting that with one more assumption of low Mach number, eq. (2.14) can lead to a direct relation between Reynold averaged and Favre averaged values as well as a meaningful expansion of scalar flux $\widetilde{u''c''}$:

$$\widetilde{u_i''c''} = \widetilde{u_i c} - \tilde{u}_i\tilde{c} = \tilde{c}(1-\tilde{c})(\bar{u}_i^b - \bar{u}_i^u) \tag{2.15}$$

where $\bar{u}_i^b$ and $\bar{u}_i^u$ denotes the mean velocities conditional on burnt and unburnt gases respectively. For thermal expansion across the flame brush $\bar{u}_i^b$ can be greater than $\bar{u}_i^u$ which leads to counter-gradient transport (i.e. the scalar flux assuming same sign as the scalar gradient, $\widetilde{u_i''c''} \times \partial\tilde{c}/\partial x_i > 0$). Thus eq. (2.15) provides a theoretical proof of the counter-gradient behaviours of scalar flux, which was later confirmed in experiments (Bray et al., 1981).

However, the modelling of mean reaction rate is still unresolved by BML model which can be mathematically explained as:

$$\overline{\dot{w}(x)} = \int_0^1 \dot{w}(c)\,p(c,x)dc = \gamma(x)\int_0^1 \dot{w}(c)\,f(c,x)dc \approx 0 \text{ for } Da >> 1 \tag{2.16}$$

As the chemical reaction rate $\dot{w}$ is weighted by γ which is negligible for $Da >> 1$, eq.(2.16) dose not yield a finite non-zero value of $\dot{w}$. Based on the BML model, three alternative approaches have been developed to close the mean reaction rate in RANS, which are respectively based on flame crossing frequency, flame surface density (FSD) and scalar dissipation rate. The approach based on scalar dissipation rate approach will be introduced in detail in section 2.2. The flame crossing frequency based reaction rate closure and flame surface density approach will be discussed here.

2.1.3 Flame crossing frequencies

The central logic of this approach is given by the following statement. At a given point, the number of times of the flame front crossing is assumed to have more influence on the mean reaction rate than the local temperature and species mass fraction (Bray,1984; Bray and Libby, 1986). According to this assumption, the mean reaction rate can be mathematically expressed as:

$$\bar{\dot{w}} = \dot{w}_f \upsilon_f \tag{2.17}$$

where $\dot{w}_f$ and υ_f represent the reaction rate per flame crossing and the flame crossing frequency respectively. The flame crossing frequency is evaluated based on the statistical function of a telegraph signal in the following manner:

$$\upsilon_f = 2\frac{\bar{c}(1-\bar{c})}{\hat{T}} \tag{2.18}$$

where $\hat{T}$ denotes the mean period of the telegraph signal, which is typically taken to be the eddy turn over time $\tilde{\tau}_t \sim \tilde{k}/\tilde{\epsilon}$ for $\bar{\dot{w}}$ closure. The reaction rate per flame crossing $\dot{w}_f$ is often modelled as:

$$\dot{w}_f = \frac{\rho_0 S_L}{\delta_L / t_t} \tag{2.19}$$

where ρ_0 denotes the density of fresh gases, δ_L is the laminar flame thickness and S_L is the laminar flame speed and t_t represents the transit time between the two isosurfaces $c = 0$ and $c = 1$. Subsequently, the eq. (2.17) can be written as:

$$\bar{\dot{w}} = \frac{2\rho_0 S_L}{\delta_L / t_t} \frac{\tilde{\varepsilon}}{\tilde{k}} \bar{c}(1 - \bar{c}) \tag{2.20}$$

However, it is often not straightforward to estimate t_t and therefore the model has been later recast in terms of FSD.

2.1.4 Flame Surface Density (FSD) approach

As a well-established modelling approach, the flame surface density Σ, which characterises the flame surface area per unit volume by measuring the flame front convolution. According to FSD based closure, the mean reaction rate is expressed as:

$$\bar{\dot{w}} = \rho_0 \langle s_c \rangle_s \Sigma \tag{2.21}$$

where s_c is the flame consumption speed and $\langle ... \rangle_s$ denotes the averaging operation over the flame surface (Marble and Broadwell, 1977). The mean surface averaged flame consumption speed $\langle s_c \rangle_s$ was estimated by (Vervisch and Veynante, 2002):

$$\langle s_c \rangle_s = \int_0^{+\infty} s_c(\kappa) p(\kappa) d\kappa \tag{2.22}$$

where $p(\kappa)$denotes the probability and κ is the stretch rate. A 'stretch factor' I_0 was introduced (Bray, 1990) to account the ratio of mean flamelet consumption speed and the laminar flame speed as:

$$I_0 = \frac{1}{S_L} \int_0^{+\infty} s_c(\kappa) p(\kappa) d\kappa \tag{2.23}$$

Subsequently, eq. (2.21) can be rewritten as:

$$\bar{\dot{w}} = \rho_0 S_L I_0 \Sigma \tag{2.24}$$

It worth noting that FSD Σ itself requires modelling which could be achieved through either an algebraic closure or solving a transport equation. This approach is valid for both RANS and LES.

2.2 Review of scalar dissipation rate in turbulent combustion modelling

This section focuses on the reaction rate closure based on scalar dissipation rate, which itself is unclosed in both RANS and LES simulations. A brief review of the roles played by SDR in turbulent combustion modelling will be provided below. The mathematical background of the SDR in turbulent premixed combustion modelling will be introduced in Chapter 3 in detail, however, the SDR based reaction rate closure derived from BML model will be introduced here in order to demonstrate the strength of this methodology.

2.2.1 Reaction rate closure

The instantaneous transport equation of reaction progress variable c is written as:

$$\frac{\partial \rho c}{\partial t}+\frac{\partial}{\partial x_i}(\rho u_i c)=\frac{\partial}{\partial x_i}\left(\rho D\frac{\partial c}{\partial x_i}\right)+\dot{w} \tag{2.25}$$

Reynolds averaging equation (2.25) one obtains the transport equation of Favre averaged progress variable $\tilde{c}$ as:

$$\frac{\partial \bar{\rho}\tilde{c}}{\partial t}+\frac{\partial}{\partial x_i}(\bar{\rho}\tilde{u}_i\tilde{c})=\overline{\frac{\partial}{\partial x_i}\left(\rho D\frac{\partial c}{\partial x_i}\right)}+\bar{\dot{w}}-\frac{\partial}{\partial x_j}[\overline{\rho u_j c}-\bar{\rho}\tilde{u}_j\tilde{c}] \tag{2.26}$$

An alternative transport equation for $c(1-c)$ can be derived from eq. (2.25) in the following form (Bray and Moss, 1977):

$$\frac{\partial\left[\rho c(1-c)\right]}{\partial t}+\frac{\partial\left[\rho u_i c(1-c)\right]}{\partial x_i}=\frac{\partial}{\partial x_i}\left(\rho D\frac{\partial}{\partial x_i}\left[c(1-c)\right]\right)+2\rho D\frac{\partial c}{\partial x_i}\frac{\partial c}{\partial x_i}-2c\dot{w}+\dot{w} \tag{2.27}$$

According to BML approach where the probability of finding $0<c<1$ is negligible, the term $c(1-c)$ assumes zero value which leads eq. (2.27) to:

$$2\rho D\frac{\partial c}{\partial x_i}\frac{\partial c}{\partial x_i}=(2c-1)\dot{w} \tag{2.28}$$

where $N_c \equiv D\frac{\partial c}{\partial x_i}\frac{\partial c}{\partial x_i}$ is the instantaneous scalar dissipation rate (SDR). Reynolds averaging eq. (2.28) yields the following equation:

$$2\overline{\rho N_c} = 2\overline{\rho D\frac{\partial c}{\partial x_i}\frac{\partial c}{\partial x_i}} = \overline{(2c-1)\dot{w}} \tag{2.29}$$

Bray (1980) proposed the SDR based reaction rate closure by recasting eq. (2.29) into the following form:

$$\bar{\dot{w}} = \frac{2}{2c_m - 1}\overline{\rho D\frac{\partial c}{\partial x_i}\frac{\partial c}{\partial x_i}} = \frac{2}{2c_m - 1}\bar{\rho}\tilde{N}_c \tag{2.30}$$

where $\tilde{N}_c = \overline{\rho N_c}/\bar{\rho}$ denotes the Favre averaged SDR and the thermo-physical parameter c_m is given by:

$$c_m = \frac{\overline{\dot{w}c}}{\bar{\dot{w}}} = \frac{\int_0^1 [\dot{w}cf(c)]_L dc}{\int_0^1 [\dot{w}f(c)]_L dc} \tag{2.31}$$

where $f(c)$ is the burning mode pdf of c and the subscript 'L' refers to the values in unstrained planar laminar premixed flames. Equation (2.30) relates the mean reaction rate $\bar{\dot{w}}$ to the turbulent mixing through SDR $\tilde{N}_c$ and chemical reaction through the thermo-chemical parameter c_m, which assumes values between 0.7~0.9 (Bray, 1980).

In order to explain the central role played by SDR in the reaction rate closure for RANS, it is useful to start from the transport equation of the scalar variance $\widetilde{c''^2}$ (noting $c = \tilde{c} + c''$) (Bray, 1980; Veynante & Vervisch, 2002):

$$\frac{\partial \bar{\rho}\widetilde{c''^2}}{\partial t}+\frac{\partial \bar{\rho}\tilde{u}_i\widetilde{c''^2}}{\partial x_i}+\frac{\partial \bar{\rho}\widetilde{u_i''c''^2}}{\partial x_i}=\overbrace{\frac{\partial}{\partial x_i}\overline{\left(\rho D\frac{\partial c''^2}{\partial x_\iota}\right)}+2\overline{c''\frac{\partial}{\partial x_\iota}\left(\rho D\frac{\partial \tilde{c}}{\partial x_\iota}\right)}}^{molecular\ diffusion}$$

$$\underbrace{-2\bar{\rho}\widetilde{u_i''c''}\frac{\partial \tilde{c}}{\partial x_i}}_{production}+\underbrace{2\overline{\dot{w}c''}}_{chemical\ reaction}-\underbrace{2\rho D\frac{\partial \widetilde{c''}}{\partial x_i}\frac{\partial \widetilde{c''}}{\partial x_i}}_{scalar\ dissipation} \tag{2.32}$$

The three terms on the left hand side (LHS) denote the transient term, advection term and turbulent transport term of scalar variance respectively. The first term on the right hand side (RHS) is the molecular diffusion of scalar variance which is often ignored in RANS of high Reynolds number flows. The 'production' term in eq. (2.32) characterises the scalar fluctuation for gradient transport of scalar flux. Many previous analyses on scalar fluxes of turbulent premixed flames in RANS reported both gradient and counter-gradient type transport (Bray *et al*.,1985; Moss, 1980; Shephard *et al*., 1982; Frank *et al*.,1999; Kalt *et al*.,2002; Rutland and Cant, 1994; Veynante *et al*. 1997; Swaminathan *et al*., 2001; Nishiki *et al*., 2006; Chakraborty and Cant, 2009). The reaction rate related term can be modelled based on eq. (2.31) as:

$$\overline{\dot{w}c''}=\overline{\dot{w}c}-\bar{\dot{w}}\tilde{c}=(c_m-\tilde{c})\bar{\dot{w}} \tag{2.33}$$

The last term on RHS of eq. (2.32) denotes the scalar dissipation of scalar variance, the mean SDR is defined as $\widetilde{\varepsilon_c}\equiv\overline{\rho D}\frac{\partial \widetilde{c''}}{\partial x_i}\frac{\partial \widetilde{c''}}{\partial x_i}/\bar{\rho}$ whose relation with Favre averaged SDR is written as:

$$\bar{\rho}\widetilde{N_c}=\overline{\rho D\frac{\partial c}{\partial x_\iota}\frac{\partial c}{\partial x_\iota}}=\overline{\rho D}\frac{\partial \tilde{c}}{\partial x_i}\frac{\partial \tilde{c}}{\partial x_i}+\overline{2\rho D\frac{\partial c''}{\partial x_\iota}\frac{\partial \tilde{c}}{\partial x_i}}+\overline{\rho D\frac{\partial c''}{\partial x_\iota}\frac{\partial c''}{\partial x_\iota}} \tag{2.34}$$

In the context of RANS, the first two terms on RHS of eq. (2.34) are often neglected due to small values of the mean scalar gradient in comparison to the gradient of scalar fluctuations which results in $\bar{\rho}\widetilde{N_c}\approx\bar{\rho}\widetilde{\varepsilon_c}$, which has been applied in the reaction rate closure (i.e. eq. (2.30)) based on SDR. However, in the context of LES the first term on the RHS cannot be simply neglected and further information of this will be elaborated in Chapter 3. It worth noting that this scalar dissipation rate (SDR) $\widetilde{\varepsilon_c}$ itself is unclosed

which require closure in RANS. A traditional approach to model the SDR $\widetilde{\varepsilon_c}$ is the linear relaxation model which is often used for passive scalar mixing:

$$\bar{\rho}\widetilde{\varepsilon_c} = \frac{\overline{\rho c''^2}}{\tau_t} \tag{2.35}$$

Based on the BML model and using the large-scale turbulent time scale scaling $\tau_t \sim \tilde{k}/\tilde{\varepsilon}$ subsequently leads to:

$$\bar{\rho}\widetilde{\varepsilon_c} = \frac{\overline{\rho c''^2}}{\tau_t} \approx \frac{\bar{\rho}\tilde{c}(1-\tilde{c})}{\tau_t} = \bar{\rho}\frac{\tilde{\varepsilon}}{\tilde{k}}\tilde{c}(1-\tilde{c}) \tag{2.36}$$

Substituting in eq. (2.30) and using $\bar{\rho}\widetilde{N_c} \approx \bar{\rho}\widetilde{\varepsilon_c}$ for large Reynolds number turbulent premixed flames, eq. (2.36) yields:

$$\bar{\dot{w}} \approx C_{EBU}\frac{\overline{\rho c''^2}}{\tau_t} \approx C_{EBU}\bar{\rho}\frac{\tilde{\varepsilon}}{\tilde{k}}\tilde{c}(1-\tilde{c}) \tag{2.37}$$

Equation (2.37) is commonly known as the Eddy-Break-Up (EBU) model (Mason & Spalding, 1973) which is one of the first attempts to close the chemical reaction rate of turbulent premixed flames. Due to the simple mathematical expression solely based on the resolved quantities, the EBU model has attracted extensive attention and is already implemented in commercial codes for both premixed and non-premixed turbulent flames simulations. However, this model adopted the assumption of passive scalar mixing and the chemistry process is assumed too fast to affect $\dot{w}$ through the existence of any burning mixtures. The separation of chemical kinetics from the turbulence in the EBU model results in a lack of interaction between flames and turbulence. The EBU model has been reported to overestimate the chemical reaction rate in the context of RANS. However, a few attempts in LES of EBU model provided reasonable predictions for bluff body stabilised flames (Fureby and Möler, 1995), but the model parameter C_{EBU} needed tuning for different flow parameters (Fureby and Löfstörm,1994).

2.2.2 Review on modelled SDR transport equation in RANS

One possible way to model SDR $\widetilde{\varepsilon_c}$ is based on the closure of the transport equation of Favre averaged SDR, which has been recently studied extensively in the context of

RANS. The exact unclosed transport equation of $\widetilde{\varepsilon_c}$ takes the following form (Borghi, 1978, 1990; Mantel and Borghi, 1990; Swaminathan and Bray, 2005):

$$\bar{\rho}\frac{\partial\widetilde{\varepsilon}_c}{\partial t}+\bar{\rho}\,\tilde{u}_j\frac{\partial\widetilde{\varepsilon}_c}{\partial x_j}=\underbrace{\frac{\partial}{\partial x_j}\left[\overline{\rho\,D\frac{\partial\varepsilon_c}{\partial x_j}}\right]}_{D_1}+T_1+T_2+T_3+T_4-D_2+f(D) \tag{2.38}$$

On the LHS the two terms respectively denotes the transient and mean advection terms. The term D_1 denotes the molecular diffusion of $\widetilde{\varepsilon_c}$ and term T_1 denotes the turbulent transport of $\widetilde{\varepsilon_c}$ which takes the following form:

$$T_1=\underbrace{-\frac{\partial(\overline{\rho u_j''\varepsilon_c})}{\partial x_j}}_{T_{11}}\quad\underbrace{\overline{-2\rho D u_j''\left(\frac{\partial c''}{\partial x_k}\right)\left(\frac{\partial^2\tilde{c}}{\partial x_j\partial x_k}\right)}}_{T_{12}} \tag{2.39}$$

The term T_2 arises due to density change resulting from heat release and is given by:

$$\begin{aligned}T_2=&-2\overline{\frac{D}{\rho}\left(\dot{w}+\frac{\partial}{\partial x_j}\rho D\frac{\partial c}{\partial x_j}\right)\frac{\partial c}{\partial x_k}\frac{\partial\rho}{\partial x_k}}\\&+2\frac{\bar{D}}{\bar{\rho}}\frac{\partial\tilde{c}}{\partial x_k}\frac{\partial\bar{\rho}}{\partial x_k}\left[\overline{\left(\dot{w}+\frac{\partial}{\partial x_j}\rho D\frac{\partial c}{\partial x_j}\right)}-\frac{\partial(\overline{\rho u_l''c''})}{\partial x_l}\right]\end{aligned} \tag{2.40}$$

The term T_3 originates due to the reaction progress variable gradient ∇c alignment with local principal strain rates, which is commonly referred to as the turbulence-scalar interaction term. The term T_3 takes the following form:

$$T_3=\underbrace{-2\overline{\rho D}\frac{\partial\tilde{c}}{\partial x_j}\frac{\widetilde{\partial u_j''}}{\partial x_k}\frac{\widetilde{\partial c''}}{\partial x_k}}_{T_{31}}\underbrace{-2\overline{\rho D}\frac{\partial c''}{\partial x_j}\frac{\widetilde{\partial u_j''}}{\partial x_k}\frac{\partial c''}{\partial x_k}}_{T_{32}}\underbrace{-2\overline{\rho D}\frac{\widetilde{\partial c''}}{\partial x_j}\frac{\widetilde{\partial c''}}{\partial x_k}\frac{\partial\widetilde{u_j}}{\partial x_k}}_{T_{33}} \tag{2.41}$$

The term T_4 representing the fluctuation of reaction rate gradient assumes the following form:

$$T_4=2\overline{D\frac{\partial\dot{w}}{\partial x_k}\frac{\partial c}{\partial x_k}}-2\bar{D}\frac{\partial\bar{\dot{w}}}{\partial x_k}\frac{\partial\tilde{c}}{\partial x_k} \tag{2.42}$$

The term ($-D_2$) denotes the molecular dissipation of $\widetilde{\varepsilon_c}$ and is given by:

$$-D_2 = -2\overline{\rho D^2 \frac{\partial^2 c''}{\partial x_k \partial x_i} \frac{\partial^2 c''}{\partial x_k \partial x_i}} \tag{2.43}$$

The term $f(D)$ arises from the variation of mass diffusion and the mathematical expression of $f(D)$ is given as:

$$\begin{aligned} f(D) = {} & \overline{2D \frac{\partial c}{\partial x_k} \frac{\partial(\rho D)}{\partial x_k} \frac{\partial^2 c}{\partial x_j \partial x_j}} + \overline{2D \frac{\partial c}{\partial x_k} \frac{\partial^2(\rho D)}{\partial x_j \partial x_k} \frac{\partial c}{\partial x_j}} - \overline{\frac{\partial}{\partial x_j}\left(\rho N_c \frac{\partial D}{\partial x_j}\right)} \\ & - \overline{2\rho D \frac{\partial D}{\partial x_j} \frac{\partial}{\partial x_j}\left(\frac{\partial c}{\partial x_k}\frac{\partial c}{\partial x_k}\right)} + \overline{\rho \frac{\partial c}{\partial x_k}\frac{\partial c}{\partial x_k}\left[\frac{\partial D}{\partial t} + u_j \frac{\partial D}{\partial x_j}\right]} - 2\tilde{D}\frac{\partial \tilde{c}}{\partial x_k}\frac{\partial(\bar{\rho}\tilde{D})}{\partial x_k}\frac{\partial^2 \tilde{c}}{\partial x_j \partial x_j} \\ & - 2\tilde{D}\frac{\partial \tilde{c}}{\partial x_k}\frac{\partial^2(\bar{\rho}\tilde{D})}{\partial x_j \partial x_k}\frac{\partial \tilde{c}}{\partial x_j} + \frac{\partial}{\partial x_j}\left(\bar{\rho}\tilde{D}\frac{\partial \tilde{c}}{\partial x_k}\frac{\partial \tilde{c}}{\partial x_k}\frac{\partial \tilde{D}}{\partial x_j}\right) \\ & + 2\bar{\rho}\tilde{D}\frac{\partial \tilde{D}}{\partial x_j}\frac{\partial}{\partial x_j}\left(\frac{\partial \tilde{c}}{\partial x_k}\frac{\partial \tilde{c}}{\partial x_k}\right) - \bar{\rho}\frac{\partial \tilde{c}}{\partial x_k}\frac{\partial \tilde{c}}{\partial x_k}\left[\frac{\partial \tilde{D}}{\partial t} + u_j \frac{\partial \tilde{D}}{\partial x_j}\right] \end{aligned} \tag{2.44}$$

The term $f(D)$ sometimes is neglected in RANS by assuming constant diffusivity D (Swaminathan and Bray, 2005). Moreover density has been assumed to be constant in an earlier derivation of the above transport equation (Borghi, 1990; Mantel & Borghi, 1994; Mura & Borghi, 2003). The terms $T_1, T_2, T_3, T_4, (-D_2)$ and $f(D)$ are the unclosed terms and these terms need to be modelled in order to solve the $\tilde{\varepsilon}_c$ transport equation. For a statistically stationary point of view, the contribution of $[\overline{\rho \nabla c . \nabla c (\partial D / \partial t)} - \bar{\rho} \nabla \tilde{c} . \nabla \tilde{c} (\partial \tilde{D} / \partial t)]$ can be considered to be negligible and thus has been neglected in most studies (Borghi and Dutyoa,1978; Borghi, 1990; Mantel and Borghi, 1994; Mura and Borghi, 2003; Swaminathan and Bray, 2005; Swaminathan and Grout, 2006; Chakraborty and Swaminathan, 2007a, 2007b, 2010, 2011, 2013; Chakraborty *et al*., 2008, 2010, 2011a; Mura *et al*., 2008, 2009; Kolla *et al*., 2009). Swaminathan and Bray (2005) proposed an order-of-magnitude analysis for the above unclosed terms by using unburned gas density ρ_0 and laminar flame velocity S_L and thickness δ_{th}. This yields the following scaling estimates for the SDR transport equation upon normalisation with respect to $\rho_0 S_L^2 / \delta_{th}^2$:

$$T_{11} \sim O(Da^{-1}) \,;\; T_{12} \sim O(\mathrm{Re}_t^{\,-1} Da^{-1}) \,; \tag{2.45}$$

$$T_2 \sim O(1) \,; \tag{2.46}$$

$$T_{31} \sim O(\mathrm{Re}_t^{-1/2}\, Da^{-1/2})\,;\; T_{32} \sim O(1)\,;\; T_{33} \sim O(Da^{-1} U_{ref}/u')\,; \tag{2.47}$$

$$T_4 \sim O(1)\,; \tag{2.48}$$

$$(-D_2) \sim O(1) \tag{2.49}$$

where U_{ref} is a velocity scale representing the Favre mean velocity. The diffusivity gradient term $f(D)$ can be scaled in the following manner upon normalising with respect to $\rho_0 S_L^{\ 2}/\delta_{th}^2$ (Gao et al., 2014):

$$f(D) \sim O(1) \tag{2.50}$$

An alternative order of magnitude analysis was proposed by Mantel and Borghi (1994), where the root-mean-square (rms) turbulent velocity fluctuation u' and Taylor micro-scale λ are used to scale the velocity fluctuations and the gradients of the fluctuating quantities respectively following Tennekes and Lumley (1972). The scaling analysis by Mantel and Borghi (1991) yields the following scaling estimates for the unclosed terms of the SDR transport equation upon normalisation with respect to $\rho_0 u'^2/l^2$:

$$T_{11} \sim O(1)\,;\; T_{12} \sim O(\mathrm{Re}_t^{-1/2})\,; \tag{2.51}$$

$$T_{31} \sim O(1)\,;\; T_{32} \sim O(\mathrm{Re}_t^{1/2})\,;\; T_{33} \sim O(1) \tag{2.52}$$

One obtains the following scaling estimate for $(-D_2)$ in non-reacting flows if the second-derivatives of fluctuating quantities are scaled using the Kolmogorov length scale, η:

$$(-D_2) \times l^2/\rho_0 u'^2 \sim O(\mathrm{Re}_t) \tag{2.53}$$

Equations (2.52) and (2.53) indicate that T_{32} and $(-D_2)$ are the leading order contributors to the $\widetilde{\varepsilon}_c$ transport in high Re_t non-reacting flows. The terms T_2, T_4 and $f(D)$ are identically zero for non-reacting isothermal flows. The above order of magnitude analysis suggests that $T_2, T_3, T_4, (-D_2)$ and $f(D)$ are the leading order terms of $\widetilde{\varepsilon}_c$ transport which has been confirmed later by DNS data (Chakraborty et al., 2011). According to eqs. (2.45) and (2.51), the contribution of T_1 can potentially play an

important role for $Da<1$ combustion, however, the magnitude of T_1 is reported to be negligible comparing with $T_2, T_3, T_4, (-D_2)$ and $f(D)$ for turbulent premixed flames with $Da<1$ (Chakraborty and Swaminathan, 2013). The modelling of these unclosed terms, T_1, T_2, T_3, T_4 and $(-D_2)$, are discussed next.

Review modelling of turbulent transport term, T_1

The scaling estimates in eq. (2.45) indicate that $T_{11}/T_{12} \sim O(\mathrm{Re}_t)$ and T_{12} contribution is negligible compared to T_{11} in high Re_t flows. A similar observation can also be made using the alternative scaling given by eq. (2.51), therefore T_1 can be written as

$$T_1 \approx -\nabla.(\overline{\rho u'' \varepsilon_c}) \tag{2.54}$$

Equation (2.54) indicates that the modelling of T_1 translates to the modelling of turbulent flux, $\overline{\rho u_j'' \varepsilon_c}$ (Chakraborty and Swaminathan, 2010, 2013). A conventional modelling approach is to follow the gradient hypothesis for passive scalar mixing in the following manner:

$$\overline{\rho u_j'' \varepsilon_c} = -\frac{\mu_t}{\sigma_\varepsilon}\frac{\partial \tilde{\varepsilon}_c}{\partial x_j} \tag{2.55}$$

where $\mu_t = C_\mu \bar{\rho}\frac{\tilde{k}^2}{\tilde{\varepsilon}}$ is the eddy viscosity, $\tilde{k} = 0.5\frac{\overline{\rho u_i'' u_i''}}{\bar{\rho}}$ denotes the turbulent kinetic energy and σ_ε is the turbulent Schmidt number and $C_\mu = 0.09$ is a model parameter. Counter-gradient transport of the turbulent flux of scalar gradients has been reported by previous studies for the flames where counter-gradient behaviour for turbulent scalar flux $\overline{\rho u_j'' c''}$ is observed. (Veynante *et al.*, 1997; Chakraborty and Cant, 2009; Chakraborty and Swaminathan, 2010, 2013). The scalar flux was modelled in BML approach (i.e. eq (2.14)) in terms of slip velocity as: $\widetilde{u_i'' c''} = \tilde{c}(1-\tilde{c})(\bar{u}_i^b - \bar{u}_i^u)$ for high Damköhler number flames (Bray et al., 1985). The slip velocity was modelled in the following manner as (Veynante et al., 1997):

$$\bar{u}_i^b - \bar{u}_i^u = -\alpha_E\sqrt{2\tilde{k}/3} + \tau S_L \tag{2.56}$$

with α_E being an appropriate efficiency function (Veynante et al., 1997). A model of $\overline{\rho u_i'' \varepsilon_c}$ was proposed to accommodate both gradient and counter-gradient transports in the following manner (Chakraborty and Swaminathan, 2013):

$$\overline{\rho u_i'' \varepsilon_c} = (1-2\tilde{c}) \underset{[c''^2+\tilde{c}(1-\tilde{c})]}{\underbrace{\overline{\rho u_i'' c''} - \alpha_1 \bar{\rho} \tilde{c}(1-\tilde{c})\sqrt{2\tilde{k}/3} M_i}} \tilde{\varepsilon}_c - \alpha_2 \mu_t \frac{\partial \tilde{\varepsilon}_c}{\partial x_i} \tag{2.57}$$

where $M_i = -(\partial \tilde{c} / \partial x_i) / |\nabla \tilde{c}|$ is the i^{th} component of the flame brush normal vector. The model parameters are given as $\alpha_1 = 0.22$; $\alpha_2 = 4.0[1-0.5erf(\mathrm{Re}_L/6)]$ and $\Phi = 1-0.5erf(\mathrm{Re}_L/3)$, where $\mathrm{Re}_L = \rho_0 \tilde{k}^2 / \mu_0 \tilde{\varepsilon}$ is the local turbulent Reynolds number with ρ_0 and μ_0 being the unburned gas density and unburned gas viscosity respectively.

Review modelling of density variation term, T_2

The term T_2 denotes the correlation between the dissipation and dilatation rates. The dilatation rate assumes non-zero values inside the flame front for low Mach number combustion. T_2 and the contribution of γ_0 in eq. (2.10) can be expressed in terms of mean reaction rate to propose a model of T_2 as follows (Swaminathan and Bray, 2005):

$$T_2 = \frac{4K_c}{2C_m - 1}\left(\frac{S_L}{\delta_{th}}\right)\bar{\rho}\tilde{\varepsilon}_c \quad \text{with} \quad K_c = \left(\frac{\delta_{th}}{S_L}\right)\frac{\int [\rho N_c (\nabla . \mathrm{u})]_L f(c) dc}{\int [\dot{w}]_L f(c) dc} \tag{2.58}$$

where L denotes the laminar flame quantities and $f(c)$ is the burning mode pdf. The quantity K_c has been found to be strongly dependent on heat release parameter τ and equivalence ratio (Rogerson and Swaminathan, 2007), which has been improved by modifying eq. (2.58) in the following form (Kolla et al., 2009):

$$T_2 = 2K_c^*\left(\frac{S_L}{\delta_{th}}\right)\bar{\rho}\tilde{\varepsilon}_c \quad \text{with} \quad K_c^* = \left(\frac{\delta_{th}}{S_L}\right)\frac{\int [\rho N_c (\nabla . \mathrm{u})]_L f(c) dc}{\int [\rho N_c (]_L f(c) dc} \tag{2.59}$$

where K_c^* can be obtained from laminar flame solutions and K_c^* / τ has been found to be insensitive to the changes in equivalence ratio. Both eqs (2.58) and (2.59) attempt to

account for the intensity of heat release through a thermochemical parameter and both models are strictly valid for flames of large *Da*. Recently, a simple algebraic closure of T_2 has been proposed to overcome the above limitation. The gas density ρ for low Mach number combustion can be expressed as (Bray *et al*., 1985):

$$\rho = \frac{\rho_0}{(1+\tau T)} \tag{2.60}$$

Equation (2.60) has been rewritten based on the progress variable *c* for flames with unity Lewis number as:

$$\rho = \frac{\rho_0}{1+\tau c}; \quad \bar{\rho} = \frac{\rho_0}{1+\tau \tilde{c}} \tag{2.61}$$

Using eq. (2.61) along with conservation equations of *c* (i.e. eq. (2.25)) and $\tilde{c}$ (i.e. eq.(2.26)) yield the following relation:

$$-2\overline{D\frac{[\dot{w}+\nabla.(\rho D\nabla c)]}{\rho}\frac{\partial c}{\partial x_k}\frac{\partial \rho}{\partial x_k}} = \overline{2\rho N_c \frac{\partial u_j}{\partial x_j}} \tag{2.62}$$

$$2\frac{\overline{D}}{\bar{\rho}}\frac{\partial \tilde{c}}{\partial x_k}\frac{\partial \bar{\rho}}{\partial x_k}\left[\overline{\dot{w}+\nabla.(\rho D\nabla c)} - \frac{\partial(\overline{\rho u_l'' c''})}{\partial x_l}\right] = -2\overline{\rho D}\nabla\tilde{c}.\nabla\tilde{c}\frac{\partial \tilde{u}_j}{\partial x_j} \tag{2.63}$$

Subsequently an alternative expression for T_2 for unity Lewis number flames can be obtained (Swaminathan and Bray, 2005):

$$\begin{aligned} T_2 &= \overline{2\rho N_c \frac{\partial u_j}{\partial x_j}} - 2\bar{\rho}\bar{D}\nabla\tilde{c}.\nabla\tilde{c}\frac{\partial \tilde{u}_j}{\partial x_j} \\ &= \underbrace{\overline{2\rho\varepsilon_c \frac{\partial u_j}{\partial x_j}}}_{T_{21}} + \underbrace{\overline{4\rho D\frac{\partial c''}{\partial x_j}\frac{\partial u_k}{\partial x_k}\frac{\partial \tilde{c}}{\partial x_j}}}_{T_{22}} + \underbrace{2\nabla\tilde{c}.\nabla\tilde{c}\overline{\rho D\frac{\partial u_j''}{\partial x_j}}}_{T_{23}} \end{aligned} \tag{2.64}$$

The three components of eq. (2.64) were scaled as (Swaminathan and Bray, 2005):

$$T_{21} \sim O\left(\frac{S_L^2}{\delta_{th}^2}\right);\ T_{22} \sim O\left(\frac{S_L^2}{\delta_{th}^2}\frac{1}{\sqrt{\mathrm{Re}_t\, Da}}\right) \text{ and } T_{23} \sim O\left(\frac{S_L^2}{\delta_{th}^2}\frac{1}{\mathrm{Re}_t\, Da}\right) \tag{2.65}$$

For turbulent premixed flames of high turbulent Reynolds number, the magnitude of T_{22} and T_{23} are expected to be much smaller than T_{21}, such that T_2 and T_{21} are almost indistinguishable (Chakraborty and Swaminathan, 2013). A model of T_2 was proposed based on the scaling estimates of scalar dissipation rate $\tilde{\varepsilon}_c$ and dilatation rate $\nabla.\vec{u}$ in term of laminar flame speed S_L and thermal flame thickness δ_{th}:

$$\nabla.\vec{u} \sim \tau \frac{S_L}{\delta_{th}} \text{ and } \tilde{\varepsilon}_c \sim \frac{S_L}{\delta_{th}} \tag{2.66}$$

The term T_2 arises due to heat release with the reaction zone maintaining quasi-laminar structure, which justifies the choice of the laminar burning velocity S_L and the flame thickness δ_{th} for the scaling analysis. A model of T_2 was proposed in the following manner (Chakraborty and Swaminathan, 2010):

$$T_2 = 2C_{T_2}\tau \frac{S_L}{\delta_{th}} \overline{\rho}\tilde{\varepsilon}_c \tag{2.67}$$

where the model parameter C_{T_2} is given by

$$C_{T_2} = \frac{B_{T_2}}{\sqrt{1 + C_K (S_L)^{-3/2} (\tilde{\varepsilon}\delta_{th})^{1/2}}} \tag{2.68}$$

with B_{T_2} and C_K are the model parameters of order unity (Chakraborty and Swaminathan, 2010):

$$Ka_L \approx C_K \frac{(\tilde{\varepsilon}\delta_{th})^{1/2}}{(S_L)^{3/2}} \tag{2.69}$$

Review modelling of scalar-turbulence interaction term, T_3

The modelling of term T_3 is usually divided into the modelling of the three components T_{31}, T_{32} and T_{33} separately (Mantel and Borghi, 1994; Swaminathan and Bray, 2005) Equation (2.52) indicates that T_{32} is expected to be the dominant contributor to T_3 for high turbulent Reynolds number Re_t turbulent premixed flames, whereas eq. (2.47) further indicates that for low Damköhler number combustion ($Da < 1$) T_{31} and T_{33} are likely to be of the same order of magnitude as that of T_{32} which has been confirmed in DNS

assessments, where contributions of T_{31} and T_{33} to T_3 have been found to play important roles (Chakraborty and Swaminathan, 2010; 2013).

The statistical behaviour of T_3 and its components can be explained by expressing the scalar-turbulence interaction contribution $\Lambda = -\overline{2\rho D \frac{\partial c}{\partial x_i}\frac{\partial u_i}{\partial x_j}\frac{\partial c}{\partial x_j}}$ in the following manner (Swaminathan and Bray, 2005; Chakraborty *et al.*, 2008):

$$\begin{aligned}\Lambda &= -\overline{2\rho D \frac{\partial c}{\partial x_i}\frac{\partial u_i}{\partial x_j}\frac{\partial c}{\partial x_j}} = -2\overline{\rho(e_\alpha \cos^2\theta_\alpha + e_\beta \cos^2\theta_\beta + e_\gamma \cos^2\theta_\gamma)N_c} \\ &= T_{31} + T_{32} + T_{33} - 2\overline{\rho D}\frac{\partial \tilde{c}}{\partial x_i}\frac{\partial \tilde{u}_i}{\partial x_j}\frac{\partial \tilde{c}}{\partial x_j}\end{aligned} \tag{2.70}$$

where e_α, e_β and e_γ are the most extensive, intermediate and most compressive principal strain rates with $\theta_\alpha, \theta_\beta$ and θ_γ being the angles between ∇c and e_α, e_β and e_γ respectively. Equation (2.70) indicates that the statistical behaviour of T_{32} is principally determined by the alignment of ∇c with the local principal strain rates. A preferential alignment of ∇c with e_α leads to a negative contribution of Λ and T_{32}, which is expected to happen for high values of Da, where the strain rate induced by flame normal acceleration dominates over turbulent straining effects. On the other hand in low Da combustion the turbulent straining is expected to overcome the heat release effects and thus the scalar gradient ∇c tends to align with the most compressive principal strain rate e_γ (Ashurst *et al*., 1987; Batchelor, 1952), leading to a positive contribution of Λ and T_{32} (Swaminathan and Grout, 2006; Chekraborty *et al*., 2008; Chakraborty and Swaminathan, 2013)

Following the same scaling approach of Swaminathan and Bray (2005), $-2\overline{\rho D}\frac{\partial \tilde{c}}{\partial x_i}\frac{\partial \tilde{u}_i}{\partial x_j}\frac{\partial \tilde{c}}{\partial x_j}$ scales in the following manner:

$$-2\overline{\rho D}\frac{\partial \tilde{c}}{\partial x_i}\frac{\partial \tilde{u}_i}{\partial x_j}\frac{\partial \tilde{c}}{\partial x_j} \times \frac{\delta_{th}^2}{\rho_0 S_L^2} \sim O\left(\frac{U_{ref}}{S_L}\frac{1}{\mathrm{Re}_t^{3/2} Da^{3/2}}\right) \tag{2.71}$$

the contribution of $-2\overline{\rho D}(\partial\tilde{c}/\partial x_i)(\partial\tilde{u}_i/\partial x_j)(\partial\tilde{c}/\partial x_j)$ remains negligible in comparison to the contributions of T_{31}, T_{32} and T_{32}, and the contribution of T_{32} remains the major contributor to Λ. The above discussion suggests that the modelling for the components of T_3 should be proposed in such a manner that they can address the alignment of ∇c with local strain rate. Various of models have been proposed for T_{31}, T_{32} and T_{33} by different researchers (Mantel and Borghi, 1990; Chakraborty and Swaminathan, 2007a, 2010; Mura *et al.*, 2009; Mura *et al*., 2009). The existing models for T_{31}, T_{32} and T_{33} are summarised in Tables 2.1, 2.2 and 2.3 respectively. The models for T_{31}, T_{32} and T_{33} proposed by Mantel and Borghi (1994) are referred to as the T31-MB, T32-MB and T33-MB models. Another series of models for T_{31}, T_{32} and T_{33} has been proposed (Mura *et al.*, 2008, 2009). However, different modelling suggestions for the same component of T_3 were made at the same time, therefore the models are named as: T31-M1 and T31-M2 for T_{31} modelling (Mura et al., 2009), T32-M1 and T32-M2 for T_{32} modelling (Mura et al., 2008), T33-M1, T33-M2 and T33-M3 for T_{33} modelling (Mura et al., 2009). Independently, an alternative set of the models for T_{31}, T_{32} and T_{33} was proposed later by Chakraborty and Swaminathan (2007) and these models were subsequently modified to account for different values of Re_t, Le and τ (Chakraborty and Swaminathan, 2010, 2013). The latest version of the models by Chakraborty and Swaminathan (2013) are referred to T31-CS, T32-CS and T33-CS models here.

Model names	**Model expression**
T31-MB	$T_{31} = -\overline{\rho u_j'' c''}\left(\frac{\partial\tilde{c}}{\partial x_j}\right)\left(\frac{\tilde{\varepsilon}}{\tilde{k}}\right)$
T31-M1	$T_{31} = -\bar{\rho}\frac{\tilde{\varepsilon}_c}{c''^2}\widetilde{u_j'' c''}\frac{\partial\tilde{c}}{\partial x_j}$
T31-M2	$T_{31} = -\tau.S_L\bar{\rho}\tilde{\varepsilon}_c < \vec{n}_f.\vec{x}_j > \frac{\partial\tilde{c}}{\partial x_j}$ where $\vec{n}_f = \nabla c/\lvert\nabla c\rvert$ is a local flamelet normal vector
T31-CS-R2	$T_{31} = -\left[C_1 + C_2 \mathrm{Da}_\mathrm{L}^*\right]\bar{\rho}\left(\frac{\tilde{\varepsilon}}{\tilde{k}}\right)\widetilde{u_j'' c''}\left(\frac{\partial\tilde{c}}{\partial x_j}\right) - C_3\tau.S_L\bar{\rho}\tilde{\varepsilon}_c < \vec{n}_f.\vec{x}_j > \frac{\partial\tilde{c}}{\partial x_j}\tilde{c}^{1.5}$ with C_1=0.5 ; $C_2 = \frac{0.4\,Ka_L^2}{(1+Ka_L)^2}$ and $C_3 = \frac{1.2+0.6erfc(\mathrm{Re}_L/5)}{1+\exp[-10(Ka_L-1)]}$

Table 2.1: Summary of the existing models for T_{31}

Model name	**Model expression**
T32-MB	$T_{32} = A_e\left(\frac{\tilde{\varepsilon}}{\tilde{k}}\right)\bar{\rho}\tilde{\varepsilon}_c$ where $A_e = 0.9$
T32-M1	$T_{32} = \bar{\rho}[\frac{\tilde{\varepsilon}}{\tilde{k}} - 1.2\tau.\mathrm{Da}_\mathrm{L}\tilde{\varepsilon}_c]\tilde{\varepsilon}_c$
T32-M2	$T_{32} = \bar{\rho}[\frac{\tilde{\varepsilon}}{\tilde{k}} - 3.2\ln(\tau+1).\mathrm{Da}_\mathrm{L}\tilde{\varepsilon}_c]\ \tilde{\varepsilon}_c$
T32-CS-R1	$T_{32} = \left[\underbrace{1.0 + 2.0erf\left(\frac{\mathrm{Re}_L+1}{5}\right)}_{C_3^*} - \underbrace{\frac{1}{(1+Ka_L)^{\zeta}}}_{C_4^*}\frac{(1-\tilde{c})^{\Phi}}{Le^{2.57}}\tau\mathrm{Da}_\mathrm{L}^*\right]\left(\frac{\tilde{\varepsilon}}{\tilde{k}}\right)\bar{\rho}\tilde{\varepsilon}_c$ where $\zeta = 0.4 + 0.15erf\left(\frac{\mathrm{Re}_L+1}{80}\right)$

Table 2.2: Summary of the existing models for T_{32}

Model name	**Model expression**
T33-MB	$T_{33} = -\bar{\rho}\tilde{\varepsilon}_c\left(\frac{\widetilde{u_j''u_k''}}{\tilde{k}}\right)\left(\frac{\partial\tilde{u}_j}{\partial x_k}\right)$
T33-CS	$T_{33} = -\bar{\rho}\tilde{\varepsilon}_c(1+1.2Ka_L^{-0.23})\left[\psi_i\psi_j + \frac{1}{3}\delta_{ij}(1-\psi_k\psi_k)\right]\frac{\partial\tilde{u}_i}{\partial x_j}$ where $\psi_i = \left(-\frac{\partial\varphi}{\partial x_i}\right)\sqrt{\frac{\rho_0 D_0}{\bar{\rho}\tilde{\varepsilon}_c}}$; $\varphi = \frac{\tau}{1+\tau\tilde{c}}\tilde{c}(1-\tilde{c})$ and D_0 is the unburned gas diffusivity
T33-M1	$T_{33} = -\frac{2}{3}\bar{\rho}\tilde{\varepsilon}_c\frac{\partial\tilde{u}_i}{\partial x_i}$
T33-M2	$T_{33} = -2\bar{\rho}\tilde{\varepsilon}_c^{\,2}\frac{\overline{\rho u_i''c''}.\overline{\rho u_j''c''}}{\tilde{\varepsilon}.(\overline{\rho c''^2})^2}.\frac{\partial\tilde{u}_i}{\partial x_j}$
T33-M3	$T_{33} = -2\bar{\rho}\tilde{\varepsilon}_c^{\,2}(\tau.S_L)^2\frac{<\vec{n}_f.\vec{x}_i><\vec{n}_f.\vec{x}_j>}{\tilde{\varepsilon}.}\frac{\partial\tilde{u}_i}{\partial x_j}$ where $\vec{n}_f = \nabla c/\lvert\nabla c\rvert$ is a local flamelet normal vector

Table 2.3: Summary of the existing models for T_{33}

Review modelling of the combined reaction rate and molecular dissipation terms (T_4- D_2)

Based on the transport equation of N_c as (Chakraborty *et al.*, 2008):

$$\rho\frac{\partial N_c}{\partial t}+\rho u_j\frac{\partial N_c}{\partial x_j}=-2\rho D\frac{\partial c}{\partial x_j}\frac{\partial c}{\partial x_i}\frac{\partial u_i}{\partial x_j}+2\rho S_d\frac{\partial n_i}{\partial x_i}N_c-2D\frac{\partial(\rho S_d n_i|\nabla c|)}{\partial x_i}|\nabla c| + 2S_d n_i\frac{\partial\rho}{\partial x_i}N_c+\rho|\nabla c|^2\left(\frac{\partial D}{\partial t}+u_j\frac{\partial D}{\partial x_j}\right) \tag{2.72}$$

where $\vec{n}=-\nabla c/|\nabla c|$ is the local flame normal vector and $S_d\equiv\left[\dot{w}+\nabla.(\rho D\nabla c)\right]/\rho|\nabla c|$ is the local flame displacement speed (Swaminathan and Bilger, 2001). Subsequently, the combined contribution of the terms D_1, T_4, $f(D)$ and $(-D_2)$ can be expressed as (Mantel & Borghi, 1994; Mura & Borghi, 2003; Swaminathan and Bray, 2005; Chakraborty et al., 2008; Gao et al. , 2014):

$$\begin{aligned}D_1+T_4-D_2+f(D)\approx&-2\overline{D\nabla.(\rho S_d\vec{n}|\nabla c|)|\nabla c|}+2\widetilde{D}\nabla.(\overline{\rho S_d|\nabla c|}\vec{m})\overline{|\nabla c|}\\&+2\overline{\rho D(S_r+S_n)\nabla.\vec{n}|\nabla c|^2}-2\widetilde{D}\overline{\rho(S_r+S_n)}\nabla.\vec{m}\overline{|\nabla c|}\\&-2\overline{\rho D^2(\nabla.\vec{n})^2|\nabla c|^2}+2\widetilde{D}\overline{\rho D(\nabla.\vec{n})|\nabla c|}\nabla.\vec{m}\overline{|\nabla c|}\end{aligned} \tag{2.73}$$

where $\vec{m}=-\nabla\tilde{c}/\overline{|\nabla c|}$ is the resolved flame normal and $S_r=\dot{w}/\rho|\nabla c|$, $S_n=\vec{N}\cdot\nabla(\rho D\vec{N}\cdot\nabla c)/\rho|\nabla c|$ are the reaction and normal diffusion components of the displacement speed respectively (Peters *et al*., 1998; Echekki and Chen, 1999; Swaminathan and Bilger, 2001). Equation (2.73) indicates that the the net contribution of $[D_1+T_4-D_2+f(D)]$ originates due to flame normal propagation and flame curvature. It worth noting that *f*(*D*) was assumed to be negligible in RANS in most of previous studies. Mantel and Borghi (1994) proposed a model for the net contribution of $T_4^*=(T_4+D_1-D_2)$ in the following manner:

$$T_4^*=T_4+D_1-D_2=-\frac{2}{3}\beta_1\overline{\rho}\frac{\widetilde{\varepsilon}_c^{\,2}}{\widetilde{c}(1-\widetilde{c})}\left[\frac{3}{2}-C_{\varepsilon_c}\frac{S_L}{\sqrt{\widetilde{k}}}\right] \tag{2.74}$$

where β_1 = 4.2 and $C_{\varepsilon_c}=0.1$ are model constants. The molecular diffusion term D_1 is a closed term and its magnitude is likely to be small for large Reynolds number Re_t flames according to the following scaling estimates (Swaminathan and Bray, 2005):

$$D_1\sim\frac{\rho_0 S_L^2}{\delta_{th}^2}\times\frac{1}{Da\times Re_t} \tag{2.75}$$

A similar conclusion can be reached using the scaling estimate (Mantel and Borghi, 1994):

$$D_1 \sim \frac{\rho_0 u'^2}{l^2} \times \frac{1}{Re_t} \tag{2.76}$$

As D_1 is a closed term and assumes negligible value for high Re_t flows, a model for $(T_4 - D_2)$ was proposed as (Chakraborty et al., 2008):

$$(T_4 - D_2) = -\beta_2 \bar{\rho} \frac{\tilde{\varepsilon}_c^{\,2}}{\tilde{c}(1-\tilde{c})} \tag{2.77}$$

where $\beta_2 = 6.7$ is the model parameter, which has been modified subsequently for a wide range of values of turbulent Reynolds number as: $\beta_2 = 3.9 + 2.8 erf(\mathrm{Re}_L/10)$ (Chakraborty and Swaminathan, 2013).

2.2.3 Review on algebraic closures of SDR in RANS

An algebraic closure of $\widetilde{\varepsilon_c}$ may be developed for turbulent premixed flames by assuming the leading order unclosed source and sink terms of the SDR transport equation (Mantel and Borghi, 1994; Mura and Borghi, 2003; Swaminathan and Bray, 2005; Kolla *et al*. 2009). Based on the above assumption, an algebraic model was initially proposed by Mantel and Borghi (1994) following the BML approach (eq. (2.36)) as:

$$\widetilde{\varepsilon_c} = \left(1 + \frac{2C_{\varepsilon_c} S_L}{3\sqrt{\tilde{k}}}\right)\left(C_D \frac{\tilde{\varepsilon}}{\tilde{k}}\right)\widetilde{c''^2} \text{ with } C_{\varepsilon_c} = 0.1;\ C_D = 0.21 \tag{2.78}$$

It worth noting that the analysis by Mantel and Borghi (1994) was carried out for constant density flow and thus the contribution of the dilatation term T_2 was not included in eq. (2.78). Swaminathan and Bray (2005) revised the model by Mantel and Borghi (1994) to take into the effects of T_2 in the below manner:

$$\widetilde{\varepsilon_c} = \left(1 + \frac{2C_{\varepsilon_c} S_L}{3\sqrt{\tilde{k}}}\right)\left(C_{D_c} \frac{S_L}{\delta_L} + C_D \frac{\tilde{\varepsilon}}{\tilde{k}}\right)\widetilde{c''^2} \text{ with } C_{D_c} \propto \frac{K_c}{2c_m - 1} \tag{2.79}$$

The model parameter C_{D_c} was suggested to be 0.24 (Swaminathan and Bray, 2005). It worth noting that the alignment between the scalar gradient with the compressive principal strain rates was implicitly considered in eq. (2.79). Subsequently, an algebraic model was proposed by Kolla *et al*. (2009) where the effects of *Da* and τ on ∇c alignment are explicitly taken into account:

$$\widetilde{\varepsilon_c} \simeq \frac{1}{\beta'}\left(2K_c^* \frac{S_L}{\delta_{th}} + [C_3 - \tau C_4 Da_L]\frac{\tilde{\varepsilon}}{\tilde{k}}\right)\widetilde{c''^2} \tag{2.80}$$

where model parameters are given as:

$$C_3 = \frac{1.5\sqrt{Ka_L}}{1+\sqrt{Ka_L}}, C_4 = \frac{1.1}{(1+Ka_L)^{0.4}} \text{ and } \beta' = 6.7 \tag{2.81}$$

Further refinements of this model have been attempted to capture the differential diffusion effects due to non-unity Lewis number *Le* (Chakraborty and Swaminathan, 2010). Lewis number *Le* is defined as the ratio of thermal diffusivity α_T to mass diffusivity D. For $Le = 1.0$, heat and mass diffuse at the same rate. Differential diffusion of heat and mass occurs for $Le \neq 1.0$ (Chakraborty and Swaminathan, 2010). By including the non-unity *Le* effects in the modelling of the leading order terms of the SDR $\widetilde{\varepsilon_c}$ transport equation, eq. (2.80) has been revised in the following form (Chakraborty and Swaminathan, 2010):

$$\widetilde{\varepsilon_c} = \left(2\frac{K_c^*}{Le^{1.88}}\frac{S_L}{\delta_{th}} + \frac{2.0\sqrt{Ka_L}}{1+\sqrt{Ka_L}}\frac{\tilde{\varepsilon}}{\tilde{k}} - \tau\frac{1.2(1-\tilde{c})^{\Phi}}{(1+Ka_L)^{0.4}Le^{2.57}}Da_L\frac{\tilde{\varepsilon}}{\tilde{k}}\right)\frac{\tilde{c}(1-\tilde{c})}{\beta'} \tag{2.82}$$

where $\Phi = 0.2 + 1.5|1 - Le|$. Another model of $\widetilde{\varepsilon_c}$ was proposed by Vervisch *et al*. (2004) in terms of the flame wrinkling factor $\Xi = \overline{|\nabla c|}/|\nabla \bar{c}|$ as:

$$\widetilde{\varepsilon_c} = \frac{(2c_m - 1)}{2\bar{\rho}}\rho_0 S_L \Xi |\nabla \bar{c}| \frac{\widetilde{c''^2}}{\tilde{c}(1-\tilde{c})} \tag{2.83}$$

Mura *et al*. (2007) proposed an alternative model by linking the scalar dissipation rate for turbulent premixed flames for the thin flamelet and thickened flame regimes which reads:

$$\widetilde{\varepsilon_c} = g\left(-\frac{\overline{\rho D}}{\bar{\rho}}\nabla\tilde{c}.\nabla\tilde{c} + \frac{\bar{\dot{w}}}{2\bar{\rho}}[2\tilde{c}-1] + \frac{1}{\bar{\rho}}[\overline{\dot{w}c} - \bar{\dot{w}}\tilde{c}]\right) + (1-g)C_Y\frac{\tilde{\varepsilon}}{\tilde{k}}\widetilde{c''^2} \quad (2.84)$$

The C_Y is the model parameter and g is the segregation factor defined as:

$$g = \frac{\widetilde{c''^2}}{\tilde{c}(1-\tilde{c})} \quad (2.85)$$

The segregation factor g assumes a value equal to unity in the strict thin flamelet regime where the pdf of c can be approximated by a bimodal distribution with impulses at $c = 0$ and $c = 1$. This yields:

$$\widetilde{c''^2} = \tilde{c}(1-\tilde{c}) \quad (2.86)$$

However $\tilde{c}(1-\tilde{c})$ is the maximum possible value of $\widetilde{c''^2}$ and $\widetilde{c''^2}$ decreases in comparison to $\tilde{c}(1-\tilde{c})$ with decreasing *Da* as the underlying combustion shows the attributes of the thicken flames regimes.

2.3 Other modelling approaches for turbulent premixed combustion

2.3.1 G-equation Level Set Approach

Williams (1985) introduced the *G*-equation (i.e. level-set approach) concept which was further developed by Peters (2000) later. This approach approximates the assumed thin flame surface with a level surface of scalar field *G*. The scalar *G* assumes a given level G_0 at the flame front and the balance equation of *G* is proposed in the following form:

$$\frac{\partial G}{\partial t} + \vec{u}.\nabla G = S_d\left|\nabla G\right| \quad (2.87)$$

Due to the lack of specific definition of *G*, it is often taken as the distance of a certain isosurface of *G* from the flame surface in the local flame normal direction. Therefore the eq. (2.36) describe the advection and propagation of this isosurface with respect to the flame surface. It has been argued that rather than taking *G* equation approach as an explicit model of turbulent premixed combustion, it may be of more physical to treat it as a mathematical framework for modelling (Cant, 2011), which provides a novel perspective to describe the premixed turbulent combustion. In the context of RANS and

LES modelling, the Favre averaged balance equation can be obtained by substituting $G = \tilde{G} + G''$ into eq. (2.87):

$$\bar{\rho}\frac{\partial \tilde{G}}{\partial t} + \bar{\rho}\tilde{u}_j \frac{\partial \tilde{G}}{\partial x_j} = \overline{\rho S_d \left|\nabla G\right|} - \overline{\nabla.(\rho u'' G'')} \tag{2.88}$$

where the first term on the RHS denotes the flame front propagation and the second term presents the turbulent flux of *G*. It worth noting that the diffusion effects was not taken into consideration in *G*-equation approach as the framework relies on kinematic description of the flame front. The first unclosed terms on the RHS of eq. (2.88) have been modelled as:

$$\overline{\rho S_d \left|\nabla G\right|} = \rho_0 S_T \left|\nabla \tilde{G}\right| \tag{2.89}$$

where S_T the turbulent burning velocity henceforth $\rho_0 S_T$ denotes the mass flow across the flame brush and the G flux terms can be modelled according to gradient hypothesis as (Chakraborty *et al*., 2011a):

$$\overline{\nabla.(\rho u'' G'')} = -\nabla.(\bar{\rho} D_T \nabla \tilde{G}) \tag{2.90}$$

where D_T reads the diffusivity of *G*. The RHS of eq. (2.90) was further deducted (Peters, 2000) by only keeping the tangential components, which leads to the well-known Favre averaged form of the G-equation:

$$\bar{\rho}\frac{\partial \tilde{G}}{\partial t} + \bar{\rho}\tilde{u}_j \frac{\partial \tilde{G}}{\partial x_j} = \rho_0 S_T \left|\nabla \tilde{G}\right| - \bar{\rho} D_t \tilde{\kappa} \left|\nabla \tilde{G}\right| \tag{2.91}$$

where $\tilde{\kappa} = \nabla.(-\nabla \tilde{G} / \left|\nabla \tilde{G}\right|)$ is the Favre averaged curvature. The turbulent flame speed is modelled in terms of laminar flame speed in the following manner (Abdel-Gayed *et al*., 1984; Gulder, 1990; Yakhot *et al*., 1992; Pocheau, 1994):

$$\frac{S_T}{S_L} = 1 + A\left(\frac{u'}{S_L}\right)^n \tag{2.92}$$

where both *A* and *n* denote constants. Peters (2000) also derived the transport equation of the variance $\widetilde{G''^2}$, which can be taken as a measure of the flame brush thickness. *G* equation has been of practical interest in RANS modelling (Peters, 2000), which has been recently extended to LES (Kim, 1999; Pitsch, 2002; Oberlack, 2001). A new mathematical description was presented recently (Pitsch, 2005, 2006) for which the *G* equation does not require filtering in LES, which is beyond the scope of this document, interest readers are referred to the papers.

2.3.2 Artificially Thickened Flame

Artificially thickened flame (ATF) approach was initially proposed in purpose of thickening the reaction zone for adequate flame resolution with limited computational power (Butler and O'Rourke, 1977) without compromising the flame speed characteristics. As the turbulent premixed flame brush is expected to be thickened by LES filtering, the ATF concepts have been revisited and adopted into LES of turbulent premixed combustion by Veynante and Poinsot (1997).

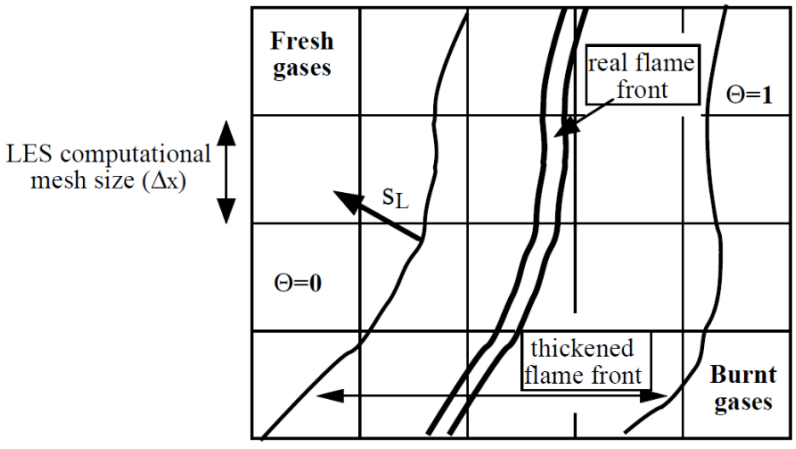

Figure 2.2: Schematic diagram of thickened flame approach (Poinsot and Veynante, 2001).

Following the theories of laminar premixed flame (Williams, 1985; Kuo, 1986), the flame speed and the Zel'dovich flame thickness can be expressed as:

$$S_L \propto \sqrt{\alpha_T B} \quad \text{and} \quad \delta_L \propto \frac{\alpha_T}{S_L} = \sqrt{\frac{\alpha_T}{B}} \tag{2.93}$$

where *B* denotes the pre-exponential factor of single step Arrhenius law of normalised form of chemical reaction $\dot{w}$. By simultaneously increasing the thermal diffusivity α_T and decreasing B with a same factor *F*, the flame speed is conserved while the flame thickness has been increased by factor *F*, therefore it is possible to thicken the flame front to scales which can be more easily resolvable on LES grids. A schematic diagram is shown in Fig. 2.2 to demonstrate the thickening of the flame brush.

This method shows advantages in dealing with ignition, flame stabilisation and flame/wall interactions where flame-turbulence interaction is mainly determined by large scales. The balance equation of a single step Arrhenius chemistry, the balance equation for reaction progress variable *c* reads:

$$\frac{\partial(\rho c)}{\partial t}+\frac{\partial(\rho u_j c)}{\partial x_j}=\frac{\partial}{\partial x_j}\left[\rho D\frac{\partial c}{\partial x_j}\right]+B(1-c)\exp\left[\frac{-\beta(1-T)}{1-\alpha(1-T)}\right] \tag{2.95}$$

which will be modified in ATF approach into the following form:

$$\frac{\partial(\rho c)}{\partial t}+\frac{\partial(\rho u_j c)}{\partial x_j}=\frac{\partial}{\partial x_j}\left[\rho DF\frac{\partial c}{\partial x_j}\right]+\frac{1}{F}\rho B(1-c)\exp\left[\frac{-\beta(1-T)}{1-\alpha(1-T)}\right] \tag{2.96}$$

The two terms on the RHS of eq. (2.95) have been recast into the form of eq. (2.96) which model the conventional unclosed terms arising from the sub-grid flux and reaction rate implicitly. The thickening of the flame brush leading to an increase in the flame time scale, which subsequently decreases Damköhler number *Da* by the same factor *F* (i.e. *Da*/*F*). and the ratio between integral length scale *l* and laminar flame thickness δ_{th} also decreases by a factor of *F*. Therefore the flame brush is expected to lose partial sensitivity to turbulent motions. This brings an interesting comparison between the conventional LES filtering and ATF approach. The response of flame to sub-grid turbulent motions is dealt with by additional unclosed terms in the filtered transport equation of a general progress variable. The filtering operation is mimicked by broadening the reaction zone where the flame stretch requires to be handled in the latter, which has been attempted by introducing an efficiency function *E* (Poinsot et al., 1991; Angelberger et al., 1998). An obvious link can be observed between the above treatments with a RANS approach of turbulent strain rate, known as intermittent turbulent net flame stretch (ITNFS) method

(Meneveau and Poinsot,1991). The efficiency function *E* builds a link between the actual flame wrinkling with the thickened flame wrinkling. The efficiency function is implemented by modifying the diffusivity *D* and the pre-exponential factor *B* in eq. (2.96) as follows:

$$\frac{\partial(\rho c)}{\partial t}+\frac{\partial(\rho u_j c)}{\partial x_j}=\frac{\partial}{\partial x_j}\left[EF\rho D\frac{\partial c}{\partial x_j}\right]+\frac{E}{F}\rho B^{*}(1-c)\exp\left[\frac{-\beta(1-T)}{1-\alpha(1-T)}\right] \tag{2.96}$$

An inequality condition between the thickening factor F and the efficiency factor E was proposed by Colin *et al*. (2000) based on an analysis involving flame wrinkling factor:

$$1\le E\le F^{2/3} \tag{2.98}$$

2.3.3 Probability density function Approach

If the joint probability density functions (pdf) of all the thermochemical quantities in turbulent premixed flames are known, the mean reaction rate can be directly calculated based on the conditional probability transport equations, which is a central motivation behind the transported pdf approach. A modelled transport equation for the conditional pdfs of the thermochemical scalars in turbulent reacting flows was derived by Dopazo and O'Brien (1974) for the first time based on a presumed pdf shape of thermochemical quantities, usually known as 'presumed pdf approach'. The mostly adopted shape of the presumed pdf is the β function, which is able to change from shape of a mono-modal distribution to a Gaussian distribution. The β function in terms of *c* in range of $0<c<1$ is given by:

$$\tilde{p}(c)=\frac{1}{B(a,b)}c^{a-1}(1-c)^{b-1}=\frac{\Gamma(a+b)}{\Gamma(a)\Gamma(b)}c^{a-1}(1-c)^{b-1} \tag{2.99}$$

where $B(a,b)=\int_0^1 c^{a-1}(1-c)^{b-1}dc$ is a normalisation factor and $\Gamma(x)=\int_0^\infty e^{-t}t^{x-1}dt$.

Two model parameters are evaluated based on *c* and $\widetilde{c''^2}$ as:

$$a=\tilde{c}\left[\frac{\bar{\rho}\tilde{c}(1-\tilde{c})}{\overline{\rho c''^2}}-1\right];\ b=\frac{a}{\tilde{c}}-a \tag{2.100}$$

A limitation of the presumed pdf is the lack of information for unburnt ($c=0$) and fully burnt gas ($c=1$). The transport equation of the scalar variance $\widetilde{c''^2}$ (i.e. eq. (2.32) also requires closure in simulations, which has been looked into by previous studies (Chakraborty et al, 2010) in the context of RANS.

An alternative pdf approach focuses on solving the pdf transport equation, which was proposed firstly through the investigation of the link between the particle transport models and the pdf description (Pope, 1979) and commonly known as the 'pdf transport approach'. An advantage of the pdf transport equation is the incorporation of multi-variables (species, mass, temperature, velocities etc.) by their joint probabilities. The pdf considered in this approach is a one-point, one-time of the velocity vectors $\boldsymbol{u}$, composition variable $\boldsymbol{N}_\Phi$ and a turbulent frequency $\boldsymbol{\omega}$ (Haworth, 2010). The composition variable $\boldsymbol{N}_\Phi$ denotes a finite number of variables sufficient to describe the thermochemical properties. The Favre average pdf is denoted as $\tilde{f}_{\boldsymbol{uN_\Phi\omega}}(\boldsymbol{V},\boldsymbol{\psi},\boldsymbol{\theta};\boldsymbol{x},t)$, where $\boldsymbol{V},\boldsymbol{\psi},\boldsymbol{\theta}$ denotes the corresponding variables related to $\boldsymbol{u}$, $\boldsymbol{N}_\Phi$ and $\boldsymbol{\omega}$ respectively. By integration of $\tilde{f}_{\boldsymbol{uN_\Phi\omega}}(\boldsymbol{V},\boldsymbol{\psi},\boldsymbol{\theta};\boldsymbol{x},t)$ over the sample space the complete statistical information of velocity, composition and turbulent frequency at a given point can be obtained for a given instance of time. Therefore, the mean chemical reaction rate is a closed term and can be deterministically evaluated using $\tilde{f}_{\boldsymbol{uN_\Phi\omega}}(\boldsymbol{V},\boldsymbol{\psi},\boldsymbol{\theta};\boldsymbol{x},t)$ which is the most important advantage of the pdf transport approach. Meanwhile, one of the central challenges of this approach is the model to characteristic rate of micro-mixing, which is represented by the SDR in the pdf transport approach. The most popular models of SDR for the pdf transport approach are IEM (Villermaux and Devillon, 1975), variants of Curl's model (Curl, 1963; Spielman et al., 1965) and the Euclidean minimum spanning tree model (Subramaniam and Pope, 1998). For premixed combustion with high Damköhler number, a mixing closure was proposed by Lindstedt and Vaos (2006).

The numerical simulations of the pdf transport approach has been developed extensively in the last decade. A hybrid Lagrangian particle/Eulerian mesh (LPEM) algorithm is the most widely adopted pdf methodology in turbulent steady flow simulations (Anand et al., 1989).

2.3.4 Dynamic modelling approach

The dynamic approach was initially proposed to model the turbulent residual Reynolds stresses for passive turbulent flows based on the scale similarity assumption (Bardina et al., 1981). Later the scalar similarity assumption was extended to model the filtered reaction rate (Germano et al., 1997), however, a model parameter is required to be specified. Dynamic modelling of unresolved stresses therefore was motivated by the fact the model parameters are directly evaluated based on the resolved quantities automatically. A review of the dynamic model of unresolved stresses in LES can be found somewhere else (Sarghini et al., 1999). However, modelling of filtered reaction rate in LES using dynamic approach is not very straight-forward. A Germano-identity like procedure was adopted to model the reaction rate after introducing an exponential dependence for filtered reaction rate (Charlette et al., 2002) as:

$$\bar{\dot{w}} = \dot{w}(\tilde{Q}, \bar{\Delta})[1 + f(u'_{\bar{\Delta}}, \dots)]^{\alpha_c} \tag{2.101}$$

where $\dot{w}(\tilde{Q}, \bar{\Delta})$ is referred as 'resolved' reaction rate which was calculated based on the known resolved quantities $\tilde{Q}$ (including temperature, species mass fraction) and the filter width $\bar{\Delta}$. Thus $\dot{w}(\tilde{Q}, \bar{\Delta}) \neq \bar{\dot{w}}$ and $f(u'_{\bar{\Delta}}, \dots)$ denotes a certain function which ensures $\dot{w}(\tilde{Q}, \bar{\Delta}) f(u'_{\bar{\Delta}}, \dots)$ can be a closure of $\bar{\dot{w}}$. The Germano-like identity then can be recast into the following form (Germano et al., 1997):

$$\widehat{\dot{w}(Q, \Delta)[1 + f(u'_{\bar{\Delta}}, \dots)]^{\alpha_c}} = \dot{w}(\hat{\tilde{Q}}, \hat{\Delta})[1 + f(u'_{\hat{\Delta}}, \dots)]^{\alpha_c} \tag{2.102}$$

where the $\hat{\tilde{Q}}$ denotes the filtered quantity based on a test filter width $\hat{\Delta}$, which is larger than original filter size Δ. Therefore the model parameter α_c can be deduced from eq. (2.102) by taking the logarithm function of both sides simultaneously as:

$$\alpha_c = \frac{log\left[\widehat{\dot{w}(Q, \Delta)} / \dot{w}(\hat{\tilde{Q}}, \hat{\Delta})\right]}{log[(1 + f(u'_{\hat{\Delta}}, \dots))/1 + f(u'_{\bar{\Delta}}, \dots)]} \tag{2.103}$$

2.3.5 Conditional Moment Closure (CMC) Approach

Conditional moment Closure (CMC) was originally proposed for non-premixed flames (Klimenko, 1990; Bilger, 1993) based on the correlation between mixture fraction and the reactive scalar species which links the fluctuations in both scalar space and mixture fraction space. A comprehensive review of CMC approach for non-premixed flames can be found in Klimenko and Bilger (1999) and the recent development has been reviewed by Kronenburg and Mastorakos (2011). The CMC shares some similarities with the flamelet assumption in premixed combustion by assuming that the fluctuations of the reactive scalars are well correlated with the fluctuations of one sole quantity: reaction progress variable in premixed flames. The global averaged quantity can be expressed in terms of conditional mean as:

$$\overline{Y(\vec{x},t)} = \int \langle Y|c=\zeta\rangle p(\zeta)\, d\zeta \tag{2.104}$$

where ζ denotes the sample space of progress variable c and $Q(\zeta,\vec{x},t) = \langle Y|c=\zeta\rangle$ is the conditional mean value of a reactive scalar Y with $\langle ... \rangle$ denoting ensemble averaging. A decomposition of the quantity $Y(\vec{x},t)$ reads $Y(\vec{x},t) = Q(\zeta,\vec{x},t) + y(\vec{x},t)$, where $y(\vec{x},t)$ denotes the conditional fluctuation. Subsequently, the transport equation of the conditional mean Q (Klimenko and Bilger, 1999; Swaminathan and Bilger, 2001) of reactive scalar Y_i is derived as:

$$\left\langle \rho|\zeta \right\rangle \frac{\partial Q_i}{\partial t} + \left\langle \rho u_i|\zeta \right\rangle \frac{\partial Q_i}{\partial x_i} = \left\langle \rho|\zeta \right\rangle \left\langle N_c|\zeta \right\rangle \frac{\partial^2 Q_i}{\partial \zeta^2} + \left\langle \dot{w}_i|\zeta \right\rangle - \left\langle \dot{w}|\zeta \right\rangle \frac{\partial Q_i}{\partial \zeta} + e_{Q_i} + e_{y_i} \tag{2.105}$$

where $\dot{w}_i$ is the generation rate of the scalar and e_{Q_i} denotes the contribution of molecular diffusion, e_{y_i} denotes the conditional transport of scalar fluctuation. The expressions of e_{Q_i} and e_{y_i} are (Swaminathan and Bilger, 2001):

$$\begin{aligned} e_{Q_i} &= \frac{\partial}{\partial x_i}\left(\rho D_i \frac{\partial Q_i}{\partial x_i} \right) + \left\langle \frac{\partial Q_i}{\partial \zeta} \frac{\partial}{\partial x_i}\left([1-Le_i]\rho D_i \frac{\partial c}{\partial x_i} \right) \middle| \zeta \right\rangle + \left\langle \rho D_i \frac{\partial c}{\partial x_i} \frac{\partial}{\partial x_i}\left(\frac{\partial Q_i}{\partial \zeta} \right) \middle| \zeta \right\rangle \\ e_{y_i} &= -\left\langle \rho \frac{\partial y_i}{\partial t} + \rho \vec{u}.\frac{\partial y_i}{\partial x_i} - \frac{\partial}{\partial x_i}\left(\rho D_i \frac{\partial y_i}{\partial x_i} \right) \middle| \zeta \right\rangle \end{aligned} \tag{2.106}$$

The terms of eq. (2.105) require modelling are: $e_{y_i}, \left\langle \rho u_i|\zeta \right\rangle, \left\langle \dot{w}_i|\zeta \right\rangle, \left\langle N_c|\zeta \right\rangle$. A model of e_{y_i} was proposed as (Klimenko and Bilger, 1999):

$$e_{y_i} \approx \frac{1}{\tilde{p}(\zeta)} \frac{\partial}{\partial x_i} \left(\left\langle \rho u_i'' y_i \middle| \zeta \right\rangle \tilde{p}(\zeta) \right) \tag{2.107}$$

where u_i'' is the conditional velocity fluctuation and $\tilde{p}(\zeta)$ is the Favre pdf of ζ. It worth noting that the terms $\left\langle \rho u_i'' y_i \middle| \zeta \right\rangle$ and $\tilde{p}(\zeta)$ require further closures. The modelling of $\left\langle \rho u_i \middle| \zeta \right\rangle$ was attempted (Swaminathan and Bilger, 2001) by a linear model which yields good agreement. Closures are required for the terms in eq. (2.105), among which $\left\langle \dot{w}_i \middle| \zeta \right\rangle$ can be addressed by first order Taylor series expansion (Klimenko and Bilger, 1999):

$$\left\langle \dot{w}_i(Y_1, ...Y_N, T) \middle| \zeta \right\rangle \approx \left\langle \dot{w}_i(Q_1, ...Q_N, Q_T) \middle| \zeta \right\rangle = \dot{w}_i(Q_1, ...Q_N, Q_T) \tag{2.108}$$

It has been reported that eq. (2.108) perform satisfactorily for major species whereas high fluctuations were observed for minor species (Swaminathan and Bilger, 2001). A key issue in CMC methodology is the modelling of conditional mean SDR $\left\langle N_c \middle| \zeta \right\rangle$ in eq. (2.105). Despite the advantage of validity of this method for both slow and fast chemistry, the computational cost of CMC is expected to be much higher than the flamelet approach, which may possibly be incorporated by the fast development of high performance computing.

2.4 Final Remarks

A review of the development of flamelet approach in turbulent premixed combustion has been provided, where the chemistry is assumed to occur within a thin region which propagates normal to itself towards the reactants in turbulent premixed flames. This approach is mostly widely used approach in the modelling of turbulent premixed flames. The scalar dissipation rate is found to have direct link to the reaction rate closure irrespective of the nature of chemical reaction as long as the flamelet assumption remains valid. The SDR determines the time scale for molecular mixing, which can be taken as a measure of reaction rate in the turbulent reacting flow where the heat release is strongly correlated with the molecular mixing process. A review of the SDR approach in turbulent premixed combustion modelling in RANS provides a useful theoretical ground and a modelling platform for SDR based closure in the context of LES, which is the central topic of this merit.

The application of popular modelling approaches for non-premixed flames (i.e. pdf transport approach, CMC approach) in turbulent premixed combustion have been discussed briefly. The advantage of transport pdf approach is it can be used irrespective of the magnitude of characteristic chemical time scales but at the expense of high computational cost and modelling of molecular micro-mixing. The CMC approach is another successful approach in non-premixed turbulent combustion modelling, which is in its infancy in modelling turbulent premixed combustion. A few unclosed terms require modelling as expected in the transport equation of conditional mean of a reactive scalar. However, the definition of the reference space, i.e. the reaction progress variable space, remain a key issue in CMC approach which inherently characterises the turbulent premixed combustion process by multiple reactive scalars. The higher computational cost of CMC than flamelet approach need to be accommodated as well.

Nevertheless, the SDR has been found to play a key role in closure of pdf transport and CMC approaches, which justifies the importance of modelling this quantity in turbulent premixed flames, using Direct Numerical Simulation data. In addition, both the quantitative and qualitative behaviours of SDR with respect to LES grid size/ filter widths are essential for adopting SDR approach into LES, which is becoming increasingly popular as a tool for designing next generation combustors by explicitly filtering the simulation results obtained from DNS with a range of different filter widths. The statistical behaviours of the Favre-filtered scalar dissipation rate for different LES filter widths will be analysed based on DNS data and scaling arguments in this merit. Both the algebraic closure of SDR and reaction rate and transported SDR closure for turbulent premixed combustion in the context of LES will be discussed in the remaining chapters of this thesis.

Chapter 3. Mathematical Background

In this chapter the important physical features and governing equations of premixed combustion for both laminar flow and turbulent flow are presented. The mathematical theory of reaction rate closure for turbulent premixed combustion in the context of LES is demonstrated. The derivations of transport equation of instantaneous, Favre filtered SDR and the resolved components of SDR are provided. The explicit filtering operations of the DNS results are presented with discussion of the numerical efficiency and accuracy of LES filtering.

3.1 Laminar premixed flames

Turbulent combustion is often categorised based on the extent of mixing of the reactants approaching the reaction zone. Premixed flames denotes the combustion process where the fuel and oxidizer are homogeneously mixed before entering the reaction zone. In premixed combustion the reaction zone tends to be a very thin surface, which separates the well-mixed reactants from fully-burnt products. The well mixed reactants are pre-heated by the intensive heat release from the chemical reaction taking place in the reaction zone. The temperature of the reactants increase during the preheating process, which triggers burning of preheated reactants as a continuous process. A schematic diagram of typical laminar premixed flame is shown below in Figure 3.1.

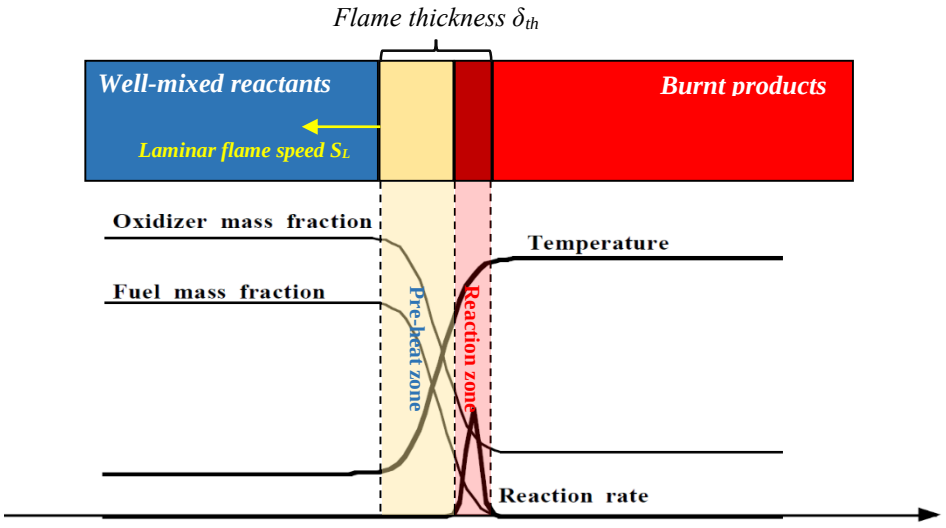

Figure 3.1: Schematic diagram of a one-dimensional laminar premixed flame

In Fig. 3.1, thermal flame thickness δ_{th} is defined based on temperature as (Williams, 1980):

$$\delta_{th} = \frac{(T_{ad} - T_0)}{\max\left|\nabla \hat{T}\right|_L} \tag{3.1}$$

where T_{ad}, T_0 and $\hat{T}$ denotes the adiabatic temperature, temperature of unburnt reactant and instantaneous temperature respectively. Figure 3.1 also shows that the sharp gradient of temperature occurs within the reaction zone, which will subsequently generate a strong thermal flux towards the fresh gases which heats up the cold fresh gases in the pre-heat zone. The flame thickness of this is typically 10 times of the reaction zone thickness δ_δ. In lean premixed combustion, the flame front propagates towards the unburnt reactants at a flame speed known as the laminar burning velocity S_L which is dependent on the initial temperature of the reactants, thermochemistry of the mixture and pressure.

A single-step irreversible Arrhenius chemical reaction can be generically presented as:

$$Reactants \rightarrow Products$$

and the premixed flame is often characterised by defining a reaction progress variable *c* in such a manner that $c = 0$ in the unburned gases and $c = 1$ in the fully burnt products and *c* increases monotonically from $c = 0$ to $c = 1$. This reaction progress can be defined based on mass fraction of a suitable reactant or product mass fraction (i.e. Y_R or Y_P) as:

$$c = \frac{Y_{R0} - Y_R}{Y_{R0} - Y_{R\infty}} \text{ or } c = \frac{Y_P - Y_{P0}}{Y_{P\infty} - Y_{P0}} \tag{3.2}$$

where 0, ∞ denotes the corresponding variable in unburnt fresh gases and fully burnt products respectively. For a single-step Arrhenius chemistry, the reaction rate is given by:

$$w = B^* \rho (1 - c) exp\left[\frac{-E}{R_0 \hat{T}}\right] \tag{3.3}$$

where B^* is the pre exponential factor and E is activation energy. A non-dimensional number characterising the ratio between the initial flow speed u_0 and sonic a_0 is known as Mach number $Ma = u_0/a_0$. As introduced in Chapter 2, for unity Lewis number *Le* flame, heat and mass diffuse at the same rate. For low Ma and unity *Le* flames, the reaction progress variable is equivalently defined based on temperature T in the following manner:

$$c = \frac{T - T_u}{T_b - T_u} \tag{3.4}$$

with T, T_u, T_b being the instantaneous , unburnt reactants' and burnt products' temperatures.

3.2 Governing Equations

The three dimensional compressible reactive flows are governed by a series of conservation equations. The dimensional form of these equations are shown below in Cartesian tensor notation.

- Mass conservation equation:

$$\frac{\partial \rho}{\partial t} + \frac{\partial}{\partial x_k}\left(\rho u_k\right) = 0 \tag{3.5}$$

where and ρ is the density, u_k is the k^{th} component of the velocity vector,

- Momentum conservation equation (Navier-Stockes equation):

$$\frac{\partial}{\partial t}\left(\rho u_i\right) + \frac{\partial}{\partial x_k}\left(\rho u_k u_i\right) = -\frac{\partial P}{\partial x_i} + \frac{\partial}{\partial x_k}\tau_{ki} \tag{3.6}$$

where P is the pressure and τ_{ki} is the viscous stress tensor, given by:

$$\tau_{ki} = \mu\left(\frac{\partial u_i}{\partial x_j} + \frac{\partial u_j}{\partial x_i}\right) - \frac{2}{3}\mu\frac{\partial u_k}{\partial x_k}\delta_{ij} \tag{3.7}$$

where μ is the kinematic viscosity.

- Species conservation equation of species α present in the reacting gas mixture:

$$\frac{\partial}{\partial t}\left(\rho Y_\alpha\right) + \frac{\partial}{\partial x_k}\left(\rho u_k Y_\alpha\right) = \dot{w}_\alpha - \frac{\partial}{\partial x_k}\left(\rho V_{\alpha,k} Y_\alpha\right) \text{ with } \alpha = 1,\ldots\ldots,N \tag{3.8}$$

where $V_{\alpha,k}$ is the diffusion velocity of species α, Y_α is the mass fraction of the species α in the reacting mixture where N is the total number of species, $\dot{w}_\alpha$ is the mass production of the species α by chemical reactions.

- Internal energy conservation equation:

$$\frac{\partial}{\partial t}(\rho E) + \frac{\partial}{\partial x_k}(\rho u_k E) = -\frac{\partial}{\partial x_k}(P u_k) + \frac{\partial}{\partial x_k}(\tau_{ki} u_i) - \frac{\partial}{\partial x_k} q_k \tag{3.9}$$

where the total specific internal energy is defined as:

$$E = C_V \hat{T} + \frac{1}{2} u_k u_k + \sum_{\alpha=1}^{N} h_\alpha^0 Y_\alpha \tag{3.10}$$

where C_V is the mixture heat capacity at constant volume. q_k in eq (3.9) is the heat flux vector, which is given by:

$$q_k = -\lambda \frac{\partial \hat{T}}{\partial x_k} + \rho \sum_{\alpha=1}^{N} h_\alpha V_{\alpha,k} Y_\alpha \tag{3.11}$$

where λ is thermal conductivity, $\hat{T}$ is the temperature, h_α is the enthalpy of the species α defined as:

$$h_\alpha = \int_{T_0}^{T} c_{p,\alpha} dT + h_\alpha^0 \tag{3.12}$$

where h_α^0 is the enthalpy of formation of species α. The thermal equation of state is given by the ideal gas law:

$$P = \rho R_0 \hat{T} \sum_{\alpha=1}^{N} \frac{Y_\alpha}{W_\alpha} \tag{3.13}$$

where R_0 is the universal gas constant and W_α is the molar mass of species α.

A reaction rate involving N species and M steps can be described in generic form as:

$$\sum_{\alpha=1}^{N} \nu'_{\alpha,m} M_\alpha \rightarrow \sum_{\alpha=1}^{N} \nu''_{\alpha,m} M_\alpha \text{ with } m = 1, \ldots, M \tag{3.14}$$

where m, $\nu''_{\alpha,m}, \nu'_{\alpha,m}$ are respectively the product and reactant stoichiometric coefficients. The chemical reaction rate of species α is given by:

$$\dot{w}_\alpha = W_\alpha \sum_{m=1}^{M} \left[(\nu''_{\alpha,m} - \nu'_{\alpha,m}) A_m \hat{T}^{n_m} \exp\left(\frac{-E_m}{R^0 \hat{T}} \right) \prod_{\beta=1}^{N} \left(\frac{\rho Y_\beta}{W_\beta} \right)^{\nu'_{\beta,m}} \right] \tag{3.15}$$

where A_m, n_m, E_m are respectively, the frequency factor, temperature exponent and activation energy. The compatibility conditions for species mass fraction, the diffusion velocities and reaction rates are respectively:

$$\sum_{\alpha=1}^{N} Y_\alpha = 1;\ \sum_{\alpha=1}^{N} V_{\alpha,k} Y_\alpha = 0 \text{ and } \sum_{\alpha=1}^{N} \dot{w}_\alpha = 0 \tag{3.16}$$

In current study, a single-step irreversible Arrhenius chemical reaction was assumed in all DNS datasets analysed here, where the simplified form of the equations of state become

$$P = \rho R \hat{T} \tag{3.17}$$

$$E = C_V \hat{T} + \frac{1}{2} u_k u_k + H(1-c) \tag{3.18}$$

where H is the heat of reaction per unit mass of reactants consumed.

- The simplified heat flux vector reads:

$$q_k = -\lambda \frac{\partial \hat{T}}{\partial x_k} + \rho D H \frac{\partial c}{\partial x_k} \tag{3.19}$$

- All the above governing equations can be non-dimensionalised based on a set of standard values of the principal variables including a reference velocity u_0 which is often taken as the laminar flame burning velocity S_L, a length scale l_0, a time scale $t_0 (= l_0 / u_0)$, the reference density usually based on the density ρ_0 of unburned gas and the unburned gas temperature T_0 is taken to be the reference temperature. The reference pressure P_0 is defined based on a dynamic perspective only as $P_0 = \rho_0 u_0^2$. In the mass transfer formulation the Soret effect and Dufour effect are assumed negligible.

- The specific heats C_P and C_V, dynamic viscosity μ, thermal conductivity λ and density weighted ρD are taken to be constant and independent of temperature.

- The temperature is non-dimensionalised as:

$$T = \frac{\hat{T} - T_0}{T_{ad} - T_0} \tag{3.20}$$

where T_0 is the initial temperature and T_{ad} is adiabatic flame temperature, given by $T_{ad} = T_0 + H / C_P$. The internal energy E is normalised with respect to $C_P T_0$. It has been discussed earlier that for low Mach number unity Le combustion condition, the above normalised temperature and reaction progress variable are equivalent to each other, i.e. $c = T$.

Based on the above assumptions all the governing equations can be recast into the following non-dimensional form:

- Mass conservation equation:

$$\frac{\partial \rho}{\partial t} + \frac{\partial (\rho u_k)}{\partial x_k} = 0 \tag{3.21}$$

- Momentum conservation equation:

$$\frac{\partial (\rho u_i)}{\partial t} + \frac{\partial (\rho u_k u_i)}{\partial x_k} = -\frac{\partial P}{\partial x_k} + \frac{1}{Re}\frac{\partial (\tau_{ki})}{\partial x_k} \tag{3.22}$$

where the viscous stress tensor τ_{ki} and reaction rate term $\dot{w}$ are given by:

$$\tau_{ki} = \mu\left[\frac{\partial u_i}{\partial x_j} + \frac{\partial u_j}{\partial x_i}\right] - \frac{2}{3}\delta_{ij}\mu\left[\frac{\partial u_k}{\partial x_k}\right] \tag{3.23}$$

- Energy conservation equation:

$$\begin{aligned}\frac{\partial (\rho E)}{\partial t} + \frac{\partial (\rho u_k E)}{\partial x_k} = &-(\gamma - 1)Ma^2 \frac{\partial (P u_k)}{\partial x_k} + \frac{1}{Re}(\gamma - 1)Ma^2 \frac{\partial (\tau_{ki} u_i)}{\partial x_k} \\ &+ \frac{\tau}{RePr}\frac{\partial}{\partial x_k}\left[\lambda \frac{\partial T}{\partial x_k}\right] - \frac{\tau}{\mathrm{Re}\,Sc}\frac{\partial}{\partial x_k}\left[\rho D \frac{\partial c}{\partial x_k}\right]\end{aligned} \tag{3.24}$$

where the non-dimensional equations of state become:

$$P = \frac{1}{\gamma Ma^2}\rho(1+\tau T) \tag{3.25}$$

$$E = \frac{1}{\gamma}(1+\tau T) + \frac{1}{2}(\gamma-1)Ma^2 u_k u_k + \tau(1-c) \tag{3.26}$$

- Species conservation equation:

$$\frac{\partial(\rho c)}{\partial t} + \frac{\partial(\rho u_k c)}{\partial x_k} = \dot{w} + \frac{1}{ReSc}\frac{\partial}{\partial x_k}\left[\rho D \frac{\partial c}{\partial x_k}\right] \tag{3.27}$$

where the heat release rate is given by:

$$\dot{w} = B\rho(1-c)\exp\left[-\frac{\beta(1-T)}{1-\alpha(1-T)}\right] \tag{3.28}$$

The parameters in the governing equations are replaced by a series of non-dimensional parameters including:

Reynolds number: $Re = \frac{\rho_0 u_0 l_0}{\mu_0}$ (3.29)

Prandtl number: $Pr = \frac{\mu_0 C_{P0}}{\lambda_0}$ which is taken as 0.7 (3.30)

Schmidt number: $Sc = \frac{\mu_0}{\rho_0 D_0}$ (3.31)

Mach number: $Ma = \frac{u_0}{a_0}$ with $a_0 = \sqrt{\gamma R T_0}$ = sonic speed (3.32)

The ratio of specific heats: $\gamma = \frac{C_{P0}}{C_{V0}}$ (3.33)

Heat release parameters: $\tau = \frac{\alpha}{(1-\alpha)} = \frac{(T_{ad}-T_0)}{T_0}$ (3.34)

Zel'dovich number: $\beta = \frac{E(T_{ad}-T_o)}{RT_{ad}^2}$ (3.35)

The non-dimensional pre-exponential factor: $B = \frac{B^*}{\rho_0 u_0}\exp\left[-\frac{\beta}{\alpha}\right]$ (3.36)

3.3 Filtering: a DNS perspective

In Large Eddy Simulation, the large structures of the turbulent reactive flows are explicitly calculated through the filtered governing equations. Filtering is mathematically a convolution process in either spectral space or physical space with respect to the filter widths, which may be expressed as:

$$\overline{f(x)} = \int f(\varsigma)F(x-\varsigma)d\varsigma \tag{3.37}$$

where F is the filter kernel function. Cut-off filtering function is widely used in spectral space, whereas box filter and Gaussian filter are the most popular filtering functions in physical space (Poinsot and Veynante, 2001). Therefore the governing equations applied in generating DNS database will need to be derived into their filtered forms. In this study, DNS database of turbulent premixed combustion are generated by solving the instantaneous governing equations in Section 3.2, which have been post-processed by applying convolution operation on the three dimensional variables extracted from DNS data.

3.3.1 Favre decomposition

Turbulence is characteristic of random fluctuations of various physical variables (Kolmogorov, 1941). In low Mach number non-reactive turbulent flow, density variation is usually expected to be small and density can be considered to be constant. Thus, the variables are decomposed into a mean and a fluctuating part according to convention Reynolds decomposition. However, in turbulent reacting flows, the density variation is significant due to the strong heat release from the chemical reaction (see eq. (3.12)). Thus, the fluctuation of density cannot be ignored which leads to unclosed terms involving density fluctuations in the Reynolds averaged mass conservation equation. This difficulty can be avoided by decomposing a general variable Q into the Favre averaged/resolved part $\tilde{Q}$ and fluctuation Q'' as:

$$Q = \tilde{Q} + Q'' \tag{3.38}$$

with $$\bar{\rho}(x)\tilde{Q}(x) = \int \rho(\varsigma)Q(\varsigma)F(x-\varsigma)d\varsigma \tag{3.39}$$

Therefore $\bar{\rho}(x)\tilde{Q}(x) = \overline{\rho(x)Q(x)}$, which is often adopted to calculate the Favre averaged values. It worth noting that the mean of the fluctuations Q'' is not 0 while the density weighted mean is null:

$$\overline{Q''} \neq 0; \overline{\rho Q''} = 0 \tag{3.40}$$

3.3.2 Gaussian filter and its efficiency

A Gaussian filter is defined as:

$$F(\vec{x}) = F(x_1, x_2, x_3) = \left(\frac{6}{\pi\Delta^2}\right)^{3/2} \exp\left[-\frac{6}{\Delta^2}(x_1^2 + x_2^2 + x_3^2)\right] \tag{3.41}$$

where Δ denotes the filter widths which is equivalent to grid size in LES. It worth noting eq. (3.41) is the normalised form of the filter such that:

$$\int_{-\infty}^{+\infty}\int_{-\infty}^{+\infty}\int_{-\infty}^{+\infty} F(x_1, x_2, x_3)\, dx_1 dx_2 dx_3 = 1 \tag{3.42}$$

Explicit filtering has been applied to simple chemistry DNS database, where the Gaussian filter kernel was firstly discretised with finite difference method and then directly calculated which may be demonstrated below:

$$\bar{Q}(x, y, z) = \left(\frac{6}{4\pi}\right)^{3/2} \sum_{i=-N}^{N}\sum_{j=-N}^{N}\sum_{k=-N}^{N} \frac{Q(i, j, k)}{N^3} \underbrace{\exp\left[-\frac{6}{(2N)^2}\left(i^2 + j^2 + k^2\right)\right]}_{F_{i,j,k}} \tag{3.43}$$

where $N = \Delta/2$ denotes the grid points involved in the filter on each direction which is equal to half of the digital filter width for isotropic filters. Considering the speciality of exponential function, under the assumption that the filtering function F can be decomposed into three orthogonal, independent components, a more efficient digital filter was proposed as follows (Klein et al., 2003):

$$\tilde{Q}(x, y, z) = \left(\frac{6}{4\pi}\right)^{3/2} \sum_{i=-N}^{N} f_i \sum_{j=-N}^{N} f_j \sum_{k=-N}^{N} f_k Q(i, j, k) \tag{3.44}$$

where $F_{i,j,k} = f_i f_j f_k$. Equation (3.44) has been used for filtering the detail chemistry DNS results. More information on numerical implementation and DNS datasets will be provided in Chapter 4.

3.3.3 Filtered transport equations

The governing transport equations in Section 3.2 are revised into the Favre filtered form below. Favre filtered/averaged mass conservation equation:

$$\frac{\partial \bar{\rho}}{\partial t} + \frac{\partial}{\partial x_k}(\bar{\rho}\tilde{u}_k) = 0 \tag{3.41}$$

Favre filtered/averaged momentum conservation equation:

$$\frac{\partial}{\partial t}(\bar{\rho}\tilde{u}_i) + \frac{\partial}{\partial x_i}(\bar{\rho}\tilde{u}_i\tilde{u}_j) = -\frac{\partial \bar{P}}{\partial x_i} + \frac{\partial}{\partial x_i}\left[\bar{\tau}_{ij} - \bar{\rho}(\widetilde{u_i u_j} - \tilde{u}_i\tilde{u}_j)\right] \tag{3.42}$$

Favre filtered/averaged conservation equation of reactant species α:

$$\frac{\partial}{\partial t}\left(\bar{\rho}\tilde{Y}_\alpha\right) + \frac{\partial}{\partial x_k}\left(\bar{\rho}\tilde{u}_k\tilde{Y}_\alpha\right) = \overline{\dot{w}_\alpha} - \frac{\partial}{\partial x_k}\left[\overline{D_{\alpha,k}Y_\alpha} + \left(\overline{\rho u_i Y_\alpha} - \bar{\rho}\tilde{u}_i\tilde{Y}_\alpha\right)\right] \text{ with } \alpha = 1,\ldots\ldots,N \tag{3.43}$$

The transport equation of the Favre filtered reaction progress variable $\tilde{c}$:

$$\bar{\rho}\left[\frac{\partial \tilde{c}}{\partial t} + \tilde{u}_j\frac{\partial \tilde{c}}{\partial x_j}\right] = \overline{\frac{\partial}{\partial x_j}\left[\rho D\frac{\partial c}{\partial x_j}\right]} + \overline{\dot{w}} - \frac{\partial}{\partial x_j}[\overline{\rho u_j c} - \bar{\rho}\tilde{u}_j\tilde{c}] \tag{3.44}$$

The two terms on LHS of eq. (3.44) indicate the transient and the resolved advection effects. The terms on the RHS denote the filtered molecular diffusion, chemical reaction rate and the sub-grid turbulent transport of the reaction progress variable respectively. The filtered reaction rate $\overline{\dot{w}}$ and the turbulent transport term $-\partial[\overline{\rho u_j c} - \bar{\rho}\tilde{u}_j\tilde{c}]/\partial x_j$ are unclosed and thus need to be modelled in LES. The filtered molecular diffusion term $\overline{\nabla\cdot(\rho D\nabla c)}$ is often approximated as $\overline{\nabla\cdot(\rho D\nabla c)} \approx \nabla\cdot(\bar{\rho}\tilde{D}\nabla\tilde{c})$.

3.4 SDR based reaction rate closure for LES

Reaction rate closure based on SDR $\tilde{N}_c$ has already introduced in Chapter 2 (Section 2.2.1) where a proportional relationship between the mean reaction rate and Favre-averaged SDR was proposed by Bray(1980) (see eq.2.30) for high Damkölar number $Da \gg 1$ flames, which has been further adopted to model $\tilde{\varepsilon}_c$ in RANS as:

$$\overline{\dot{w}} \approx \frac{2\bar{\rho}\tilde{\varepsilon}_c}{2c_m - 1} \tag{3.45}$$

Equation (3.45) has been assessed later by DNS analysis and it is found to remain valid even for $Da<1$ turbulent premixed flames in RANS (Chakraborty and Swaminathan, 2010). A recent analysis has recast eq. (3.45) back into the form of eq. (2.30), i.e. $\bar{\dot{w}}=2\bar{\rho}\tilde{N}_c/\left(2c_m-1\right)$, for the purpose of assessing and extending this relationship for LES (Dunstan et al., 2013). The analysis of Dunstan *et al.* (2013) suggested that for filter size greater than thermal flame thickness (i.e. $\Delta>\delta_{th}$), eq. (2.30) is valid for LES. However, for filter width comparable $\Delta\approx\delta_{th}$ or smaller $\Delta<\delta_{th}$ than thermal flame thickness, the local behaviour of filtered reaction rate $\bar{\dot{w}}$ is not accurately predicted by eq. (2.30). The reason for this discrepancy will be discussed in detail in Chapter 5 of this thesis.

3.5 SDR transport equations

3.5.1 Instantaneous SDR transport equation

The transport equation of the instantaneous SDR N_c can be derived from the transport equation of the reaction progress variable *c* (eq. (2.25)). To demonstrate the derivation process, the eq. (2.25) is recast in the following manner:

$$\rho\frac{\partial c}{\partial t}+\rho u_i\frac{\partial c}{\partial x_i}=\frac{\partial}{\partial x_i}\left(\rho D\frac{\partial c}{\partial x_i}\right)+\dot{w} \tag{3.46}$$

Dividing both sides of eq. (3.46) by ρ and then differentiating them with $\frac{\partial}{\partial x_i}$ reads:

$$\frac{\partial}{\partial x_i}\left(\frac{\partial c}{\partial t}+u_i\frac{\partial c}{\partial x_i}\right)=\frac{\partial}{\partial x_i}\left(\frac{1}{\rho}\left[\frac{\partial}{\partial x_i}(\rho D\frac{\partial c}{\partial x_i})\right]\right)+\frac{\partial}{\partial x_i}\left(\frac{\dot{w}}{\rho}\right) \tag{3.47}$$

Multiplying both sides of eq. (3.47) with $\left(2\frac{\partial c}{\partial x_i}\right)$ leads to:

$$\begin{aligned}\frac{\partial}{\partial t}\left(\nabla c.\nabla c\right)+u_i\frac{\partial}{\partial x_j}\left(\nabla c.\nabla c\right)=&-\frac{2}{\rho^2}\frac{\partial c}{\partial x_i}\frac{\partial\rho}{\partial x_i}[\dot{w}+\frac{\partial}{\partial x_j}(\rho D\frac{\partial c}{\partial x_j})]-2\frac{\partial c}{\partial x_i}\frac{\partial u_j}{\partial x_i}\frac{\partial c}{\partial x_j}\\&+\frac{2}{\rho}\frac{\partial c}{\partial x_i}\frac{\partial^2}{\partial x_i\partial x_j}(\rho D\frac{\partial c}{\partial x_j})+\frac{2}{\rho}\frac{\partial c}{\partial x_i}\frac{\partial\dot{w}}{\partial x_i}\end{aligned} \tag{3.48}$$

Multiplying diffusivity on both sides of eq. (3.48) generates the following equation:

$$\rho\frac{\partial N_c}{\partial t}+\rho\frac{\partial}{\partial x_j}\left(u_i N_c\right)=-\frac{2D}{\rho}\frac{\partial c}{\partial x_i}\frac{\partial \rho}{\partial x_i}[\dot{w}+\frac{\partial}{\partial x_j}(\rho D\frac{\partial c}{\partial x_j})]-2\rho D\frac{\partial c}{\partial x_i}\frac{\partial u_j}{\partial x_i}\frac{\partial c}{\partial x_j}$$
$$+2D\frac{\partial c}{\partial x_i}\frac{\partial^2}{\partial x_i\partial x_j}(\rho D\frac{\partial c}{\partial x_j})+2D\frac{\partial c}{\partial x_i}\frac{\partial \dot{w}}{\partial x_i} \tag{3.49}$$
$$+\rho\nabla c.\nabla c[\frac{\partial D}{\partial t}+u_i\frac{\partial D}{\partial x_j}]+\rho N_c\frac{\partial u_j}{\partial x_j}$$

Incorporating continuity equation into eq. (3.49) will lead to the final form of the instantaneous SDR transport equation as follows:

$$\frac{\partial(\rho N_c)}{\partial t}+\frac{\partial(\rho u_j N_c)}{\partial x_j}=\overbrace{\frac{\partial}{\partial x_j}\left(\rho D\frac{\partial N_c}{\partial x_j}\right)}^{\text{Molecular diffusion: } D_{1I}}\overbrace{-\frac{2D}{\rho}\frac{\partial \rho}{\partial x_j}\frac{\partial c}{\partial x_j}[\dot{w}+\nabla.(\rho D\nabla c)]}^{\text{Density variation: } T_{1I}}$$
$$\underbrace{-2\rho D\frac{\partial c}{\partial x_i}\frac{\partial u_i}{\partial x_j}\frac{\partial c}{\partial x_j}}_{\text{Scalar turbulence interaction: } T_{2I}} \tag{3.50}$$
$$+\underbrace{2D\frac{\partial \dot{w}}{\partial x_j}\frac{\partial c}{\partial x_j}}_{\text{Chemical reaction: } T_{3I}}\underbrace{-2\rho D^2\frac{\partial^2 c}{\partial x_i\partial x_j}\frac{\partial^2 c}{\partial x_i\partial x_j}}_{\text{Molecular dissipation: } (-D_{2I})}+\underbrace{f(D)_I}_{\text{Diffusivity variation}}$$

where

$$f(D)=\underbrace{2D\frac{\partial c}{\partial x_k}\frac{\partial(\rho D)}{\partial x_k}\frac{\partial^2 c}{\partial x_j\partial x_j}}_{T_{D1}}+\underbrace{2D\frac{\partial c}{\partial x_k}\frac{\partial^2(\rho D)}{\partial x_j\partial x_k}\frac{\partial c}{\partial x_j}}_{T_{D2}}\underbrace{-\frac{\partial}{\partial x_j}\left(\rho N_c\frac{\partial D}{\partial x_j}\right)}_{T_{D3}} \tag{3.51}$$
$$\underbrace{-2\rho D\frac{\partial D}{\partial x_j}\frac{\partial(\nabla c.\nabla c)}{\partial x_j}}_{T_{D4}}+\underbrace{\rho\nabla c.\nabla c\left[\frac{\partial D}{\partial t}+u_j\frac{\partial D}{\partial x_j}\right]}_{T_{D5}}$$

The first two terms on the left hand side of eq. (3.50) represent the transient and advection effects, whereas the first term on the RHS D_{1I} denotes molecular diffusion of SDR. The second term on the RHS of eq. (3.50) T_{1I} originates due to density variation and will henceforth be referred to as the density variation term. The third term T_{2I} represents the effects of fluid-dynamic straining, whereas the fourth term T_{3I} denotes the reaction rate contribution to the SDR transport. The penultimate term on the RHS of eq. (3.50) $(-D_2)$ denotes molecular dissipation of N_c and terms involving temporal and spatial gradients of diffusivity are collectively referred to as $f(D)_I$ shown in eq. (3.51) (Gao et al., 2014). The behaviours of the above terms will be provided and analysed in detail in Chapters 6 and 7 later in this thesis.

Although the statistical behaviours of $|\nabla c|$ and the terms of its transport equation were analysed earlier, the terms of N_c transport equation are fundamentally different from the terms of the $|\nabla c|$ transport equation, which can be written for a given *c* isosurface in the following manner (Chakraborty and Cant, 2005):

$$\frac{\partial|\nabla c|}{\partial t}+\frac{\partial(u_j|\nabla c|)}{\partial x_j}=(\delta_{ij}-n_i n_j)\frac{\partial u_i}{\partial x_j}|\nabla c|+S_d\frac{\partial n_i}{\partial x_i}-\frac{\partial(S_d n_i|\nabla c|)}{\partial x_i} \tag{3.52}$$

where

$$n_i=-\frac{1}{|\nabla c|}\left(\frac{\partial c}{\partial x_i}\right) \tag{3.53}$$

is the i^{th} component of flame normal vector and

$$S_d=\frac{\dot{w}+\nabla.(\rho D\nabla c)}{\rho|\nabla c|} \tag{3.54}$$

is the local flame displacement speed. It is evident from eqs. (3.52) – (3.54) that the statistical behaviour of N_c transport is likely to be different from $|\nabla c|$ transport although the quantities N_c and $|\nabla c|$ are closely related to each other (i.e. $N_c=D|\nabla c|^2$).

3.5.2 Favre averaged SDR transport equation

The transport equation of Favre averaged/filtered SDR $\tilde{N}_c$ is obtained by LES filtering Eq. (3.50):

$$\begin{aligned}\frac{\partial(\overline{\rho N_c})}{\partial t}+\frac{\partial(\overline{\rho u_j N_c})}{\partial x_j}=&\overline{\frac{\partial}{\partial x_j}\left(\rho D\frac{\partial N_c}{\partial x_j}\right)}-\overline{\frac{2D}{\rho}\frac{\partial\rho}{\partial x_j}\frac{\partial c}{\partial x_j}[\dot{w}+\nabla.(\rho D\nabla c)]}\\&-\overline{2\rho D\frac{\partial c}{\partial x_i}\frac{\partial u_i}{\partial x_j}\frac{\partial c}{\partial x_j}}\\&+\overline{2D\frac{\partial\dot{w}}{\partial x_j}\frac{\partial c}{\partial x_j}}-\overline{2\rho D^2\frac{\partial^2 c}{\partial x_i\partial x_j}\frac{\partial^2 c}{\partial x_i\partial x_j}}+\overline{f(D)}\end{aligned} \tag{3.55}$$

$$\overline{f(D)} = \overline{2D\frac{\partial c}{\partial x_k}\frac{\partial(\rho D)}{\partial x_k}\frac{\partial^2 c}{\partial x_j \partial x_j}} + \overline{2D\frac{\partial c}{\partial x_k}\frac{\partial^2(\rho D)}{\partial x_j \partial x_k}\frac{\partial c}{\partial x_j}} - \overline{\frac{\partial}{\partial x_j}\left(\rho N_c \frac{\partial D}{\partial x_j}\right)}$$
$$-\overline{2\rho D\frac{\partial D}{\partial x_j}\frac{\partial(\nabla c.\nabla c)}{\partial x_j}} + \overline{\rho\nabla c.\nabla c\left[\frac{\partial D}{\partial t} + u_j\frac{\partial D}{\partial x_j}\right]} \quad (3.56)$$

where

Then dividing the term $\frac{\partial(\overline{\rho u_j N_c})}{\partial x_j}$ into three components as:

$$\frac{\partial(\overline{\rho u_j N_c})}{\partial x_j} = \frac{\partial(\bar{\rho}\tilde{u}_j\tilde{N}_c)}{\partial x_j} + \frac{\partial}{\partial x_j}\left(\overline{\rho u_j N_c} - \bar{\rho}\tilde{u}_j\tilde{N}_c\right) \quad (3.57)$$

will lead to the final form of the Favre averaged/filtered SDR transport equation shown below:

$$\frac{\partial(\bar{\rho}\tilde{N}_c)}{\partial t} + \frac{\partial(\bar{\rho}\tilde{u}_j\tilde{N}_c)}{\partial x_j} = \underbrace{\overline{\frac{\partial}{\partial x_j}\left(\rho D\frac{\partial N_c}{\partial x_j}\right)}}_{D_1} + T_1 + T_2 + T_3 + T_4 - D_2 + f(D) \quad (3.58)$$

where u_j is the j^{th} component of velocity vector and the terms on the left hand side denote the transient effects and the resolved advection of $\tilde{N}_c$ respectively. The term D_1 represents the molecular diffusion of $\tilde{N}_c$ and the other terms $T_1, T_2, T_3, T_4, (-D_2)$ and $f(D)$ are all unclosed and given by:

$$T_1 = -\frac{\partial}{\partial x_j}\left(\overline{\rho u_j N_c} - \bar{\rho}\tilde{u}_j\tilde{N}_c\right) \quad (3.59)$$

$$T_2 = \overline{-2\frac{D}{\rho}\left[\dot{w} + \frac{\partial}{\partial x_i}\left(\rho D\frac{\partial c}{\partial x_i}\right)\right]\frac{\partial c}{\partial x_j}\frac{\partial \rho}{\partial x_j}} \quad (3.60)$$

$$T_3 = \overline{-2\rho D\frac{\partial c}{\partial x_i}\frac{\partial u_i}{\partial x_j}\frac{\partial c}{\partial x_j}} \quad (3.61)$$

$$T_4 = \overline{2D\frac{\partial \dot{w}}{\partial x_i}\frac{\partial c}{\partial x_i}} \quad (3.62)$$

$$(-D_2) = \overline{-2\rho D^2\frac{\partial^2 c}{\partial x_i \partial x_j}\frac{\partial^2 c}{\partial x_i \partial x_j}} \quad (3.63)$$

$$f(D)=\overline{f_1(D)}=\underbrace{\overline{2D\frac{\partial c}{\partial x_k}\frac{\partial(\rho D)}{\partial x_k}\frac{\partial^2 c}{\partial x_j\partial x_j}}}_{FD1}+\underbrace{\overline{2D\frac{\partial c}{\partial x_k}\frac{\partial^2(\rho D)}{\partial x_j\partial x_k}\frac{\partial c}{\partial x_j}}}_{FD2}-\underbrace{\overline{\frac{\partial}{\partial x_j}\left(\rho N_c\frac{\partial D}{\partial x_j}\right)}}_{FD3}$$
$$\underbrace{-\overline{2\rho D\frac{\partial D}{\partial x_j}\frac{\partial}{\partial x_j}\left(\frac{\partial c}{\partial x_k}\frac{\partial c}{\partial x_k}\right)}}_{FD4}+\underbrace{\overline{\rho\left(\frac{\partial c}{\partial x_k}\frac{\partial c}{\partial x_k}\right)\left[\frac{\partial D}{\partial t}+u_j\frac{\partial D}{\partial x_j}\right]}}_{FD5} \quad (3.64)$$

The term T_1 represents the effects of sub-grid convection, whereas T_2 denotes the effects of density-variation due to heat release. The term T_3 is determined by the alignment of ∇c with local strain rates $e_{ij}=0.5(\partial u_i/\partial x_j+\partial u_j/\partial x_i)$, and this term is commonly referred to as the scalar-turbulence interaction term. The term T_4 arises due to reaction rate gradient while $(-D_2)$ denotes the molecular dissipation of SDR and these terms will henceforth be referred to as the reaction rate term and dissipation term respectively. The term $f(D)$, as in eq. (3.64), indicates the effects of variation of mass diffusivity, D, and its interaction with scalar gradients.

3.5.3 The transport equation of the resolved components of $\tilde{N}_c$

Equation (2.34) presents the expansion form of $\bar{\rho}\tilde{N}_c$ which can be recast into the following form:

$$\widetilde{N_c}=\overline{\rho D\frac{\partial c}{\partial x_\iota}\frac{\partial c}{\partial x_\iota}}\Big/\bar{\rho}=\widetilde{D}\frac{\partial\tilde{c}}{\partial x_i}\frac{\partial\tilde{c}}{\partial x_i}+N_{sg}+\tilde{\varepsilon}_c \quad (3.65)$$

As the term $N_{sg}=2\widetilde{D\frac{\partial c''}{\partial x_\iota}\frac{\partial\tilde{c}}{\partial x_i}}$ tends to be small. The resolved component of $\tilde{N}_c$ is usually denoted as: $\tilde{D}\nabla\tilde{c}.\nabla\tilde{c}$. The transport equation of the resolved component of SDR $\tilde{D}\nabla\tilde{c}.\nabla\tilde{c}$ can be derived from the transport eqaution of $\tilde{c}$ eq. (3.44) which has been recast in the following form:

$$\frac{\partial\tilde{c}}{\partial t}+\tilde{u}_j\frac{\partial\tilde{c}}{\partial x_j}=\frac{1}{\bar{\rho}}\left[\dot{\bar{w}}+\overline{\nabla.(\rho D\nabla c)}\right]-\frac{1}{\bar{\rho}}\frac{\partial}{\partial x_j}\left(\overline{\rho u_j c}-\bar{\rho}\tilde{u}_j\tilde{c}\right) \quad (3.66)$$

Similarly with the derivation of the transport equation of instantaneous SDR N_c, eq. (3.66) are differentiated with respect to x_i on both sides:

$$\frac{\partial}{\partial t}\left(\frac{\partial \tilde{c}}{\partial x_i}\right)+\tilde{u}_j\frac{\partial}{\partial x_j}\left(\frac{\partial \tilde{c}}{\partial x_i}\right)=-\frac{1}{\bar{\rho}^2}\left[\dot{\bar{w}}+\nabla.\left(\overline{\rho D\nabla c}\right)\right]\frac{\partial \bar{\rho}}{\partial x_i}$$
$$+\frac{1}{\bar{\rho}}\left[\frac{\partial \dot{\bar{w}}}{\partial x_i}+\frac{\partial^2}{\partial x_i\partial x_j}\left(\overline{\rho D\frac{\partial c}{\partial x_j}}\right)\right]-\frac{1}{\bar{\rho}}\frac{\partial}{\partial x_j\partial x_i}\left(\overline{\rho u_j c}-\bar{\rho}\tilde{u}_j\tilde{c}\right) \quad (3.67)$$
$$+\frac{1}{\bar{\rho}^2}\frac{\partial}{\partial x_j}\left(\overline{\rho u_j c}-\bar{\rho}\tilde{u}_j\tilde{c}\right)\frac{\partial \bar{\rho}}{\partial x_i}-\frac{\partial \tilde{u}_j}{\partial x_i}\frac{\partial \tilde{c}}{\partial x_j}$$

Multiplying eq. (3.67) with $\left(2\frac{\partial \tilde{c}}{\partial x_i}\right)$ then using chain rule leads to:

$$\frac{\partial}{\partial t}\left(\nabla\tilde{c}.\nabla\tilde{c}\right)+\tilde{u}_j\frac{\partial}{\partial x_j}\left(\nabla\tilde{c}.\nabla\tilde{c}\right)$$
$$=-\frac{2}{\bar{\rho}^2}\left[\dot{\bar{w}}+\nabla.\left(\overline{\rho D\nabla c}\right)\right]\frac{\partial \bar{\rho}}{\partial x_i}\frac{\partial \tilde{c}}{\partial x_i}$$
$$+\frac{2}{\bar{\rho}}\frac{\partial \tilde{c}}{\partial x_i}\left[\frac{\partial \dot{\bar{w}}}{\partial x_i}+\frac{\partial^2}{\partial x_i\partial x_j}\left(\overline{\rho D\frac{\partial c}{\partial x_j}}\right)\right]-\frac{2}{\bar{\rho}}\frac{\partial \tilde{c}}{\partial x_i}\frac{\partial}{\partial x_j\partial x_i}\left(\overline{\rho u_j c}-\bar{\rho}\tilde{u}_j\tilde{c}\right) \quad (3.68)$$
$$+\frac{2}{\bar{\rho}^2}\frac{\partial \tilde{c}}{\partial x_i}\frac{\partial}{\partial x_j}\left(\overline{\rho u_j c}-\bar{\rho}\tilde{u}_j\tilde{c}\right)\frac{\partial \bar{\rho}}{\partial x_i}-2\frac{\partial \tilde{c}}{\partial x_i}\frac{\partial \tilde{u}_j}{\partial x_i}\frac{\partial \tilde{c}}{\partial x_j}$$

By multiplying $\tilde{D}$ on both sides of eq. (3.68), an exact form of the transport equation of the resolved component of filtered SDR $\tilde{D}\nabla\tilde{c}.\nabla\tilde{c}$ can be obtained as follows:

$$\frac{\partial}{\partial t}\left(\bar{\rho}\tilde{D}\nabla\tilde{c}.\nabla\tilde{c}\right)+\frac{\partial}{\partial x_j}\left(\bar{\rho}\tilde{u}_j\tilde{D}\nabla\tilde{c}.\nabla\tilde{c}\right)$$
$$=-2\tilde{D}\frac{\partial \tilde{c}}{\partial x_i}\frac{\partial^2}{\partial x_j\partial x_i}\left(\overline{\rho u_j c}-\bar{\rho}\tilde{u}_j\tilde{c}\right)$$
$$-\frac{2\tilde{D}}{\bar{\rho}}\frac{\partial \bar{\rho}}{\partial x_i}\frac{\partial \tilde{c}}{\partial x_i}\left[\dot{\bar{w}}+\nabla.\left(\overline{\rho D\nabla c}\right)-\frac{\partial}{\partial x_j}\left(\overline{\rho u_j c}-\bar{\rho}\tilde{u}_j\tilde{c}\right)\right]$$
$$-2\bar{\rho}\tilde{D}\frac{\partial \tilde{c}}{\partial x_i}\frac{\partial \tilde{u}_j}{\partial x_i}\frac{\partial \tilde{c}}{\partial x_j}+2\tilde{D}\frac{\partial \tilde{c}}{\partial x_i}\frac{\partial \dot{\bar{w}}}{\partial x_i} \quad (3.69)$$
$$+\bar{\rho}\tilde{D}\nabla\tilde{c}.\nabla\tilde{c}\frac{\partial \tilde{u}_j}{\partial x_j}+2\tilde{D}\frac{\partial \tilde{c}}{\partial x_i}\frac{\partial^2}{\partial x_i\partial x_j}\left(\overline{\rho D\frac{\partial c}{\partial x_j}}\right)$$
$$+\bar{\rho}\nabla\tilde{c}.\nabla\tilde{c}\left(\frac{\partial \tilde{D}}{\partial t}+\tilde{u}_j\frac{\partial \tilde{D}}{\partial x_j}\right)+\tilde{D}\nabla\tilde{c}.\nabla\tilde{c}\left(\frac{\partial \bar{\rho}}{\partial t}+\tilde{u}_j\frac{\partial \bar{\rho}}{\partial x_j}\right)$$

A simple assumption is made to express $2\tilde{D}\nabla\tilde{c}.\nabla\left[\nabla.(\overline{\rho D}\nabla\tilde{c})\right]$ in the following form:

$$2\tilde{D}\frac{\partial\tilde{c}}{\partial x_i}\frac{\partial^2}{\partial x_i\partial x_j}\left(\overline{\rho D\frac{\partial c}{\partial x_j}}\right)\approx 2\tilde{D}\frac{\partial\tilde{c}}{\partial x_i}\frac{\partial^2}{\partial x_i\partial x_j}\left(\bar{\rho}\tilde{D}\frac{\partial\tilde{c}}{\partial x_j}\right) \tag{3.70}$$

This yields the transport equation of the resolved component of SDR $\tilde{D}\nabla\tilde{c}.\nabla\tilde{c}$ as:

$$\begin{aligned}
&\frac{\partial}{\partial t}\left(\bar{\rho}\tilde{D}\nabla\tilde{c}.\nabla\tilde{c}\right)+\frac{\partial}{\partial x_j}\left(\bar{\rho}\tilde{u}_j\tilde{D}\nabla\tilde{c}.\nabla\tilde{c}\right)\\
&\qquad\overbrace{\approx -2\tilde{D}\frac{\partial\tilde{c}}{\partial x_i}\frac{\partial^2}{\partial x_j\partial x_i}\left(\overline{\rho u_j c}-\bar{\rho}\tilde{u}_j\tilde{c}\right)}^{T_{1R}}\\
&\qquad\overbrace{-\frac{2\tilde{D}}{\bar{\rho}}\frac{\partial\bar{\rho}}{\partial x_i}\frac{\partial\tilde{c}}{\partial x_i}\left[\bar{\dot{w}}+\nabla.\left(\overline{\rho D\nabla c}\right)-\frac{\partial}{\partial x_j}\left(\overline{\rho u_j c}-\bar{\rho}\tilde{u}_j\tilde{c}\right)\right]}^{T_{2R}}\\
&\qquad\underbrace{-2\bar{\rho}\tilde{D}\frac{\partial\tilde{c}}{\partial x_i}\frac{\partial\tilde{u}_j}{\partial x_i}\frac{\partial\tilde{c}}{\partial x_j}}_{T_{3R}}\underbrace{+2\tilde{D}\frac{\partial\tilde{c}}{\partial x_i}\frac{\partial\bar{\dot{w}}}{\partial x_i}}_{T_{4R}}\\
&\qquad\underbrace{+\frac{\partial}{\partial x_j}\left(\bar{\rho}\tilde{D}\frac{\partial}{\partial x_j}\left[\tilde{D}\nabla\tilde{c}.\nabla\tilde{c}\right]\right)}_{D_{1R}}\underbrace{-2\bar{\rho}\tilde{D}\frac{\partial^2\tilde{c}}{\partial x_i\partial x_j}\frac{\partial^2\tilde{c}}{\partial x_i\partial x_j}}_{-D_{2R}}+f(D)_R
\end{aligned} \tag{3.71}$$

where

$$\begin{aligned}
f(D)_R=&-\frac{\partial\tilde{D}}{\partial x_j}\frac{\partial(\bar{\rho}\tilde{D})}{\partial x_j}\frac{\partial\tilde{c}}{\partial x_k}\frac{\partial\tilde{c}}{\partial x_k}-4\bar{\rho}\tilde{D}\frac{\partial\tilde{D}}{\partial x_j}\frac{\partial\tilde{c}}{\partial x_k}\frac{\partial^2\tilde{c}}{\partial x_k\partial x_j}-\bar{\rho}\tilde{D}\nabla\tilde{c}.\nabla\tilde{c}\frac{\partial^2\tilde{D}}{\partial x_j\partial x_j}\\
&+2\tilde{D}\frac{\partial\tilde{c}}{\partial x_k}\frac{\partial\tilde{c}}{\partial x_j}\frac{\partial^2(\bar{\rho}\tilde{D})}{\partial x_k\partial x_j}+2\tilde{D}\frac{\partial\tilde{c}}{\partial x_k}\frac{\partial(\bar{\rho}\tilde{D})}{\partial x_j}\frac{\partial^2\tilde{c}}{\partial x_k\partial x_j}\\
&+\tilde{D}\nabla\tilde{c}.\nabla\tilde{c}(\frac{\partial\bar{\rho}}{\partial t}+\tilde{u}_j\frac{\partial\bar{\rho}}{\partial x_j})+\bar{\rho}\nabla\tilde{c}.\nabla\tilde{c}(\frac{\partial\tilde{D}}{\partial t}+\tilde{u}_j\frac{\partial\tilde{D}}{\partial x_j})+\bar{\rho}\tilde{D}\nabla\tilde{c}.\nabla\tilde{c}\frac{\partial\tilde{u}_j}{\partial x_j}
\end{aligned} \tag{3.72}$$

3.6 Summary

In this chapter, the governing transport equations and the underlying assumptions of the DNS were presented. The diffusion velocities were characterized by the Fick's law. The reaction mechanism was accounted with respect to a single reaction progress variable. This reaction progress variable can be defined based on the mass fraction of a deficient reactant/product as well as temperature. All the transport equation were non-dimensionalised with respect to the numeraire of the unburned reactants. The SDR based

reaction rate closure in the context of RANS was discussed and the derivation of the transport equations of instantaneous SDR, Favre filtered SDR and its resolved component were introduced. In next chapter, the DNS database used will be introduced in detail.

Chapter 4 Numerical Implementation

Several Direct Numerical Simulation (DNS) databases are post-processed in the current work for analysing the statistical behaviours of both instantaneous SDR, filtered SDR and the terms of their transport equations. Based on *a-priori* analysis of the simple chemistry DNS database, the current work has attempted to model the Favre-filtered SDR and different unclosed terms of its transport equation in the context of LES for turbulent premixed flames with different non-dimensional parameters, which will be further elaborated in Chapters 5, 6 and 7. The models based on *a-priori* DNS analysis of simple chemistry DNS database are further assessed in detail chemistry DNS data in Chapter 7. The purpose of this chapter is firstly to demonstrate general numerical procedure behind DNS simulation and secondly to provide description of both simple and detailed chemistry DNS databases used for the a-priori analysis conducted in this thesis. The filtering operation and the filtered scalar field of both sets of DNS database are provided.

4.1 DNS in turbulent combustion

Recent significant development in computational power has established DNS as a precise numerical technique of turbulent combustion research. However, the computational cost of DNS is still too high for simulating industrial combustors. In addition, the information provided by DNS may need further simplifications for research purpose to investigate the effects of a particular physiochemical element in isolation. Therefore, simplifications and assumptions of different levels are often made in DNS (Poinsot and Veynante, 2005). Another central issue for solving the governing partial differential equations (PDE) through DNS is the set-up of proper initial conditions and boundary conditions, which are deterministic to the PDE solutions. At the early stage of 1990s, when DNS as a simulation tool for combustion research just started up, the DNS was often restricted into two dimensional domains, where the vortex-stretching mechanism were inherently ignored. In the current work, both simple chemistry and detail chemistry fully compressible DNS databases are considered. The description of chemistry raises another main approximation in DNS. For the current analysis, the modelling of SDR and its transport is addressed using a-priori analysis of simple chemistry DNS database for different values of heat release parameter τ, global Lewis number Le and turbulent Reynolds number Re_t. Although, three dimensional DNS simulations with detail chemistry are now possible to

carry out, they involve several million CPU hours (Chen, 2009) and thus are not ideally suitable for a detailed parametric analysis. Furthermore, it is not convenient to analyse the effects of τ and Le in isolation using detailed chemistry DNS data because these effects are often interlinked in the context of detailed chemistry and transport. However, it is useful to assess the validity of the models proposed based on the analysis of simple chemistry DNS databases in the context of detailed chemistry and transport. Thus the models developed based on a-priori DNS analysis using simple chemistry DNS database are assessed again for detail chemistry DNS data in Chapter 8.

4.2 Spatial and temporal resolution

In the current work, DNS databased of both statistical planar flame and V-shape flames are considered. The relationship between the domain size and the mesh size of DNS for turbulent premixed flames are generally required to be:

- The simulation should carried out a domain size which accommodates a number of large scale (i.e. integral) eddies so that there are enough statistical independent samples within the domain.
- The mesh should be fine enough such that the turbulent flow are fully resolved, therefore the grid size is often smaller or comparable with Kolmogorov scales.
- The inner flame structure should be resolved by the mesh as well.

When the largest and smallest scales of turbulent motions are approximately addressed by the DNS grid, the turbulent flow is considered to be correctly resolved. Take a cubic domain with side of length L with N+1 grid points on it, leading to the grid size $\Delta x = L/N$. The largest spatial scales in turbulent flow is often considered as integral length scale l and the velocity field of turbulent flow is often characteristic by the large-scale velocity fluctuations u'. The smallest spatial scales of turbulent flow is considered as Kolmogorov length scale η. Therefore a relation is obtained to meet the above requirements as:

$$\frac{l}{N} \leq \Delta x \leq \eta \tag{4.1}$$

which ensures that the whole domain size is no smaller than integral length scale (i.e. $L \geq l$) and the Kolmogorov scale is resolved by the mesh. Based on the work of Kolmogorov (1941), it is known that for isotropic turbulence a relationship can be obtained for the turbulent cascading process as:

$$\eta \sim \frac{l}{(Re_t)^{3/4}} \tag{4.2}$$

Combining eqs. (4.1) and (4.2) reads:

$$N > \frac{l}{\eta} \approx (Re_t)^{3/4} \text{ or } Re_t < N^{4/3} \tag{4.3}$$

The inequalities shown in eq. (4.3) provides a direct relationship between the given turbulent Reynolds number Re_t and the required number of grid points N or the maximum achievable Re_t based on the number of grid points in each direction.

Another feature of DNS is the number of grids resolving the inner flame, which is often characterised by thermal flame thickness $\delta_{th} \equiv (T_{ad} - T_0)/\max|\nabla T|_L$. For simplified chemistry, at least ten grid points are required to resolve the flame structure. If the number of grid points resolving the flame brush is denoted as Q, then the size of domain can be expressed with respect to the flame thickness as:

$$L \approx \left(\frac{N}{Q}\right)\delta_{th} \tag{4.4}$$

Substituting $L \geq l$ into eq. (4.4) leads to:

$$\frac{l}{\delta_{th}} < \frac{L}{\delta_{th}} < \frac{N}{Q} \tag{4.5}$$

The flame is often characterised based on another flame thickness, known as Zel'dovich/diffusive flame thickness δ_Z, which can be expressed as:

$$\delta_Z \equiv \frac{\alpha_T}{S_L} \quad \frac{\nu}{S_L} \tag{4.6}$$

Thus, eq. (4.5) can be recast in terms of turbulent Reynolds number Re_t and Damköhler number Da as:

$$Re_t Da \sim \frac{l^2 S_L}{\upsilon \delta_z} \sim \left(\frac{l}{\delta_Z}\right)^2 \tag{4.7}$$

Another computational grid condition is obtained as :

$$Re_t Da < \left(\frac{N}{Q}\right)^2 \tag{4.8}$$

It worth noting that δ_Z is usually an approximation rather than an exact calculated values, however, the scaling argument $\delta_Z \quad \nu/S_L$ holds even under approximation, therefore eq. (4.8) is useful for defining the resolution of chemical scales considering the physical representation of Damköhler number is $Da = \tau_t/\tau_c$ whereas the resolution of turbulence structure is limited in terms of turbulent Reynolds number Re_t by eq. (4.3).

Temporal resolution is another important requirement for DNS, which affects the computational cost directly. The time step Δt and the number of time steps required of DNS are determined based on two time scales: Kolmogorov time scale τ_η and large eddy turn over time scale which is often defined based on integral length scale as $\tau_t = l/u'$. In order to resolve the flame structure in temporal space as well, the time step Δt is required to meet the following relation:

$$\Delta t \le \tau_\eta \text{ or } \Delta t \le \left(\frac{\nu}{\varepsilon}\right)^{1/2} \tag{4.9}$$

Another criterion of time step Δt is prescribed by Courant-Friedrichs-Lewy (CFL) condition which restricts the travel distance of acoustic wave *a* in unit time step Δt within unit grid size Δx as:

$$C = \frac{|u' \pm a|\,\Delta t}{\Delta x} \le 1 \tag{4.10}$$

Equation (4.10) can be recast to determine the maximum allowable time step size as:

$$\Delta t \le \frac{\Delta x}{|u' \pm a|} \tag{4.11}$$

where *C* is the CFL number, which has been suggested to be around $C \approx 1/20$ in practice to ensure the acoustic wave only travels a fraction of the unit grid in one time step Δt (Pope, 2000).

4.3 Discretisation: DNS domain setup

4.3.1 Statistically planar turbulent premixed flames

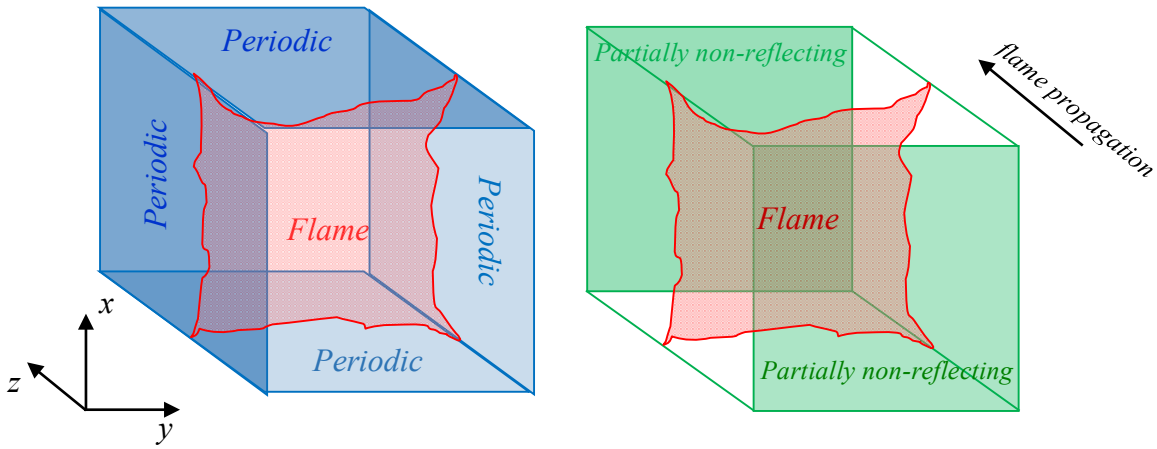

Figure 4.1: Description of computational domain for statistically turbulent premixed flames for both simple and detail chemistry DNS.

The statistically planar flames of turbulent premixed combustion with simplified one-step chemistry was generated by a three dimensional compressible DNS code SENGA (Jenkins and Cant, 1999), in order to investigate the effects of non-dimensional numbers such as Lewis number Le (0.34-1.2), heat release parameter τ (2.0-6.0) and turbulent Reynolds number Re_t (22.0-110.0) on Favre-averaged SDR and its transport equation characterised for different LES filter widths Δ. An updated version of SENGA code: SENGA2 (Cant, 2012) was used to generate the DNS solution for a detailed turbulent methane-air premixed flames, which is post-processed here for the assessment of the modelling of SDR and its transport equation in the context of detail chemistry and transport. A schematic diagram of the above two DNS databases is shown in Fig. 4.1, where the DNS domain is considered to be a rectangular box with the flame propagating in the negative x-direction. The boundary condition in the direction of main flame propagation is chosen to be partially non-reflecting and are specified according to the Navier-Stokes Characteristic Boundary Condition (NSCBC) formalism in conjunction with Local One-Dimensional Inviscid (LODI) approximation (Poinsot and Lele, 1992; Jenkins and Cant, 1999). The transverse boundaries are chosen to be periodic to reduce the computational complexity.

Numerical scheme of high accuracy is essential for DNS of turbulent combustion. In the above DNS solutions, a 10^{th} order central-difference scheme is used to evaluate spatial derivatives at the internal grid points as:

$$f_i^{'} = \sum_{j=1}^{j=m/2} \frac{a_j}{2jh}(f_{i+j} - f_{i-j}) \tag{4.12}$$

where m is the order of the approximation which is always even for a central difference scheme. Values of the constants a_j are obtained by Taylor expansion and equating coefficients of successive orders in h (Jenkins and Cant, 1999). A stencil width of eleven points is demanded for explicitly 10^{th} order central difference scheme to ensure 5 grid points in each directions, which is feasible only at the inner grid points, whereas boundary points are treated with explicit finite differences of decreasing order of accuracy as the boundary is approached. The order of differentiation gradually drops to a one-sided 4^{th} order scheme near non-periodic boundaries. The time-advancement is carried out using a 3^{rd} order low storage Runge-Kutta scheme (Wray, 1990). One does not obtain any spurious fluctuations due to the 10^{th} order central difference scheme and its transition to the lower-order finite difference scheme for sufficiently small grid spacing (e.g. $\Delta x \leq \eta$ where Δx and η are the grid spacing and the Kolmogorov length scale respectively). Thus it was not necessary to use numerical filter to eliminate spurious oscillations. For detail chemistry database, the methane-air combustion is simulated based on a skeletal mechanism consisting of 16 species and 36 elementary reactions (Smooke, 1991).

The initial velocity field of both simple and detail chemistry DNS databases were generated under the continuity constraint of incompressible flow (i.e. $\nabla.\vec{u} = 0$) in spectral space where the turbulent kinetic energy spectrum $E(\kappa)$, with κ being the wave number magnitude in the Fourier space, has been specified according to Bachelor and Townsend (1948). A standard pseudo-spectral method has been used to generate the initial turbulent velocity field (Rogallo, 1981), whereas an unstrained planar steady laminar premixed flame solution has been used to initialise the flame.

The simple chemistry DNS database consists of thirteen cases for the purpose of an extensive parametric analysis which is in turn used for developing algebraic and transport equation based SDR closure. The initial parameters of these thirteen cases are set in such a manner that the effects of Lewis number Le (0.34-1.2), heat release parameter τ (2.0-

6.0) and turbulent Reynolds number Re_t (22.0-110.0) can be investigated independently of each other. Table 4.1 lists the initial values of the important simulation parameters for the simply chemistry DNS database, which are the normalised rms velocity fluctuation u'/S_L, normalised integral length scale l/δ_{th}, turbulent Reynolds number Re_t, Damköhler number *Da*, Karlovitz number *Ka*, heat release parameter τ and the global Lewis number *Le*. Standard values are taken for the Prandtl number (i.e. $\mathrm{Pr} = 0.7$), ratio of specific heat capacities (i.e. $\gamma = C_P / C_V = 1.4$) and the Zel'dovich number (i.e. $\beta = T_{ac}(T_{ad} - T_0)/T_{ad}^2 = 6.0$) where T_{ac} is the activation temperature. The computational domain is taken to be a cube of size $24.1\delta_{th} \times 24.1\delta_{th} \times 24.1\delta_{th}$ for cases A-E and cases K-M, which has been discretised with a uniform Cartesian grid of $230 \times 230 \times 230$, with about 10 grid points kept within δ_{th} for all cases considered here.

Case	u'/S_L	l/δ_{th}	Re_t	*Da*	*Ka*	τ	*Le*
A	7.5	2.45	47.0	0.33	13.2	4.5	0.34
B	7.5	2.45	47.0	0.33	13.2	4.5	0.6
C	7.5	2.45	47.0	0.33	13.2	4.5	0.8
D	7.5	2.45	47.0	0.33	13.2	4.5	1.0
E	7.5	2.45	47.0	0.33	13.2	4.5	1.2
F	5.0	1.67	22.0	0.33	8.67	4.5	1.0
G	6.25	1.44	23.5	0.23	13.0	4.5	1.0
H	7.5	2.50	48.0	0.33	13.0	4.5	1.0
I	9.0	4.31	100	0.48	13.0	4.5	1.0
J	11.25	3.75	110	0.33	19.5	4.5	1.0
K	7.5	2.45	47.0	0.33	13.2	2.0	1.0
L	7.5	2.45	47.0	0.33	13.2	3.0	1.0
M	7.5	2.45	47.0	0.33	13.2	6.0	1.0

Table 4.1: Initial parameters for simple chemistry DNS database

It can be seen from Table 4.1 that the value of *Le* number changes from 0.34 to 1.2 in cases A-E, but all remaining parameters are kept identical and thus the effects of *Le* can be investigated independently of other parameters using these cases. The three dimensional field of progress variable *c* ranging 0.1 to 0.9 at $t_c = \delta_{th}/S_L$ is shown for cases A-E in Figure 4.1. It is evident from Fig. 4.1 that the flame is wrinkled by the turbulence and the extent of flame wrinkling increases with decreasing *Le*, which will be explained in detail in the following subsection.

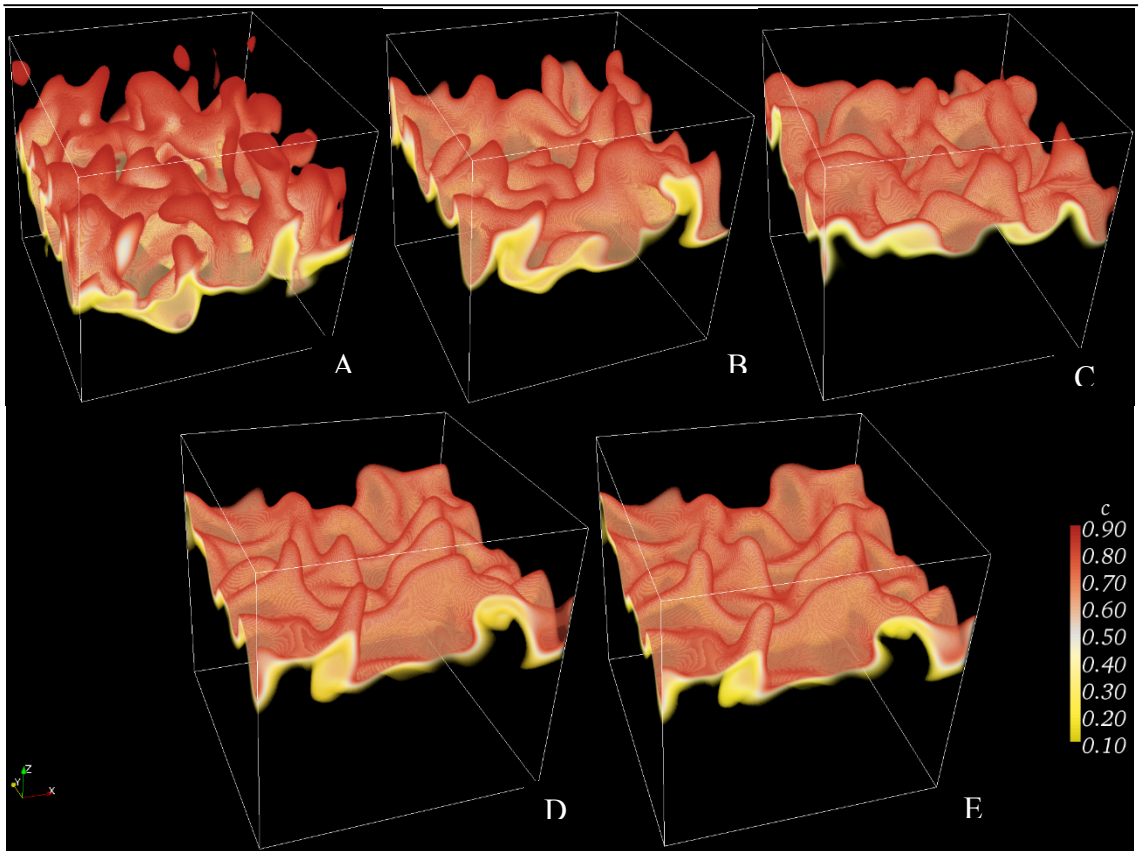

Figure 4.2: Instantaneous field of 0.1 < c < 0.9 isosurfaces at $t_c = \delta_{th}/S_L$ for cases A-E.

Cases F-J are generated by changing *Da* (cases G-I) and *Ka* (cases F, H, J) independently of each other to bring about the change in Re_t from 22.0 to 110.0 as Re_t scales as $\mathrm{Re}_t \sim Da^2 Ka^2$ (Peters, 2000). The computational domain for cases F-J is considered to be a rectangular parallelepiped of size $36.1\delta_{th} \times 24.1\delta_{th} \times 24.1\delta_{th}$, which has been discretised with a uniform Cartesian grid of $345 \times 230 \times 230$, with about 10 grid points kept within δ_{th} for all cases considered here. The Instantaneous view of 0.01< c <0.99 isosurfaces at $t_c = \delta_{th}/S_L$ for cases F-J are shown in Fig. 4.3, which demonstrates that the extent of wrinkling of the flame surface increases considerably with increasing turbulence intensity u'/S_L. The cases D, K-M share identical parameters except the heat release parameter τ. It worth noting that for the cases, which are used to analyse the effects of τ and Re_t, Lewis number is kept as unity.

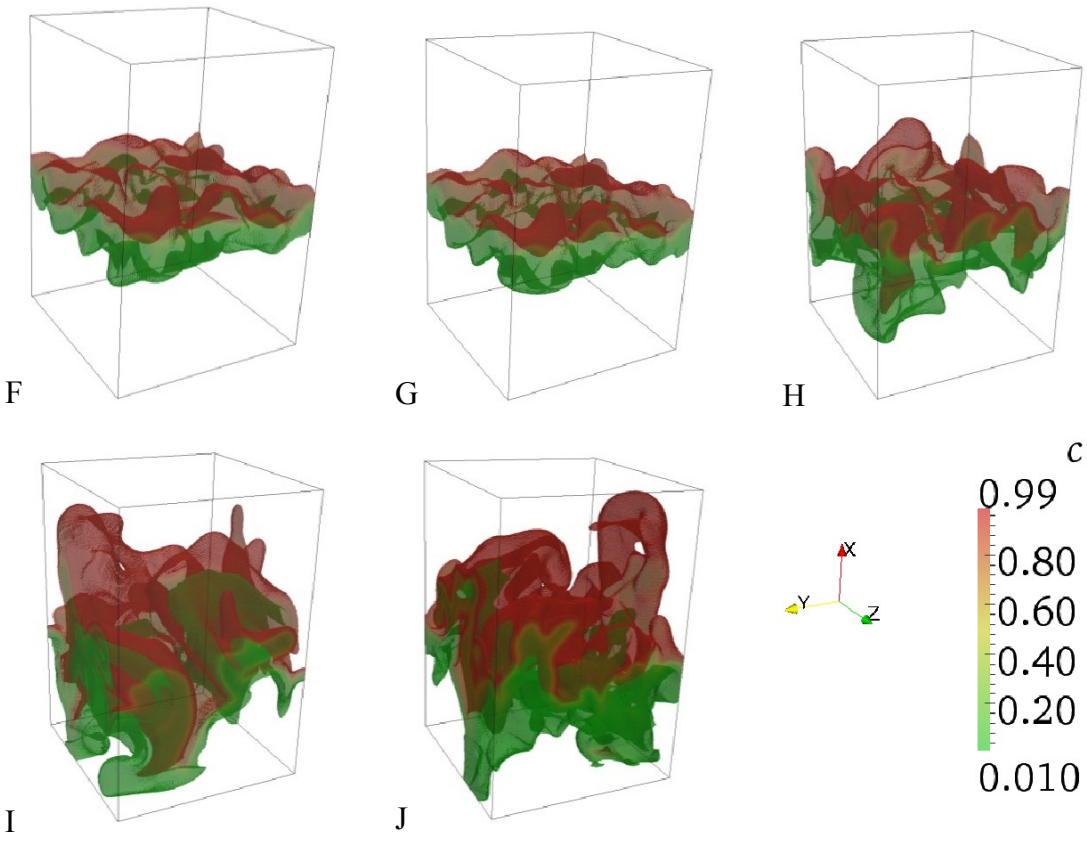

Figure 4.3: Instantaneous field of 0.01 < c < 0.99 isosurfaces at $\tau_c = \delta_{th}/S_L$ for cases F-J.

In all simple chemistry cases flame-turbulence interaction takes place under decaying turbulence, which necessitates the simulation time $\tau_{sim} \geq Max(\tau_f, \tau_c)$, where $\tau_f = l/u'$ is the initial eddy turn over time and $\tau_c = \delta_{th}/S_L$ is the chemical time scale. In all cases statistics were extracted after one chemical time scale τ_c. Chemical time scale τ_c corresponds to a time equal to $3.0\tau_f$ in cases A-E (where *Le* number differs), cases F, H and J (where *Ka* is varied) and cases K-M (where τ varies), $2.0\tau_f$ in case I and $4.34\tau_f$ for case H respectively. It is worth noting that the thermo-chemical parameters for the cases are chosen in such a manner that chemical time scale τ_c remains the same for all cases. The present simulation time is comparable to several previous DNS studies (Boger *et al.,* 1998; Charlette *et al.,* 2002a,b; Swaminathan and Bray, 2005; Swaminathan and Grout, 2006; Grout, 2007; Han and Huh, 2008,2009; Reddy and Abraham, 2012), which have contributed significantly to the fundamental understanding and modelling of the turbulent premixed combustion. By the time the statistics were extracted, the global turbulent kinetic energy and its dissipation rate in the unburned gas ahead of the flame were no longer changing rapidly with time. The global level of turbulent velocity fluctuation had decayed by about 50%, 52.66%, 61.11%, 45%, 24% and 34% in

comparison to the initial values for cases A-E and K-M, F, G, H, I and J respectively. By contrast, the integral length scale increased by factors 1.5 to 2.25 for cases A-M, ensuring that sufficient numbers of turbulent eddies were retained in each direction to obtain useful statistics. It worth noting that *Ka* remains larger than unity and the thermal flame thickness δ_{th} is greater than the Kolmogorov length scale η at the time of analysis, suggesting that combustion takes place in the thin reaction zones regime for all the cases here (Peters, 2000). The DNS cases considered here have been used extensively in several previous publications (Chakraborty *et al*., 2009; Chakraborty and Swaminathan, 2010, 2011, 2013; Chakraborty and Cant, 2009a-c, 2011, 2013; Chakraborty *et al*., 2011b-d; Chakraborty and Lipatnikov, 2013a,b) to analyse different aspects of turbulent premixed combustion and interested readers are referred to these publications for further information regarding these cases and for the conditions under which statistics were extracted.

4.3.2 Turbulent V-flames

Three detailed chemistry DNS cases of turbulent premixed V-flames of stoichiometric hydrogen air mixture at 0.1 MPa have been post-processed here. These cases consider 27 elementary reactions involving 12 reactive species (H_2, O_2, H_2O, O, H, OH, HO_2, H_2O_2, N_2, N, NO_2, and NO) (Minamoto et al., 2011). CHEMKIN-II package have been used to calculate the temperature dependence of the viscosity, thermal conductivity, and diffusion coefficients (Kee et al., 1986, 1989). The diffusion velocity was modelled based on Fickian type diffusion with the diffusion effects of Soret, Dufour, and pressure gradient neglected. The unburnt reactant temperature is set to 700K for all these flames. A third-order low storage Runge-Kutta method was used for time advance on the uniform grid mesh. The reaction terms are implicitly dealt with by using point implicit method.

Figure 4.4 shows a schematic of the V-flame DNS configuration. The turbulent flame is anchored through a hot rod which is positioned at a distance of about 2.5 to 5mm away from the inflow boundary with a diameter $d \approx \delta_{th}$. The temperature inside the rod is fixed at $T_{rod} = 2000K$. The velocity of the grid points on the rod are set to be zero and the mass fraction of these grid points are given the value of the mass fraction of the corresponding species in the burned gas $Y_{i,rod} = Y_{i,b}$, which subsequently creates a region of discontinuity for the values of velocities and mass fractions. In order to resume the continuity of the simulation grids, a Gaussian function *G* has been applied to the turbulent velocity field and scalar field (temperature and species mass fractions) which is expressed as:

$$G(r,t=0)=(G_{rod}-G_{\infty})\exp\left[\frac{(r-r_w)^2}{2r_w^2}\right]+G_{\infty} \tag{4.13}$$

where G can denote flow velocity components, temperature or species mass fractions, r is the radial distance from the centre of the rod. $r_w = d/2$ denotes the radius of the rod and the subscript "∞" denotes the free stream value which is equal to the values at inflow boundary, where the fluid velocity u is assumed to be a sum of an average velocity $U_{av} = (u_{av}, 0, 0)$ and the inlet turbulent velocity fluctuation u'_{in} which was obtained from an incompressible turbulent flow solution, as $u = U_{av} + u'_{in}$. The simulation has run for 3 flow through time $\tau_D = L_x / u_{av}$ after initialisation, where L_x is the length of the domain in main flow stream direction (see Fig. 4.4). The simulation parameters for turbulent V-flames post-processed are listed in Table 4.3.

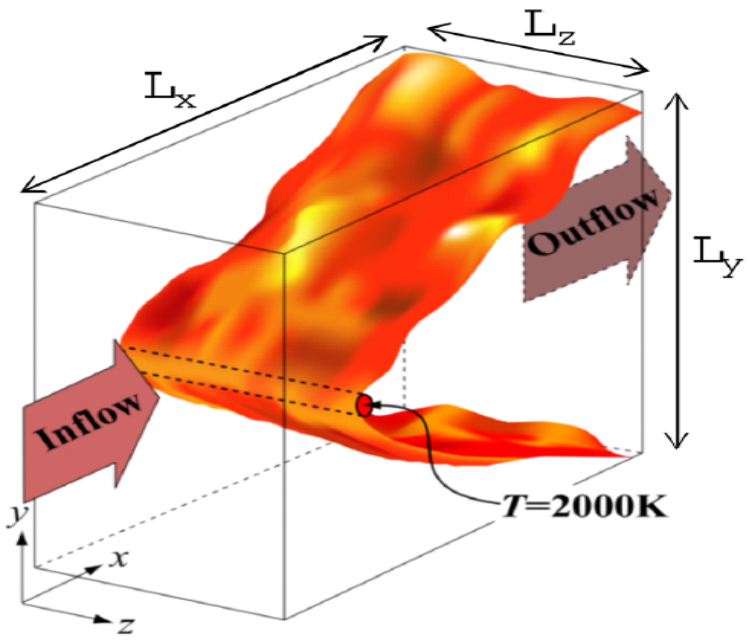

Figure 4.4: Schematic diagram of the V-shape flame DNS domain.

Case	u'/S_L	u_{av}/S_L	l/δ_{th}	Re_t	Da	Ka
V	2.2	10	1.6	60.8	0.73	1.3

Table 4.2: Initial conditions of V-shape flames based on inflow turbulence characteristics

The computational domain of case V is given in Table 4.4 below.

Case	Domain size (mm)	Grid size
V	10×5×5	513×257×257

Table 4.3: Domain configurations of V-shape flames

The grid spacing of the three V-shape flame cases ensures that the thermal flame thickness δ_{th} is resolved by no less than 20 grids. The boundary layers near the rod are also resolved by the computational grid as well. The x-directions are taken to be inlet and outlet, whereas outflow boundaries are considered for y-direction boundaries. The NSCBC technique is used to specify inflow and outflow boundaries. The boundaries in Z-direction are considered to be periodic.

4.3.3 Effects of Lewis number Le

The instantaneous views of reaction progress variable isosurfaces corresponding to $0.1 \leq c \leq 0.9$ at $t = t_c = \delta_{th} / S_L$ and c field at the central x_1 - x_2 plane of the DNS domain after three eddy turn over time for cases A-E are shown in Figs. 4.1 and 4.5 respectively. Figure 4.5 shows that the level of flame wrinkling increases significantly with decreasing Le, which is consistent with several previous analyses (Chakraborty and Cant, 2011; Sivashinsky, 1977; Clavin, and Williams, 1982). The extent of the augmentation of flame wrinkling with decreasing Lewis number can be quantified from the values of normalised turbulent flame surface area A_T / A_L, which are presented in Table 4.4, where flame surface area A is evaluated using the volume integral:

$$A = \int_V |\nabla c| \, dV \tag{4.14}$$

and the subscripts 'T' and 'L' are used to refer to turbulent and laminar flame values respectively. An increase in flame wrinkling is reflected in the increase in burning rate in turbulent flames.

Case	Le	A_T / A_L	S_T / S_L
A	0.34	3.93	13.70
B	0.6	2.66	4.58
C	0.8	2.11	2.53
D	1.0	1.84	1.83
E	1.2	1.76	1.50

Table 4.4: The effects of Lewis number on normalised flame surface area A_T / A_L and normalised turbulent flame speed S_T / S_L when the statistics were extracted.

The extent of burning rate augmentation can be quantified from the values of the normalised turbulent burning velocity S_T / S_L, which for cases A-E are also presented in Table 4.4 where S_T is evaluated as:

$$S_T = \frac{1}{\rho_0 A_P} \int_V w dV \tag{4.15}$$

with A_P being the projected area in the direction of mean flame propagation. The values of A_T / A_L and S_T / S_L in Table 4.4 reveal that $(S_T / S_L) \approx (A_T / A_L)$ roughly holds only for the $Le = 1.0$ case but S_T / S_L assumes greater (smaller) values than A_T / A_L in the flames with $Le < 1$ ($Le > 1$).[1]

In the $Le < 1$ flames, the heat diffues at a slower rate than the rate at which fresh reactants diffuse into the reaction zone, which leads to the simultaneous presence of high temperature and reactant concentration, giving rise to faster flame propagation, higher extent of flame wrinkling, and greater burning rate than the unity Lewis number flame with statistically similar turbulence in the unburned gas.

The simultaneous presence of high temperature and reactants concentration in the reaction zone significantly increases the overall consumption rate of reactants per unit area in comparison to the corresponding laminar flame value for the flames with $Le < 1$. Higher rate of thermal diffusion from the reaction zone than the rate of diffusion of fresh reactants in the $Le > 1$ cases gives rise to simultaneous presence of low temperature and reactant concentration, which in turn leads to a reduction in the overall consumption rate of reactants per unit area in comparison to the corresponding laminar flame values.

[1] It has been found $S_T / S_L > A_T^t / A_L^t$ for $Le << 1.0$ flames even when the area A^t is evaluated as $A^t = \int_V |\nabla T| dV$ where $T = (\hat{T} - T_0) / (T_{ad} - T_0)$ is the non-dimensional temperature. However, $S_T / S_L \approx A_T^t / A_L^t$ is maintained for the globally adiabatic low Mach number $Le \approx 1.0$ flames.

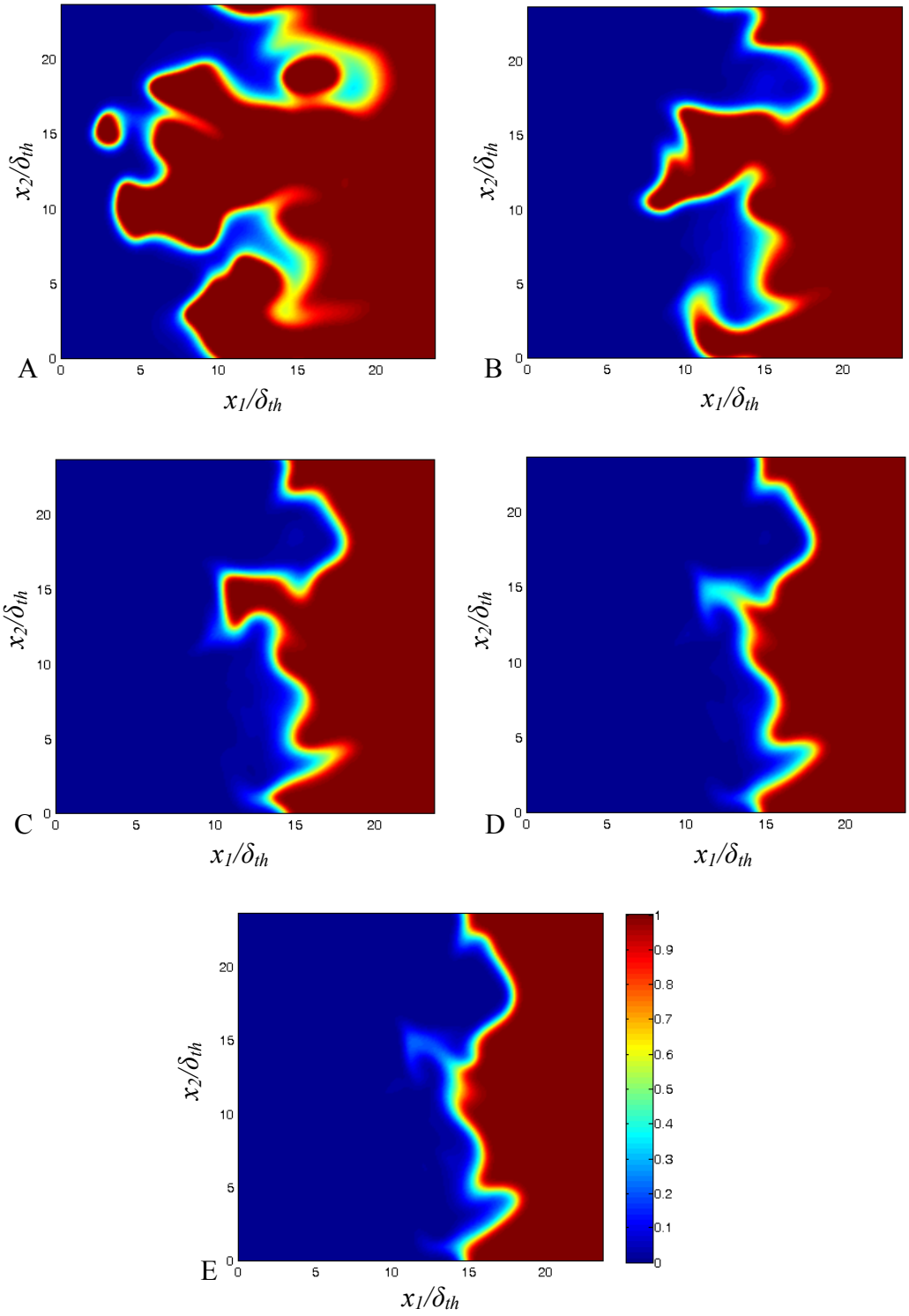

Figure 4.5: The reaction progress variable *c* field at the central x1 - x2 plane of the DNS domain after three eddy turn over time, for cases A-E.

This leads to $(S_T / S_L) < (A_T / A_L)$ in the $Le = 1.2$ case (i.e. case E) considered here (see Table 4.5). In the flamelet regime of combustion (Peters, 2000), the consumption rate of reactants per unit area remains similar to the laminar flame values for unity Lewis number flames, which gives rise to $(S_T / S_L) \approx (A_T / A_L)$ in case D. As the mean/filtered reaction

rate has been found to be directly proportional to density-weighted Favre-mean/Favre-filtered SDR (Bray, 1980) through BML approach (i.e. $\overline{\dot{w}} \propto \overline{\rho}\widetilde{N}_c$), the turbulent flame speed can be expressed as :

$$S_T \propto \frac{1}{\rho_0 A_P}\int_V (\overline{\rho} N_c) dV \tag{4.16}$$

Therefore the effects of Le on S_T / S_L and A_T / A_L are expected to be reflected in the statistical behaviour of the SDR transport.

4.3.4 Effects of turbulent Reynolds number Re_t

The contours of reaction progress variable in the central $x_1 - x_2$ plane for cases F-J are shown in Fig. 4.6, where the flame wrinkling increases with increasing u'/S_L, which can be explained through the scaling relation:

$$u'/S_L \sim \left(\frac{Re_t}{Da}\right)^{1/2} \sim Re_t^{1/4} Ka^{1/2} \tag{4.17}$$

The normalised turbulent flame speed S_T / S_L and normalised turbulent flame area A_T / A_L for cases F-J are listed in Table 4.6. This quantitatively demonstrates the augmentation of the flame surface area due to stronger turbulent wrinkling, leading to higher reaction rates. An increase in Re_t for a given value of *Da* leads to an increase in *Ka*, which separates the length scale between δ_{th} and η. Thus, turbulent eddies with sufficient energy are more likely to penetrate into the flame and distort the thermo-diffusive balance within the preheat zone for high values of *Ka.*

Case	Re_t	A_T / A_L	S_T / S_L
F	22.0	1.1	1.83
G	23.0	1.25	1.83
H	47.0	1.85	1.83
I	100.0	3.75	1.83
J	110.0	3.80	1.83

Table 4.5: The effects of turbulent Reynolds number Re_t on normalised flame surface area A_T / A_L and normalised turbulent flame speed S_T / S_L when the statistics were extracted.

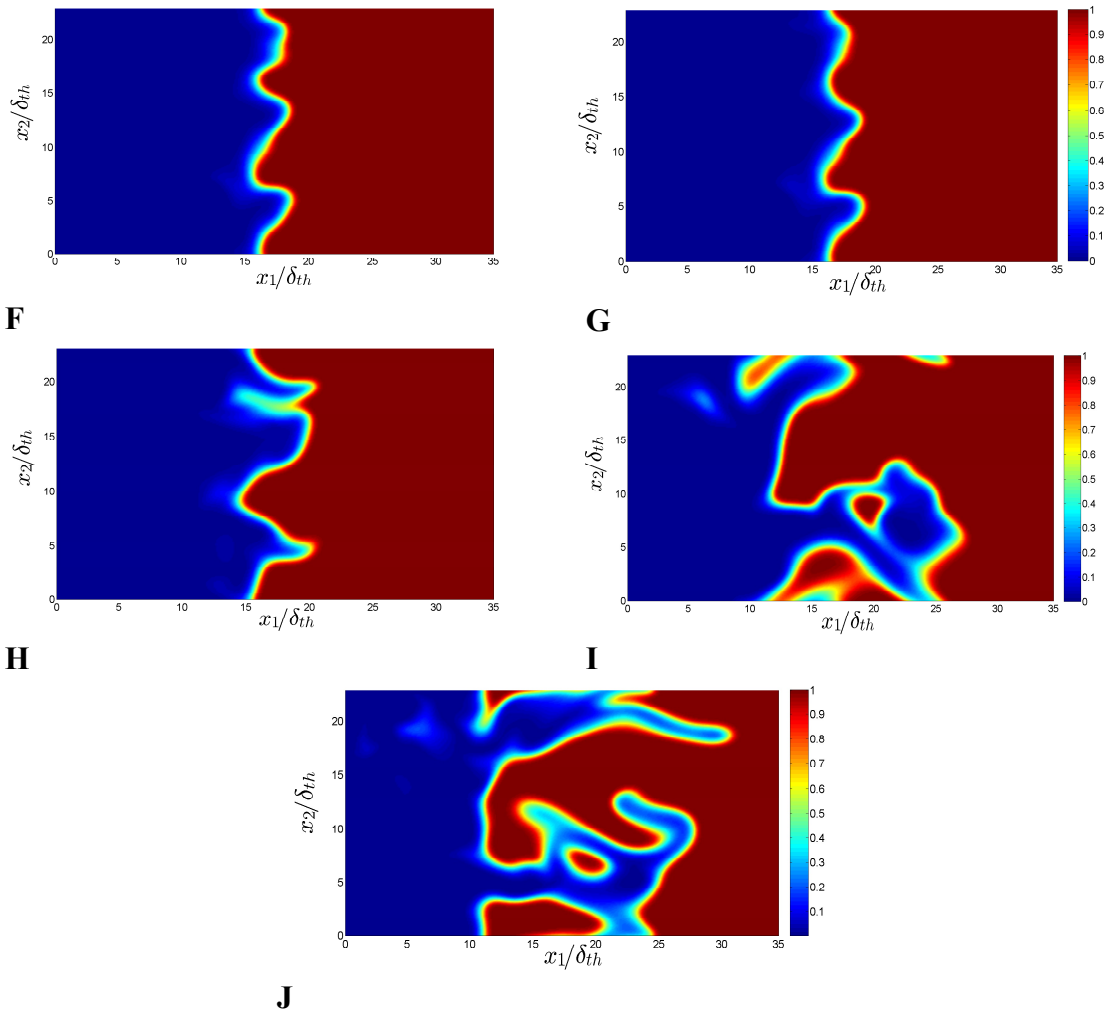

Figure 4.6: Contours of c in the central $x_1 - x_2$ plane for cases F-J at $t_c = \delta_{th} / S_L$.

Case	τ	A_T / A_L	S_T / S_L
K	2.0	2.04	2.01
L	3.0	1.95	1.92
D	4.5	1.84	1.83
M	6.0	1.74	1.76

Table 4.6: The effects of heat release parameter τ on normalised flame surface area A_T / A_L and normalised turbulent flame speed S_T / S_L when the statistics were extracted.

4.3.5 Effects of heat release parameter τ

The heat release parameter τ characterises the temperature increase with respect with the initial temperature or temperature of the unburnt reactants. It is shown in Table 4.6 that an increase in heat release parameter τ will lead to a slight decrease in both S_T / S_L and A_T / A_L. The scalar gradient is expected to increase with decreasing τ, which will enhance

the dilatational effects of smoothing the wrinkled flame surface (Chakraborty and Cant, 2006).

4.4 Summary

In this chapter the governing equations and the underlying assumptions of the DNS databases were mentioned. These assumptions for the simple chemistry DNS databse are that the reaction mechanism was determined by a single step irreversible Arrhenius rate law, whereby allowing for the species held to be represented using a reaction progress variable, which is based on the product mass fraction. Additionally, the diffusion velocities was accounted for by using Fick's law. In the following chapter the reaction rate closure based on SDR in the context of LES will be introduced with a brief discussion of the modelling strategy for SDR based reaction rate closure.

Chapter 5. Reaction rate closure for LES: SDR approach

SDR based reaction rate closure in the context of RANS has been introduced in detail in Chapter 2, where the Reynolds averaged chemical reaction rate can be seen to be modelled directly by the unresolved SDR. The model has been recast for the purpose of LES recently (Dunstan *et al.*, 2013) based on *a-priori* DNS analysis of a single database turbulent premixed V-flame, which was introduced in Section 3.4. The SDR based reaction rate closure (eq. 2.30) for LES was reported to capture the filtered reaction rate closure for filter widths much larger than thermal flame thickness but cannot capture the local behaviours for relatively small filter widths, where further investigation and improvement are required. Therefore, in this chapter, the relationship between filtered chemical reaction rate and the filtered SDR for different filter widths will be discussed based on the explicitly filtered DNS data for different values of heat release parameter τ, Lewis number *Le* and turbulent Reynolds number Re_t. The modelling assumptions will be elaborated from a statistical perspective in Sections 5.2 & 5.3, based on which a new reaction rate closure for LES using SDR approach of turbulent premixed combustion will be introduced in Section 5.4.

5.1 Assessment of SDR based reaction rate closure for LES

A recent *a-priori* DNS analysis (Dunstan *et al.*, 2013) assessed the SDR based reaction rate closure which was originally proposed for RANS (i.e. eq. (2.30)) in the context of LES. The reaction rate model expression analysed by Dunstan *et al*. (2013) is given here as the original expression proposed by Bray (1979) was in the context of RANS:

$$\overline{\dot{w}} = \frac{2\overline{\rho}\tilde{N}_c}{2c_m - 1} \tag{5.1}$$

where $\tilde{q}$ indicates Favre filtered value of a general quantity q and the $\overline{q}$ indicates a simple LES filtering operation. Eq. (5.1) was reported to remain valid for $\Delta >> \delta_{th}$ based on a single V-shape flame DNS database with $Le = 1.0$ and the effects of heat release

parameter τ and turbulent Reynolds number Re_t on the applicability of eq. (5.1) was not considered.

The above analysis is extended here by assessing eq. (5.1) with an DNS database of a range of different values of global Lewis number Le, heat release parameter τ and turbulent Reynolds number Re_t.

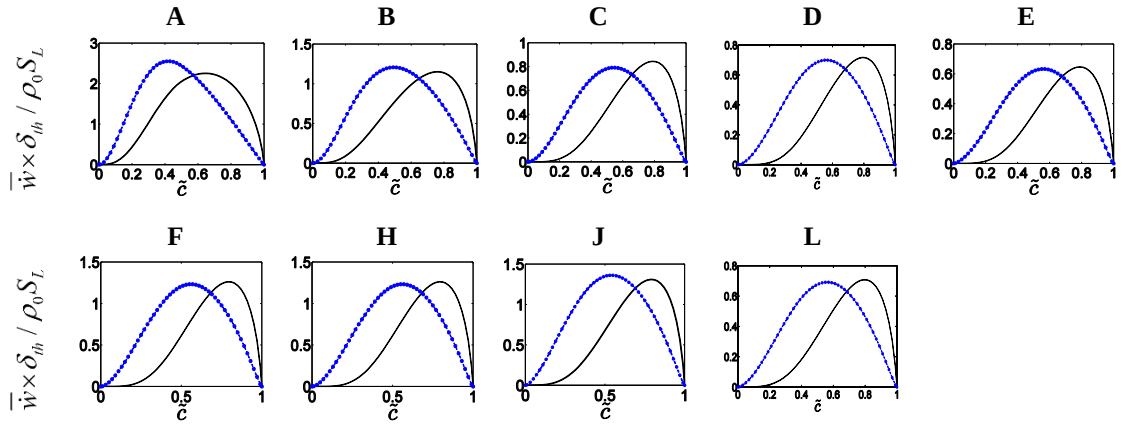

Figure 5.1: Variation of mean values of normalised reaction rate $\overline{\dot{w}}^{+}$ (———), normalised SDR based closure $\overline{\dot{w}}^{+}_{\mathrm{mod}}$ (-·-·-) conditional on $\tilde{c}$ across the flame brush at $\Delta \approx 0.8\delta_{th}$ for cases A-E, F, H, J and K.

The variations of the normalised filtered reaction rate $\overline{\dot{w}}^{+} = \overline{\dot{w}} \times \delta_{th} / \rho_0 S_L$ and the prediction given by eq. (5.1) $\overline{\dot{w}}^{+}_{model} = 2\bar{\rho}\tilde{N}_c / (2c_m - 1) \times \delta_{th} / \rho_0 S_L$ conditional on $\tilde{c}$ values at $\Delta \approx 0.8\delta_{th}$ and $\Delta \approx 2.8\delta_{th}$ in cases A-J and L are shown in Figs. 5.1 and 5.2 respectively, which show that $\overline{\dot{w}}^{+}_{model}$ does not adequately predict $\overline{\dot{w}}^{+}$ for $\Delta < \delta_{th}$, but satisfactorily predicts $\overline{\dot{w}}^{+}$ for $\Delta > \delta_{th}$.

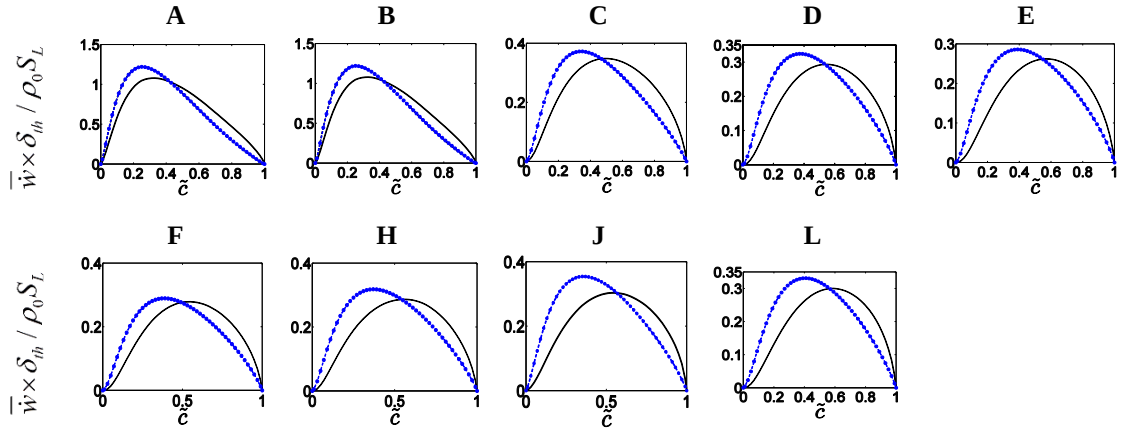

Figure 5.2: Variation of mean values of normalised reaction rate $\overline{\dot{w}}^{+}$ (———), normalised SDR based closure $\overline{\dot{w}}^{+}_{\mathrm{mod}}$ (-·-·-) conditional on $\tilde{c}$ across the flame brush at $\Delta \approx 2.8\delta_{th}$ for cases A-E, F, H, J and K.

Since the cases G and I are qualitatively similar to cases F and J, the results of these two cases are not shown in Figs. 5.1 and 5.2 and in subsequent figures. Figures 5.1 and 5.2 show that the agreement between the normalised reaction rates obtained form DNS and SDR based closure (i.e. $\overline{\dot{w}}^{+}$ and $\overline{\dot{w}}^{+}_{model}$) improves with increasing Δ, which is consistent with the previous findings (Dunstan *et al*., 2013). The SDR closure eq. (5.1) was proposed based on two major assumptions (Bray, 1979):

1. Fast chemical reaction: $Da >> 1$
2. Presumed bi-modal probability density function of c with impulses at $c = 0$ and $c = 1$

According to the above assumptions, the probability of finding burning mixtures is negligible, and it needs to be assessed if such an assumption is valid within the sub-filter volume. The above assumptions are assessed in the following sub-sections.

The above observation has been explained by showing the pdf of c at a given iso-surface, where the assumption of bi-modal pdf was found invoked for filter width close $\Delta \approx \delta_{th}$ and smaller than thermal flame thickness $\Delta < \delta_{th}$. Although LES will leave the premixed flame brush unresolved as a sub-grid phenomenon, where filter size $\Delta > \delta_{th}$, the above mismatch requires further investigation and simultaneously the behaviour of eq. (2.30) is subject to improvement in order to smoothly transfer the well behaved reaction rate closure in RANS eq.(3.45) into a LES feasible form.

5.2 Sub-grid Damköhler number for different filter widths

For the assessment of an LES model, the sub-grid/local Damköhler number Da_{Δ} is more relevant than the global Damköhler number Da. The sub-grid Damköhler number Da_{Δ} can be defined as:

$$Da_{\Delta} \equiv \frac{\Delta S_L}{u'_{\Delta}\delta_{th}} \tag{5.2}$$

where u'_{Δ} is sub-grid turbulent velocity fluctuation and can be defined based on sub-grid turbulent kinetic energy k_{sg} in the following manner:

$$u'_{\Delta} = \sqrt{2k_{sg}/3}\,, \text{ where } k_{sg} = \frac{1}{2}\left(\frac{\overline{\rho u_i u_i}}{\bar{\rho}} - \tilde{u}_i\tilde{u}_i\right) \tag{5.3}$$

where u_i denotes the i^{th} component of the velocity vector. It worth noting that u'_{Δ} can be explicitly calculated by post-processing DNS database as done here, but it requires modelling in actual LES.

The variations of Da_{Δ} conditional on $\tilde{c}$ values for filter widths ranging from $\Delta \approx 0.4\delta_{th}$ to $\Delta \approx 2.8\delta_{th}$ are shown in Fig. 5.3 for cases A-F, H, J and L. It can be seen from Fig. 5.3 that Da_{Δ} increases with increasing filter width Δ for all cases, which justifies the observed mismatch between $\overline{\dot{w}}^{+}$ and $\overline{\dot{w}}^{+}_{model}$ for $\Delta \leq \delta_{th}$ filter widths comparable or smaller than thermal flame thickness, as the assumption of $Da >> 1$ is not maintained.

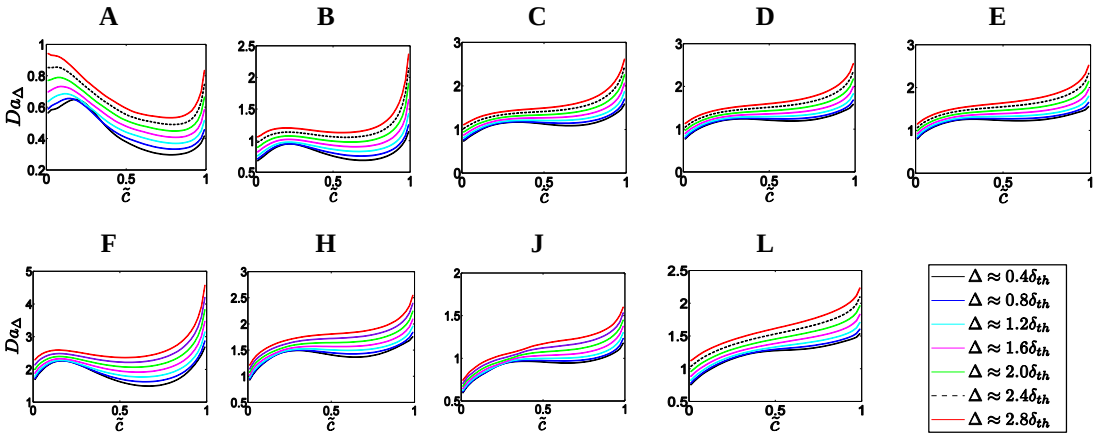

Figure 5.3: Variation of Da_{Δ} at filter widths ranging from $\Delta \approx 0.4\delta_{th}$ up towards $\Delta \approx 2.8\delta_{th}$ for cases A-E, F, H, J and K.

5.3 Validity of presumed probability density function of reaction progress variable

The pdfs of c within the filter volume corresponding to $\tilde{c} = 0.5$ are shown in Figs. 5.4a and 5.4b for $\Delta \approx 0.8\delta_{th}$ and $\Delta \approx 2.8\delta_{th}$ respectively. It can be observed from the pdf profile that the for small filter width (i.e. $\Delta \approx 0.8\delta_{th}$), there exists considerable probability to find $c \approx \tilde{c} \approx 0.5$, which represents burning mixtures. Although the pdf of c does not become bi-modal with increasing Δ, the probability of finding $c \neq \tilde{c}$ increases with increasing Δ (compare Figs 5.4a and b for $\Delta \approx 0.8\delta_{th}$ and $\Delta \approx 2.8\delta_{th}$). Therefore, the second assumption is likely to be invalid in the context of LES for filter widths $\Delta \leq \delta_{th}$.

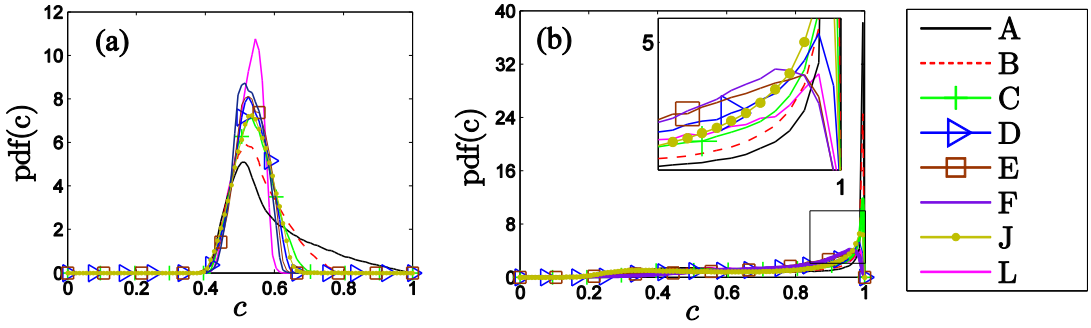

Figure 5.4: Pdfs of c at $\tilde{c}=0.5$ within the filter volume for (a) $\Delta \approx 0.8\delta_{th}$ and (b) $\Delta \approx 2.8\delta_{th}$ for cases A-F, H, J and L.

Figures 5.3 and 5.4 together demonstrate that the probability of finding $c \neq \tilde{c}$ within the filter volume increases significantly with increasing Δ and Da_{Δ}, which subsequently improves the agreement between the normalised reaction rates obtained from DNS and the SDR based closure (i.e. $\overline{\dot{w}}^{+}$ and $\overline{\dot{w}}^{+}_{model}$) as shown in Figs. 5.1 and 5.2. This observation is found to be consistent with previous findings by Dunstan *et al.* (2013). Therefore, the behaviours of eq. (5.1) for small filter widths (i.e. $\Delta \leq \delta_{th}$). It worth noting that in most practical LES, Δ often assumes greater values than the largest filter width used here (i.e. $\Delta > 2.8\delta_{th}$), where eq. (5.1) remain valid for the closure of $\overline{\dot{w}}$ according to Figs 5.1 and 5.2, provided $\tilde{N}_c$ is appropriately modelled.

5.4 A new reaction rate closure using SDR approach

In order to improve the prediction of $\overline{\dot{w}}$ for $\Delta \leq \delta_{th}$ as well as satisfying the limiting condition given by: $\lim_{\Delta \to 0} \overline{\dot{w}} = \dot{w}$, a modified closure for $\overline{\dot{w}}$ in the context of LES is proposed as:

$$\overline{\dot{w}} = f_1(\bar{\rho},\tilde{c},\tilde{T})\exp\left(-\varphi\frac{\Delta}{\delta_{th}}\right)+\left[1-\exp\left(-\varphi\frac{\Delta}{\delta_{th}}\right)\right]\frac{2\bar{\rho}\tilde{N}_c}{(2c_m-1)} \tag{5.4}$$

where the model parameter φ is given by:

$$\varphi = 0.56\frac{\delta_L}{\delta_Z} \tag{5.5}$$

where $\delta_L = 1/\max\left|\nabla c\right|_L$ is an alternative flame thickness defined based on reaction progress variable *c*. It can be shown that

- $\delta_L = \delta_{th}$ for flames with $Le = 1.0$,
- $\delta_L > \delta_{th}$ for flames with $Le < 1$,
- $\delta_L < \delta_{th}$ for flames with $Le > 1$.

In the new model (i.e. eq. (5.4)), f_1 is a function which follows the Arrhenius law of chemical reaction rate (i.e. eq. (2.9)) but is based on the filtered density $\bar{\rho}$, filtered reaction progress variable $\tilde{c}$ and filtered temperature $\tilde{T}$ in the following manner:

$$f_1(\bar{\rho},\tilde{c},\tilde{T}) = B\bar{\rho}(1-\tilde{c})\exp\left[-\frac{\beta(1-\tilde{T})}{1-\alpha(1-\tilde{T})}\right] \tag{5.6}$$

which ensures that

$$\lim_{\Delta\to 0} f_1(\bar{\rho},\tilde{c},\tilde{T}) = f(\rho,c,T) = B\rho(1-c)\exp\left[-\frac{\beta(1-T)}{1-\alpha(1-T)}\right] = \dot{w} \tag{5.7}$$

where $T = \left(\hat{T} - T_0\right)\Big/\left(T_{ad} - T_0\right)$ is the non-dimensional temperature, $\alpha = \tau\big/\left(1+\tau\right)$ is a heat release parameter and $B = B^* \exp\left(-\beta/\alpha\right)$ with B being the pre-exponential factor. For multi-step chemistry, the reaction progress variable c can be defined in terms of a suitable reactant mass fraction Y_R or product mass fraction Y_P of a species which is closely related to the chemical heat release as:

$$c = \frac{Y_{R0} - Y_R}{Y_{R0} - Y_{R\infty}} \text{ or } c = \frac{Y_P - Y_{P0}}{Y_{P\infty} - Y_{P0}} \tag{5.8}$$

Thus the overall reaction rate can be defined as

$$\dot{w} = -\frac{\dot{w}_R}{Y_{R0} - Y_{R\infty}} \text{ or } \dot{w} = \frac{\dot{w}_P}{Y_{P\infty} - Y_{P0}} \tag{5.9}$$

where $\dot{w}_R$ and $\dot{w}_P$ are the reaction rate of the reacting species and product species based on which the progress variable is defined respectively, which can be expressed as: $\dot{w} = f_1(\rho,\hat{T},[q])$ where $[q] = [Y_1, Y_2, ..., Y_N]$ is the scalar matrix with $Y_1, Y_2, ..., Y_N$ being the species mass fractions. Therefore in the context of multi-step multi-variate scenario the first term on the right hand side of Eq. (5.4) needs to be replaced by $f_1(\bar{\rho},\tilde{\hat{T}},[\tilde{q}])\exp(-\varphi\Delta/\delta_{th})$ where $[\tilde{q}] = [\tilde{Y}_1, \tilde{Y}_2, ..., \tilde{Y}_N]$. Furthermore most industrial LES

are carried out for $\Delta >> \delta_{th}$ where the first term on the right hand side of Eq. (5.4) effectively vanishes so the exact form of f_1 is unlikely play an important role.

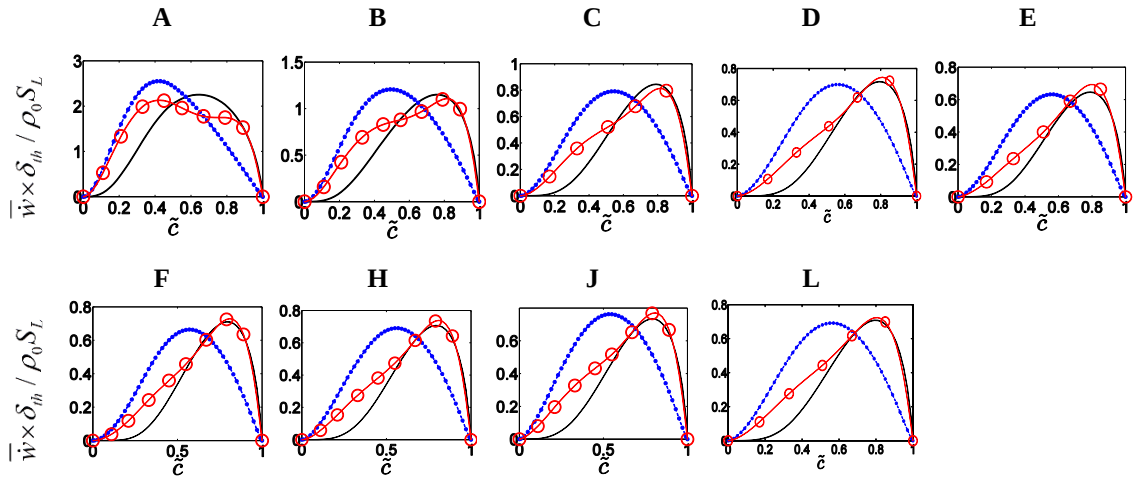

Figure 5.5: Variation of mean values mean values of normalised reaction rate $\overline{\dot{w}}^{+}$ (———), normalised SDR based closure $\overline{\dot{w}}^{+}_{model}$ (—×—) and the prediction of new reaction rate model (i.e. eq. 5.4) (—○—) conditional on $\tilde{c}$ across the flame brush at $\Delta \approx 0.8\delta_{th}$ for cases A-E, F, H, J and K.

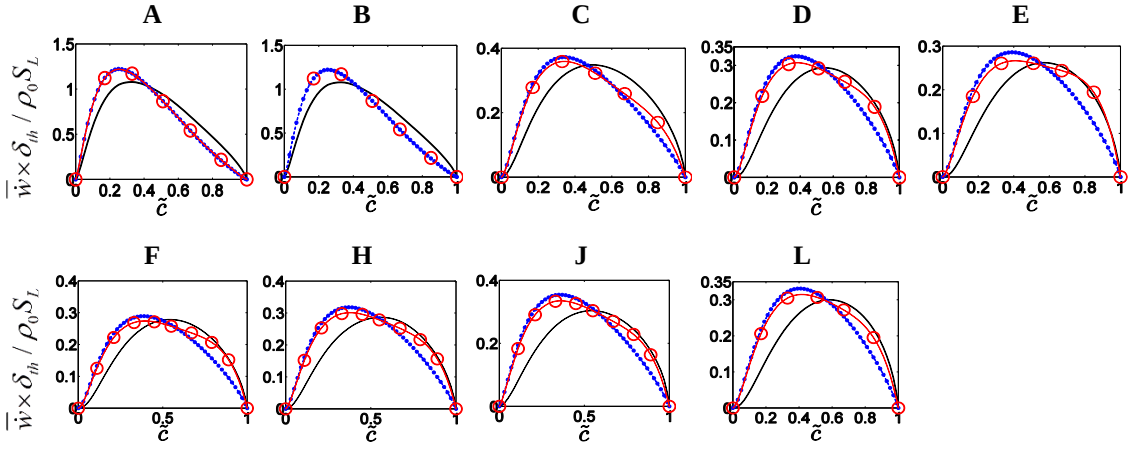

Figure 5.6: Variation of mean values mean values of normalised reaction rate $\overline{\dot{w}}^{+}$ (———), normalised SDR based closure $\overline{\dot{w}}^{+}_{model}$ (—×—) and the prediction of new reaction rate model (i.e. eq. 5.4) (—○—) conditional on $\tilde{c}$ across the flame brush at $\Delta \approx 2.8\delta_{th}$ for cases A-E, F, H, J and K.

Figures 5.5 and 5.6 show the predictions of filtered reaction rate by eq. (5.4) along with the predictions of eq. (5.1). Equation (5.4) ensures that the right hand side becomes $\dot{w}$ when $\Delta \to 0$ (i.e. $\Delta << \delta_{th}$) and $\overline{\dot{w}} = 2\overline{\rho}\tilde{N}_c / (2c_m - 1)$ is obtained for $\Delta >> \delta_{th}$. In addition it is possible to scale Δ / δ_{th} as:

$$\frac{\Delta}{\delta_{th}} \sim \frac{u'_{\Delta}}{S_L} Da_{\Delta} \sim \mathrm{Re}_{\Delta}^{1/2} Da_{\Delta}^{1/2} \tag{5.10}$$

which suggests that eq. (5.4) can be rewritten as:

$$\overline{\dot{w}} = f_1(\bar{\rho}, \tilde{c}, \tilde{T}) \exp\left(-\varphi_1 Da_{\Delta} \frac{u'_{\Delta}}{S_L}\right) + \left[1 - \exp\left(-\varphi_1 Da_{\Delta} \frac{u'_{\Delta}}{S_L}\right)\right] \frac{2\bar{\rho}\tilde{N}_c}{(2c_m - 1)} \tag{5.11}$$

$$\overline{\dot{w}} = f_1(\bar{\rho}, \tilde{c}, \tilde{T}) \exp\left(-\varphi_2 \mathrm{Re}_{\Delta}^{1/2} Da_{\Delta}^{1/2}\right) + \left[1 - \exp\left(-\varphi_2 \mathrm{Re}_{\Delta}^{1/2} Da_{\Delta}^{1/2}\right)\right] \frac{2\bar{\rho}\tilde{N}_c}{(2c_m - 1)} \tag{5.12}$$

where $\varphi_1 = \varphi$ and $\varphi_2 = 0.626\varphi$ for the simple chemistry cases are the appropriate model coefficients.

The eqs. (5.11) and (5.12) tend towards $\overline{\dot{w}} = 2\bar{\rho}\tilde{N}_c / (2c_m - 1)$ for high values of Da_{Δ} for a given value of u'_{Δ} / S_L and Re_{Δ} respectively, which is consistent with improved agreement between $\overline{\dot{w}}$ and $2\bar{\rho}\tilde{N}_c / (2c_m - 1)$ with increasing Da_{Δ} (compare Figs. 5.4-5.6). Figures 5.5 and 5.6 suggest that eq. (5.4) satisfactorily predicts $\overline{\dot{w}}$ for all cases considered here for both $\Delta < \delta_{th}$ and $\Delta > \delta_{th}$.

5.5 Summary

It has been found that eq. (5.1) starts to satisfactorily predict $\overline{\dot{w}}$ obtained for DNS data for $\Delta \geq 2.0\delta_{th}$ for all assessed DNS cases of simple chemistry. In most engineering calculations Δ remains much greater than $2.0\delta_{th}$ so eq. (5.1) is likely to predict $\overline{\dot{w}}$ satisfactorily for most industrial LES. However, the LES model given by eq. (5.1) fail to approach to the correct asymptotic value (i.e. $\dot{w}$) for small values of Δ (i.e. $\Delta \to 0$) for which an LES simulation approaches a DNS simulation which has been addressed by eqs. (5.4), (5.11) and (5.12). The satisfactory performance of eq. (5.4) indicates that $\overline{\dot{w}}$ can be closed using SDR if $\tilde{N}_c$ is adequately modelled, as filtered SDR itself requires modelling in LES as well. The modelling approaches of filtered SDR will be presented in Chapters 6 and 7 in detail.

Chapter 6. Algebraic Closure of SDR in the context of LES

As introduced in Chapter 5, it is possible to close the chemical reaction rate of turbulent premixed combustion based on properly modelled scalar dissipation rate. In non-premixed combustion, SDR is often modelled by introducing the eddy diffusivity to characterise the turbulence effects on scalar mixing. However, such an approach ignores the involvement of chemical time-scale in the SDR in turbulent premixed combustion. The validity of eq. (5.1) provides the proof that SDR in premixed flames is dependent on chemical time scales along with turbulent mixing time scales. In turbulent premixed combustion, the transport equation of SDR can be closed if all unclosed terms in SDR transport equation is properly modelled in the context of both RANS and LES. Under the condition when the equilibrium is maintained for the generation and destruction of scalar gradient, it is possible to derive an algebraic closure of Favre-filtered/averaged SDR in both RANS and LES, which will be discused in detail here. Dunstan *et al*. (2013) investigated the possibility of extending an algebraic closure for the Favre-averaged SDR $\tilde{\varepsilon}_c$ proposed by Kolla *et al*. (2009) for the SDR closure in the context of LES. The *a-priori* analysis by Dunstan *et al.* (2013) showed a good agreement between the SDR extracted from DNS and the model predictions. It worth noting that the analysis of Dunstan *et al.* (2013) was based on a single V-flame DNS data with unity global Lewis number and the effects of global Lewis number, heat release parameter τ and turbulent Reynolds number Re_t were not addressed, which motivates the analysis presented here.

Chakraborty and Swaminathan (2011) demonstrated that the algebraic $\tilde{\varepsilon}_c$ model by Kolla *et al.* (2009) was inadequate for $Le \neq 1.0$ flames and proposed modifications. This modified SDR model for RANS is extended to LES. The performance of this new model is evaluated using the DNS results for $\tilde{N}_c$. Furthermore, this model performance is compared to a power-law based closure with a global exponent and inner cut-off scale (Dunstan *et al*.,2013) and a conventional model (Girimaji and Zhou, 1996), which is widely used for SDR closure in the context of passive scalar mixing.

The sub-grid turbulent velocity fluctuation (i.e. $u'_\Delta = \sqrt{2k_{sg}/3}$) (where u_i is the i^{th} component of fluid velocity and $k_{sg} = 0.5(\overline{\rho u_i u_i}/\bar{\rho} - \tilde{u}_i\tilde{u}_i)$ is the sub-grid kinetic energy) is an input parameter to the algebraic model for $\tilde{N}_c$, which needs to be modelled in actual LES. In order to assess the effects of u'_Δ modelling on $\tilde{N}_c$ closure, the results of an algebraic SDR model with u'_Δ evaluated according to the Smagorinsky-Lily model (Smagorinsky, 1963) of sub-grid eddy viscosity have been compared to the corresponding $\tilde{N}_c$ predictions where the sub-grid turbulent velocity fluctuation u'_Δ has been extracted from DNS data.

6.1 Statistical analysis of filtered SDR and its transport equation

For the purpose of convinience, the transport equation of SDR $\tilde{N}_c$, which is eqs. (3.58-3.64) in Chapter 3, is repeated here as (Swaminathan and Bray, 2005):

$$\frac{\partial(\bar{\rho}\tilde{N}_c)}{\partial t} + \frac{\partial(\bar{\rho}\tilde{u}_j\tilde{N}_c)}{\partial x_j} = \underbrace{\overline{\frac{\partial}{\partial x_j}\left(\rho D\frac{\partial N_c}{\partial x_j}\right)}}_{D_1} + T_1 + T_2 + T_3 + T_4 - D_2 + f(D) \tag{6.1}$$

where u_j is the j^{th} component of velocity vector and the terms on the left hand side denote the transient effects and the resolved advection of $\tilde{N}_c$ respectively. The term D_1 represents the molecular diffusion of $\tilde{N}_c$ and the other terms $T_1, T_2, T_3, T_4, (-D_2)$ and $f(D)$ are all unclosed and given by:

$$T_1 = -\frac{\partial}{\partial x_j}\left(\overline{\rho u_j N_c} - \bar{\rho}\tilde{u}_j\tilde{N}_c\right) \tag{6.2}$$

$$T_2 = \overline{-2\frac{D}{\rho}\left[\dot{w} + \frac{\partial}{\partial x_i}\left(\rho D\frac{\partial c}{\partial x_i}\right)\right]\frac{\partial c}{\partial x_j}\frac{\partial \rho}{\partial x_j}} \tag{6.3}$$

$$T_3 = \overline{-2\rho D\frac{\partial c}{\partial x_i}\frac{\partial u_i}{\partial x_j}\frac{\partial c}{\partial x_j}} \tag{6.4}$$

$$T_4 = \overline{2D\frac{\partial \dot{w}}{\partial x_i}\frac{\partial c}{\partial x_i}} \tag{6.5}$$

$$(-D_2) = \overline{-2\rho D^2\frac{\partial^2 c}{\partial x_i \partial x_j}\frac{\partial^2 c}{\partial x_i \partial x_j}} \tag{6.6}$$

$$f(D) = \overline{f_1(D)} = \underbrace{\overline{2D\frac{\partial c}{\partial x_k}\frac{\partial(\rho D)}{\partial x_k}\frac{\partial^2 c}{\partial x_j \partial x_j}}}_{FD1} + \underbrace{\overline{2D\frac{\partial c}{\partial x_k}\frac{\partial^2(\rho D)}{\partial x_j \partial x_k}\frac{\partial c}{\partial x_j}}}_{FD2} - \underbrace{\overline{\frac{\partial}{\partial x_j}\left(\rho N_c \frac{\partial D}{\partial x_j}\right)}}_{FD3}$$
$$\underbrace{-\overline{2\rho D\frac{\partial D}{\partial x_j}\frac{\partial}{\partial x_j}\left(\frac{\partial c}{\partial x_k}\frac{\partial c}{\partial x_k}\right)}}_{FD4} + \underbrace{\overline{\rho\left(\frac{\partial c}{\partial x_k}\frac{\partial c}{\partial x_k}\right)\left[\frac{\partial D}{\partial t} + u_j\frac{\partial D}{\partial x_j}\right]}}_{FD5} \quad (6.7)$$

6.1.1 Local behaviours of $\tilde{N}_c$

The variation of $\widetilde{N}_c \times \delta_{th}/S_L$ with $\tilde{c}$ is shown in Fig. 6.1 for cases F, H, J and V where values of $\widetilde{N}_c \times \delta_{th}/S_L$ have been ensemble-averaged on $\tilde{c}$ isosurfaces for $0.4\delta_{th}$, $1.6\delta_{th}$ and $2.8\delta_{th}$. The filter sizes $0.4\delta_{th}$ and $2.8\delta_{th}$ are representative of the situations where the flame is partially resolved and fully unresolved respectively. The cases G and I are not shown because of their qualitative similarity to cases F and J. It can be seen from Fig. 6.1 that $\widetilde{N}_c \times \delta_{th}/S_L$ remains slightly skewed towards the burned gas side (i.e. $\tilde{c} > 0.5$) for $\Delta << \delta_{th}$ (e.g. $\Delta = 0.4\delta_{th}$) but the profile becomes more symmetric with the peak occurring close to $\tilde{c} \approx 0.5$ for $\Delta >> \delta_{th}$ (e.g. $\Delta = 2.8\delta_{th}$). It can also be seen from Fig. 6.1 that the magnitude of $\widetilde{N}_c \times \delta_{th}/S_L$ decreases with increasing filter width Δ due convolution operation over a larger volume where the contributions arising from the close to the centre of the filter volume are weighted more heavily. However, Fig. 6.1 suggests that $\widetilde{N}_c \times \delta_{th}/S_L$ remains of the order of unity for all values of Δ for all cases.

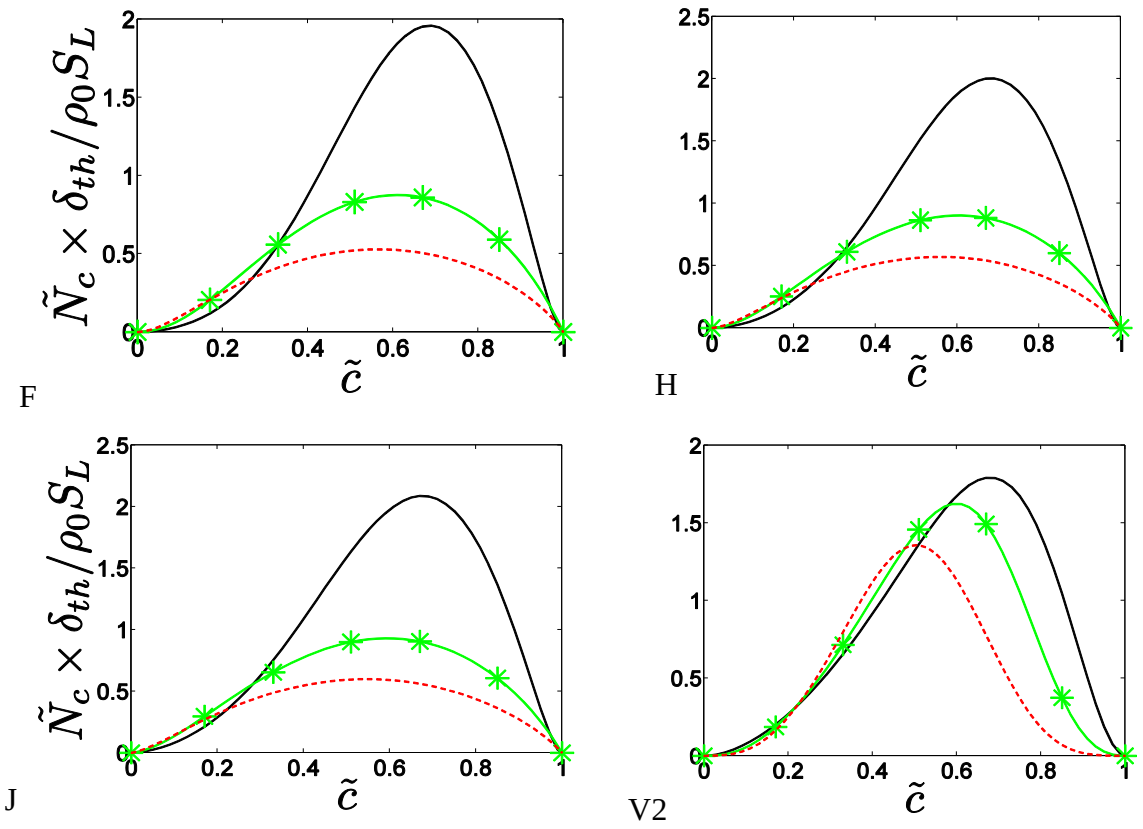

Figure 6.1 : Variation of $\tilde{N}_c \times \delta_{th} / S_L$ with $\tilde{c}$ at Δ=0.4δ_{th} (——), Δ= 1.6δ_{th} (—*—) and Δ= 2.8δ_{th} (– – –) for cases F, H, J and V2.

Following Swaminathan and Bray (2005) the sub-grid part of ∇c can be scaled as:

$$(\nabla c)_{sg} \sim \frac{1}{\delta_{th}} \tag{6.8}$$

whereas the molecular diffusivity D can be taken to scale as $D \sim S_L \delta_{th}$ with $(\tilde{Q})_{sg}$ and referring to sub-grid parts of $\tilde{Q}$ respectively. Thus, the sub-grid component of $\tilde{N}_c$ can be expressed as:

$$(\tilde{N}_c)_{sg} = [\tilde{N}_c - \tilde{D}\nabla\tilde{c}.\nabla\tilde{c}] \sim \frac{S_L}{\delta_{th}} \tag{6.9}$$

The resolved part of $\tilde{N}_c$ in turn scales as:

$$(\tilde{N}_c)_{res} = \tilde{D}\nabla\tilde{c}.\nabla\tilde{c} \sim \frac{S_L}{\delta_{th}} \quad \text{for } \Delta << \delta_{th} \tag{6.10}$$

$$(\tilde{N}_c)_{res} \sim \frac{S_L \delta_{th}}{\Delta^2} \sim \frac{S_L}{\delta_{th}} \frac{1}{Re_\Delta Da_\Delta} \quad \text{for } \Delta >> \delta_{th} \tag{6.11}$$

where $(\tilde{Q})_{res}$ refers to resolved parts of $\tilde{Q}$, $Da_\Delta = \frac{\Delta S_L}{\delta_{th} u'_\Delta}$ and $Re_\Delta = \frac{\rho_0 u'_\Delta \Delta}{\mu_0}$ are the local Damköhler and turbulent Reynolds number respectively with u'_Δ, ρ_0 and μ_0 are the sub-grid scale velocity fluctuation, unburned gas density and viscosity respectively. Equations (6.9-6.11) suggest that $(\tilde{N}_c)_{res}$ remains comparable to $(\tilde{N}_c)_{sg}$ for small values of Δ (i.e. $\Delta << \delta_{th}$) but $(\tilde{N}_c)_{res}$ decreases progressively in comparison to $(\tilde{N}_c)_{sg}$ with increasing Δ, and for $\Delta >> \delta_{th}$ the Favre-filtered SDR $\tilde{N}_c$ is principally made up of $(\tilde{N}_c)_{sg}$ (i.e. $\tilde{N}_c \approx (\tilde{N}_c)_{sg}$). As $(\tilde{N}_c)_{res}$ decreases with increasing Δ, the magnitude of $\tilde{N}_c$ decreases progressively with increasing Δ but remains of the order of S_L / δ_{th} due to $(\tilde{N}_c)_{sg} \sim S_L / \delta_{th}$.

6.1.2. Statistical nature of $\tilde{N}_c$ transport

The variations of the mean values of D_1, T_1, T_2, T_3, T_4, ($-D_2$) and $f(D)$ conditional on $\tilde{c}$ values for $0.4\delta_{th}$, $1.6\delta_{th}$ and $2.8\delta_{th}$ for cases F, H, J and V2 are shown in Fig. 6.2. It is evident that T_2, and ($-D_2$) remain leading-order source and sink terms respectively for all filter widths. The contribution of T_4 remains positive for the major portion of the flame brush before becoming negative towards the burned gas side for $\Delta << \delta_{th}$ (e.g. $\Delta = 0.4\delta_{th}$) but for $\Delta >> \delta_{th}$ (e.g. $\Delta = 2.8\delta_{th}$) the contribution of T_4 remains a leading-order source term throughout the flame brush. For the cases considered here the contribution of T_3 remains negative (positive) throughout the flame brush for all filter widths in cases F-J (case V2), whereas $f(D)$ assumes negative (positive) values towards the unburned (burned) gas side of the flame brush for all cases for all filter widths. The magnitude of T_1 remains negligible in comparison to the magnitudes of T_2, T_3, T_4, ($-D_2$) and $f(D)$ for all filter widths in all cases. The molecular diffusion term D_1 plays a key role for $\Delta << \delta_{th}$ (e.g. $\Delta = 0.4\delta_{th}$) assuming comparable magnitudes as those of T_2, T_3, T_4, ($-D_2$) and $f(D)$.

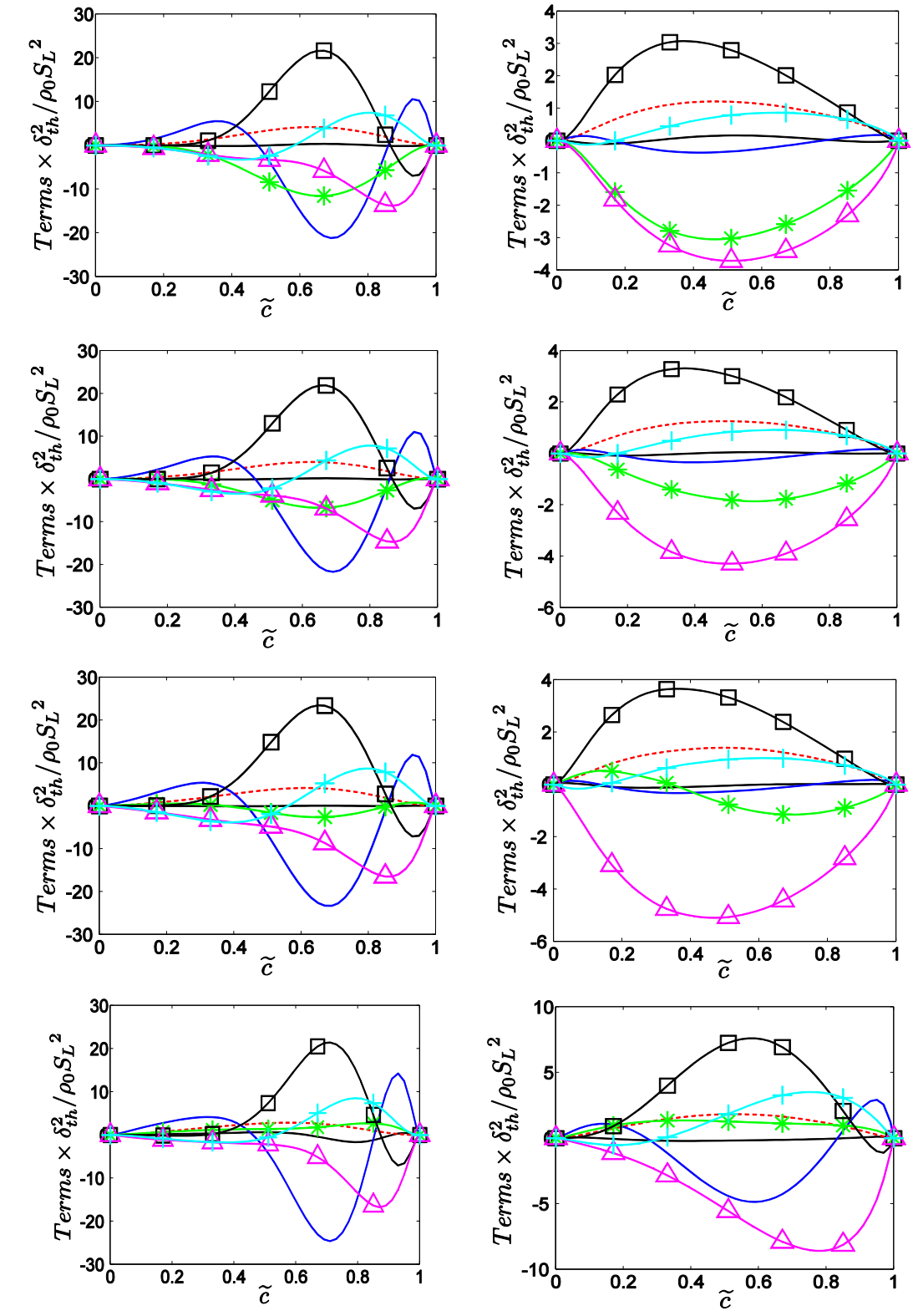

Figure 6.2: Variation of D_1 (——), T_1 (——), T_2(- - -), T_3 (—*—), T_4 (—□—), (-D_2) (—△—) and f(D) (—+—) with $\tilde{c}$ at Δ=0.4δ_{th} (1st column) and 2.8δ_{th} (2nd column) for cases: F (1st row), H (2nd row), J (3rd row) and V2 (4th row).

However, the magnitude of D_1 becomes negligible in comparison to the magnitudes of T_2, T_3, T_4, ($-D_2$) and $f(D)$ for $\Delta>>\delta_{th}$ (e.g. $\Delta=2.8\delta_{th}$). The molecular diffusion term D_1 scales in the following manner if the spatial gradients are scaled with respect to Δ:

$$D_1 \sim \frac{\rho_0 S_L^2}{\Delta^2} \sim \frac{\rho_0 S_L^2}{\delta_{th}^2} \frac{1}{Re_\Delta Da_\Delta} \text{ for } \Delta>>\delta_{th} \tag{6.12}$$

$$D_1 \sim \frac{\rho_0 S_L^2}{\delta_{th}^2} \text{ for } \Delta<<\delta_{th} \tag{6.13}$$

Equations (6.12) and (6.13) suggest that the magnitude of D_1 is expected to decrease with increasing Δ. Figure 6.2 further indicates that the magnitudes of T_2, T_3, T_4, ($-D_2$) and $f(D)$ decrease with increasing Δ and the observed behaviours in response to Δ will be explained.

6.1.3. Statistical behaviour of T_1

The variations of the mean values of T_1, conditional on $\tilde{c}$ values for cases F, H, J and V2 are shown in Fig. 6.3 for different filter widths. It is evident from Fig. 6.3 that T_1 assumes both positive and negative values across the flame brush. The behaviour of T_1 depends on the statistical behaviour of the sub-grid flux of SDR (i.e. $\overline{\rho u_i N_c} - \bar{\rho}\tilde{u}_i\tilde{N}_c$). The distributions of $(\overline{\rho u_i N_c} - \bar{\rho}\tilde{u}_i\tilde{N}_c)M_i$ and $(\partial\tilde{N}_c/\partial x_i)M_i$ conditionally averaged on $\tilde{c}$ isosurfaces are shown in Fig. 6.3 where $M_i = -(\partial\bar{c}/\partial x_i)/|\nabla\bar{c}|$ is the i^{th} component of the resolved flame normal vector. Comparing the signs of $(\overline{\rho u_i N_c} - \bar{\rho}\tilde{u}_i\tilde{N}_c)M_i$ and $(\partial\tilde{N}_c/\partial x_i)M_i$ it is evident that the sub-grid flux of SDR shows predominantly gradient type transport (i.e. $\overline{\rho u_i N_c} - \bar{\rho}\tilde{u}_i\tilde{N}_c = -(\mu_t/Sc_\Sigma)\partial\tilde{N}_c/\partial x_i$) for the case V2 but counter-gradient transport has been observed for cases F-J. It is worth noting the sub-grid flux $\overline{\rho u_i N_c} - \bar{\rho}\tilde{u}_i\tilde{N}_c$ assumes negligible values for $\Delta<<\delta_{th}$ (e.g. $\Delta=0.4\delta_{th}$) and its magnitude increases with increasing Δ, as most of the turbulent transport takes place at the sub-grid level. If the sub-grid velocity fluctuations are scaled with respect to S_L (Swaminathan and Bray, 2005) one obtains the following scaling argument for $(\overline{\rho u_i N_c} - \bar{\rho}\tilde{u}_i\tilde{N}_c)$:

$$\overline{\rho u_i N_c} - \bar{\rho}\tilde{u}_i\tilde{N} \sim \frac{\rho_0 S_L^2}{\delta_{th}} \tag{6.14}$$

Alternatively, sub-grid scale velocity fluctuation can be scaled using u'_Δ which yields:

$$\overline{\rho u_i N_c} - \bar{\rho}\tilde{u}_i\tilde{N} \sim \frac{\rho_0 S_L u'_\Delta}{\delta_{th}} \quad \text{for} \quad \Delta >> \delta_{th} \tag{6.15}$$

Using eq. (6.14) and scaling resolved gradients with respect Δ lead to the following scaling of T_1:

$$T_1 \sim \frac{\rho_0 S_L^2}{\Delta\delta_{th}} \sim \frac{\rho_0 S_L^2}{\delta_{th}^2}\frac{1}{Da_\Delta^{0.5} Re_\Delta^{0.5}} \quad \text{for} \quad \Delta >> \delta_{th} \tag{6.16}$$

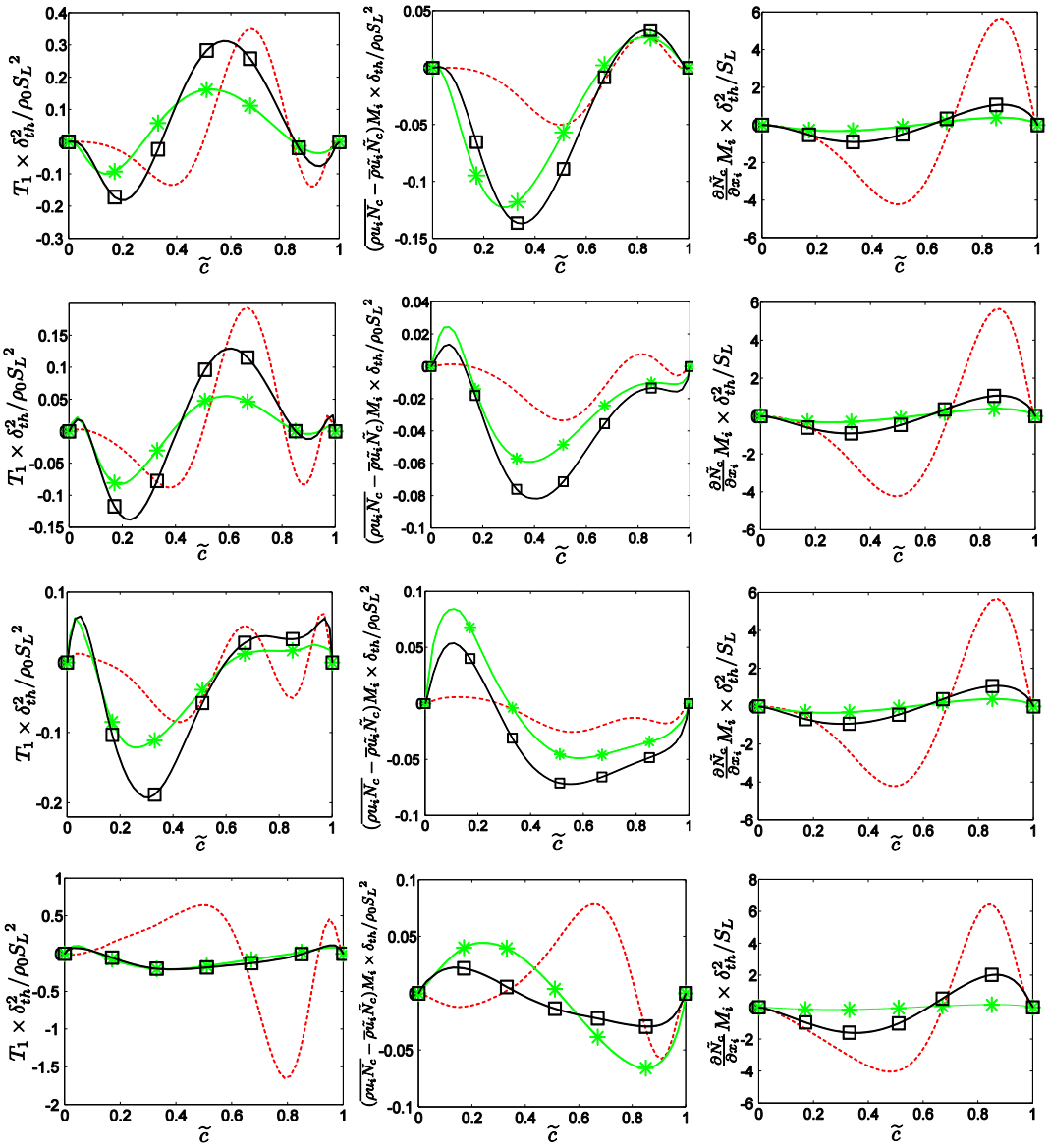

Figure 6.3: The variation of T_1, (1st column), $(\overline{\rho u_i N_c} - \bar{\rho}\tilde{u}_i\tilde{N}_c)M_i$ (2nd column) and $(\partial\tilde{N}_c/\partial x_i)M_i$ (3rd column) with $\tilde{c}$ at Δ= $0.4\delta_{th}$ (- - -) , $1.6\delta_{th}$ (—□—) and $2.8\delta_{th}$(—✳—) for cases F (1st row), H (2nd row), J (3rd row) and V (4th row).

Similarly, eq. (6.15) yields:

$$T_1 \sim \frac{\rho_0 S_L u'_\Delta}{\Delta \delta_{th}} \sim \frac{\rho_0 S_L^2}{\delta_{th}^2} \frac{1}{Da_\Delta} \tag{6.17}$$

The values of Da_Δ and Re_Δ increase with increasing Δ (Dunstan et al., 2013) so it is expected that the magnitude of T_1 decreases in comparison to $\rho_0 S_L^2 / \delta_{th}^2$ with increasing Δ. Moreover, eqs. (6.16) and (6.17) indicate that the magnitude of T_1 is expected to decreases with increasing Δ, which can be confirmed from Fig. 6.3.

6.1.4. Statistical behaviour of T_2 and T_3

The variations of the mean values of T_2 and T_3, conditional on $\tilde{c}$ values for cases F, H, J and V2 are shown in Fig. 6.4 for different filter widths. Using $\rho = \rho_0 / (1+\tau c)$ for low Mach number unity Lewis number flames leads to the following expression:

$$T_2 = \overline{\rho \nabla . \vec{u} N_c} \tag{6.18}$$

The dilatation rate $\nabla . \vec{u}$ can be taken to scale with $\tau S_L / \delta_{th}$ (i.e. $\nabla . \vec{u} \sim \tau S_L / \delta_{th}$) (Chakraborty et al., 2007) and thus the sub-grid and resolved component of T_2 can be scaled as:

$$(T_2)_{sg} \sim \frac{\rho_0 \tau S_L^2}{\delta_{th}^2} \tag{6.19}$$

$$\text{For } \Delta << \delta_{th},\ (T_2)_{res} = \bar{\rho} \tilde{D} \nabla \tilde{c} . \nabla \tilde{c} \frac{\partial \tilde{u}_i}{\partial x_i} \sim \frac{\rho_0 U_{ref} S_L}{\delta_{th}^2} \tag{6.20}$$

$$\text{For} \Delta >> \delta_{th},\ (T_2)_{res} \sim \frac{\rho_0 S_L^2}{\delta_{th}^2} \frac{U_{ref}}{S_L} \frac{1}{Re_\Delta^{1.5} Da_\Delta^{1.5}} \tag{6.21}$$

where U_{ref} is a velocity scale representing the Favre-filtered velocity components $\tilde{u}_i$. Equations (6.19-6.21) demonstrate that $(T_2)_{sg}$ remains of the order of $\rho_0 \tau S_L^2 / \delta_{th}^2$ irrespective of Δ. By contrast, the magnitude of $(T_2)_{res}$ remains comparable to $(T_2)_{sg}$ for $U_{ref} \sim S_L$ for $\Delta << \delta_{th}$ but the magnitude of $(T_2)_{res}$ decreases with increasing Δ. Thus, the

magnitude of $T_2 = (T_2)_{res} + (T_2)_{sg}$ decreases with increasing Δ but remains of the order of $\rho_0 \tau S_L^2 / \delta_{th}^2$.

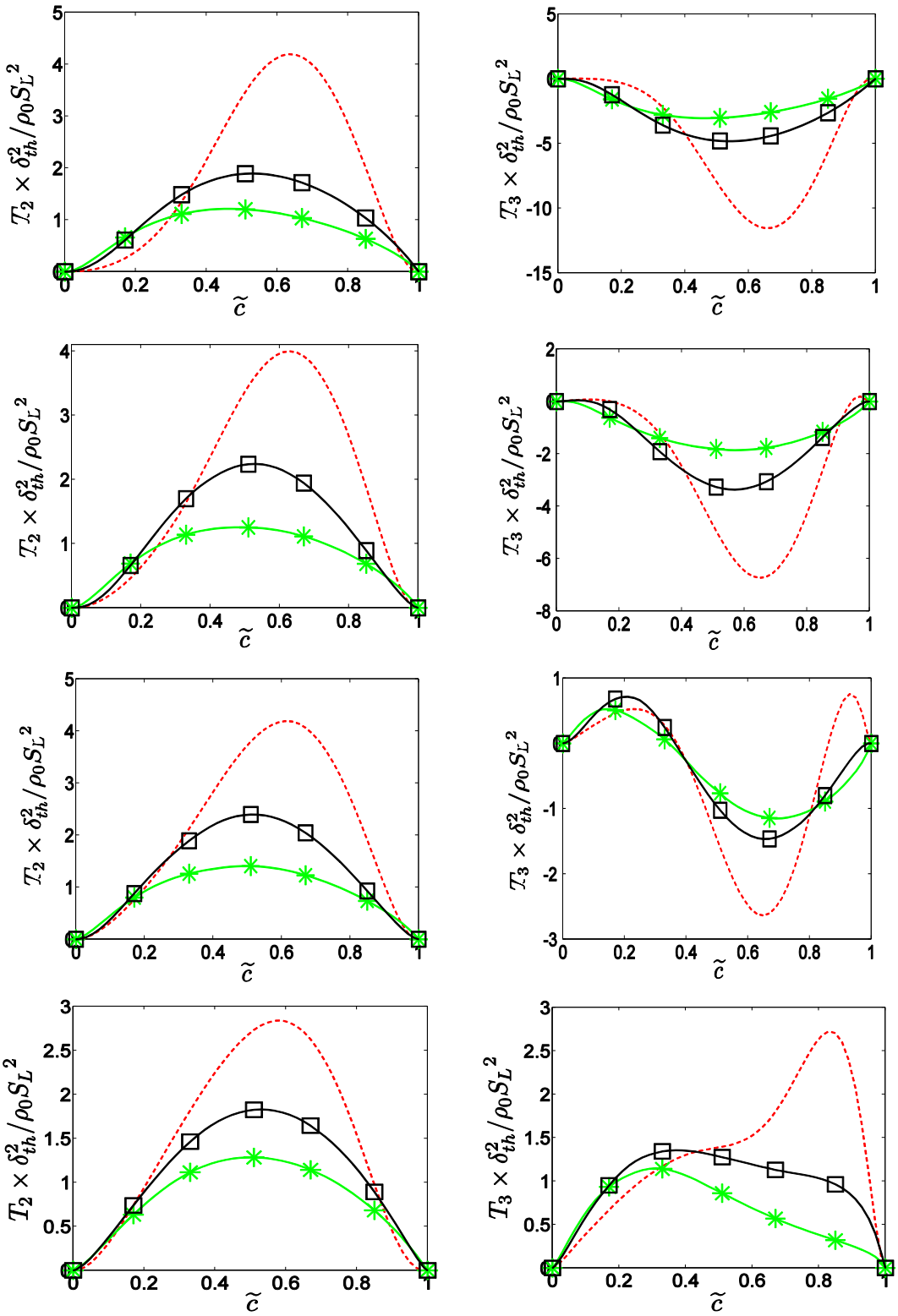

Figure 6.4: The variation of T_2, (1st column) and T_3 (2nd column) with $\tilde{c}$ at $\Delta = 0.4\delta_{th}$ (- - -), $1.6\,\delta_{th}$ (—□—) and $2.8\,\delta_{th}$ (—✳—) for cases F (1st row), H (2nd row), J (3rd row) and V2 (4th row).

The contribution of T_3 can be expressed as:

$$T_3 = -\overline{2\rho(e_\alpha \cos^2\alpha + e_\beta \cos^2\beta + e_\gamma \cos^2\gamma)N_c} \tag{6.22}$$

where e_α, e_β and e_γ are the most extensive, intermediate and the most compressive principal strain rates and their angles with ∇c are given by α, β and γ respectively.

The scalar gradient ∇c aligns with e_α when the effects of strain rate induced by chemical reaction a_{chem} overcome the effects of turbulent straining a_{turb} and *vice versa* (Chakraborty et al., 2007). The strain rate induced by chemical heat release is expected to scale as $a_{chem} \sim \tau S_L / \delta_{th}$. Following Meneveau and Poinsot (1991) the turbulent strain rate a_{turb} can be scaled as: $a_{turb} \sim u'/l$, which leads to $a_{chem} / a_{turb} \sim \tau Da$ (Chakraborty and Swaminathan, 2007).

As $\tau Da > 1$ for the cases F-J, ∇c aligns with e_α for the major portion of the flame brush leading to negative values of T_3. In case V2, the effects of a_{turb} dominate over the effects of a_{chem} to give rise predominant alignment of ∇c with e_γ leading to positive values of T_3. The contributions of $(T_3)_{res}$ and $(T_3)_{sg}$ can be scaled as:

$$(T_3)_{sg} \sim \frac{\rho_0 S_L^2}{\delta_{th}^2} \tag{6.23}$$

$$\text{For } \Delta << \delta_{th}: (T_3)_{res} = -\overline{\rho}\tilde{D}\frac{\partial \tilde{c}}{\partial x_i}\frac{\partial \tilde{u}_i}{\partial x_j}\frac{\partial \tilde{c}}{\partial x_j} \sim \frac{\rho_0 U_{ref} S_L}{\delta_{th}^2} \tag{6.24}$$

$$\text{For } \Delta >> \delta_{th}: (T_3)_{res} \sim \frac{\rho_0 S_L^2}{\delta_{th}^2}\frac{U_{ref}}{S_L}\frac{1}{Re_\Delta^{1.5} Da_\Delta^{1.5}} \tag{6.25}$$

Equations (6.23-6.25) demonstrate that $(T_3)_{sg}$ remains of the order of $\rho_0 S_L^2 / \delta_{th}^2$ irrespective of Δ. By contrast, the magnitude of $(T_3)_{res}$ remains comparable to $(T_3)_{sg}$ for $U_{ref} \sim S_L$ for $\Delta << \delta_{th}$ but the magnitude of $(T_3)_{res}$ decreases with increasing Δ. Thus, the magnitude of $T_3 = (T_3)_{res} + (T_3)_{sg}$ decreases with increasing Δ but remains of the order of $\rho_0 S_L^2 / \delta_{th}^2$.

6.1.5. Statistical behaviour of T_4, ($-D_2$) and f(D)

The variations of the mean values of T_4, ($-D_2$) and $f(D)$ conditional on $\tilde{c}$ values for cases F, H, J and V2 are shown in Fig. 6.5 for different filter widths. The term T_4 can be expressed as: $T_4 = -\overline{2D\partial\dot{w}/\partial n|\nabla c|}$ where n is the spatial coordinate in the local flame normal direction and the flame normal vector $\vec{n} = -\nabla c/|\nabla c|$ points towards the unburned gas side of the flame. For single step chemistry considered here the maximum value of reaction rate $\dot{w}$ occurs close to $c \approx 0.85$ (Chakraborty and Cant, 2004). This suggests that the probability of finding negative (positive) values of $\partial\dot{w}/\partial n$ is significant for $c < 0.85$ ($c > 0.85$), which gives rise to positive (negative) mean value of T_4 towards the unburned (burned) gas side of the flame brush. The molecular dissipation term ($-D_2$) remains deterministically negative according to eq. (6.6).

It is worth noting from Figs. 6.2 and 6.5 that $f(D)$ remains weakly negative towards the unburned gas side before assuming positive values towards the burned gas side for all cases. The magnitude of the mean contribution of $f(D)$ cannot be neglected even for cases F-J where ρD is considered to be constant.

In cases F-J, $\overline{\rho N_c[\partial D/\partial t + u_j \partial D/\partial x_j]}$ for constant ρD can be expressed as:

$$\overline{\rho N_c\left[\frac{\partial D}{\partial t} + u_j\frac{\partial D}{\partial x_j}\right]} = \overline{\rho D N_c\left(\frac{\partial u_j}{\partial x_j}\right)} = \frac{T_2}{2} \tag{6.26}$$

and the first three terms on the right hand side vanish for constant values of ρD. The contributions of the third and fourth terms on the right hand side of eq. (6.7) are responsible for the change in sign of $f(D)$ in cases F-J. These terms are also principally responsible for sign change of $f(D)$ in case V. Scaling the sub-grid reaction progress variable and reaction rate gradients using δ_{th} leads to following scaling estimates for $(T_4)_{sg}$, $(-D_2)_{sg}$ and $f(D)_{sg}$:

$$(T_4)_{sg} \sim \frac{\rho_0 S_L^2}{\delta_{th}^2};\ (-D_2)_{sg} \sim \frac{\rho_0 S_L^2}{\delta_{th}^2};\ f(D)_{sg} \sim \frac{\rho_0 S_L^2}{\delta_{th}^2}; \tag{6.27}$$

where the reaction rate $\dot{w}$ is taken to scale with $\rho_0 S_L/\delta_{th}$ (Swaminathan and Bray, 2005).

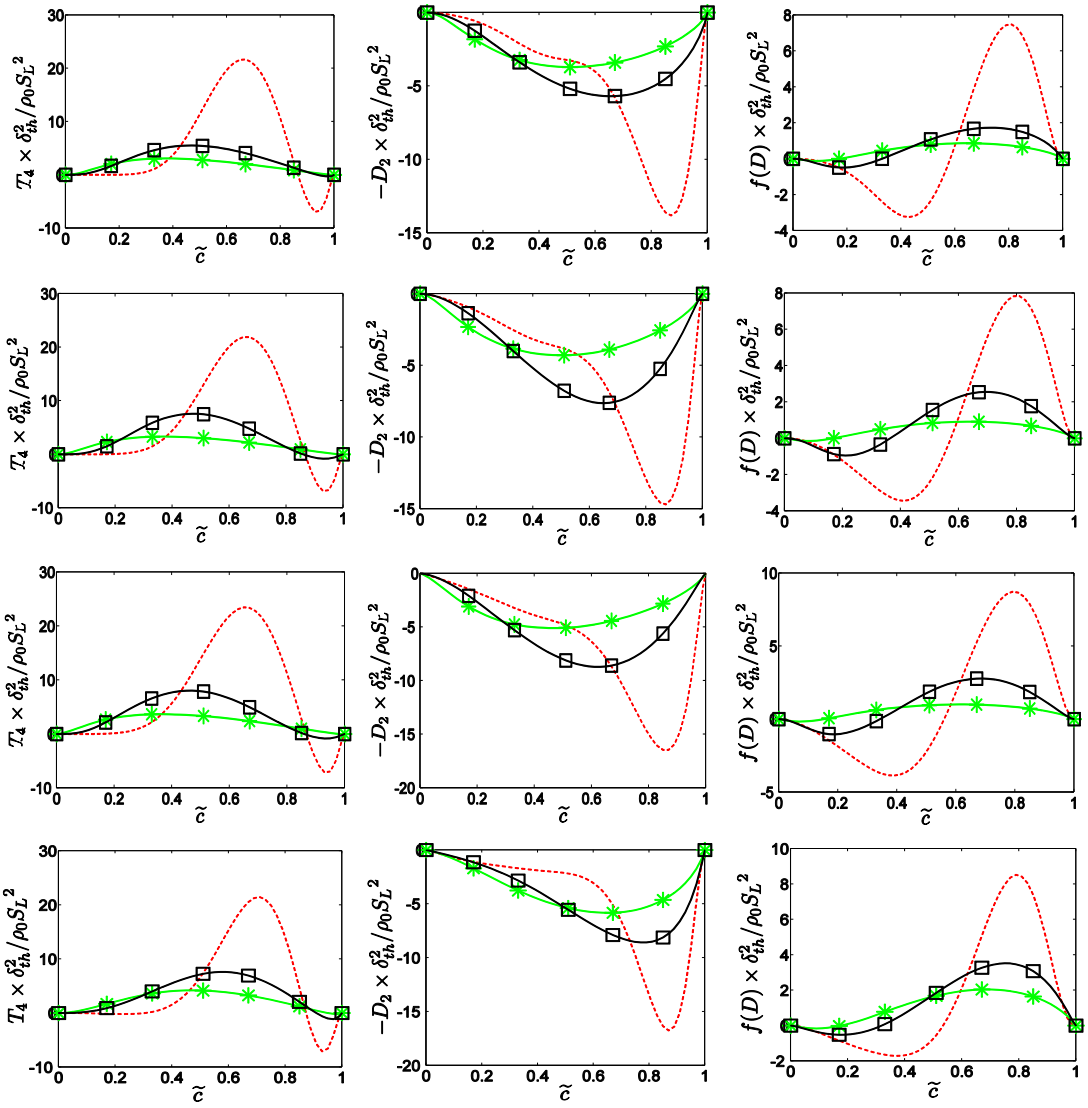

Figure 6.5: The variation of T_4, (1st column) and ($-D_2$) (2nd column) and f(D) (3rd column) with $\tilde{c}$ at $\Delta = 0.4\delta_{th}$ (- - -), $1.6\delta_{th}$ (—□—) and $2.8\delta_{th}$ (—✳—) for cases F (1st row), H (2nd row), J (3rd row) and V (4th row).

The resolved parts of T_4, ($-D_2$) and $f(D)$ can in turn be scaled in the following manner for $\Delta >> \delta_{th}$:

$$(T_4)_{res} = 2\tilde{D}\frac{\partial \dot{\bar{w}}}{\partial x_i}\frac{\partial \tilde{c}}{\partial x_i} \sim \frac{\rho_0 S_L^2}{\delta_{th}^2}\frac{1}{Re_\Delta Da_\Delta} \tag{6.28}$$

$$(-D_2)_{res} = -2\bar{\rho}\tilde{D}^2\frac{\partial^2 \tilde{c}}{\partial x_i \partial x_j}\frac{\partial^2 \tilde{c}}{\partial x_i \partial x_j} \sim \frac{\rho_0 S_L^2}{\delta_{th}^2}\frac{1}{Re_\Delta^2 Da_\Delta^2} \tag{6.29}$$

$$f(D)_{res} \sim \frac{\rho_0 S_L^2}{\delta_{th}^2}\frac{1}{Re_\Delta^2 Da_\Delta^2} \tag{6.30}$$

Equations (6.27-6.30) demonstrate that $(T_4)_{sg}$, $(-D_2)_{sg}$ and $f(D)_{sg}$ remain of the order of $\rho_0 S_L^2/\delta_{th}^2$ irrespective of Δ. By contrast, the magnitude of $(T_4)_{res}$, $(-D_2)_{res}$ and $f(D)_{res}$ decrease with increasing Δ. Thus, the magnitude of $T_4=(T_4)_{res}+(T_4)_{sg}$, $(-D_2)=(-D_2)_{res}+(-D_2)_{sg}$ and $f(D)=f(D)_{res}+f(D)_{sg}$ decreases with increasing Δ but remains of the order of $\rho_0 S_L^2/\delta_{th}^2$.

6.2 Differential diffusion (Lewis number) effects on SDR and its transport equation

The above section showed the behaviours of $\tilde{N}_c$ and its transport for unity Lewis number flames of different turbulent Reynolds number and flame configuartion, however, the differential diffusion effects on SDR and its transport has not been shown yet. Lewis number has been reported to affect the behaviours of SDR and its transport equation significantly in the context of RANS (Chakraborty et al., 2009; Chakraborty and Swaminathan, 2010). The effects of *Le* on SDR and its transport in the context of LES will be demonstrated here in this section. The five cases A-E will be used here to demonstrate the effects of *Le* on the SDR $\tilde{N}_c$ transport.

6.2.1 Effects of *Le* on the statistical behaviour of SDR $\tilde{N}_c$

The variations of the mean values of $\tilde{N}_c^+=\tilde{N}_c\times\delta_{th}/S_L$ conditional on bins of $\tilde{c}$ for cases A-E are shown in Fig. 6.6 for $\Delta\approx 0.4\delta_{th}$, $1.6\delta_{th}$ and $2.8\delta_{th}$. It can be seen from Fig. 6.6 that the magnitude of $\tilde{N}_c$ decreases with increasing *Le* for a given Δ. It has been discussed elsewhere (Chakraborty and Cant, 2011; Chakraborty and Swaminathan, 2010; Trouvé and Poinsot, 1994; Chakraborty and Klein, 2008) that the probability of finding high values of $|\nabla c|$ increases with decreasing *Le*. The augmentation of $|\nabla c|$ and $\dot{w}$ with decreasing *Le* is particularly prevalent for $Le<<1.0$ cases (e.g. $Le=0.34$ and 0.6), which can be substantiated from the values A_T/A_L and S_T/S_L reported in Table 4.5. The increased probability of finding high values of $|\nabla c|$ with decreasing *Le* gives rise to an increase in the mean value of $\tilde{N}_c^+$ conditional on $\tilde{c}$ for a given Δ. It is worth noting that the thermo-physical parameters for cases A-E have been chosen to yield identical values of S_L and δ_{th} in all cases. Thus a comparison between the normalised values of SDR (i.e.

$\tilde{N}_c^+$) in Fig. 6.6 provides information regarding the relative magnitudes of SDR between the cases considered here. Figure 6.6 shows that the variation of $\tilde{N}_c^+$ is skewed towards the burned side of the flame brush with a peak value of SDR at $\tilde{c} > 0.5$ for $\Delta < \delta_{th}$ (e.g. $\Delta \approx 0.4\delta_{th}$). However, the location of peak value of $\tilde{N}_c^+$ progressively shifts close to $\tilde{c} = 0.5$ with increasing Δ for the $Le \approx 1.0$ flames. However, the peak value location shifts towards $\tilde{c} < 0.5$ for the $Le = 0.34$ and 0.6 flames. A Gaussian filter kernel assigns more weight at the centre of the filtered domain and high values of $|\nabla c|$ are concentrated near the middle of the flame front.

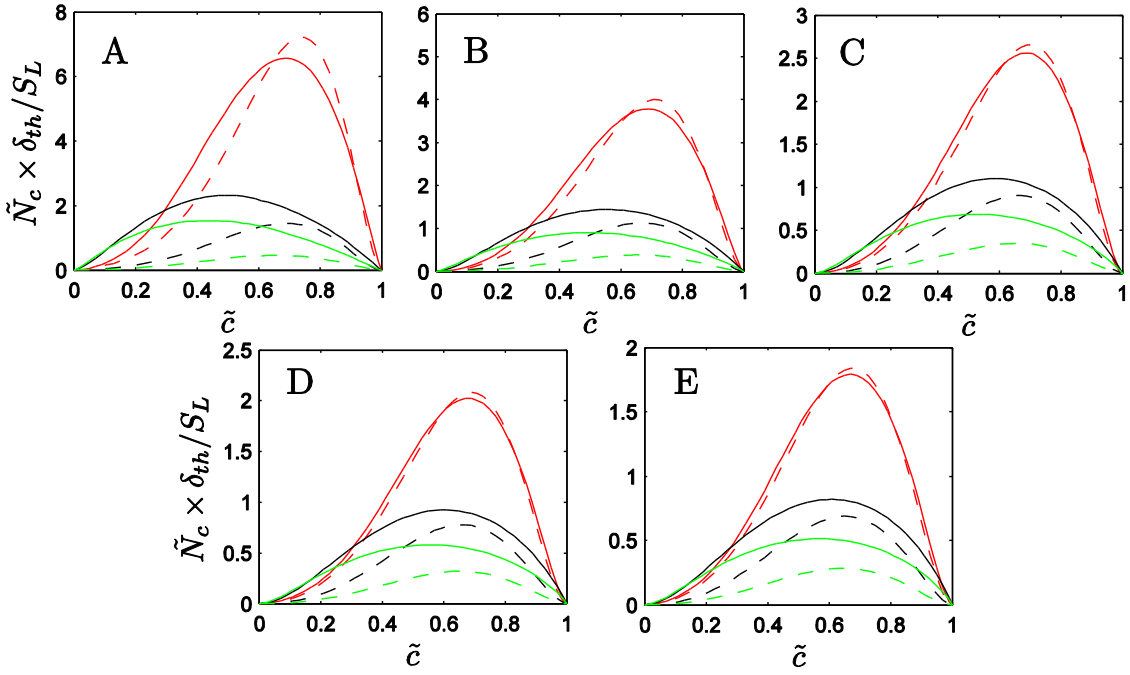

Figure 6.6: Variation of mean values of $\tilde{N}_c^+ = \tilde{N}_c \times \delta_{th}/S_L$ (solid line) and $\tilde{D}\nabla\tilde{c}.\nabla\tilde{c} \times \delta_{th}/S_L$ (dash line) conditional on bins of $\tilde{c}$ across the flame brush at $\Delta \approx 0.4\delta_{th}$ (red), $\Delta \approx 1.6\delta_{th}$ (black) and $\Delta \approx 2.8\delta_{th}$ (green) for the Le=0.34(A), Le=0.6(B), Le=0.8(C), Le=1.0(D), Le=1.2(E) cases.

These act to produce high values of $\tilde{N}_c^+$ close to $\tilde{c} \approx 0.5$ for $\Delta >> \delta_{th}$ (e.g. $\Delta \approx 2.8\delta_{th}$) for flames with $Le \approx 1.0$ (e.g. cases C-E). The reaction progress variable c field in the $Le << 1.0$ flames is significantly different from non-dimensional temperature $T = (\hat{T} - T_0)/(T_{ad} - T_0)$ field, and $\bar{\rho}$ in these flames is dependent on both $\tilde{c}$ and $\tilde{T}$ unlike $Le \approx 1.0$ flames where $\tilde{c}$ and $\tilde{T}$ are almost (identially equal for $Le = 1.0$) equal to each other. The $Le << 1.0$ flames show higher extent of $\tilde{T}$ variation for a given value of $\tilde{c}$

than in the $Le \approx 1.0$ cases due to weaker thermal diffusion. This increases the probability of obtaining smaller values of $\overline{\rho}$ in the $Le \ll 1.0$ flames than in the $Le \approx 1.0$ cases for a given value of $\widetilde{c}$, which leads to a shift in the peak value location of $\widetilde{N}_c^+$ towards $\widetilde{c} < 0.5$ as a result of Favre-filtering for the $Le \ll 1$ cases considered here (see cases A and B in Fig. 6.6).

The variation of $\widetilde{N}_c^+$ with $\widetilde{c}$ shown in Fig. 6.6 is qualitatively consistent with previous results in the context of RANS (Chakraborty et al., 2011). Figure 6.6 further indicates that the magnitude of $\widetilde{N}_c^+$ decreases with increasing Δ for all cases considered here. Based on the definition of $\delta_L = 1/(Max|\nabla c|_L)$, the Favre-filtered SDR $\widetilde{N}_c$ can be scaled as:

$$\widetilde{N}_c \sim \frac{S_L}{\delta_L} \text{ irrespective of } \Delta \tag{6.31}$$

where the molecular diffusivity D is scaled with respect to $S_L\delta_L$ (i.e. $D \sim S_L\delta_L$). Figure 6.6 reveals that $\widetilde{N}_c^+$ remains of the order of 1.0,

$$\widetilde{N}_c \times \delta_{th} / S_L \sim O(1) \text{ irrespective of } \Delta \text{ due to } \delta_{th}/\delta_L \sim 1.0 \text{ (see Table 6.1)} \tag{6.32}$$

The resolved part of the SDR (i.e. $\widetilde{D}\nabla\widetilde{c}.\nabla\widetilde{c}$) for $\Delta >> \delta_{th}$ can be scaled as:

$$\widetilde{D}\nabla\widetilde{c}\cdot\nabla\widetilde{c} \sim \frac{S_L\delta_L}{\Delta^2} \sim \frac{S_L}{\delta_L}\frac{1}{Le^2 Re_\Delta Da_\Delta} \text{ and } \left(\frac{\Delta}{\delta_{th}}\right)^2 \sim Re_\Delta Da_\Delta \tag{6.33}$$

where the gradients of the resolved quantities are scaled with respect to Δ. Therefore $\widetilde{D}\nabla\widetilde{c}.\nabla\widetilde{c}$ is expected to decrease with increasing Δ and $\widetilde{D}\nabla\widetilde{c}.\nabla\widetilde{c}$ assumes comparable values to that of $\widetilde{N}_c$ only for $\Delta \le \delta_L$. This behaviour can be substantiated from Fig. 6.6, which shows that the difference between $\widetilde{N}_c$ and $\widetilde{D}\nabla\widetilde{c}\cdot\nabla\widetilde{c}$ increases with increasing Δ and the sub-grid contribution $(\widetilde{N}_c)_{sg} = (\widetilde{N}_c - \widetilde{D}\nabla\widetilde{c}\cdot\nabla\widetilde{c})$ increases with an increase in Δ. For $\Delta >> \delta_{th}$ (or $\mathrm{Re}_\Delta Da_\Delta >> 1$) $\widetilde{D}\nabla\widetilde{c}.\nabla\widetilde{c}$ remains much smaller than $\widetilde{N}_c$, which indicates the sub-grid part of SDR $(\widetilde{N}_c)_{sg}$ also remains of the order of S_L/δ_L for $\Delta >> \delta_L$

(i.e. $[\tilde{N}_c - \tilde{D}\nabla\tilde{c}\cdot\nabla\tilde{c}] \sim S_L/\delta_L$). As shown by eqs. (6.31-6.33), it is expected that the peak value of $\tilde{N}_c$ conditional on bins of $\tilde{c}$ decreases with increasing Δ, which is consistent with the observations from Fig. 6.6. Moreover, the weighted averaging process involved in LES filtering leads to a decrease in the peak value of $\tilde{N}_c$ conditional on bins of $\tilde{c}$ with an increase in Δ, as the sub-filter volume includes an increasing number of samples with small values of $N_c = D\nabla c\cdot\nabla c$ for $\Delta >> \delta_{th}$.

Quantities	**Scaling estimates**
$\tilde{N}_c$	$\frac{S_L}{\delta_L}$
$\tilde{D}\nabla\tilde{c}.\nabla\tilde{c}$	$\frac{S_L}{\delta_L} Le^{-2}\,\mathrm{Re}_\Delta^{-1}\,Da_\Delta^{-1}$
T_1	$\frac{\tau g_2(Le)\rho_0 S_L^2}{\delta_{th}^2}\times Le\times Da_\Delta^{-0.5}\,\mathrm{Re}_\Delta^{-0.5}$ **alternatively** $\frac{\rho_0 S_L^2}{\delta_{th}^2}\times Le\times Da_\Delta^{-1}$ **The above expressions can be combined as** $\frac{(\overline{\rho u_i c}-\overline{\rho}\tilde{u}_i\tilde{c})\tilde{N}_c}{\Delta}$
T_2	$\frac{\tau\rho_0 S_L^2}{Le^{m-1}\delta_{th}^2}$
$(T_2)_{res}$	$\frac{\rho_0 S_L^2}{\delta_{th}^2}\times\frac{U_{ref}}{S_L}\times Le^{-1}\,\mathrm{Re}_\Delta^{-1.5}\,Da_\Delta^{-1.5}$
T_3	$\frac{\tau\rho_0 S_L^2}{Le^{n-1}\delta_{th}^2}$ **alternatively** $\frac{\rho_0 S_L^2}{\delta_{th}^2}\times Le\times \mathrm{Pr}^{-1/2}\times Ka_\Delta$
$(T_3)_{res}$	$\frac{\rho_0 S_L^2}{\delta_{th}^2}\times\frac{U_{ref}}{S_L}\times Le^{-1}\,\mathrm{Re}_\Delta^{-1.5}\,Da_\Delta^{-1.5}$
T_4	$\frac{\phi(Le)\rho_0 S_L^2}{\delta_{th}^2}$
$(T_4)_{res}$	$\frac{\phi_1(Le)\rho_0 S_L^2}{\delta_{th}^2}\times\mathrm{Re}_\Delta^{-1}\,Da_\Delta^{-1}Le^{-1}$
$(-D_2)$	$\frac{\rho_0\Psi(Le)^2 S_L^2}{\delta_{th}^2}\times Le^{-2}$ alternatively $(-D_2)\sim\frac{\rho_0 S_L^2}{\delta_{th}^2}\times\frac{Ka_\Delta^2}{Pr^3 Le^2}$
$(-D_2)_{res}$	$\frac{\rho_0 S_L^2}{\delta_{th}^2}\times Le^{-2}\,\mathrm{Re}_\Delta^{-2}\,Da_\Delta^{-2}$
$f(D)$	$\frac{\rho_0\tau S_L^2}{Le^{m-1}\delta_{th}^2}$
$f(D)_{res}$	$\frac{\rho_0 S_L^2}{\delta_{th}^2}\times Le^{-2}\,\mathrm{Re}_\Delta^{-2}\,Da_\Delta^{-2}$

Table 6.1: Summary of the scaling estimates of $\tilde{N}_c$ and the terms of its tranport equation.

6.2.2 Effects of *Le* on SDR $\tilde{N}_c$ transport

The variations of the mean values of the unclosed terms of the SDR transport equation conditional on $\tilde{c}$ values for $\Delta \approx 0.4\delta_{th}$ and $2.8\delta_{th}$ are shown in Fig. 6.7 where the magnitudes of these terms are normalised by $\rho_0 S_L^2 / \delta_{th}^2$, which remains the same for all cases considered here. It can be seen from Fig. 6.7 that the magnitude of T_1 remains negligible in comparison to the magnitudes of $T_2, T_3, T_4, (-D_2)$ and $f(D)$ for all filter widths in all cases so that $T_2, T_3, T_4, (-D_2)$ and $f(D)$ remain leading order contributors to the SDR $\tilde{N}_c$ transport irrespective of Δ, which is consistent with previous findings in the context of RANS (Chakraborty and Swaminathan, 2010). It can be seen from Fig. 6.7 that T_2 acts as a source term for both $\Delta >> \delta_{th}$ and $\Delta << \delta_{th}$ in all cases irrespective of *Le*. The magnitude of T_2 shows an increasing trend with decreasing Le and especially for the $Le = 0.34$ and 0.6 cases T_2 assumes much greater values than in the $Le \approx 1.0$ cases (i.e. cases C-E) for a given value of Δ. It can be seen from the S_T / S_L values in Table 4.5 that the rate of burning in turbulent flames increases with decreasing *Le*, which acts to produce greater extent of density-change for small values of Le, leading to an increasing magnitude of T_2 with decreasing *Le*. For low Mach number globally adiabatic flames with *Le*=1.0 yields $T_2 = 2\overline{\rho(\nabla \cdot \vec{u})N_c}$. As dilatation rate $(\nabla \cdot \vec{u})$ remains predominantly positive in premixed flames, the density-variation term T_2 assumes positive values throughout the flame brush for case D. The non-dimensional temperature *T* increases with increasing c within the flame front, which leads to a positive value of $\nabla T \cdot \nabla c$ throughout the flame front for all cases. This along with the predominant positive values of the reaction-diffusion balance $\left[\dot{w} + \nabla \cdot (\rho D \nabla c)\right]$ leads to positive values of T_2 throughout the flame brush for all cases irrespective of the value of Le.

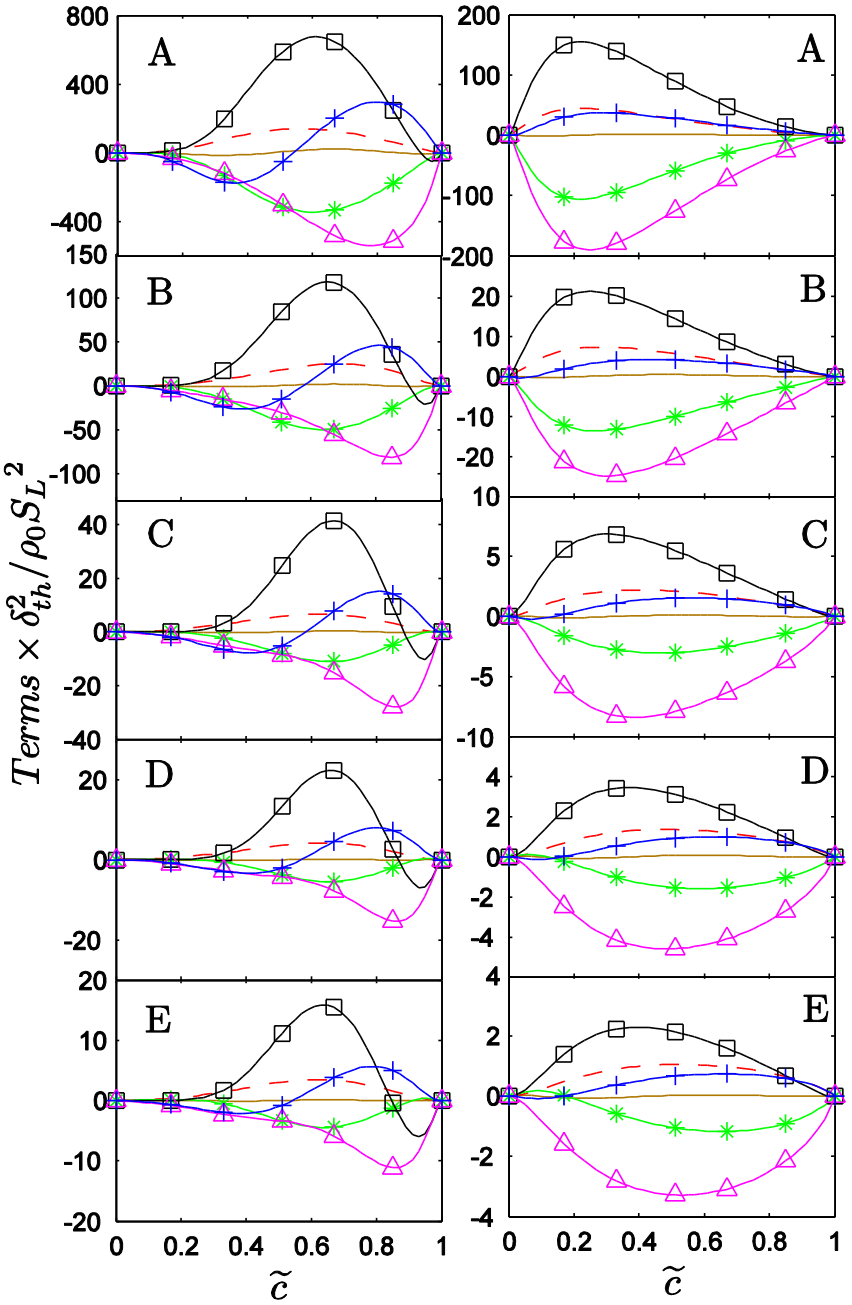

Figure 6.7: Variation of mean values of T_1 (——), T_2 (– – –), T_3 (—✳—), T_4 (—□—), (-D_2) (—△—) and f(D) (—+—) conditional on bins of $\tilde{c}$ at $\Delta \approx 0.4\delta_{th}$ (1st column) and $2.8\delta_{th}$ (2nd column). All the terms are normalised by $\rho_0 S_L^2/\delta_{th}^2$ for the *Le*=0.34 (A), *Le*=0.6 (B), *Le*=0.8 (C), *Le*=1.0 (D), *Le*=1.2(E) cases.

The term T_3 assumes negative values throughout the flame brush for the *Le* = 0.34 and 0.6 cases, whereas this term assumes positive values near both the unburned and burned sides of the flame brush for $\Delta << \delta_{th}$ (e.g. $\Delta \approx 0.4\delta_{th}$) for the $Le \approx 1.0$ cases. The scalar turbulence interaction term T_3 assumes negative values for the major part of the flame brush but positive values can be discerned towards the unburned gas side of the flame

brush for the $Le \approx 1.0$ cases for $\Delta >> \delta_{th}$. As shown in the previous section, the term T_3 can alternatively be expressed as eq. (6.22):

$$T_3 = \overline{-2\rho N_c (e_\alpha \cos^2\alpha + e_\beta \cos^2\beta + e_\gamma \cos^2\gamma)}$$

where e_α, e_β and e_γ are the most extensive, intermediate and most compressive principal strain rates and α, β and γ are the angles between ∇c and e_α, e_β and e_γ respectively.

It is evident that a predominant collinear alignment between ∇c and e_α (e_γ) leads to a negative (positive) contribution of T_3. The probability density functions (pdfs) of $|\cos\alpha|$ and $|\cos\gamma|$ on five different c isosurfaces across the flame front are shown in Fig. 6.8. A high probability of finding $|\cos\alpha| \approx 1.0$ ($|\cos\gamma| \approx 1.0$) indicates a predominant collinear alignment of ∇c with e_α (e_γ). Figure 6.8 shows that ∇c aligns predominantly with e_α for the *Le* = 0.34 and 0.6 cases (i.e. cases A and B), which leads to negative contributions of T_3 in these cases. By contrast, in the $Le \approx 1.0$ cases ∇c aligns predominantly with e_γ both on unburned and burned gas sides of the flame, where the effects of heat release are weak. However, in the $Le \approx 1.0$ cases ∇c starts to align predominantly with e_α for the major part of the flame brush, where the effects of heat release are strong. This alignment statistics for the $Le \approx 1.0$ cases lead to predominantly negative contribution of T_3 for the major part of the flame brush but the local alignment of ∇c with e_γ both on unburned and burned gas sides of the flame leads to positive contribution of T_3 near both the unburned and burned sides of the flame brush for $\Delta << \delta_{th}$ (e.g. $\Delta \approx 0.4\delta_{th}$). The local information is progressively smeared with increasing Δ due to the convolution operation associated with LES filtering, and thus only positive values of T_3 have been observed towards the leading edge of the flame brush for $\Delta >> \delta_{th}$ for the $Le = 1.0$ and 1.2 cases.

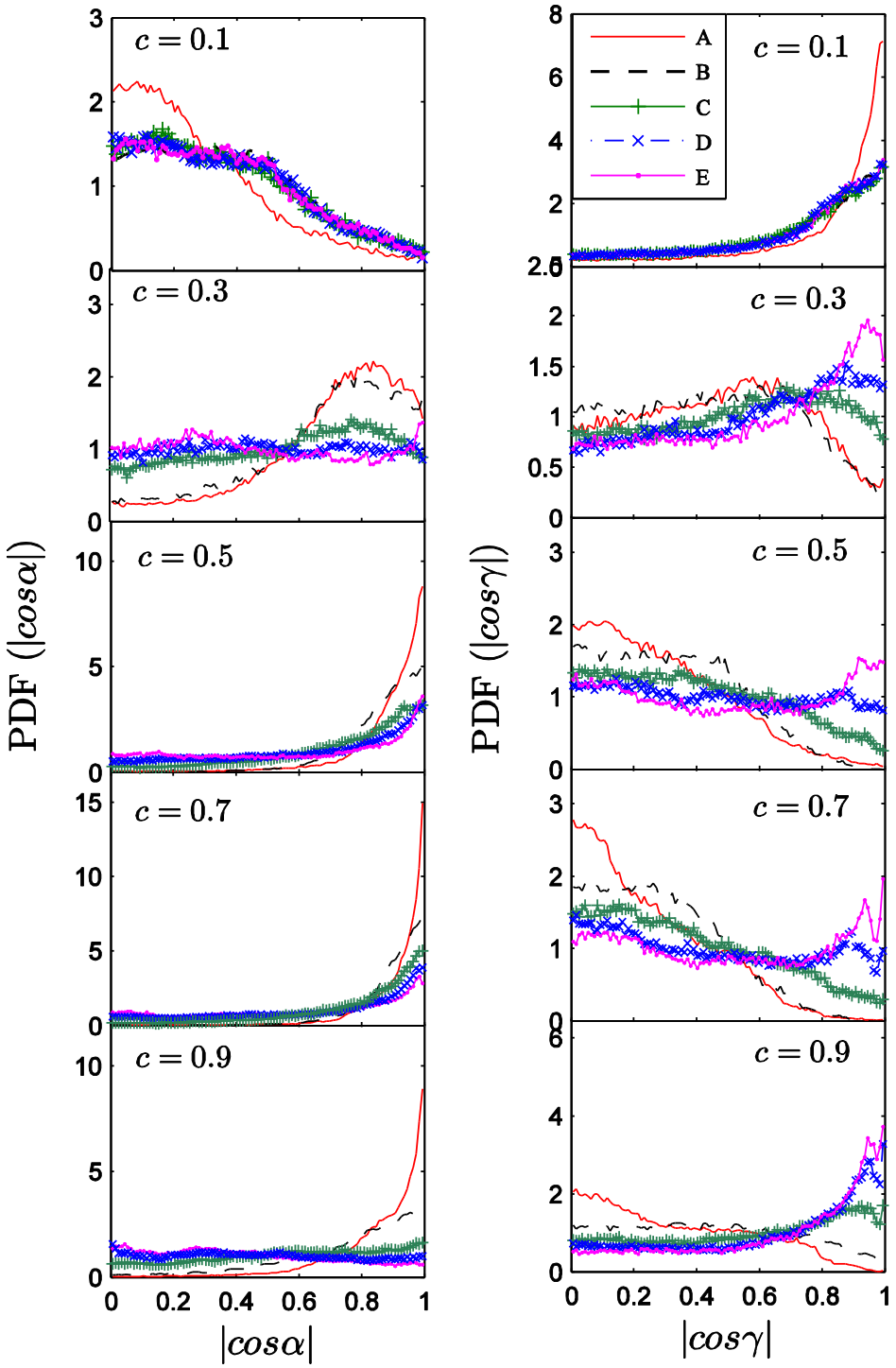

Figure 6.8: Pdfs of $|\cos\alpha|$ (1st column) and $|\cos\gamma|$ (2nd column) on c = 0.1, 0.3, 0.5, 0.7 and 0.9 isosurfaces for the Le = 0.34(A), Le = 0.6(B), Le = 0.8(C), Le = 1.0(D), Le = 1.2(E) cases.

The strain rate a_{chem} arising from flame normal acceleration can be taken to scale as:

$$a_{chem} \sim \tau\, g(Ka, Le) \times \left(\frac{S_L}{\delta_{th}} \right) \tag{6.34}$$

where g is a function which is expected to decrease with increasing Ka as the reacting flow field for high values of Karlovitz number starts to show attributes of the broken reaction zones regime (Peters, 2000) where the effects of heat release are expected to be weak. However, g is also expected to increase with decreasing Le as the effects of flame normal acceleration strengthen with decreasing Le due to augmentation of burning rate (see Table 4.5)[1]. Scaling a_{turb} as: $a_{turb} \sim u'/l$ (Meneveau and Poinsot, 1991) or $a_{turb} \sim u'/\lambda$ (Tennekes and Lumley, 1972) where λ is the Taylor micro-scale, yields respectively:

$$\frac{a_{chem}}{a_{turb}} \sim \tau g(Ka, Le)\, Da \tag{6.35}$$

$$\frac{a_{chem}}{a_{turb}} \sim \tau\, g(Ka, Le)\left(\frac{Da}{\mathrm{Re}_t^{1/2}}\right) \sim \frac{\tau g(Ka, Le)}{Ka} \tag{6.36}$$

As g increases with decreasing Le, the strain rate due to flame normal acceleration a_{chem} dominates over turbulent straining a_{turb} to give rise to a preferential alignment of ∇c with e_α for the $Le = 0.34$ and 0.6 cases. In the *Le* = 0.8, 1.0 and 1.2 cases a_{chem} dominates over a_{turb} only in the region where the flame normal acceleration due to heat release is strong enough to induce $a_{chem} > a_{turb}$. However, a_{turb} dominates over a_{chem} on both unburned and burned gas sides of the flame brush where the effects of heat release are relatively weak. For $Le << 1$ cases (e.g. $Le = 0.34$ and 0.6 flames considered here) $a_{chem} >> a_{turb}$, leading to large negative contributions of T_3, which are comparable to the magnitude of the molecular dissipation term $(-D_2)$. For the low Damköhler number $Le \approx 1.0$ cases considered here (e.g. cases C-E) $a_{chem} \sim a_{turb}$ and thus the effects of a_{chem} are partially nullified by the influences of a_{turb}. This results in a relatively smaller magnitude of T_3 in the $Le \approx 1.0$ cases than in the $Le << 1$ cases (see Fig. 6.7).

[1] The exact form of g is not important for the purpose of this scaling analysis.

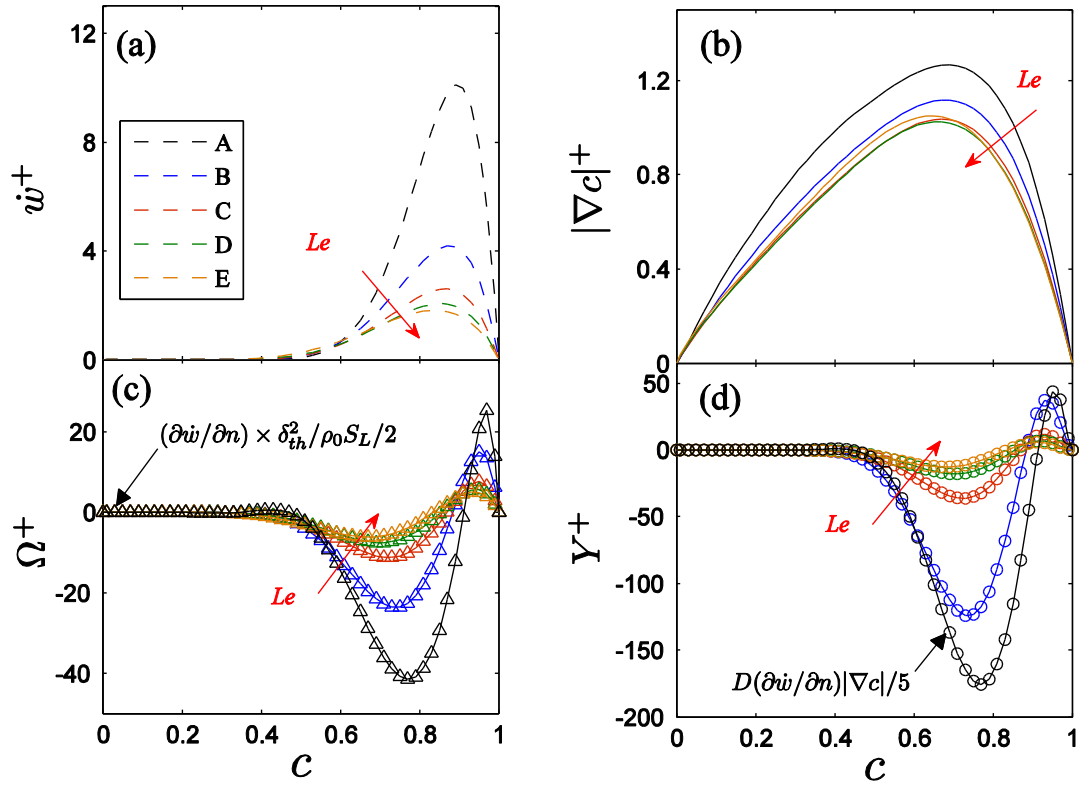

Figure 6.9: Variations of (a) $\dot{w}^+ = \dot{w}\times\delta_{th}/(\rho_0 S_L)$ (- - - -), (b) $|\nabla c|^+ = |\nabla c|\times\delta_{th}$ (——), (c) $\Omega^+ = (\partial\dot{w}/\partial n)\times\delta_{th}^2/(\rho_0 S_L)$ (—△—) and (d) $Y^+ = D(\partial\dot{w}/\partial n)|\nabla c|\times\delta_{th}^2/\rho_0 S_L^2$ (—○—) with c for the *Le*=0.34(A), *Le*=0.6(B), *Le*=0.8(C), *Le*=1.0(D), *Le*=1.2(E) cases.

The term T_4 behaves as a source (sink) term towards the unburned (burned) gas sides of the flame brush for all cases for $\Delta << \delta_{th}$ (e.g. $\Delta \approx 0.4\delta_{th}$). However, T_4 acts as a leading order source term throughout the flame brush for all cases for $\Delta >> \delta_{th}$ (e.g. $\Delta = 28\Delta_m \approx 2.8\delta_{th}$). Figure 6.7 also indicates that the magnitude of T_4 increases with decreasing *Le*. The term $T_4 = 2\overline{D\nabla\dot{w}\cdot\nabla c}$ can alternatively be expressed as: $T_4 = -2\overline{D(\partial\dot{w}/\partial n)|\nabla c|}$ where n is the flame normal direction and $\vec{n} = -\nabla c/|\nabla c|$ is the flame normal vector, which points towards the unburned gas side of the flame. The variations of the mean values of nomrliased reaction rate $\dot{w}^+ = \dot{w}\times\delta_{th}/(\rho_0 S_L)$, normalised magnitude of reaction progress variable gradient $|\nabla c|^+ = |\nabla c|\times\delta_{th}$ and normalised reaction rate gradient in flame normal direction $\Omega^+ = (\partial\dot{w}/\partial n)\times\delta_{th}^2/(\rho_0 S_L)$ conditional on bins of c are shown in Fig. 6.9 , which shows Ω^+ assumes negative values for the major part of the flame brush except the burned gas side where Ω^+ is positive. For single step chemistry the maximum value of $\dot{w}$ occurs close to $c \approx 0.8$, which suggests that the probability of finding negative (positive) values of Ω^+ is significant for

$c<0.8$ ($c>0.8$). The variations of the mean values of $Y^+ = D(\partial\dot{w}/\partial n)|\nabla c| \times \delta_{th}^2 / \rho_0 S_L^2$ conditional on bins of c across the flame front for different values of Le are also shown in Fig. 6.9, which shows that Y^+ assumes negative values for the major part of the flame front before assuming positive values towards the burned gas side, and the magnitude of Y^+ increases significantly with decreasing Le. The negative (positive) values of Ω^+ and Y^+ lead to positive (negative) values of $T_4 = -2\overline{D(\partial\dot{w}/\partial n)|\nabla c|}$ when the flame is partially resolved (i.e. $\Delta < \delta_{th}$, for example $\Delta \approx 0.4\delta_{th}$), which can be confirmed by Figs. 6.7 and 6.9. For $\Delta > \delta_{th}$, the flame is completely unresolved and thus the sub-filter volume includes more positive samples with high magnitudes of $(-2D(\partial\dot{w}/\partial n)|\nabla c|)$ than the negative samples which are confined only in a small region within the flame front. This leads to predominantly positive values of T_4 throughout the flame brush for $\Delta > \delta_{th}$ (e.g. $\Delta \approx 2.8\delta_{th}$, see Fig. 6.7). It is evident from Fig. 6.9 that the magnitudes of $\dot{w}^+$, Ω^+ and Y^+ increase with decreasing Le and this trend is especially strong for the $Le \ll 1$ cases (e.g. $Le = 0.34$ and 0.6 cases considered here). The high magnitudes of $D(\partial\dot{w}/\partial n)|\nabla c|$ for small values of Le (see Fig. 6.9) give rise to an increasing magnitude of $T_4 = -2\overline{D(\partial\dot{w}/\partial n)|\nabla c|}$ with decreasing *Le*.

Figure 6.7 shows that the molecular dissipation term $(-D_2)$ acts as a leading order sink term for all cases irrespective of Δ. However, the magnitude of $(-D_2)$ also increases with decreasing *Le*. It is worth noting that the components of the tensor σ_c (where the components of σ_c are given by $\partial h_i / \partial x_j$ with h_i being $\partial c / \partial x_i$) assume non-zero values only in the flame front and $|\nabla c|^{-1}$ provides a measure of the local flame thickness where σ_c remains active. The probability of finding high values of $|\nabla c|$ increases signficantly with decreasing *Le* (see Table 4.5 and Fig. 6.9), which indicates a high probability of finding thin flame front for small values of Le. This acts to increase the magnitude of the components of σ_c, which, along with an increase in mass diffusivity D with decreasing Le, leads to high magnitudes of $(-D_2)$ for small values of Le at a given Δ.

The term $f(D) = \overline{f_1(D)}$ assumes negative (positive) values towards the unburned (burned) gas sides of the flame brush with the transition taking place close to the middle of the flame brush for all cases for $\Delta << \delta_{th}$ (e.g. $\Delta \approx 0.4\delta_{th}$). However, the magnitude of the negative contribution of $f(D)$ remains smaller than the positive contribution for $\Delta << \delta_{th}$, which indicates that the negative contribution of $f_1(D)$ on the unburned gas side also remains smaller than the positive $f_1(D)$ contribution on the burned gas side. The high magnitude of positive samples of $f_1(D)$ overcomes the negative contributions of $f_1(D)$ in the filter volume for $\Delta >> \delta_{th}$ (e.g. $\Delta \approx 2.8\delta_{th}$), which gives rise to predominantly positive values of $f(D)$ for the major part of the flame brush. In cases A-E, $FD5$ can be expressed as: $FD5 = \overline{\rho D N_c (\partial u_j / \partial x_j)}$ (i.e. for constant ρD) and the first two terms $FD1$ and $FD2$ on the right hand side of eq. (6.7) vanish for constant values of ρD. The contributions of the third and fourth terms on the right hand side of eq. (6.7) ($FD3$ and $FD4$) are responsible for the change in sign of $f(D)$ within the flame brush.

It can be seen from Fig. 6.7 that the magnitudes of $T_1, T_2, T_3, T_4, (-D_2)$ and $f(D)$ are significantly affected by Δ, and the filter size dependences of the unclosed terms of the SDR $\tilde{N}_c$ transport equation will be discussed next in thiscChapter.

6.2.3 Scaling estimate and filter size dependence of turbulent transport term T_1

The variations of the mean values of the turbulent transport term T_1 (see eq. 6.2 for its definition) conditional on bins of $\tilde{c}$ for cases A-E are shown for $\Delta \approx 0.4\delta_{th}, 1.6\delta_{th}$ and $2.8\delta_{th}$ in Fig. 6.10, which shows that T_1 assumes negative values towards both unburned and burned gas sides while attaining positive values in the middle of the flame brush for all cases considered here. Equation 6.2 and the previous section has shown that T_1 is closely related to the sub-grid flux of SDR $F_i^{sg} = (\overline{\rho u_i N_c} - \bar{\rho}\tilde{u}_i\tilde{N}_c)$. The variation of mean values of $F_i^{sg} M_i = (\overline{\rho u_i N_c} - \bar{\rho}\tilde{u}_i\tilde{N}_c) M_i$ and $(\partial \tilde{N}_c / \partial x_i) M_i$ conditional on bins of $\tilde{c}$ are also shown in Fig. 6.10. It can be seen from Fig. 6.10 that $F_i^{sg} M_i$ and $(\partial \tilde{N}_c / \partial x_i) M_i$ predominantly show same (different) signs for major portion of the flame brush in case A-C (cases D-E). A gradient hypothesis based closure for $\vec{F}^{sg}$ yields: $\vec{F}^{sg} = -(\mu_t / \sigma_N) \nabla \tilde{N}_c$ where μ_t is the eddy viscosity and σ_N is a suitable Schmidt

number. Thus, the same (different) signs of $F_i^{sg} M_i$ and $(\partial \tilde{N}_c / \partial x_i) M_i$ indicate a counter-gradient (gradient) transport of SDR. Figure 6.10 indicates that a gradient transport is prevalent (i.e. $F_i^{sg} \propto (-\partial \tilde{N}_c / \partial x_i)$) for cases D and E for $\Delta >> \delta_{th}$, whereas a predominantly counter-gradient transport has been observed for cases A-C for $\Delta >> \delta_{th}$, which is consistent with a previous analysis in the context of RANS (Chakraborty and Swaminathan, 2010). The flame normal acceleration strengthens with the augmentation of heat release with decreasing Le, and a counter-gradient transport is obtained when the effects of flame normal acceleration overcome the effects of turbulent velocity fluctuations and *vice versa*. The effects of Le on turbulent transport have been discussed elsewhere (Chakraborty and Cant, 2009; 2009a; 2009b) and thus will not be addressed here. The aforementioned scaling arguments yield:

$$T_1 \sim \frac{\rho_0 \tau g_2(Le) S_L \tilde{N}_c}{\Delta} \sim \frac{\rho_0 \tau g_2(Le) S_L^2}{\delta_{th}^2} \times Le \times Da_\Delta^{-0.5} \, \mathrm{Re}_\Delta^{-0.5} \text{ for } \Delta >> \delta_{th} \tag{6.37}$$

In eq. (6.37) the sub-grid flux of SDR is scaled as:

$$\overline{(\rho u_i N_c} - \bar{\rho} \tilde{u}_i \tilde{N}_c) \sim \rho_0 \tau g_2(Le) S_L \tilde{N}_c \sim \rho_0 \tau g_2(Le) \frac{S_L^2}{\delta_L} \tag{6.38}$$

where the sub-grid velocity fluctuations are scaled with respect to $\tau g_2(Le) S_L$ where $g_2(Le)$ is a function (the exact form is not important for the purpose of this scaling analysis) which increases with decreasing Le and accounts for strengthening of flame normal acceleration with decreasing Le .

Alternatively, the sub-grid velocity fluctuations can be scaled using u'_Δ as: $\overline{(\rho u_i N_c} - \bar{\rho} \tilde{u}_i \tilde{N}_c) \sim \rho_0 u'_\Delta \tilde{N}_c \sim \left(\rho_0 S_L u'_\Delta\right) / \delta_L$. Accordingly, T_1 could be scaled in the following manner:

$$T_1 \sim \frac{\rho_0 S_L u'_\Delta}{\Delta \delta_L} \sim \frac{\rho_0 S_L^2}{\delta_{th}^2} \times Le \times Da_\Delta^{-1} \text{ for } \Delta >> \delta_{th} \tag{6.39}$$

Equation (6.37) is more suitable for counter-gradient transport as $u'_\Delta << \tau S_L$ whereas eq. (6.39) is proper for gradient transport for $u'_\Delta >> \tau S_L$. For the cases considered here a combination of counter-gradient and gradient transport has been observed (see Fig. 6.10) and thus both eqs. (6.37) and (6.39) remain relevant. Equations (6.37) and (6.39) indicate

that the magnitude of T_1 is expected to decrease with increasing Δ, as $Da_\Delta = (\Delta/\delta_{th})(S_L/u'_\Delta)$ and $Da_\Delta \mathrm{Re}_\Delta \sim (\Delta/\delta_{th})^2$ increase with increasing Δ (Dunstan et al., 2013).

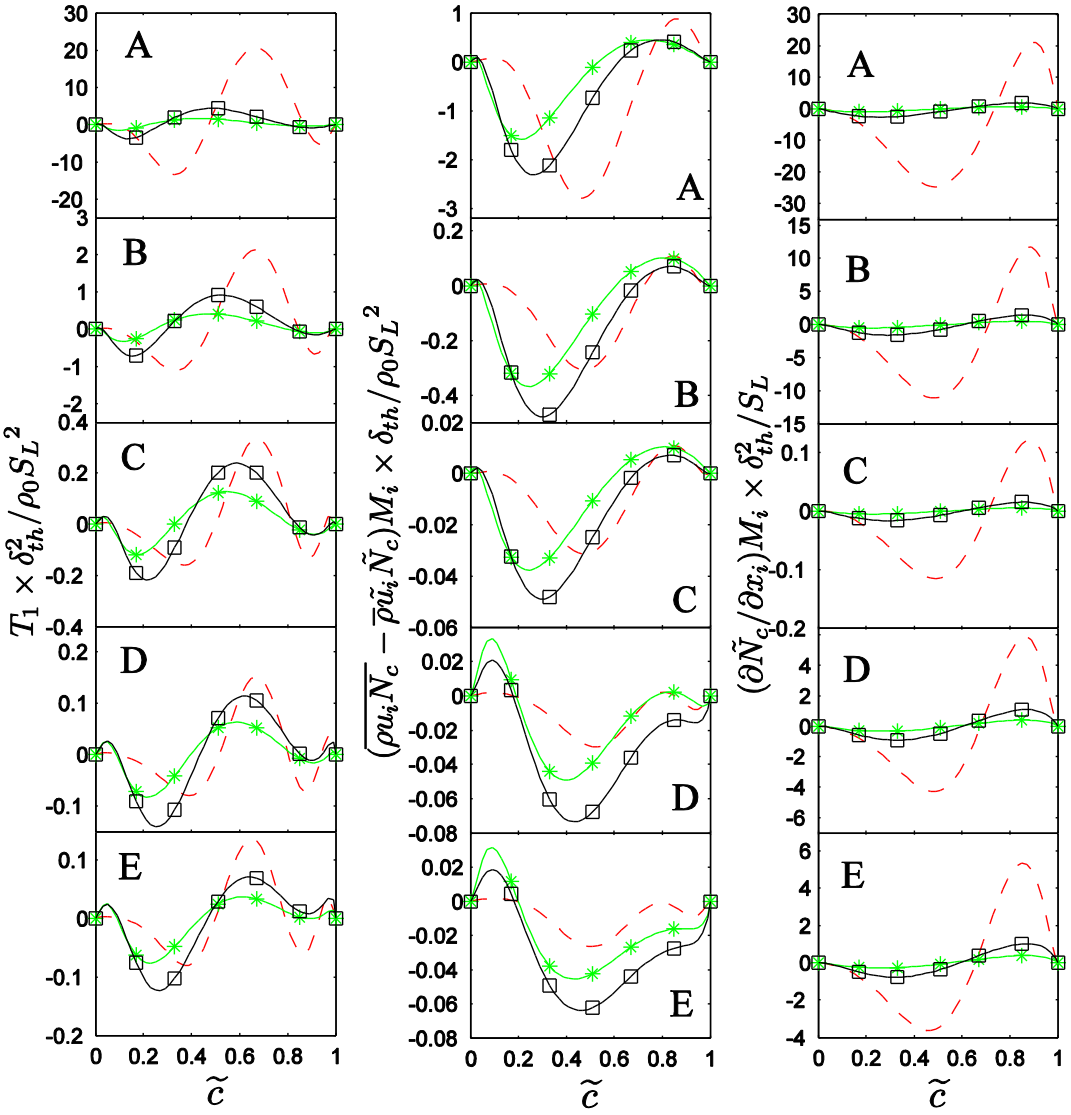

Figure 6.10: Variation of mean values of $T_1 \times \delta_{th}^2/\rho_0 S_L^2$ (1st column), $\left(\overline{\rho u_i N_c} - \bar{\rho}\tilde{u}_i\tilde{N}_c\right)M_i \times \delta_{th}/\rho_0 S_L^2$ (2nd column) and $\left(\partial\tilde{N}_c/\partial x_i\right)M_i \times \delta_{th}^2/S_L$ (3rd column) conditional on bins of $\tilde{c}$ at $\Delta \approx 0.4\delta_{th}$ (- - -), $1.6\delta_{th}$ (—▫—) and $2.8\delta_{th}$ (—✳—) for the *Le*=0.34(A), *Le*=0.6(B), *Le*=0.8(C), *Le*=1.0(D), *Le*=1.2(E) cases.

It is evident from Fig. 6.10 that the magnitude of T_1 indeed decreases with increasing Δ. Moreover, the scaling estimates $T_1 \sim \rho_0 \tau g_2(Le) S_L \tilde{N}_c/\Delta$ and $T_1 \sim \rho_0 u'_\Delta \tilde{N}_c/\Delta$ indicate an increasing trend of T_1 with decreasing Le due to high values of $\tilde{N}_c$ and $g_2(Le)$ for small values of Le. This can also be substantiated from Fig. 6.10, which shows that the magnitude of T_1 increases with decreasing Le for a given Δ.

It is worth noting that the sub-grid flux of reaction progress variable $R_i^{sg} = (\overline{\rho u_i c} - \bar{\rho}\tilde{u}_i\tilde{c})$ can be scaled with respect to $\rho_0 \tau g_2(Le) S_L$ ($\rho_0 u'_\Delta$) in the case of counter-gradient (gradient) transport where $u'_\Delta << \tau S_L$ ($u'_\Delta >> \tau S_L$). This leads to the following scaling relations for $F_i^{sg} = (\overline{\rho u_i N_c} - \bar{\rho}\tilde{u}_i\tilde{N}_c)$ and T_1:

$$\overline{(\rho u_i N_c} - \bar{\rho}\tilde{u}_i\tilde{N}_c) \sim (\overline{\rho u_i c} - \bar{\rho}\tilde{u}_i\tilde{c})\tilde{N}_c \text{ and } T_1 \sim \frac{\overline{(\rho u_i c} - \bar{\rho}\tilde{u}_i\tilde{c})\tilde{N}_c}{\Delta} \text{ for } \Delta >> \delta_{th} \qquad (6.40)$$

Equation (6.40) remains valid for both gradient and counter-gradient transport. Moreover, eq. (6.40) indicates that the modelling of sub-grid flux of SDR F_i^{sg} is closely related to the closure of sub-grid scalar flux R_i^{sg}. This is consistent with previous findings (Chakraborty and Swaminathan, 2010) in the context of RANS, which demonstrated that the statistical behaviour and modelling of Reynolds fluxes of SDR and the scalar are closely related and one obtains counter-gradient (gradient) transport of Reynolds flux of SDR where turbulent scalar flux shows counter-gradient (gradient) behaviour. Equation (6.40) further indicates that the modelling of sub-grid flux of SDR F_i^{sg} and turbulent transport term T_1 in the context of LES depends on accurate modelling of sub-grid scalar flux R_i^{sg}. Thus the models for F_i^{sg} and T_1 should be proposed in terms of R_i^{sg} so that both counter-gradient and gradient transports of SDR can be appropriately accounted for in LES of premixed turbulent combustion. It is worth noting that failing to address counter-gradient transport of F_i^{sg} could potentially lead to artificial thickening of the flame. Under extreme conditions, transported SDR could provide high unrealistic values of SDR and filtered reaction rate in the burned gas side of the flame brush in the absence of accuarate turbulent transport modelling.

6.2.4 Scaling estimates and filter size dependences of the density-variation term, T_2, and the scalar-turbulence interaction term, T_3

The contribution of the density variation term, T_2 (defined in eq. (6.3)), for low Mach number unity Lewis number flames can be expressed as $T_2 = 2\overline{\rho \nabla \cdot \vec{u} N_c}$ which does not strictly hold for non-unity Lewis number flames, but T_2 could still be scaled as:

$T_2 \sim 2\overline{\rho\nabla\cdot\vec{u}N_c}$. Chakraborty *et al*. (2009) proposed that the dilatation rate $\nabla\cdot\vec{u}$ could be scaled as:

$$\nabla\cdot\vec{u} \sim \frac{1}{Le^m}\left(\frac{\tau S_L}{\delta_{th}}\right) \tag{6.41}$$

where m is a positive number, but greater than unity (i.e. $m>1$), which suggests that T_2 can be scaled as:

$$T_2 \sim \frac{\rho_0 \tau S_L^2}{Le^{m-1}\delta_{th}^2} \tag{6.42}$$

The resolved part of T_2 (i.e. $(T_2)_{res}$) can be scaled in the following manner for $\Delta >> \delta_{th}$:

$$(T_2)_{res} \sim \bar{\rho}\tilde{D}\frac{\partial\tilde{c}}{\partial x_k}\frac{\partial\tilde{c}}{\partial x_k}\frac{\partial\tilde{u}_j}{\partial x_j} \sim \frac{\rho_0 S_L^2}{\delta_{th}^2}\times\frac{U_{ref}}{S_L}\times\frac{1}{Le\,\mathrm{Re}_\Delta^{1.5}\,Da_\Delta^{1.5}} \text{ for } \Delta>>\delta_{th} \tag{6.43}$$

where U_{ref} is a velocity scale representing the Favre-filtered velocity components $\tilde{u}_i$ and the length scale associated with resolved scale velocity gradients is taken to scale with Δ for $\Delta >> \delta_{th}$. Equations 6.42 and 6.43 show that the contribution of $(T_2)_{res}$ to T_2 decreases with increasing Δ. Also the high probability of obtaining small values of $-2(D/\rho)\left[\dot{w}+\nabla.\left(\rho D\nabla c\right)\right]\nabla c.\nabla\rho$ with increasing Δ, as large values of $-2(D/\rho)\left[\dot{w}+\nabla.\left(\rho D\nabla c\right)\right]\nabla c.\nabla\rho$ and N_c are confined within the flame front, further reduces the magnitude of T_2 with increasing Δ. However, $T_2\times\delta_{th}^2/\rho_0 S_L^2$ remains of the order of τ/Le^{m-1} irrespective of Δ. The aforementioned behaviour of T_2 in response to Δ and Le can be verified from Fig. 6.11 where the variations of the mean values of T_2 conditional on bins of $\tilde{c}$ for cases A-E are shown for $\Delta \approx 0.4\delta_{th}, 1.6\delta_{th}$ and $2.8\delta_{th}$.

The predominant negative values of the scalar turbulence interaction term T_3 (see eq. (6.4) for its definition) indicates a predominant ∇c alignment with e_α, and the dominance of a_{chem} over a_{turb}. For $Le \neq 1$ flames a_{chem} can be taken to scale with $a_{chem} \sim Le^{-n}(\tau S_L/\delta_{th})$ where n is a positive number greater than unity (i.e. $n>1$). This can be utilised to scale T_3 as:

$$T_3 \sim \overline{\rho a_{chem} N_c} \sim \frac{\tau \rho_0 S_L^2}{Le^{n-1}\delta_{th}^2} \tag{6.44}$$

whereas the resolved part of T_3 (i.e. $(T_3)_{res}$) can be scaled in the following manner for $\Delta >> \delta_{th}$:

$$(T_3)_{res} = -2\overline{\rho D \frac{\partial \tilde{c}}{\partial x_i} \frac{\partial \tilde{u}_i}{\partial x_j} \frac{\partial \tilde{c}}{\partial x_j}} \sim \frac{\rho_0 S_L^2}{\delta_{th}^2} \times \frac{U_{ref}}{S_L} \times \frac{1}{Le\, \mathrm{Re}_\Delta^{1.5}\, Da_\Delta^{1.5}} \tag{6.45}$$

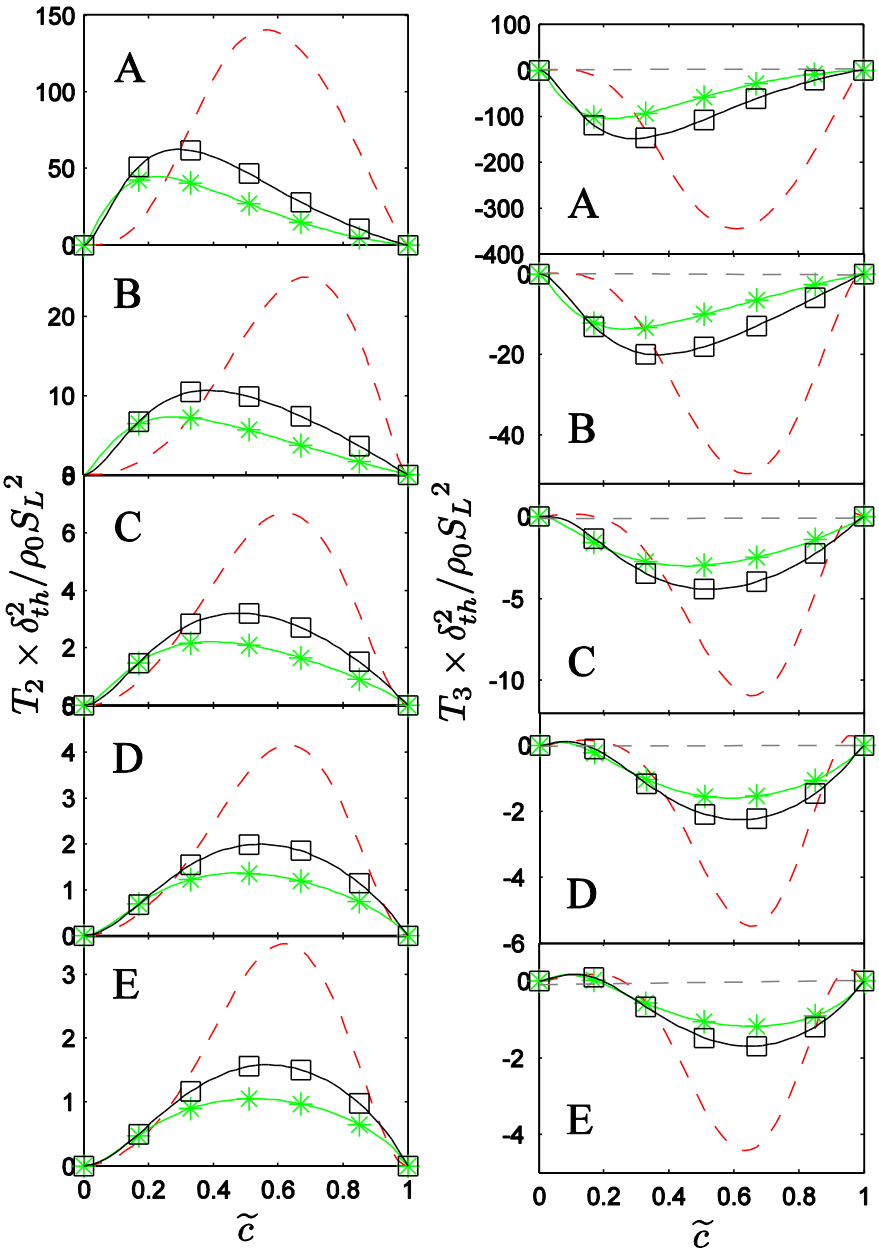

Figure 6.11: Variation of mean values of $T_2 \times \delta_{th}^2/\rho_0 S_L^2$ (1st column) and $T_3 \times \delta_{th}^2/\rho_0 S_L^2$ (2nd column) conditional on bins of $\tilde{c}$ at $\Delta \approx 0.4\delta_{th}$ (- - -), $1.6\delta_{th}$ (—□—) and $2.8\delta_{th}$ (—*—) for the *Le*=0.34(A), *Le*=0.6(B), *Le*=0.8(C), *Le*=1.0(D), *Le*=1.2(E) cases.

Equations (6.44) and (6.45) indicate that the contribution of $(T_3)_{res}$ to T_3 progressively decreases with increasing Δ, which along with an increased probability of obtaining small magnitudes of $-2\rho(e_\alpha \cos^2\alpha + e_\beta \cos^2\beta + e_\gamma \cos^2\gamma)N_c$ within the filter volume, leads to a reduction in magnitude of T_3 with increasing Δ. This can also be substantiated from Fig. 6.11 where the variations of the mean values of T_3 conditional on bins of $\tilde{c}$ for cases A-E are shown for $\Delta \approx 0.4\delta_{th}$, $1.6\delta_{th}$ and $2.8\delta_{th}$. Equations (6.44) and (6.45) indicate that the magnitude of T_3 for a given filter width is expected to show an increasing trend with decreasing Le, which is consistent with the variation of T_3 shown in Fig. 6.11.

It is worth noting that T_3 can alternatively scaled based on $a_{turb} \sim u'/\lambda$ as: $T_3 \sim \overline{\rho a_{turb} N_c}$, which yields an alternative scaling estimate of T_3 subject to the inertial range assummption $(\mu/\rho)(u'^2/\lambda^2) \sim u_\Delta'^3/\Delta$:

$$T_3 \sim \overline{\rho a_{turb} N_c} \sim \frac{\rho_0 S_L^2}{\delta_{th}^2} \times \frac{Le}{Pr^{1/2}} \times \frac{\mathrm{Re}_\Delta^{1/2}}{Da_\Delta} \sim \frac{\rho_0 S_L^2}{\delta_{th}^2} \times \frac{Le}{Pr^{1/2}} \times Ka_\Delta \tag{6.46}$$

Equation (6.46) is more appropriate for high Karlovitz number combustion where the effects of heat release are expected to be weak. However, both eqs. (6.44) and (6.46) indicate that T_3 is expected to play a key role in the SDR $\tilde{N}_c$ transport, which is consistent with the observations made from Fig. 6.7.

6.2.5 Scaling estimates and filter size dependences of the reaction rate contribution, T_4, molecular dissipation term, ($-D_2$), and the diffusivity gradient term, $f(D)$

The reaction rate gradient $\partial\dot{w}/\partial n$ can be scaled as $\partial\dot{w}/\partial n \sim \varphi(Le) \times (\rho_0 S_L/\delta_{th}^2)$ where $\phi(Le)$ is a function, which increases with decreasing *Le* in order to account for the augmentation of the magnitudes of $\partial\dot{w}/\partial n$ (see Fig. 6.12) with decreasing *Le*. The above information can be utilised to obtain following scaling estimates for the reaction rate contribution, T_4 (defined in eq. 6.6), and the resolved component of T_4 for $\Delta >> \delta_{th}$:

$$T_4 \sim \frac{\phi(Le)\rho_0 S_L^2}{\delta_{th}^2} \tag{6.47}$$

$$(T_4)_{res} = 2\tilde{D}\frac{\partial\overline{\dot{w}}}{\partial x_i}\frac{\partial\tilde{c}}{\partial x_i} \sim \frac{\varphi_1(Le)\rho_0 S_L^2}{\delta_{th}^2} \times \frac{1}{LeRe_\Delta Da_\Delta} \tag{6.48}$$

where $\dot{\bar{w}}$ is scaled as $\dot{\bar{w}} \sim \varphi_1(Le) \times (\rho_0 S_L / \delta_{th})$ with $\varphi_1(Le)$ being a function, which increases with decreasing Le to account for high burning rate for low Lewis number flames (see Table 4.5 and Fig. 6.9). It is worth noting that the exact mathematical expressions of φ and φ_1 are not important for the purpose of this scaling analysis.

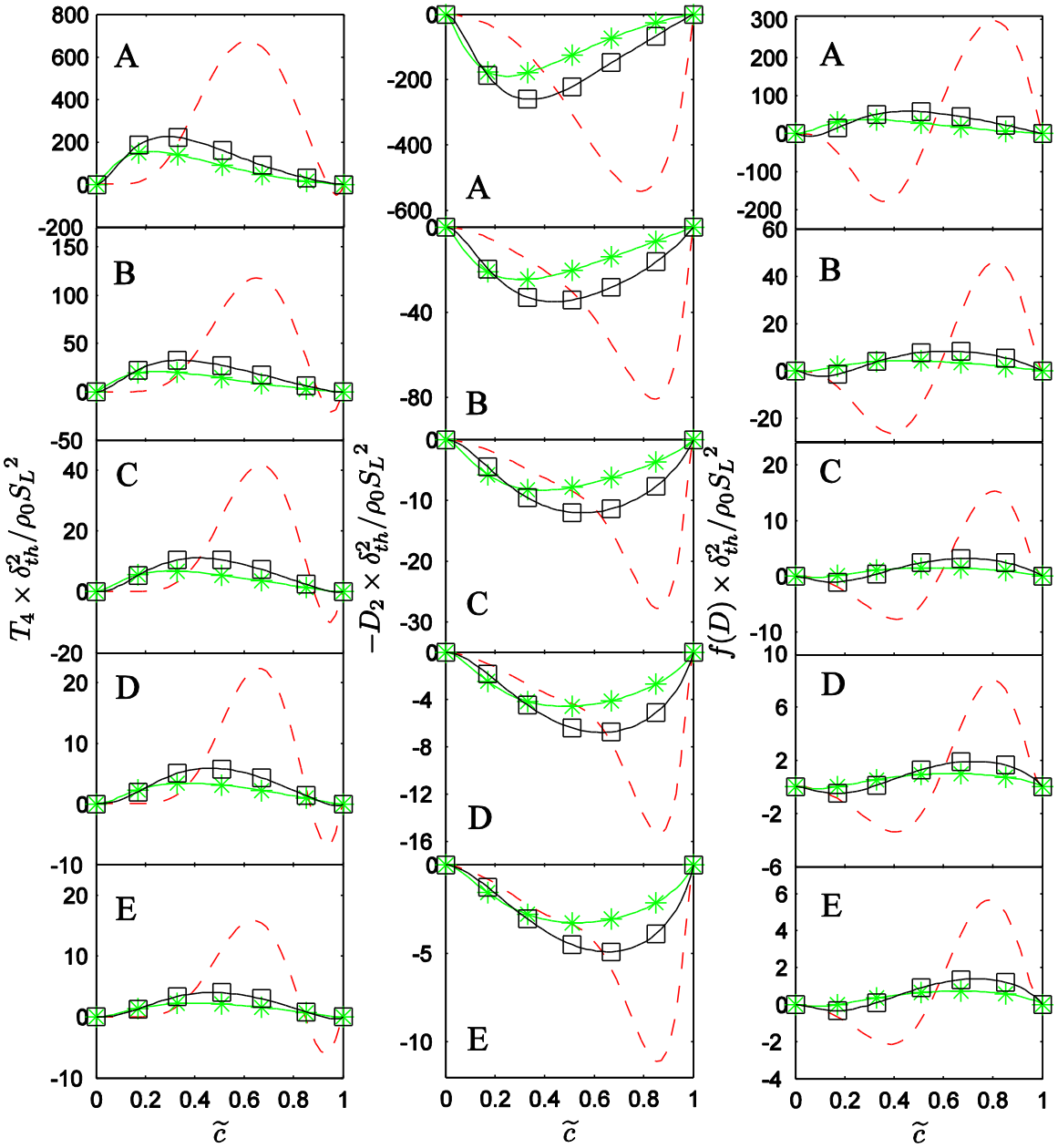

Figure 6.12: Variation of mean values of $T_4 \times \delta_{th}^2/\rho_0 S_L^2$ (1st column), $(-D_2) \times \delta_{th}^2/\rho_0 S_L^2$ (2nd column) and $f(D) \times \delta_{th}^2/\rho_0 S_L^2$ (3rd column) with $\tilde{c}$ at $\Delta \approx 0.4\delta_{th}$ (- - -), $1.6\delta_{th}$ (—□—) and $2.8\delta_{th}$ (—✳—) for the *Le*=0.34(A), *Le*=0.6(B), *Le*=0.8(C), *Le*=1.0(D), *Le*=1.2(E) cases.

It has already been discussed earlier in this analysis that the components of σ_c is expected to assume high magnitudes for small values of Le because of thinning of the flame front (see Figs. 6.6 and 6.9). Thus, the components of σ_c could be scaled as: $\sigma_c \sim \Psi(Le)/\delta_{th}^2$

where $\Psi(Le)$ is a function (again the exact mathematical expression is not important for this analysis), which increases with decreasing *Le* in order to account for the thinning of flame front for small values of Le (see Figs. 6.6 and 6.9). Using $\sigma_c \sim \Psi(Le)/\delta_{th}^2$ yields following scaling estimates for the molecular dissipation term $(-D_2)$ (see eq. (6.6) for its definition) and its resolved component $(-D_2)_{res}$ for $\Delta >> \delta_{th}$:

$$(-D_2) \sim \frac{\rho_0 \Psi(Le)^2 S_L^2}{\delta_{th}^2} \times Le^{-2} \tag{6.49}$$

$$(-D_2)_{res} = -2\bar{\rho}\tilde{D}^2 \frac{\partial^2 \tilde{c}}{\partial x_i \partial x_j} \frac{\partial^2 \tilde{c}}{\partial x_i \partial x_j} \sim \frac{\rho_0 S_L^2}{\delta_{th}^2} \times \frac{1}{Le^2 Re_\Delta^2 Da_\Delta^2} \tag{6.50}$$

Subject to the assumption of inertial scaling $u'^3/l \sim u_\Delta'^3/\Delta$ one obtains the alternative scaling when σ_c is scaled with respect to the Kolmogorov scale η similar to the passive scalar mixing:

$$(-D_2) \sim \frac{\rho_0 S_L^2}{\delta_{th}^2} \times \frac{Ka_\Delta^2}{Pr^3 Le^2}, \text{ for } \Delta >> \delta_{th} \tag{6.51}$$

For the current cases $Ka^{1/2} \sim \delta_{th}/\eta \sim O(1)$, so both eqs. (6.49) and (6.51) are expected to yield similar scaling estimates.

As ρD is treated as constant in cases A-E, the first two terms of the difffusivity gradient term *f*(*D*) (see eq. (6.7) for its definition) on the right hand side vanish and $FD5$ can be expressed as: $FD5 = \overline{\rho \nabla \cdot \vec{u} N_c}$ using the mass conservation equation. It has been discussed earlier that T_2 could be scaled as: $T_2 \sim 2\overline{\rho \nabla \cdot \vec{u} N_c}$ whereas an equality holds for the $Le = 1.0$ flames. Thus, for the present cases $f(D)$ can be scaled as: $f(D) \sim (T_2/2) + FD3 + FD4$ using $\overline{\rho N_c \nabla . \vec{u}} \sim T_2/2$. This leads to the following scaling estimation of $f(D)$ using eq. (6.42):

$$f(D) \sim T_2 \sim \frac{\rho_0 \tau S_L^2}{Le^{m-1} \delta_{th}^2} \tag{6.52}$$

whereas the resolved component $f(D)_{res}$, can be taken to scale as:

$$f(D)_{res} = 2\tilde{D}\frac{\partial\tilde{c}}{\partial x_k}\frac{\partial(\bar{\rho}\tilde{D})}{\partial x_k}\frac{\partial^2\tilde{c}}{\partial x_j\partial x_j} + 2\tilde{D}\frac{\partial\tilde{c}}{\partial x_k}\frac{\partial^2(\bar{\rho}\tilde{D})}{\partial x_j\partial x_k}\frac{\partial\tilde{c}}{\partial x_j} - \frac{\partial}{\partial x_j}\left[\bar{\rho}\tilde{D}\left(\frac{\partial\tilde{c}}{\partial x_k}\frac{\partial\tilde{c}}{\partial x_k}\right)\frac{\partial\tilde{D}}{\partial x_j}\right]$$
$$-2\bar{\rho}\tilde{D}\frac{\partial\tilde{D}}{\partial x_j}\frac{\partial}{\partial x_j}\left(\frac{\partial\tilde{c}}{\partial x_k}\frac{\partial\tilde{c}}{\partial x_k}\right) + \bar{\rho}\left(\frac{\partial\tilde{c}}{\partial x_k}\frac{\partial\tilde{c}}{\partial x_k}\right)\left[\frac{\partial\tilde{D}}{\partial t} + \tilde{u}_j\frac{\partial\tilde{D}}{\partial x_j}\right] \quad (6.53)$$
$$\sim \frac{\rho_0 S_L^2}{\delta_{th}^2}\times Le^{-2}\,\mathrm{Re}_\Delta^{-2}\,Da_\Delta^{-2}$$

Equations (6.47)-(6.53) demonstrate that the magnitudes of $(T_4)_{res}$, $(-D_2)_{res}$ and $f(D)_{res}$ decrease with increasing Δ, which along with increased probability of obtaining small magnitudes of $2D\nabla\dot{w}.\nabla c$, $-2\rho D^2(\partial h_i/\partial x_j)(\partial h_i/\partial x_j)$ and $f_1(D)$ within the filter volume for $\Delta >> \delta_{th}$, leads to reductions in magnitudes of T_4, $(-D_2)$ and $f(D)$ with increasing Δ. This behaviour can be confirmed from Fig. 6.12 where the variations of the mean values of T_4, $(-D_2)$ and $f(D)$ conditional on bins of $\tilde{c}$ for all cases are shown for $\Delta\approx 0.4\delta_{th}$, $1.6\delta_{th}$ and $2.8\delta_{th}$. Equations (6.47)-(6.53) also suggest that the magnitudes of T_4, $(-D_2)$ and $f(D)$ are expected to increase with decreasing *Le* for a given Δ, which can also be substantiated from Fig. 6.12.

Case	u'/S_L	l/δ_{th}	Re_t	*Da*	τ	*Le*	*Ka*	c_m	K_c^*/τ
A	**7.5**	**2.45**	**47.0**	**0.33**	**4.5**	**0.34**	**13.2**	**0.92**	**0.52**
B	**7.5**	**2.45**	**47.0**	**0.33**	**4.5**	**0.6**	**13.2**	**0.87**	**0.67**
C	**7.5**	**2.45**	**47.0**	**0.33**	**4.5**	**0.8**	**13.2**	**0.867**	**0.71**
D	**7.5**	**2.45**	**47.0**	**0.33**	**4.5**	**1.0**	**13.2**	**0.825**	**0.78**
E	**7.5**	**2.45**	**47.0**	**0.33**	**4.5**	**1.2**	**13.2**	**0.816**	**0.79**
F	**5.0**	**1.67**	**22.0**	**0.33**	**4.5**	**1.0**	**8.67**	**0.825**	**0.78**
G	**6.25**	**1.44**	**23.5**	**0.23**	**4.5**	**1.0**	**13.0**	**0.825**	**0.78**
H	**7.5**	**2.50**	**48.0**	**0.33**	**4.5**	**1.0**	**13.0**	**0.825**	**0.78**
I	**9.0**	**4.31**	**100**	**0.48**	**4.5**	**1.0**	**13.0**	**0.825**	**0.78**
J	**11.25**	**3.75**	**110**	**0.33**	**4.5**	**1.0**	**19.5**	**0.825**	**0.78**
K	**7.5**	**2.45**	**47.0**	**0.33**	**2.0**	**1.0**	**13.2**	**0.85**	**0.746**
L	**7.5**	**2.45**	**47.0**	**0.33**	**3.0**	**1.0**	**13.2**	**0.85**	**0.756**
M	**7.5**	**2.45**	**47.0**	**0.33**	**6.0**	**1.0**	**13.2**	**0.85**	**0.795**

Table 6.2: Initial values of simulation parameters and non-dimensional numbers relevant to the DNS database

6.2.6 Modelling implications in the context of LES

The scaling estimates for the different relevant quantities, as given by eqs. (6.37)-(6.53), are summarised in Table 6.1 for quick reference. Table 6.1 demonstrates that the terms T_2, T_3, T_4, ($-D_2$) and $f(D)$ are likely to play key roles in the SDR $\tilde{N}_c$ transport irrespective of Δ, which is consistent with previous findings in the context of RANS (Chakraborty et al., 2011; Chakraborty and Swaminathan, 2010). Moreover, Table 6.1 and Figs. (6.11)-(6.121) indicate that the magnitudes of T_2, T_3, T_4, ($-D_2$) and $f(D)$ are expected to increase with decreasing *Le* and similar observations have been made earlier by Chakraborty and Swaminathan (2010) in the context RANS. As introduced in Chapter 2 that an algebraic model of SDR was proposed (Kolla et al., 2009) based on the assumption of the equilibrium of the generation and destruction of the scalar gradients, which equivalently assumes the standing of $T_2+T_3+T_4-D_2+f(D)\approx 0$ in the context of RANS. The above model has been extended laterly to cover the differential diffusion effects of heat and mass (Chakraborty and Swamianthan, 2010). The scaling relations given by eqs. (6.37)-(6.53) indicate that $[T_2+T_3+T_4+f(D)]\sim D_2$, which allows for obtaining an algebraic estimation for $\tilde{N}_c$ by putting the model expressions for the unclosed terms $T_2, T_3, T_4, f(D)$ and $(-D_2)$ in the expression $[T_2+T_3+T_4+f(D)]\sim D_2$. It is important to note that T_1 is a transport term and thus the volume-integral of this term vanishes so it does not play any role in the generation/destruction of $\tilde{N}_c$. The variations of the mean values of $[T_2+T_3+T_4+f(D)]/D_2$ conditional on $\tilde{c}$ for different values of Δ for cases A-E are shown in Fig. 6.13. It can be seen from Fig. 6.13 that $[T_2+T_3+T_4+f(D)]/D_2$ remains of the order of unity for all values of Δ in all cases. However, $[T_2+T_3+T_4+f(D)]/D_2$ assumes a value close to unity for the major portion of the flame brush for large filter widths (i.e. $\Delta >> \delta_{th}$) and this trend strengthens with increasing Δ. This suggests that $T_2+T_3+T_4-D_2+f(D)\approx 0$ remains roughly valid for $\Delta >> \delta_{th}$. The transient term $\bar{\rho}(\partial\tilde{N}_c/\partial t)$ in the SDR transport equation for turbulent flows can be scaled as: $\bar{\rho}(\partial\tilde{N}_c/\partial t)\sim \rho_0 u'_\Delta \tilde{N}_c/\Delta \sim (\rho_0 S_L^2/\delta_{th}^2)Da_\Delta^{-1}$. This suggests that the magnitude of $\bar{\rho}(\partial\tilde{N}_c/\partial t)$ weakens with increasing Δ because Da_Δ shows an increasing trend with increasing filter width (Dunstan et al., 2013). Thus, $T_2+T_3+T_4-D_2+f(D)\approx 0$ is not

expected to hold for small values of Δ (e.g. $\Delta < \delta_{th}$) but this assumption roughly holds in an order of magnitude sense for large filter widths (i.e. $\Delta >> \delta_{th}$).

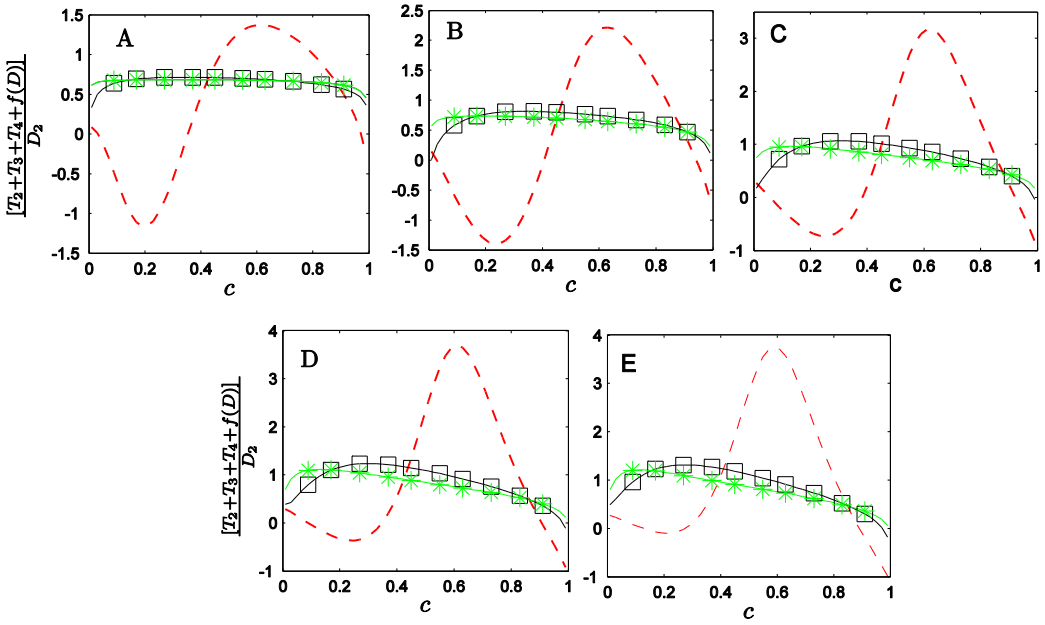

Figure 6.13: Variation of mean values of $[T_2+T_3+T_4+f(D)]/D_2$ conditional on bins of $\tilde{c}$ at $\Delta \approx 0.4\delta_{th}$ (- - -), $1.6\delta_{th}$ (—□—) and $2.8\delta_{th}$ (—*—) for the *Le*=0.34(A), *Le*=0.6(B), *Le*=0.8(C), *Le*=1.0(D), *Le*=1.2(E) cases.

Therefore, it is reasonable to expect that the algebraic models proposed based on this assumption remain feasible for the large filter widths but may require modifications for the filter widths which are comparable to or smaller than the thermal flame thickness. This will be discussed in the next section in detail together with other possible approaches to algebraicaly closure of SDR for LES.

6.3 Algebraic closure of SDR in the context of LES

A model of $\tilde{N}_c$, which is widely used for sub-grid SDR closure for passive scalar mixing is given by Girimaji and Zhou (1996) as:

$$\tilde{N}_c = (\tilde{D} + D_t)\nabla\tilde{c}.\nabla\tilde{c} \tag{6.54}$$

where D_t is the eddy diffusivity and is often modelled based on sub-grid eddy viscosity ν_t as:

$$D_t \approx \nu_t = (C_s\Delta)^2(2\tilde{S}_{ij}\tilde{S}_{ij})^{1/2} \tag{6.55}$$

where $\nu_t = (C_s\Delta)^2(2\widetilde{S}_{ij}\widetilde{S}_{ij})^{1/2}$ is the Smagorinsky-Lily model of sub-grid eddy viscosity (Smagorinsky, 1963), $\widetilde{S}_{ij} = 0.5(\partial\widetilde{u}_i/\partial x_j + \partial\widetilde{u}_j/\partial x_i)$ is the resolved strain rate, and C_s is the Smagorinsky constant which assumes a theoretical value of $C_s = 0.18$ for decaying turbulence (Girimaji and Zhou, 1996) and this value of C_s is used in the present *a-priori* DNS analysis. The model given by eq. (6.55) is referred to as the SDR-C (SDR-Conventional) model.

The SDR is closely related to the generalised Flame Surface Density (FSD) (Boger *et al*., 1998) $\Sigma_{gen} = \overline{|\nabla c|} = \overline{(N_c/D)^{1/2}}$ (Bray and Swaminathan, 2011; Vervisch and Veynante, 2002). The FSD is often modelled in terms of a wrinkling factor $\Xi_\Delta = \Sigma_{gen}/|\nabla\bar{c}|$ in the following manner (Charlette *et al*., 2002a,b; Knikker *et al.,* 2004; Chakraborty and Klein, 2008):

$$\Xi_\Delta = \frac{\Sigma_{gen}}{|\nabla\bar{c}|} = \left(\frac{\eta_O}{\eta_i}\right)^{D_F-2} \tag{6.56}$$

where η_i and η_O are the inner and outer cut-off scales and D_F is the fractal dimension based on FSD. The filter width Δ can be taken to be the outer cut-off scale η_O. Dunstan *et al.* (2013) defined a SDR based wrinkling factor Ξ_D drawing on the analogy with eq. (6.56), as follows:

$$\Xi_D = \frac{\tilde{N}_c}{\tilde{D}\nabla\tilde{c}.\nabla\tilde{c}} \tag{6.57}$$

Dunstan *et al*. (2013) also explored the possibility of modelling Ξ_D by using a power-law in the following manner:

$$\Xi_D = \left(\frac{\eta_O}{\eta_{iD}}\right)^{\alpha_D} \tag{6.58}$$

where α_D is the power-law exponent, η_{iD} is the inner cut-off scale for Ξ_D, whereas the outer cut-off scale η_O for LES can be taken to be the LES filter width Δ. According to eq. (6.57), $\bar{\dot{w}}$ can be considered to be directly proportional to $\bar{\rho}\tilde{N}_c$ for $\Delta >> \delta_{th}$, and thus

the volume-averaged value of $\overline{\rho}\tilde{N}_c = \overline{\rho N_c}$ should remain independent of Δ for $\Delta >> \delta_{th}$, which leads to $\left\langle \overline{\rho N_c} \right\rangle_V = \left\langle \overline{\rho}\tilde{N}_c \right\rangle_V$ where $\langle \ldots \rangle_V$ indicates a volume averaging operation. Using eqs. (6.57) and (6.58), it is possible to write:

$$\log \Xi_D^V = \log\left(\frac{\left\langle \overline{\rho}\tilde{N}_c \right\rangle_V}{\left\langle \overline{\rho}\tilde{D}\nabla\tilde{c}.\nabla\tilde{c} \right\rangle_V} \right) = \alpha_D \log\Delta - \alpha_D \log\eta_{iD} \tag{6.59}$$

where $\Xi_D^V = \left\langle \overline{\rho}\tilde{N}_c \right\rangle_V \Big/ \left\langle \overline{\rho}\tilde{D}\nabla\tilde{c}.\nabla\tilde{c} \right\rangle_V$ indicates the wrinkling factor based on the volume-averaged quantities. Thus a linear variation between $\log\Xi_D^V$ and $\log\Delta$ confirms the power-law behaviour postulated in eq. (6.58), which was demonstrated earlier for $\Delta >> \delta_{th}$ by Dunstan *et al.* (2013). However, it is worth noting that:

$$\lim_{\Delta\to 0}\left(\overline{\rho}\tilde{N}_c \right) = \overline{\rho}\tilde{D}\nabla\tilde{c}.\nabla\tilde{c} = \rho D\nabla c.\nabla c \tag{6.60}$$

whereas $\overline{\rho}\tilde{N}_c$ approaches zero according to eq. (6.58). Dunstan *et al*. (2013) modified eq. (6.58) in the following manner to overcome this difficulty:

$$\Xi_D^V = \exp\left(-\theta_1 \frac{\Delta}{\delta_{th}} \right) + \left[1 - \exp\left(-\theta_2 \frac{\Delta}{\delta_{th}} \right) \right] \left(\frac{\Delta}{\eta_{iD}} \right)^{\alpha_D} \tag{6.61}$$

where θ_1 and θ_2 are the model parameters (Dunstan *et al*., 2013). According to eq. (6.61) Ξ_D^V approaches unity (i.e. $\Xi_D^V \to 1$) for small values of filter width (i.e. $\Delta \to 0$), whereas one recovers eqs. (6.58) and (6.59) for $\Delta >> \delta_{th}$. Thus, it is possible to propose a model for $\tilde{N}_c$, in the following manner provided the power-law exponent α_D and η_{iD} are suitably parameterised and optimised values are used for θ_1 and θ_2:

$$\tilde{N}_c = \tilde{D}\nabla\tilde{c}.\nabla\tilde{c}\left[\exp\left(-\theta_1 \frac{\Delta}{\delta_{th}} \right) + \left[1 - \exp\left(-\theta_2 \frac{\Delta}{\delta_{th}} \right) \right] \left(\frac{\Delta}{\eta_{iD}} \right)^{\alpha_D} \right] \tag{6.62}$$

The model given by eq. (6.62) is referred to as the SDR-PL (SDR-Power-Law) model here. It is worth noting that one will obtain $\Xi_D^V = \left\langle \overline{\rho}\tilde{\tilde{N}}_c \right\rangle_V \Big/ \left\langle \overline{\rho}\tilde{\tilde{D}}\nabla\tilde{\tilde{c}}.\nabla\tilde{\tilde{c}} \right\rangle_V = 1.0$ for $\Delta \le \delta_{th}$ if η_O is not permitted to be smaller than η_{iD}. However, DNS results (see Dunstan

et al. (2013) and Fig. 6.14 later in this chapter) show $\Xi_D^V > 1.0$ even for $0 < \Delta \leq \delta_{th}$. This necessitates an expression such as eq. (6.62), which has the capability of capturing Ξ_D^V variation with Δ.

Dunstan *et al*. (2013) discussed the possibility of extending a RANS algebraic SDR closure proposed by Kolla *et al*. (2009) for the purpose of LES in the following manner:

$$\tilde{N}_c = \tilde{D}\nabla\tilde{c}.\nabla\tilde{c} + [1-\exp(-\theta\frac{\Delta}{\delta_{th}})]\left[2K_c^*\frac{S_L}{\delta_{th}} + (C_3 - \tau C_4 Da_\Delta)\frac{2u'_\Delta}{3\Delta}\right]\tilde{c}(1-\tilde{c})/\beta_1 \qquad (6.63)$$

where S_L is the unstrained laminar burning velocity. The model parameters θ, C_3, C_4 and β_1 in eq. (6.63) are given by:

$$\theta = 0.75\,;\; C_3 = \frac{1.5\sqrt{Ka_\Delta}}{1+\sqrt{Ka_\Delta}}\,;\; C_4 = \frac{1.1}{(1+Ka_\Delta)^{0.4}} \text{ and } \beta_1 = 2.4 \qquad (6.64)$$

In eq. (6.64) K_c^* is a thermo-chemical parameter which provides information regarding the SDR-weighted dilatation rate $\nabla.\vec{u}$ (Kolla *et al*., 2009) in the following manner:

$$K_c^* = \frac{\delta_{th}}{S_L}\frac{\int_0^1 [\rho N_c \nabla.\vec{u} f(c)]_L\, dc}{\int_0^1 [\rho N_c f(c)]_L\, dc} \qquad (6.65)$$

The same expressions of K_c^*, C_3 and C_4 were proposed by Kolla *et al*., (2009) in the context of RANS and the value of β_1 has been modified by Dunstan *et al.* (2013) to adopt this model for LES. The function $[1-\exp(-\theta\Delta/\delta_{th})]$ ensures that $\tilde{N}_c$ approaches $D\nabla c.\nabla c$ when the flow is fully resolved (i.e. $\Delta \to 0$) and this function and the first term on the right hand side of eq. (6.63) were absent in the model proposed by Kolla *et al*. (2009) as the RANS model was proposed only for the unresolved part of SDR (i.e. $\breve{\varepsilon}_c$). The terms $2K_c^*(S_L/\delta_{th})$ and $(C_3 - \tau C_4 Da_\Delta)(2u'_\Delta/3\Delta)$ in eq. (6.63) arise due to dilatation and normal strain rate contributions to the SDR transport, whereas $\tilde{c}(1-\tilde{c})/\beta_1$ originates due to the combined reaction and molecular dissipation contributions (Kolla *et al.*, 2009). It is worth noting that the model given by eq. (6.63) and the model of Kolla *et al.* (2009) are strictly valid for unity Lewis number (i.e. $Le = 1.0$) flames. Moreover, the

performance of eq. (6.63) was assessed for LES based on the *a-priori* analysis of a single unity Lewis number V-flame DNS database, and thus it is important to assess the performance of this modelling methodology for different values of τ, Le and Re_t.

It was demonstrated by Chakraborty and Swaminathan (2011) that global Lewis number Le has significant influence on the statistical behaviour of SDR $\tilde{\varepsilon}_c$ in the context of RANS (i.e. $\Delta/\delta_{th} \to \infty$) and the model proposed by Kolla *et al.* (2009) has been modified by Chakraborty and Swaminathan (2011) to account for non-unity Lewis number effects on $\tilde{\varepsilon}_c$ closure in RANS. This modified RANS model for $\tilde{\varepsilon}_c$ is extended for $\widetilde{N}_c$ closure in the context of LES in the following manner:

$$\widetilde{N}_c = \widetilde{D}\nabla\widetilde{c}.\nabla\widetilde{c} + (1-f)\underbrace{\left[\frac{2K_c^* S_L}{Le^{1.88}\delta_{th}} + (C_3^* - \tau.Da_\Delta C_4^*)\frac{2u'_\Delta}{3\Delta}\right]\frac{\widetilde{c}.(1-\widetilde{c})}{\beta_c}}_{N_{sg}} \qquad (6.66)$$

where $f = \exp[-\theta(\Delta/\delta_{th})^p]$ is a bridging function and C_3^*, C_4^* and β_c are the model parameters. Chakraborty and Swaminathan (2011) suggested the following expressions for C_3^* and C_4^*:

$$C_3^* = \frac{2.0\sqrt{Ka_\Delta}}{1.0+\sqrt{Ka_\Delta}},\ C_4^* = \frac{1.2(1.0-\widetilde{c})^\Phi}{Le^{2.57}(1+Ka_\Delta)^{0.4}} \text{ where } \Phi = 0.2 + 1.5\left|(1.0-Le)\right| \qquad (6.67)$$

It is worth noting that the first term on the right hand side of eq. (6.66) was absent and the second term featured without $(1-f)$ in the RANS model by Chakraborty and Swaminathan (2011). The bridging function $(1-f)$ ensures that $\widetilde{N}_c$ approaches to $N_c = D\nabla c.\nabla c$ for small values of filter size (i.e. $\lim_{\Delta\to 0}\widetilde{N}_c = N_c = D\nabla c.\nabla c$ where $f \approx 1.0$), whereas eq. (6.66) approaches to the RANS model expression proposed by Chakraborty and Swaminathan (2011) for $\Delta >> \delta_{th}$ where $f \approx 0.0$. The terms $2K_c^*(S_L/Le^{1.88}\delta_{th})$ and $(C_3^* - \tau.Da_\Delta C_4^*)(2u'_\Delta/3\Delta)$ in eq. (6.66) arise due to dilatation and strain rate contributions to the SDR transport, whereas $\widetilde{c}(1-\widetilde{c})/\beta_c$ originates due to the combined reaction and molecular dissipation contributions (Kolla *et al.*, 2009; Chakraborty and Swaminathan, 2010, 2011). Equations (6.63) and (6.66) have similar expressions, and they provide similar performances for the unity Lewis number (i.e.

$Le = 1.0$) flames, but the effects of Le are included in eq. (6.66) and thus the performances of eq. (6.66) will only be discussed in this paper for the sake of conciseness.

The model given by eq. (6.66) will henceforth be referred to as the SDR-RE (SDR-RANS Extended) model here. It is worth noting that the sub-grid turbulent velocity fluctuation (i.e. u'_Δ) needs to be modelled in actual LES and u'_Δ is often evaluated in the following manner (Pope, 2000):

$$u'_\Delta = \frac{\nu_t}{C_\nu \Delta} \tag{6.68}$$

where $C_\nu = 0.094$ is a model parameter. As u'_Δ appears explicitly in eq. (6.66) and in the definitions of Da_Δ and Ka_Δ, which are the input parameters for the SDR-RE model given by eq. (6.66). Thus, the modelling of u'_Δ is expected to play an important role in its predictive capabilities of eq. (6.66). The performances of SDR-C, SDR-PL and SDR-RE models will be compared with $\tilde{N}_c$ extracted from the DNS data for a range of filter widths Δ.

Case	A_T / A_L	θ_1	θ_2	α_D	η_{iD} / δ_{th}	β_c	β_c^*
A	3.93	0.01	0.69	1.42	0.73	4.35	4.9
B	2.66	0.01	0.55	1.32	0.88	4.35	4.9
C	2.11	0.01	0.45	1.19	0.92	4.35	4.9
D	1.84	0.01	0.42	1.07	0.93	4.35	4.9
E	1.76	0.01	0.40	1.04	0.93	4.35	4.9
F	1.1	0.01	0.33	0.86	0.93	4.8	5.5
G	1.25	0.01	0.34	0.88	0.94	4.8	5.5
H	1.85	0.01	0.41	1.11	0.98	4.1	4.9
I	3.75	0.01	0.45	1.18	0.96	4.0	4.5
J	3.80	0.01	0.48	1.26	0.97	4.0	4.5
K	2.04	0.01	0.47	1.14	0.92	2.4	2.4
L	1.94	0.01	0.45	1.13	0.90	3.3	3.8
M	1.74	0.01	0.42	1.02	0.93	4.8	4.86

Table 6.3: Normalised flame surface area when statistics were extracted and the optimum model parameters for eqs. (6.62) and (6.66).

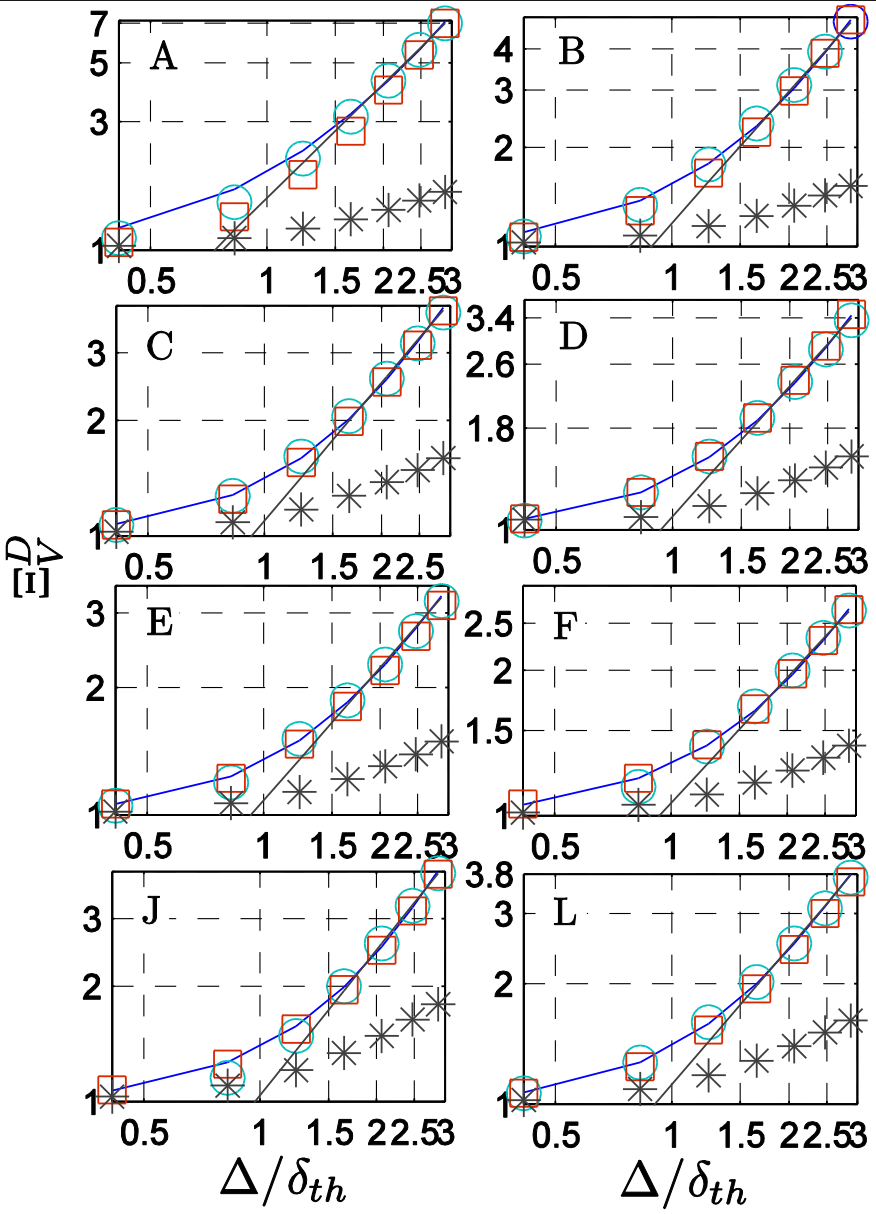

Figure 6.14: Variations of wrinkling factor based on volume averaged quantities Ξ_D^V (——) with normalised filter width Δ/δ_{th} on a log-log plot along with the predictions of SDR-C model (i.e. eq. (6.54)) (✱), SDR-PL model (i.e. eq.(6.62)) (□) and SDR-RE model (i.e. eq.(6.66)) (○) for case A-F, J and L. Power-law model (eq. (6.62)) predictions are shown for the optimum values of θ_1 and θ_2 reported in Table 6.3 and the values of α_D and η_{iD} extracted from DNS data. The SDR-RE model (eq. (6.66)) predictions are shown for the optimum values of β_c reported in Table 6.3.

The variations of Ξ_D^V (see eq. (6.58)) with normalised filter width Δ/δ_{th} in cases A-F, J and L are shown in Fig. 6.14 on a log-log plot along with the predictions of SDR-C (i.e. eq. (6.54)), SDR-PL (i.e. eq. (6.61)) models. Figure 6.14 shows that the SDR-C model underpredicts Ξ_D^V for all cases considered here for the theoretical value of Smagorinsky constant for decaying turbulence (i.e. $C_s = 0.18$). It is worth noting the predictions of the SDR-PL (i.e. eq. (6.61)) model are shown in Fig. 6.14 for optimum choices of θ_1 and θ_2

which capture the variations of Ξ_D^V with Δ/δ_{th}. Equation (6.61) is multiplied with $\bar{\rho}$ to obtain an expression for Ξ_D^V in order to estimate the optimum values of θ_1 and θ_2. The values of θ_1 and θ_2 which yield satisfactory qualitative and quantitative predictions of the variation of Ξ_D^V with Δ are estimated based on a least-squares method. It has been found that the value of θ_1, which leads to satisfactory prediction of Ξ_D^V, does not change from one case to another and the optimum value of θ_1 remains close to 0.01. For the sake of simplicity $\theta_1 = 0.01$ is taken for all cases and a least squares method is used to obtain optimum values of θ_2. The optimum values of θ_1 and θ_2 for cases A-M are shown in columns 3 and 4 of Table 6.3 respectively.

It is evident from Fig. 6.14 that a power-law between Ξ_D^V with Δ/δ_{th} (see eqs. (6.58) and (6.59)) can be obtained for $\Delta > \delta_{th}$, where $\log(\Xi_D^V)$ shows a linear relation with $\log(\Delta/\delta_{th})$, which is consistent with the previous findings by Dunstan *et al*. (2013). The slope of the best-fit straight line with the steepest slope corresponding to the linear variation of $\log(\Xi_D^V)$ with $\log(\Delta/\delta_{th})$ provides the value of power-law exponent α_D. The intersection of this best fit straight line with $\Xi_D^V = 1.0$ (i.e. $\log(\Xi_D^V) = 0.0$) provides the measure of the inner cut-off scale η_{iD}. The values of α_D and η_{iD}/δ_{th} obtained from DNS are reported in columns 5 and 6 respectively for cases A-M. It is evident from Fig. 6.14 and Table 6.3 that the inner cut-off scale η_{iD} remains of the order of δ_{th} for all the cases considered here, which is consistent with previous findings by Dunstan *et al*. (2013). This suggests that η_{iD} is not significantly affected by τ, Le and Re_t. By contrast, τ, Le and Re_t have significant influences on the power-law exponent α_D. The power-law exponent α_D increases with decreasing Le (i.e. from *Le*=1.2 in case E to *Le*=0.34 in case A), which consistent with increasing extent of flame wrinkling with decreasing *Le* which is consistent with the c isosurfaces and A_T/A_L values shown in Fig. 4.1 and column 2 of Table 6.3 respectively.

It has been found that the SDR-RE model (i.e. eq. (6.66)) satisfactorily captures the variation of Ξ_D^V with Δ/δ_{th} when f is taken to be $f = \exp[-0.7(\Delta/\delta_{th})^{1.7}]$ (for the present thermo-chemistry $f = \exp[-0.7(\Delta/\delta_{th})^{1.7}] \approx \exp[-0.325(Da_\Delta\,\mathrm{Re}_\Delta)^{0.85}]$) and the

optimum global values of β_c have been used, which can be substantiated from Fig. 6.14 where the predictions of the SDR-RE model for $f = \exp[-0.7(\Delta/\delta_{th})^{1.7}]$ and the optimum values of β_c are shown. Equation (6.61) is multiplied with $\bar{\rho}$ to obtain an expression for Ξ_D^V in order to estimate the optimum values of θ, p and β_c. The values of β_c, θ and p, which provide satisfactory qualitative and quantitative predictions of the variation of Ξ_D^V with Δ, are estimated based on a least-squares method. It has been found that the values of θ and p, which lead to satisfactory prediction of Ξ_D^V, do not change from one case to another and the optimum values of θ and p remain close to 0.7 and 1.7 respectively. For the sake of simplicity $\theta = 0.7$ and $p = 1.7$ are taken for all cases and a least squares method is used to obtain optimum values of β_c.

The global optimum values of β_c for the cases considered here are shown in column 7 of Table 6.3, which indicates that β_c increases with increasing τ (i.e. β_c =2.4 to 4.86 from τ =2.0 to 6.0), which is consistent with β_c =2.7 for the model expression given by eq. (6.66) for the flame with $\tau = 2.52$, analysed by Dunstan *et al*. (2013). Moreover, a comparison of the optimum values of β_c for cases F-J reveals a weak variation of β_c but it is difficult to ascertain if this variation originates due to statistical variation or due to the turbulent Reynolds number Re_t dependence. A recent RANS based analysis by Chakraborty and Swaminathan (2013) also revealed a weak Re_t dependence of β_c. However, the variation of β_c between cases F-J has been found to be much weaker than the dependence on the heat release parameter τ (see cases K, L, D and M). It is worth noting that a different set of optimum values of β_c can be obtained for a different expression of f but the present choice of $f = \exp[-0.7(\Delta/\delta_{th})^{1.7}]$ yields optimum values of β_c which only exhibits τ dependence and remains a weak function of Le and Re_t. This makes $f = \exp[-0.7(\Delta/\delta_{th})^{1.7}]$ as a desirable bridging function for practical applications.

The variations of mean values of normalised SDR $\tilde{N}_c^+ = \tilde{N}_c \times \delta_{th}/S_L$ conditional on $\tilde{c}$ across the flame brush at $\Delta \approx 0.8\delta_{th}$ and $\Delta \approx 2.8\delta_{th}$ for cases A-F, J and L are shown in Figs. 6.15 and 6.16 respectively along with the predictions of the SDR-C (i.e. eq. (6.54)), SDR-PL (i.e. eq. (6.61)) and SDR-RE (i.e. eq. (6.66)) models for α_D and η_{iD} extracted

from DNS data and the optimum values of θ_1, θ_2 and β_c (as reported in Table 6.3) for which the variation of Ξ_D^V with Δ/δ_{th} is accurately captured. It can be seen from Fig. 6.15 that all three models satisfactorily capture the behaviour of the mean value of normalised SDR $\widetilde{N}_c^+$ conditional on $\widetilde{c}$ for filter widths $\Delta < \delta_{th}$ (e.g. $\Delta \approx 0.8\delta_{th}$) for flames in cases B-F, J and L but the SDR-PL model (i.e. eq. (6.61)) shows overprediction for *Le*<<1.0 cases (e.g. case A with *Le*=0.34) at $\Delta \approx 0.8\delta_{th}$ even with the optimum values of θ_1 and θ_2 for which the SDR-PL model satisfactorily captures the variation of Ξ_D^V with Δ/δ_{th}. However, the SDR-C (i.e. eq. (6.54)) and SDR-RE (i.e. eq. (6.66)) models more accurately predict the mean value of normalised SDR $\widetilde{N}_c^+$ conditional on $\widetilde{c}$ for case B at $\Delta \approx 0.8\delta_{th}$ than the SDR-PL model. A comparison between Figs. 6.15 and 6.16 reveals that the differences between the predictions of the SDR-C, SDR-PL and SDR-RE models increase with increasing Δ. Figure 6.16 shows that the SDR-PL model (i.e. eq. (6.61)) overpredicts the mean value of normalised SDR $\widetilde{N}_c^+$ conditional on $\widetilde{c}$ for $\Delta > \delta_{th}$ (e.g. $\Delta \approx 2.8\delta_{th}$), and does not adequately capture the qualitative behaviour obtained from DNS data, even when α_D and η_{iD} are extracted from DNS data, and the optimum values of θ_1 and θ_2 for which the SDR-PL model satisfactorily captures the variation of Ξ_D^V with Δ/δ_{th}, are used. By contrast, the SDR-C model (i.e. eq. (6.54)) underpredicts the mean value of $\widetilde{N}_c \times \delta_{th}/S_L$ conditional on $\widetilde{c}$ at $\Delta \approx 2.8\delta_{th}$ for all the cases considered here. It is worth noting that the Smagorinsky constant C_s in eq. (6.54) (which has been taken here as $C_s = 0.18$ according to the theoretical analysis for decaying turbulence) is often taken to be $C_s = 0.1$, which will make the SDR-C (i.e. eq. (6.54)) model to underpredict further than the results shown in Figs. 6.14-6.16.

For using the SDR-PL model in an actual LES simulation, the quantities α, θ_1 and θ_2 need to be parameterised in terms of resolved-scale quantities. However, such parameterisation has not been attempted here because the SDR-PL model fails to capture the variation of the mean values of normalised SDR $\widetilde{N}_c^+$ conditional on $\widetilde{c}$ across the flame brush, especially for $\Delta > \delta_{th}$, even when the optimum values of parameters θ_1 and θ_2 for the accurate prediction of Ξ_D^V are used, and the values of α_D and η_{iD} are extracted from DNS data. The first term on the right side of eq. (6.61) (i.e.

$\tilde{D}\nabla\tilde{c}.\nabla\tilde{c}\left[\exp(-\theta_1\Delta/\delta_{th})\right]$) remains a major contributor for $\Delta < \delta_{th}$ and thus eq. (6.61) is more successful in capturing the local behaviour of $\tilde{N}_c$ for $\Delta < \delta_{th}$ than $\Delta > \delta_{th}$ (see Figs. 6.15 and 6.16). This suggests that a power-law based model with a single global value of α_D may not be suitable for capturing the correct qualitative variation of $\tilde{N}_c$ even when the optimum values of θ_1 , θ_2 , and η_{iD} are used in eq. (6.61). The discrepancy between satisfactory prediction of Ξ_D^V and inadequate prediction of the mean values of normalised SDR $\tilde{N}_c^+$ conditional on $\tilde{c}$ by the SDR-PL (i.e. eq. (6.61)) model arises possibly due to multi-fractal nature of SDR (i.e. a power law of the form $\Xi_D = (\eta_o/\eta_i)^{\alpha_D}$ has a single exponent α_D but a continuous series of exponents is necessary to describe the statistics of Ξ_D. For example $\sum X_r^q \sim X_L^q (r/L)^{\alpha_1(q)}$ where X_r is defined as $X_r = \int N_c d^3\vec{x}$ with $\alpha_1(q)$ being the exponent associated with any real number q for which the power-law behaviour is obtained. For the above description the summation is taken over a box of size r for a domain of characteristic length *L*). Interested readers are referred to (Sreenivasan *et al*., 1989; Sreenivasan, 1991; Prasad and Sreenivasan, 1990; Shivamoggi, 1995) for further information on multi-fractal nature of SDR. The performace of the SDR-PL model is also found to be consistent with earlier findings by Dunstan *et al.* (2013) for turbulent premixed flames.

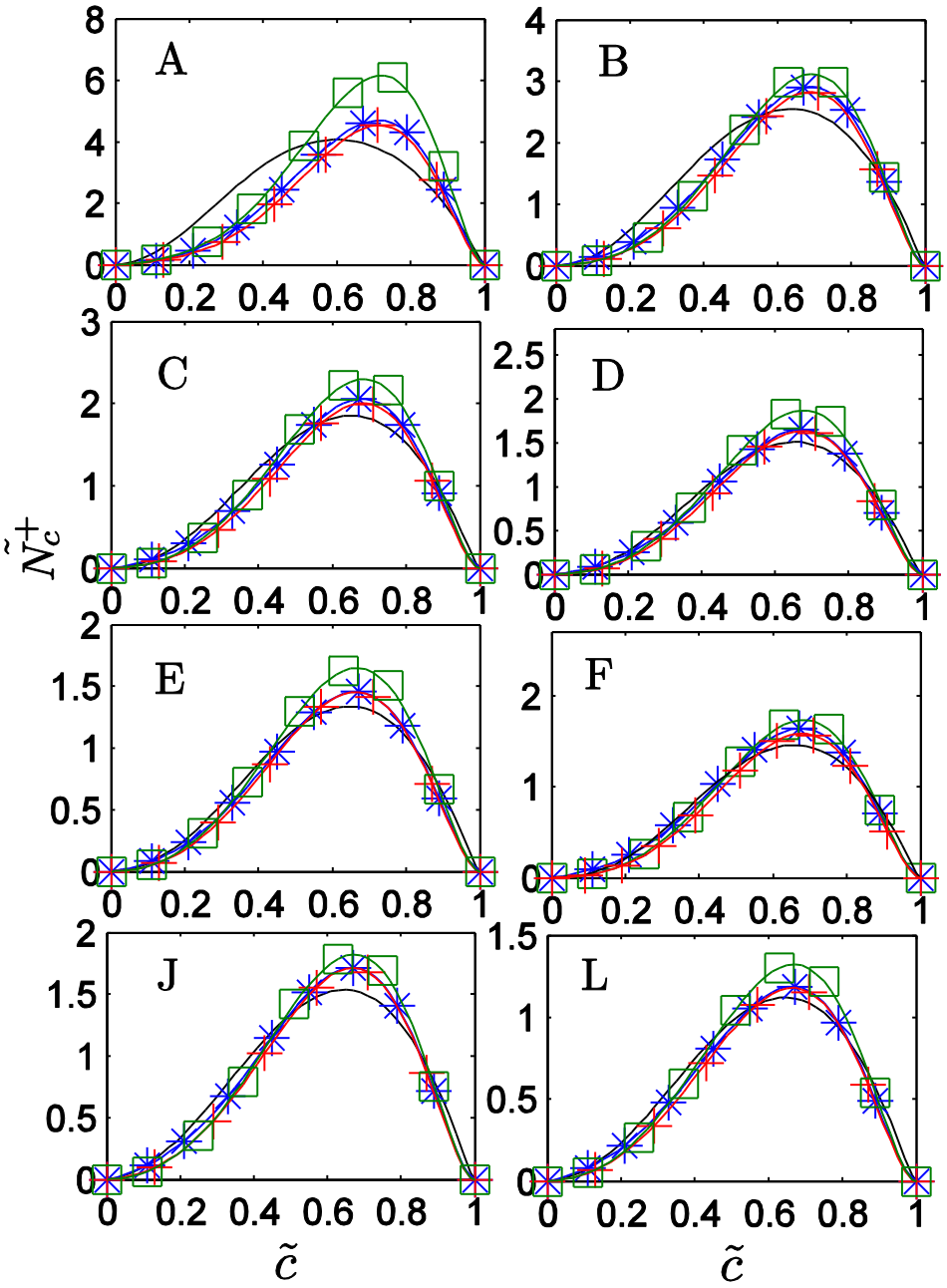

Figure 6.15: Variation of mean values of normalised SDR $\tilde{N}_c^+$ (———) conditional on $\tilde{c}$ across the flame brush along with the predictions of SDR-C model (i.e. eq. (6.54)) (—|—), SDR-PL model (i.e. eq. (6.62)) (—□—) and SDR-RE model (i.e. eq. (6.66)) (—*—) at $\Delta \approx 0.8\delta_{th}$ for cases A-F, J and L. Power-law model (eq. (6.62)) predictions are shown for the optimum values of θ_1 and θ_2 reported in Table 6.3 and the values of α_D and η_{iD} extracted from DNS data. The SDR-RE model (eq. (6.66)) predictions are shown for the optimum values of β_c reported in Table 6.3.

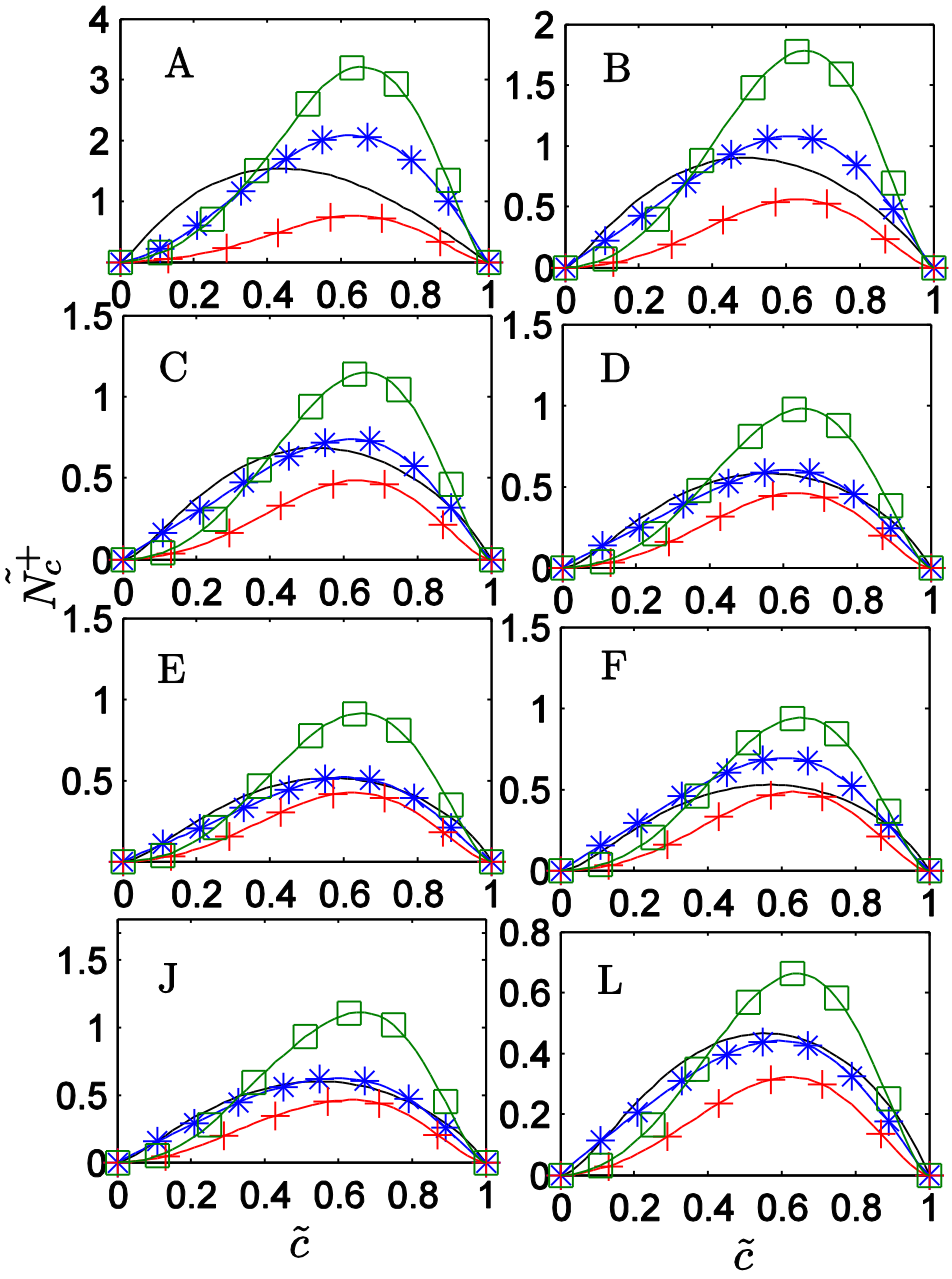

Figure 6.16 : Variation of mean values of normalised SDR $\tilde{N}_c^+$ (———) conditional on $\tilde{c}$ across the flame brush along with the predictions of SDR-C model (i.e. eq. (6.54)) (—|—), SDR-PL model (i.e. eq.(6.62)) (—□—) and SDR-RE model (i.e. eq.(6.66)) (—✳—) at $\Delta \approx 2.8\delta_{th}$ for case A-F, J and L. SDR-PL model (eq. (6.62)) predictions are shown for the optimum values of θ_1 and θ_2 reported in Table 6.3 and the values of α_D and η_{iD} extracted from DNS data. The SDR-RE model (eq. (6.66)) predictions are shown for the optimum values of β_c reported in Table 6.3.

The SDR-C model is commonly used for passive scalar mixing when the time-scale of turbulent mixing (i.e. $\tau_t \sim (D_t \nabla\tilde{c}.\nabla\tilde{c})^{-1}$) is the principal time-scale associated with the physics of micro-mixing. However, in turbulent premixed flames the time-scale associated with chemical processes also plays an important role in the SDR statistics (Swaminathan and Bray, 2005; Kolla *et al*., 2009) and this essential physics is missing in

the SDR-C model (i.e. eq. (6.54)). The effects of chemical reaction weaken with decreasing Da, and thus this model reasonably captures the qualitative variation of the mean values of normalised SDR $\widetilde{N}_c^+$ conditional on $\widetilde{c}$ across the flame brush (in spite of

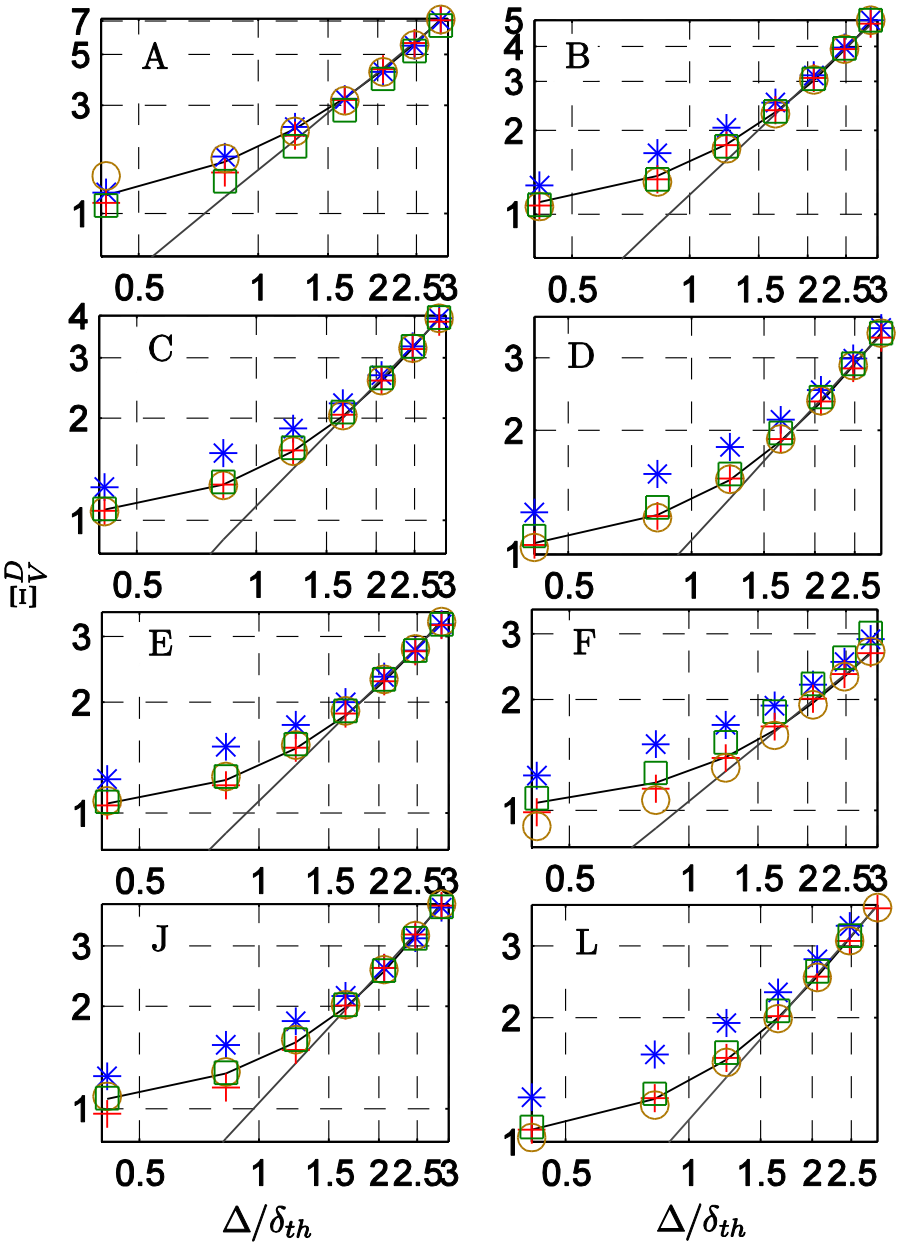

Figure 6.17: Variations of wrinkling factor based on volume averaged quantities Ξ_D^V (———) with normalised filter width Δ/δ_{th} on a log-log plot along with the predictions of the SDR-RE model for: (i) u'_Δ extracted from DNS and β_c reported in Table 6.3 (+), (ii) u'_Δ extracted from DNS and β_c according to eq. (6.69) (✱), (iii) u'_Δ modelled using eq. (6.68) and optimum values of β_c^* reported in Table 6.3 (○) and (iv) u'_Δ modelled using eq. (6.68) and β_c^* according to eq. (6.70) (□) for cases A-G and K.

some underpredictions) for $Da<1$ flames considered here, although Ξ_D^V is significantly underpredicted by the SDR-C model. The prediction of the SDR-C model is likely to be worse in the $Da>1$ flames where the effects of chemical reaction are stronger than in the $Da<1$ cases considered here, and thus cannot be ignored. The local Damköhler number Da_Δ increases with increasing filter width Δ for all cases considered here (see Fig. 5.4) and thus the SDR-C model is expected to show greater extent of underprediction of Ξ_D^V for $\Delta >> \delta_{th}$ (see Fig. 6.14).

It is evident from Figs. 6.15 and 6.16 that the SDR-RE model (i.e. eq. (6.66)) satisfactorily captures the variation of the mean values of normalised SDR $\widetilde{N}_c^+$ conditional on $\widetilde{c}$ across the flame brush except the overpredictions in cases B and F for $\Delta > \delta_{th}$ (e.g. $\Delta \approx 2.8\delta_{th}$). In the $Le<<1$ cases (e.g. $Le=0.34$ in case A) neither of the models considered here captures the correct qualitative behaviour of $\widetilde{N}_c$ for $\Delta < \delta_{th}$ (e.g. $\Delta \approx 0.8\delta_{th}$) and $\Delta > \delta_{th}$ (e.g. $\Delta \approx 2.8\delta_{th}$) but the prediction of the SDR-RE model remains closer to the DNS data than the SDR-PL and SDR-C models. Although the SDR-RE model overpredicts the mean values of normalised SDR $\widetilde{N}_c^+$ conditional on $\widetilde{c}$ at the middle of the flame brush for $\Delta > \delta_{th}$ (e.g. $\Delta \approx 2.8\delta_{th}$) in case F where Re_t remains small, the agreement between the SDR-RE model prediction and DNS data improves with increasing Re_t (i.e. going from F to J). For example, the SDR-RE model satisfactorily captures the variation of the mean values of normalised SDR $\widetilde{N}_c^+$ conditional on $\widetilde{c}$ across the flame brush for both $\Delta < \delta_{th}$ (e.g. $\Delta \approx 0.8\delta_{th}$) and $\Delta > \delta_{th}$ (e.g. $\Delta \approx 2.8\delta_{th}$) in case J. Figures 6.15 and 6.16 indicate that the SDR-RE model (i.e. eq. (6.66)) more accurately captures both global and local behaviours of $\widetilde{N}_c$ in turbulent premixed flames than the SDR-PL and SDR-C models for the range of τ, Le and Re_t considered here, provided the optimum value of β_c is used for which the variation of Ξ_D^V with Δ is accurately captured by eq. (6.66).

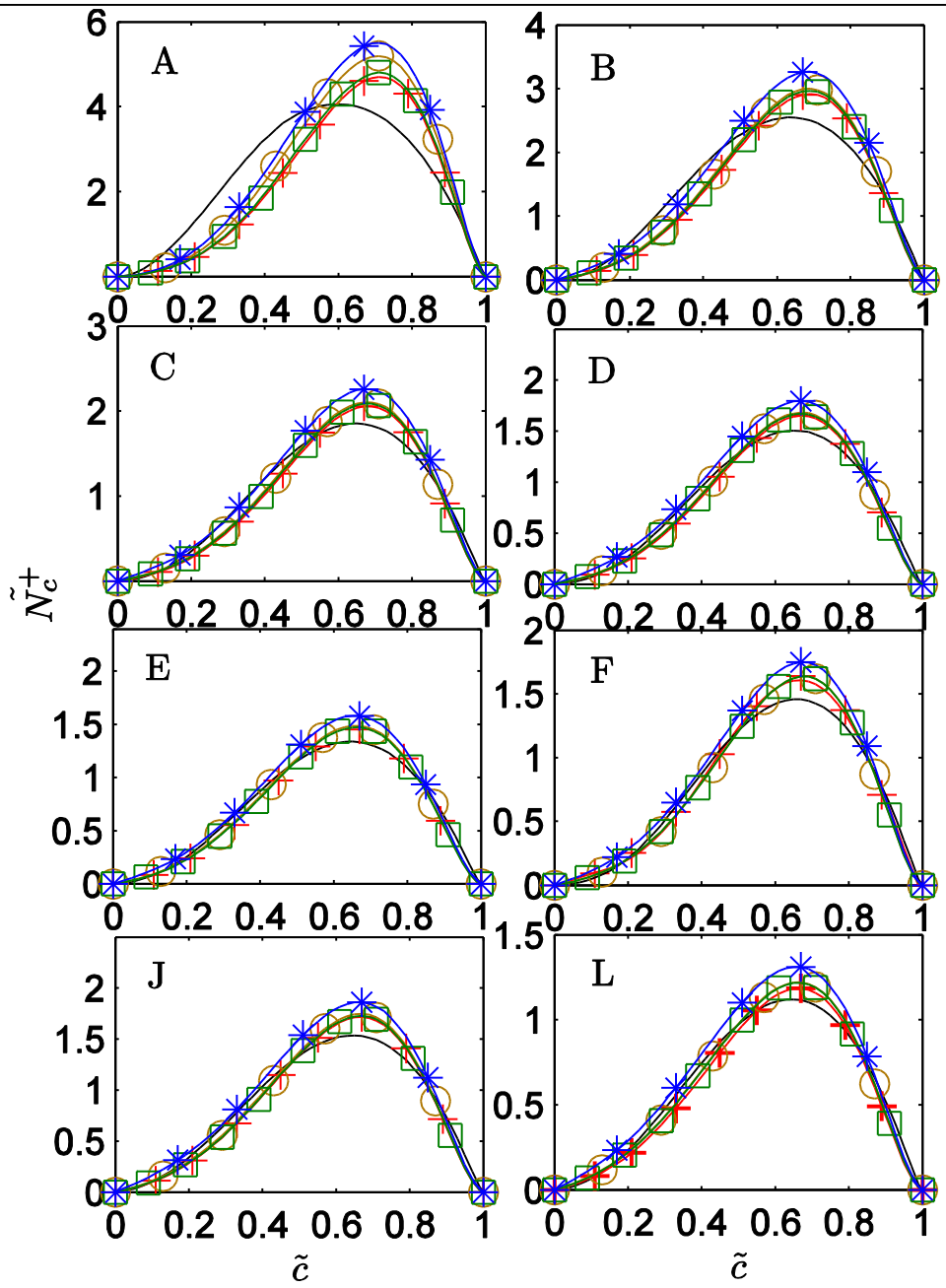

Figure 6.18: Variation of mean values of normalised SDR $\tilde{N}_c^+$ (———) conditional on $\tilde{c}$ across the flame brush along with the predictions of predictions of the SDR-RE model for: (i) u'_Δ extracted from DNS and β_c reported in Table 6.3 (—+—), (ii) u'_Δ extracted from DNS and β_c according to eq. (6.69) (—*—), (iii) u'_Δ modelled using eq. (6.68) and optimum values of β_c^* reported in Table 6.3 (—o—) and (iv) u'_Δ modelled using eq. (6.68) and β_c^* according to eq. (6.70) (—□—) at $\Delta \approx 0.8\delta_{th}$ for cases A-F, J and L.

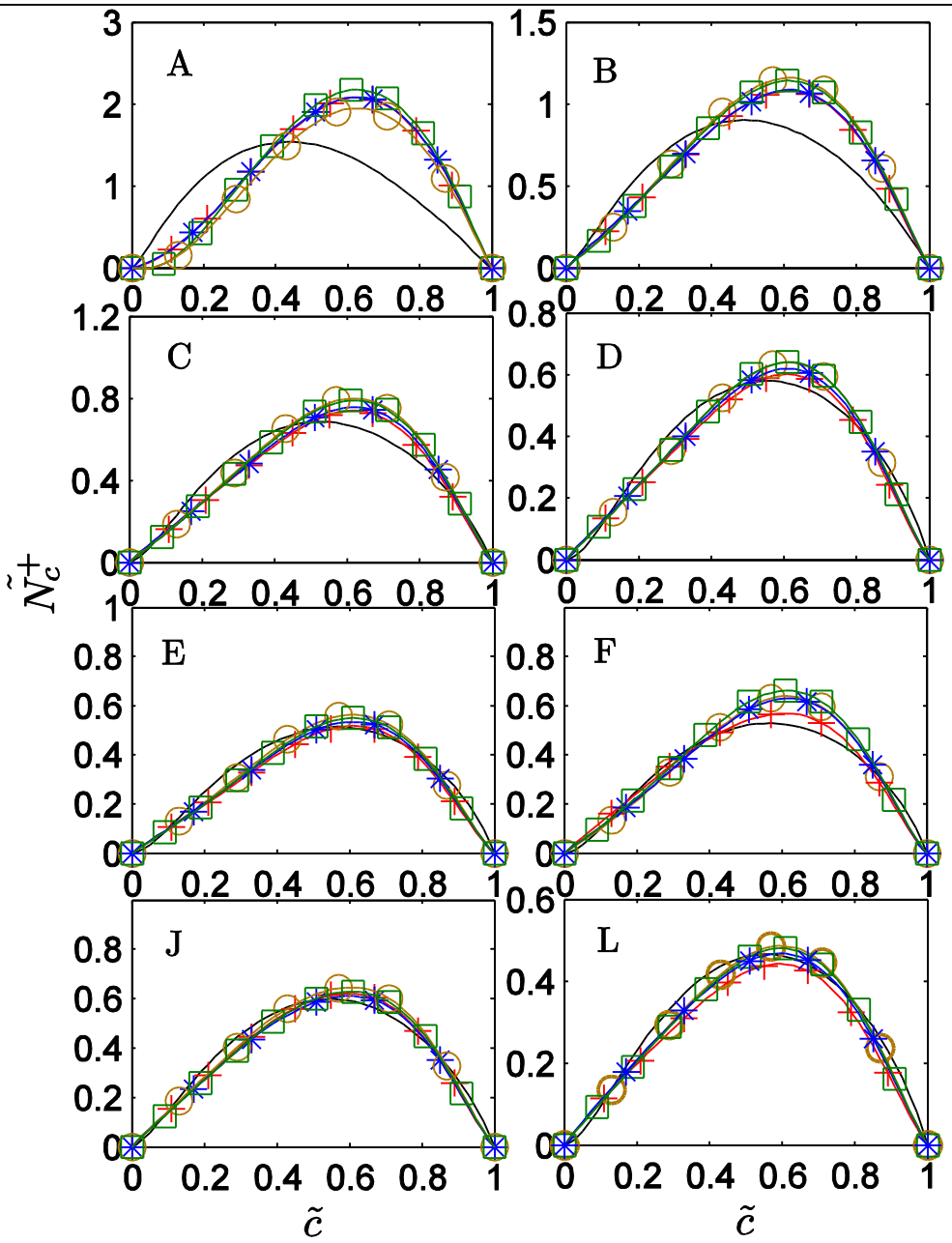

Figure 6.19: Variation of mean values of normalised SDR $\tilde{N}_c^+$ (———) conditional on $\tilde{c}$ across the flame brush along with the predictions of predictions of the SDR-RE model for: (i) u'_Δ extracted from DNS and β_c reported in Table 6.3 (—|—), (ii) u'_Δ extracted from DNS and β_c according to eq. (6.69) (—*—), (iii) u'_Δ modelled using eq. (6.68) and optimum values of β_c^* reported in Table 6.3 (—○—) and (iv) u'_Δ modelled using eq. (6.68) and β_c^* according to eq. (6.70) (—□—) at $\Delta \approx 2.8\delta_{th}$ for cases A-F, J and L.

It is worth noting that the original RANS model for $\tilde{\varepsilon}_c$, based on which eq. (6.66) was derived, implicitly assumed an equilibrium between the source and sink terms of the SDR transport equation. The first term on right hand side of eq. (6.66) indicates the resolved part of SDR (i.e. $\tilde{D}\nabla\tilde{c}.\nabla\tilde{c}$), whereas the second term on the right hand side represents the unresolved part of SDR (i.e. $\tilde{N}_c - \tilde{D}\nabla\tilde{c}.\nabla\tilde{c}$) and the expression for N_{sg} in eq. (6.66)

is obtained based on the balance of the source and sink terms of the SDR transport equation for $\Delta >> \delta_{th}$ (Chakraborty and Swaminathan, 2011). It has been demonstrated earlier by Swaminathan and Bray (2005) and Kolla *et al.* (2009) that the contributions of $T_2, T_3, T_4, f(D)$ and $(-D_2)$ remain the leading order contributors to the SDR transport for high values of Damköhler number (i.e. $Da >> 1$), and a rough equilibrium is maintained between the terms $T_2, T_3, T_4, f(D)$ and $(-D_2)$, which was utilised to develop the original RANS models leading to eqs. (6.66) and (6.67). The assumptions behind the derivations of eqs. (6.66) and (6.67) are satisfied more closely for high values of Δ. Thus, $(1-f)N_{sg}$ in eq. (6.66) is expected to predict the unresolved part of SDR (i.e. $\widetilde{N}_c - \widetilde{D}\nabla\widetilde{c}.\nabla\widetilde{c}$) reasonably accurately for $\Delta > \delta_{th}$ (e.g. $\Delta \approx 2.8\delta_{th}$). Although the assumptions behind eq. (6.66) are likely to be rendered invalid for $\Delta < \delta_{th}$ (e.g. $\Delta \approx 0.8\delta_{th}$), the resolved part of SDR (i.e. $\widetilde{D}\nabla\widetilde{c}.\nabla\widetilde{c}$) remains the major contributor to $\widetilde{N}_c$ (as evidenced by $\Xi_D^V \approx 1.0$ for $\Delta < \delta_{th}$ in Fig. 6.14) and thus eq. (6.66) continues to predict $\widetilde{N}_c$ accurately and the inaccuracy involved in evaluating the unresolved part $(\widetilde{N}_c - \widetilde{D}\nabla\widetilde{c}.\nabla\widetilde{c})$ by $(1-f)N_{sg}$ does not play a major role.

It is worth noting that the model parameters C_3^* and C_4^* in eq. (6.66) are expressed according to the original suggestion by Chakraborty and Swaminathan (2011) for the purpose of RANS modelling and here only β_c has been modified in order to extend the model for LES. In Figs. 6.15 and 6.16 the predictions of the SDR-RE are shown for the optimum values of β_c for which the variation of Ξ_D^V with Δ is appropriately captured. For actual LES simulations the optimum values of β_c are not *a-priori* known and thus it is important to parameterise the optimum values of β_c. In addition, β_c needs to satisfy $\beta_c \geq 2/(2c_m - 1)$ in order to maintain physical realisability (i.e. $\widetilde{N}_c \geq 0$) (Chakraborty *et al.*, 2008). Therefore a parameterisation for β_c has been proposed here in the following manner, which reasonably captures the variation of Ξ_D^V with Δ, as shown in Fig. 6.17 for cases A-M:

$$\beta_c = \max\left[\frac{2}{2c_m - 1}, \left(1.05\frac{\tau}{\tau+1} + 0.51\right)^{4.6}\right] \tag{6.69}$$

Equation (6.69) accounts for the increasing trend of Ξ_D^V and the peak mean value of $\widetilde{N}_c$ conditional on $\widetilde{c}$ with decreasing τ by ensuring an increasing trend of β_c with increasing τ. The minimum value of β_c has been set to be $2/(2c_m - 1)$ in eq. (6.69) in order to satisfy the physical realisability (i.e. $\widetilde{N}_c \geq 0$) according to a previous analysis by Chakraborty *et al.* (2008). In addition, β_c assumes an asymptotic constant value (i.e. $\beta_c = 7.73$) for large values of τ (i.e. $\tau \to \infty$) according to eq. (6.69), and this asymptotic value remains close to $\beta' = 6.7$ proposed by Chakraborty and Swaminathan (2011) in their SDR-RANS model. The turbulent Reynolds number Re_t dependence has not been included in eq. (6.69) for the sake of simplicity because the optimum value of β_c for $f = \exp[-0.7(\Delta/\delta_{th})^{1.7}]$ does not show any appreciable Re_t dependence (see column 7 of Table 6.2). It is worth noting that eq. (6.69) not only satisfactorily predicts the optimum values of β_c for cases A-M, but also enables eq. (6.66) to capture the variation of Ξ_D^V with Δ for the DNS dataset (where $\tau = 2.52$ and $Le = 1.0$) considered by Dunstan *et al.* (2013) (not shown here).

The predictions of the mean values of normalised SDR $\widetilde{N}_c^+$ conditional on $\widetilde{c}$ according to the SDR-RE model with β_c parameterisation using eq. (6.69) at $\Delta \approx 0.8\delta_{th}$ and $\Delta \approx 2.8\delta_{th}$ are also compared with DNS results in Figs. 6.18 and 6.19 respectively for cases A-M. A comparison between Figs. 6.17-6.19 reveals that eq. (6.69) enables the SDR-RE model to perform comparably with the model predictions when the optimum values of β_c are used. Moreover, the SDR-RE model (i.e. eq. (6.66)) satisfactorily captures the variation of the mean values of normalised SDR $\widetilde{N}_c^+$ conditional on $\widetilde{c}$ across the flame brush for both $\Delta < \delta_{th}$ (e.g. $\Delta \approx 0.8\delta_{th}$) and $\Delta > \delta_{th}$ (e.g. $\Delta \approx 2.8\delta_{th}$) for cases B-E, G-J and L except the overpredictions in cases A and F, as noted earlier in this paper.

It is worth noting that u'_Δ appears explicitly in eq. (6.66) and is used for the evaluation of Da_Δ, Re_Δ and Ka_Δ. The optimum values of β_c reported in column 7 of Table 6.2 and its parametersation using eq. (6.69) are obtained when u'_Δ is extracted from DNS data. However, modelling of u'_Δ using eq. (6.68) is likely to alter the optimum values and the parameterisation of β_c. The optimum values of β_c when u'_Δ is modelled using eq. (6.68)

show similar Le, τ and Re_t dependences as that of β_c (when u'_Δ is extracted from DNS data) for a slightly modified bridging function $f = \exp[-0.8(\Delta/\delta_{th})^{1.7}]$ ($\approx f = \exp[-0.36(Da_\Delta\,\mathrm{Re}_\Delta)^{0.85}]$ for the present thermo-chemistry). The optimum values of β_c, when u'_Δ is modelled using eq. (6.68), are reported in column 8 of Table 6.2 (denoted as β_c^* for convenience) and the corresponding predictions of the SDR-RE model with the optimum values of β_c^* are shown in Fig. 6.17, which reveals that the variation of Ξ_D^V with Δ can be appropriately captured by the SDR-RE model when u'_Δ is modelled using eq. (6.68) provided the optimum values of β_c^* are used. The optimum value of β_c^* and the corresponding bridging function f have been obtained using the same methodology which was used to extract optimum values of β_c and f when u'_Δ was extracted from DNS data.

It is evident from Table 6.3 that β_c^* shows qualitatively similar τ and Re_t dependences as that of β_c, and Le has been found not to have any major influence on β_c^*. However, the optimum values of β_c^* are slightly greater than the values for β_c (see Table 6.3). The predictions of the SDR-RE model, when u'_Δ is modelled using eq. (6.68) and the optimum values of β_c^* are used, are also shown in Figs. 6.18 and 6.19, which indicate that the performance of the SDR-RE model does not get significantly affected by u'_Δ modelling when the optimum values of β_c^* are used. The observed τ dependences of β_c^* has been parameterised here by modifying eq. (6.69) in the following manner so that the SDR-RE model captures the variation of Ξ_D^V with Δ, which can be substantiated from Fig. 6.17 for cases A-M:

$$\beta_c^* = \max\left[\frac{2}{2c_m - 1}, \left(1.05\frac{\tau}{\tau+1} + 0.55\right)^{4.6}\right] \tag{6.70}$$

Similar to eq. (6.69) the weak Re_t dependence of β_c^* has been ignored in the parameterisation of β_c^* in eq. (6.70). The predictions of eqs. (6.69) and (6.70) ensure that β_c^* remains slightly larger than β_c as demonstrated in Table 6.3 (see columns 7 and 8 of Table 6.3).

The predictions of the SDR-RE model with β_c^* (u'_Δ) according to eq. (6.69) are also shown in Figs. 6.18 and 6.19, which show that these predictions remain comparable to the predictions when u'_Δ is extracted from DNS and β_c is parameterised using eq. (6.70). Moreover, the predictions of the SDR-RE model with β_c^* according to eq. (6.70) remain comparable to the predictions when the optimum values of β_c^* reported in Table 6.3 are used. The evidences from Figs. 6.15-6.19 indicate that the performance of the SDR-RE model captures the statistical behaviours of $\widetilde{N}_c$ better than the SDR-PL and SDR-C models for turbulent premixed flames with a range of different values of τ, Le and Re_t even when u'_Δ is modelled using eq. (6.68). Thus, the SDR-RE model (i.e. eq. (6.66)) can be considered to be a viable option for the SDR closure in the context of LES simulations of turbulent premixed flames.

6.4 Dynamic approach of SDR algebraic closure

6.4.1 Dynamic power law model for $\widetilde{N}_c$

It is possible to rewrite the eqs. (6.57) and (6.58) in the following manner:

$$\overline{\rho N_c} = \bar{\rho}\widetilde{N}_c = \bar{\rho}\widetilde{D}\nabla\widetilde{c}.\nabla\widetilde{c}\left(\frac{\Delta}{\eta_{iD}}\right)^{\alpha_D} \tag{6.71}$$

where η_{iD} is the inner cut-off scale and α_D is the power-law exponent. An approach to avoid the unphysical small values of $\bar{\rho}\widetilde{N}_c$ for $\Delta \to 0$ according to eq. (6.71) is a dynamic evaluation of α_D as it (i.e. $\alpha_D \to 0$) approaches to 0 for $\Delta \to 0$. Assuming α_D does not change during test filtering operation, it is possible to evaluate it dynamically in the following manner:

$$\overline{\rho N_c} = \bar{\rho}\tilde{N}_c = \overbrace{(\bar{\rho}\tilde{D}\nabla\tilde{c}.\nabla\tilde{c})}.\left(\frac{\Delta}{\delta_{th}}\right)^{\alpha_D} = \bar{\rho}\,\tilde{D}\,\nabla\,\tilde{c}\,.\nabla\,\tilde{c}\,.\left(\frac{\bar{\Delta}}{\delta_{th}}\right)^{\alpha_D} \tag{6.72}$$

where $\overleftarrow{\overline{Q}}$ and $\overleftarrow{\widetilde{Q}}$ indicate test filtered value of a general quantity Q and Favre filtering operation at the equivalent filter width (i.e. $\overleftarrow{\widetilde{Q}} = \overleftarrow{\overline{\rho Q}}/\overleftarrow{\bar{\rho}}$) respectively, whereas the equivalent filter width after test filtering is given by $\overleftarrow{\bar{\Delta}}$. The test filter is often taken to be

a multiplier of Δ (i.e. $\tilde{\Delta} = a\Delta$ where $a > 1$ is a constant) for non-zero filter widths. Thus the equivalent filter width $\tilde{\tilde{\Delta}}$ for a Gaussian filter can be given as: $\tilde{\tilde{\Delta}} = [\Delta^2 + (\tilde{\Delta})^2]^{1/2} = \Delta\sqrt{1+a^2}$ (i.e. $\lim_{\Delta \to 0} \tilde{\tilde{\Delta}} / \Delta = \sqrt{1+a^2}$) (Pope, 2000). Therefore the ratio between $\tilde{\tilde{\Delta}}$ and Δ should be taken as a constant value. Based on eq. (6.72), it is possible to obtain an expression of α_D in the following manner:

$$\alpha_D = \frac{\ln[< \overbrace{(\bar{\rho}\tilde{D}\nabla\tilde{c}.\nabla\tilde{c})}^{} >_D / < \tilde{\bar{\rho}}\tilde{\tilde{D}}\nabla\tilde{\tilde{c}}.\nabla\tilde{\tilde{c}} >_D]}{\ln(\tilde{\tilde{\Delta}} / \Delta)} \quad \text{for } \Delta > 0 \text{; otherwise } \alpha_D = 0 \quad (6.73)$$

where $< Q >_D$ is an appropriate volume-averaging operation to avoid unphysical numerical artefacts induced by dynamic filtering operation (Charlette et al., 2002; Knikker et al., 2004). It is worth noting that eq. (6.73) relies on scale-similarity between Δ and $\tilde{\tilde{\Delta}}$, and thus the validity of this modelling approach is significantly dependent on it. Furthermore, α_D approaches 0 (i.e. $\ln 1 / \ln(\sqrt{1+a^2})$) for very small filter width (i.e. $\Delta \to 0$), as the numerator of eq. (6.73) vanishes when $\bar{\rho}\tilde{D}\nabla\tilde{c}.\nabla\tilde{c} \to \overbrace{(\bar{\rho}\tilde{D}\nabla\tilde{c}.\nabla\tilde{c})}^{}$. This leads to $\tilde{N}_c \approx \tilde{D}\nabla\tilde{c}\cdot\nabla\tilde{c}$ when the flow becomes completely resolved (i.e. $\Delta \to 0$). It is worth noting that a similar dynamic closure for FSD (i.e. $\Sigma_{gen} = |\nabla\bar{c}|(\Delta S_L / 3\alpha_{T0})^{\alpha_{FSD}}$) was proposed earlier by Knikker *et al.* (2004) where α_{FSD} was evaluated using an expression similar to eq. (6.73).

6.4.2 Dynamic evaluation of the SDR-RE model

The SDR model given by eq. (6.66) with a predetermined β_c has recently been implemented in LES simulations (Ma *et al.*, 2014; Langella *et al.*, 2013) of flow configurations for which well-documented experimental data is available for a direct comparison with simulation results and the results have been found to be either comparable or better than that obtained from established algebraic LES-FSD closures. Interested readers are referred to Ma *et al.* (2014) for further discussion in this regard.

However, the modelling of u'_Δ influences the optimum value and the parameterization of β_c. The empirical parameterisation of β_c can be avoided using a dynamic formulation which is proposed here in the following manner. Equation (6.69) can be rewritten as:

$$\overline{\rho}\widetilde{N}_c - \overline{\rho}\widetilde{D}\nabla\widetilde{c}.\nabla\widetilde{c} = f_1\left(\frac{u'_\Delta}{S_L}, \frac{\Delta}{\delta_{th}}\right)\frac{\overline{\rho}}{\beta_c} \tag{6.74}$$

where $f_1\left(\frac{u'_\Delta}{S_L}, \frac{\Delta}{\delta_{th}}\right)$ is given by:

$$f_1\left(\frac{u'_\Delta}{S_L}, \frac{\Delta}{\delta_{th}}\right) = \left[1-\exp[-\theta\left(\frac{\Delta}{\delta_{th}}\right)^p]\right]\left[\frac{2K_c^* S_L}{Le^{1.88}\delta_{th}} + (C_3^* - \tau.Da_\Delta C_4^*)\left(\frac{2u'_\Delta}{3\Delta}\right)\right]\tilde{c}(1-\tilde{c}) \tag{6.75}$$

Based on the assumption of the scale independent functional form one can write:

$$\widetilde{\overline{\rho}\widetilde{N}_c} - \widetilde{\overline{\rho}\widetilde{D}\nabla\widetilde{c}.\nabla\widetilde{c}} = \frac{1}{\beta_c}\cdot\widetilde{\overline{\rho}\, f_1\left(\frac{u'_\Delta}{S_L}, \frac{\Delta}{\delta_{th}}\right)}, \quad \widetilde{\overline{\rho N_c}} - \widetilde{\overline{\rho}}\widetilde{\widetilde{D}}\nabla\widetilde{\widetilde{c}}.\nabla\widetilde{\widetilde{c}} = \frac{\widetilde{\overline{\rho}}}{\beta_c} f_1\left(\frac{\widetilde{u'_\Delta}}{S_L}, \frac{\widetilde{\overline{\Delta}}}{\delta_{th}}\right) \tag{6.76}$$

$$\text{and } f_1\left(\frac{u'_\Delta}{S_L}, \frac{\overline{\Delta}}{\delta_{th}}\right) = \left[1-\exp[-\theta\left(\frac{\overline{\Delta}}{\delta_{th}}\right)^p]\right]\left[\frac{2K_c^* S_L}{Le^{1.88}\delta_{th}} + (C_3^* - \tau.Da_\Delta C_4^*)\frac{2u'_\Delta}{3\overline{\Delta}}\right]\tilde{c}.(1-\tilde{c}) \tag{6.77}$$

where $\widetilde{C_3^*}$, $\widetilde{C_4^*}$ and $\widetilde{Da_\Delta}$ are given by:

$$\widetilde{C_3^*} = \frac{2.0(\widetilde{Ka_\Delta})^{1/2}}{1+(\widetilde{Ka_\Delta})^{1/2}}, \quad \widetilde{C_4^*} = \frac{1.2(1.0-\widetilde{\tilde{c}})^\Phi}{Le^{2.57}(1+\widetilde{Ka_\Delta})^{0.4}} \quad \text{and} \quad \widetilde{Da_\Delta} = \frac{\widetilde{\overline{\Delta}}}{\widetilde{u'_\Delta}}\frac{S_L}{\delta_{th}} \tag{6.78}$$

In eq. (6.78) $\widetilde{Ka_\Delta}$ and $\widetilde{u'_\Delta}$ are given by:

$$\widetilde{Ka_\Delta} = \left(\frac{\widetilde{u'_\Delta}}{S_L}\right)^{1.5}\left(\frac{\widetilde{\overline{\Delta}}}{\delta_{th}}\right)^{-0.5} \quad \text{and} \quad \widetilde{u'_\Delta} = \left[\frac{1}{3}\left(\frac{\widetilde{\rho u_i u_i}}{\overline{\rho}} - \widetilde{\tilde{u}}_i\widetilde{\tilde{u}}_i\right)\right]^{0.5} \tag{6.79}$$

The volume-averaged value of the density-weighted SDR ($= \overline{\rho}\widetilde{N}_c$) should be independent of Δ (i.e. $< \widehat{\overline{\rho}\widetilde{N}_c} >_V = < \widehat{\overline{\rho N_c}} >_V \because < \hat{\bar{w}} >_V = \widehat{< \bar{w} >_V}$), which can be utilised along with eqs. (6.74) and (6.76) to obtain the following dynamic evaluation of β_c:

$$\beta_c = \frac{< \hat{\bar{\rho}} f_1 \left(\frac{\hat{u}'_\Delta}{S_L}, \frac{\hat{\bar{\Delta}}}{\delta_{th}} \right) >_D - \widehat{< \overline{\rho} f_1 \left(\frac{u'_\Delta}{S_L}, \frac{\Delta}{\delta_{th}} \right) >_D}}{\widehat{< \overline{\rho}\widetilde{D}\nabla\widetilde{c}.\nabla\widetilde{c} >_D} - < \hat{\bar{\rho}}\hat{\widetilde{D}}\nabla\hat{\widetilde{c}}.\nabla\hat{\widetilde{c}} >_D}} \tag{6.80}$$

Chakraborty *et al.* (2008) demonstrated that β_c needs to satisfy $\beta_c \geq 2/(2c_m - 1)$ in order to maintain physical realisability (i.e. $\widetilde{N}_c \geq 0$) and thus it is ensured that dynamic evaluation of β_c does not violate physical realisability in the following manner:

$$\beta_c = \max \left[\frac{2}{2c_m - 1}, \frac{< \hat{\bar{\rho}} f_1 \left(\frac{\hat{u}'_\Delta}{S_L}, \frac{\hat{\bar{\Delta}}}{\delta_{th}} \right) >_D - \widehat{< \overline{\rho} f_1 \left(\frac{u'_\Delta}{S_L}, \frac{\Delta}{\delta_{th}} \right) >_D}}{\widehat{< \overline{\rho}\widetilde{D}\nabla\widetilde{c}.\nabla\widetilde{c} >_D} - < \hat{\bar{\rho}}\hat{\widetilde{D}}\nabla\hat{\widetilde{c}}.\nabla\hat{\widetilde{c}} >_D} \right] \tag{6.81}$$

The predictions of eqs. (6.73) and (6.81) for dynamic evaluation of α_D and β_c, respectively, will be assessed with respect to explicitly filtered DNS data. The predictions of SDR-RE model with dynamic evaluation of β_c (i.e. eq. (6.81)) will also be compared to the prediction of the static version of this model where β_c is evaluated using eq. (6.69).

6.4.3 Performance of the dynamic approaches: Volume-averaged behaviour

The variation of Ξ_D^V with changing Δ/δ_{th} for cases A-M are shown in Fig. 6.20 on a log-log plot. The cases G, I, K are qualitatively similar to cases F, H and L respectively and thus are not shown in Fig. 6.20 and in subsequent figures. A linear variation of $\log(\Xi_D^V)$ with $\log(\Delta/\delta_{th})$ indicates a power-law dependence between Ξ_D^V and Δ (see eq. (6.71)), which can be seen in Fig. 6.20 for $\Delta > \delta_{th}$ but not for $\Delta < \delta_{th}$. The slope of the best-fit straight line with the steepest slope provides a global value of α_D and the intersection of

this line with the $\Xi_D^V = 1.0$ gives the measure of η_{iD}/δ_{th}. The values of α_D and η_{iD}/δ_{th} for all cases considered here. It can be seen from Table 6.3 that α_D assumes higher values for cases with smaller value of Le for a given value of u'/S_L, whereas α_D increases with increasing $u'/S_L \sim \mathrm{Re}_t^{1/4} Ka^{1/2} \sim \mathrm{Re}_t^{1/2}/Da^{1/2}$ for a given value of Le. By contrast, η_{iD} remains of the order of δ_{th} for all cases. Table 6.3 shows that $\alpha_D < 1.0$ for weakly turbulent flames (e.g. cases F and G) which also leads to $\Xi_D^V > 1.0$ for $\Delta > \delta_{th}$. An increase of α_D with decreasing Le for a given value of Le suggests an increase in the extent of flame wrinkling, which can be substantiated from the values of normalised flame surface area A_T/A_L, which is provided in Table 6.3 where the flame surface area has been evaluated using the volume integral $A = \int_V |\nabla c| dV$ with the superscripts '*T*' and '*L*' referring to turbulent and laminar flame quantities respectively. Table 6.3 further shows that flame area generation increases with increasing u'/S_L for a given value of Le, which in turn gives rise to an increasing trend of α_D with an increase in u'/S_L. It has been demonstrated in Dunstan et al. (2013) that the power-law model (i.e. eq. (6.71)) does not adequately predict the local behaviour of $\tilde{N}_c$ even when α_D and η_{iD} obtained from DNS data in Fig. 6.20 are used. Interested readers are referred to Dunstan et al. (2013) for more discussion on the performance of the static version of the power-law model.

The prediction of the SDR-RE model (i.e. eq. (6.66)) with β_c given by eq. (6.69) is also shown in Fig. 6.20, which shows that eq. (6.66) satisfactorily predicts the variation of Ξ_D^V with Δ but this is expected as the parameterisation given by eq. (6.69) is designed to capture the magnitude of $\left\langle \bar{\rho}\tilde{N}_c \right\rangle_V$. However, Fig. 6.20 suggests that an accurate estimation of $\tilde{N}_c$ can be obtained using eq. (6.66) and the empiricism involved in β_c parameterisation (i.e. similar to eq. (6.66)) can be avoided if β_c can be evaluated using eq. (6.81) according to the dynamic formulation.

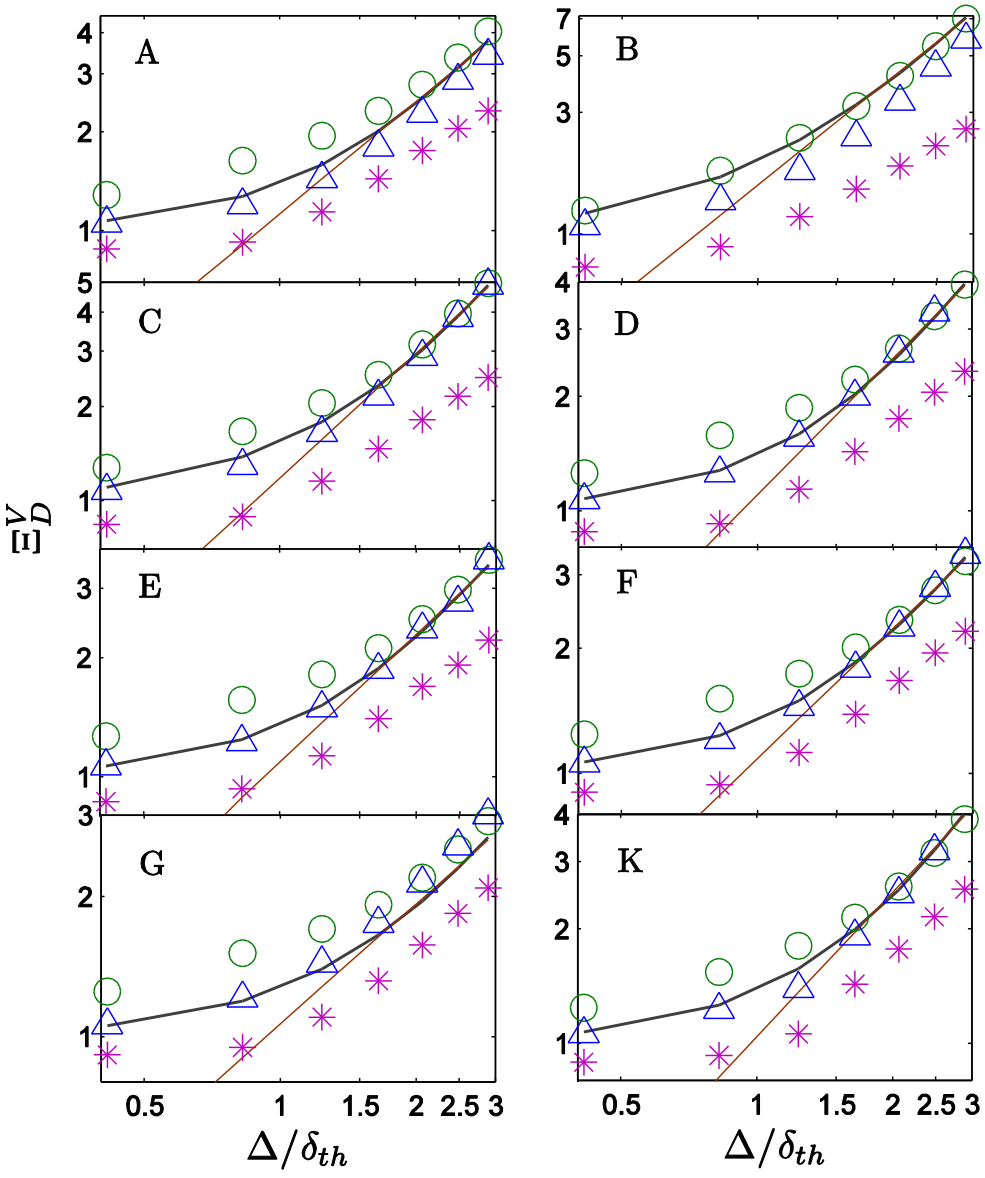

Figure 6.20: Variations of Ξ_D^V (——) with Δ/δ_{th} on a log-log plot along with the predictions of Power-law model (i.e. eq. (6.71)) (❋) with dynamic α_D, static SDR-RE model (eq. (6.66) with β_c according to eq. (6.69)) (O) and dynamic SDR-RE model (eq. (6.66) with β_c according to eq. (6.81)) (△) in cases A-F, J and L. The linear region describing the power-law given by eq. (6.71) is marked by the solid line following least-squares fit corresponding to the largest slope.

The predictions of eq. (6.71) with dynamic evaluation of α_D according to eq. (6.73) are compared to the mean value of $\tilde{N}_c$ conditional on $\tilde{c}$ obtained from DNS in Fig. 6.21 for cases A-F, J and L at $\Delta \approx 0.4\delta_{th}$ and $\Delta \approx 2.8\delta_{th}$. The volume-averaging involved in dynamic evaluation of α_D (see eq. (6.73)) is carried out by ensemble averaging the relevant quantities of using $(2n)^3$ cells around a given grid point, and it was found that results did not change significantly for n>3. Here the results are shown for n=4. The same

procedure was used for volume-averaging process involved in the dynamic evaluation of β_c using eq. (6.81). It is worth noting that α_D is a three-dimensional variable in the context of dynamic modelling and thus it is ensemble averaged conditional on bins of $\widetilde{c}$ in Fig. 6.22. The variations of the mean values of α_D conditional on $\widetilde{c}$ for cases A-F, J and L at $\Delta \approx 0.4\delta_{th}$ and $\Delta \approx 2.8\delta_{th}$ are shown in Fig. 6.22. It is clear from Fig. 6.22 that dynamic formulation according to eq. (6.73) successfully captures the increase in power-law exponent α_D with increasing Re_t for a given value of Le. Moreover, it can be seen from Fig. 6.22 that α_D increases with decreasing Le. Figure 6.22 demonstrates that α_D according to eq. (6.73) shows considerable local variation of power-law exponent within the flame brush for $\Delta > \delta_{th}$ (e.g. $\Delta \approx 2.8\delta_{th}$). Moreover, Fig. 6.22 shows that the dynamic formulation shows a reduction in α_D with decreasing Δ. It can be seen from Fig. 6.21 that the dynamic power-law model prediction under-predicts the mean value of $\widetilde{N}_c$ conditional on $\widetilde{c}$ towards the unburnt side of the flame brush for $\Delta > \delta_{th}$ for all cases, and the qualitative variation of $\widetilde{N}_c$ with $\widetilde{c}$ is not captured by the dynamic model for $Le << 1$ cases (e.g. cases A and B). However, the variation of mean value of $\widetilde{N}_c$ conditional on $\widetilde{c}$ is satisfactorily captured for $\Delta < \delta_{th}$ (e.g. $\Delta \approx 0.4\delta_{th}$) for $Le \approx 1$ cases but the dynamic model under-predicts the mean value of $\widetilde{N}_c$ conditional on $\widetilde{c}$ for $Le << 1$ cases (e.g. cases A and B) even at small filter widths (i.e. $\Delta < \delta_{th}$, for example $\Delta \approx 0.4\delta_{th}$). The predictions of Ξ_D^V according to eq. (6.71) with dynamic α_D (i.e. eq. (6.73)) evaluation are also shown in Fig. 6.20, which shows that dynamic evaluation of α_D results in the under-prediction of Ξ_D^V with increasing Δ, and this tendency increases with decreasing Le and is particularly prevalent for flames with $Le << 1$ (e.g. cases A and B).

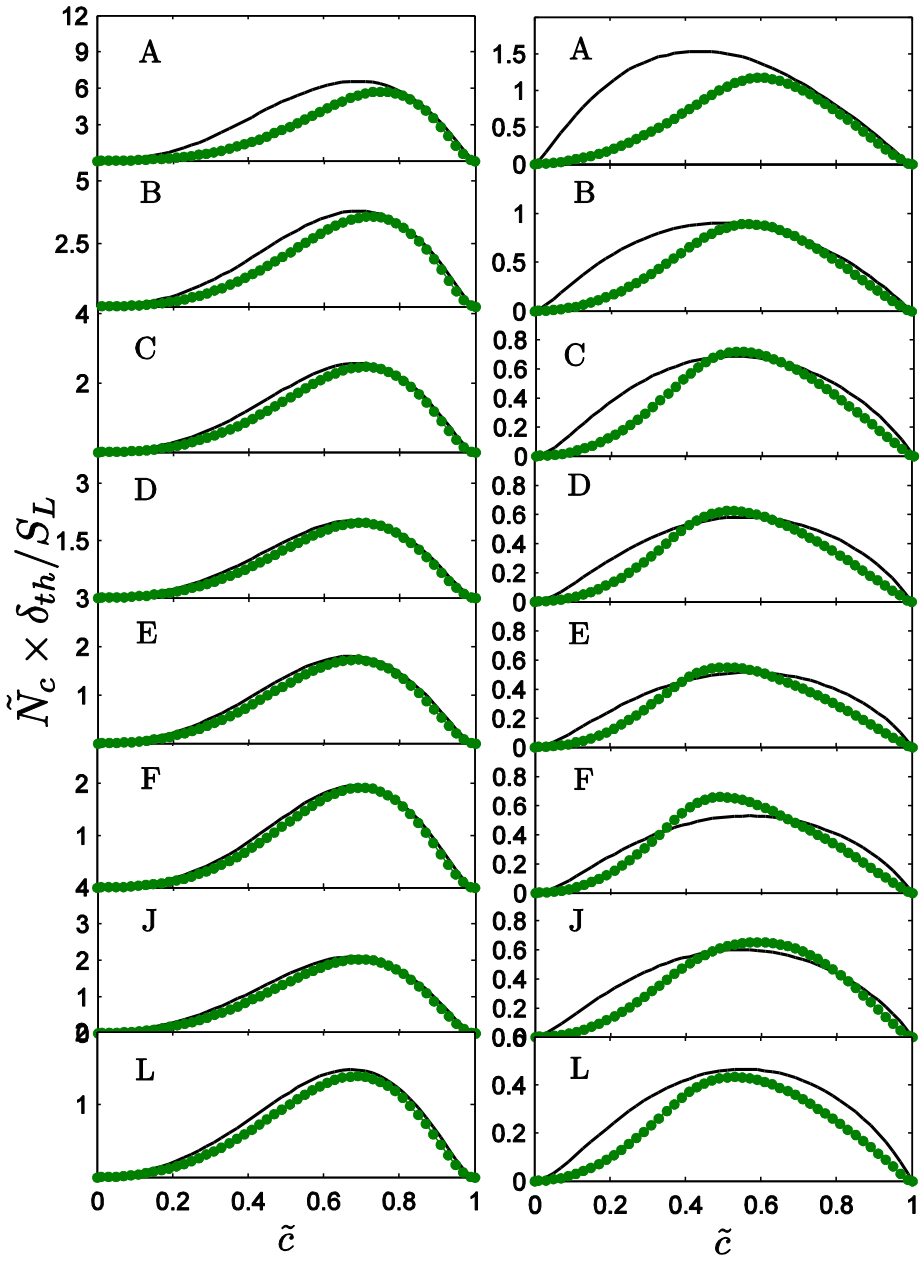

Figure 6.21: Variations of $\tilde{N}_c \times \delta_{th} / S_L$ (——) conditionally averaged in bins of $\tilde{c}$ along with the predictions of power-law model (—●—) with dynamic evaluation of α_D for $\Delta \approx 0.4\delta_{th}$ (left column) and $\Delta \approx 2.8\delta_{th}$ (right column) in cases A-F, J and L.

It is possible propose an alternative power-law model in the following manner:

$$\overline{\rho N_c} = \overline{\rho}\tilde{N}_c = \overline{\rho}\tilde{D}\nabla\tilde{c}.\nabla\tilde{c}\left(1+\frac{\Delta}{\delta_{th}}\right)^{\alpha'_D} \tag{6.82}$$

which leads to the following expression under the assumption of scale-similarity:

$$\widehat{\overline{\rho N_c}} = \widehat{\overline{\rho}\tilde{N}_c} = \widehat{(\overline{\rho}\tilde{D}\nabla\tilde{c}.\nabla\tilde{c})}.(1+\Delta/\delta_{th})^{\alpha'_D} = \hat{\overline{\rho}}\hat{\tilde{D}}\nabla\hat{\tilde{c}}.\nabla\hat{\tilde{c}}.(1+\hat{\Delta}/\delta_{th})^{\alpha'_D} \tag{6.83}$$

Equation (6.83) provides:

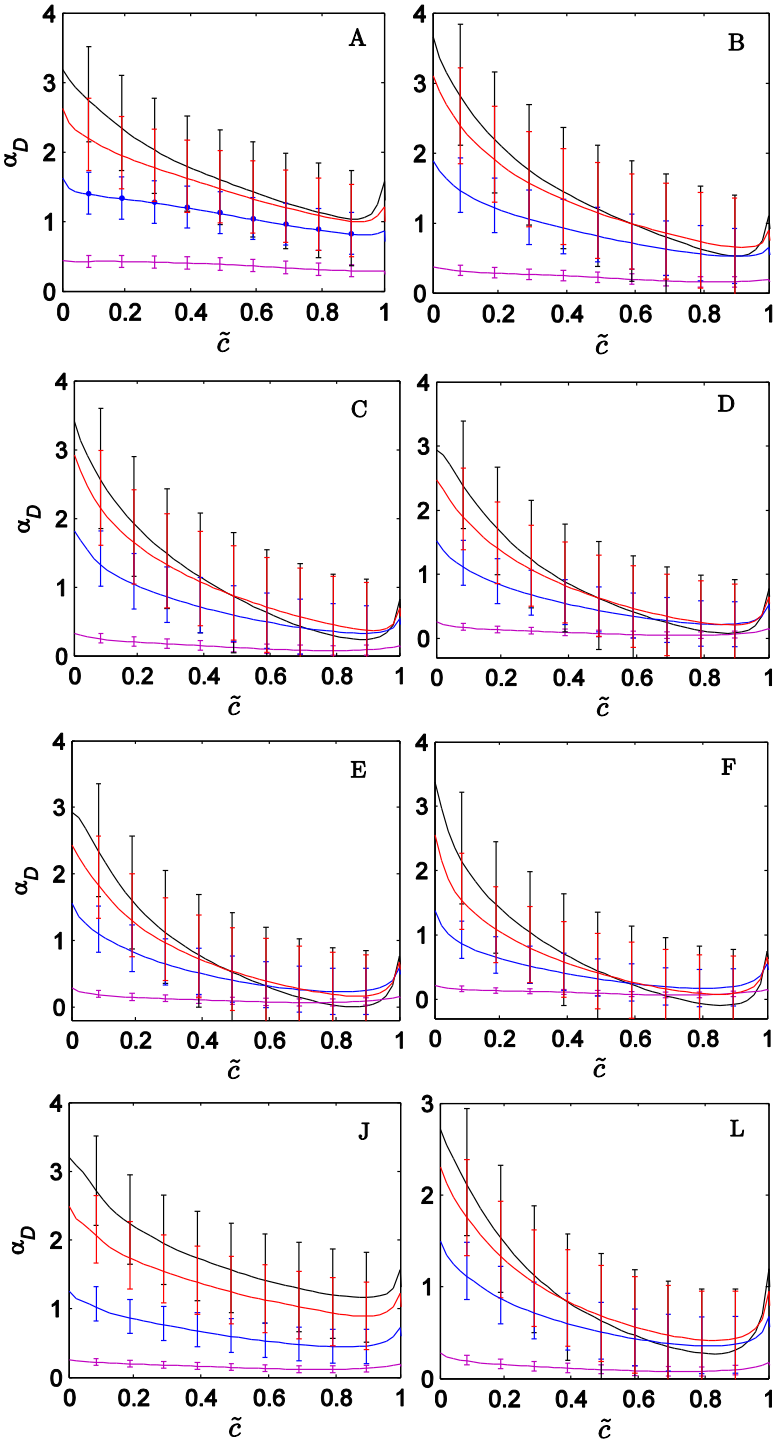

Figure 6.22: Variations of dynamically evaluated α_D (according to eq. 4) conditionally averaged in bins of $\tilde{c}$ for $\Delta \approx 0.4\delta_{th}$ (———), $\Delta \approx 1.2\delta_{th}$ (———), $\Delta \approx 2.0\delta_{th}$ (———) and $\Delta \approx 2.8\delta_{th}$ (———) with the bars indicating one standard deviation variation over the mean in cases A-F, J and L.

$$\alpha'_D = \frac{\ln[<\overbrace{(\overline{\rho}\widetilde{D}\nabla\widetilde{c}.\nabla\widetilde{c})}>_D / <\tilde{\overline{\rho}}\tilde{\widetilde{D}}\nabla\tilde{\widetilde{c}}.\nabla\tilde{\widetilde{c}}>_D]}{\ln[(1+\tilde{\overline{\Delta}}/\delta_{th})/(1+\Delta/\delta_{th})]} \tag{6.84}$$

However, the performance of eq. (6.82) remains inferior to the dynamic version of the model given by eq. (6.71) and thus are not discussed here. The applicability of scale-similarity for quantities related to scalar gradient (e.g. SDR and Flame FSD) is debatable but the assumption of scale-similarity was successfully used in the past for the closure of FSD (Charlette et al., 2002). However, the results in Figs. 6.20 and 6.21 suggest that the strong assumption regarding scale independent functional form (i.e. α_D does not change between actual and test filter scales) that has been invoked while deriving eq. (6.73) may not be strictly valid, as SDR for passive scalars is known to exhibit multi-fractal nature (Sreenivasan, 2004; Sreenivasan et al., 1989; Sreenivasan, 1991; Prasad and Sreenivasan, 1990; Shivamoggi, 1995) and a similar behaviour is likely to present also for reacting flows. Thus, a single power-law exponent may not be suitable to describe the statistical behaviour of $\widetilde{N}_c$. Thus, the inaccuracies associated with the assumption involved scale regarding the independent functional form while deriving eq. (6.73) might have strong implications for highly wrinkled flames with $Le << 1$ (e.g. case A), which leads to a discrepancy between the predictions of local and volume-integrated behaviours of SDR according to the dynamic power-law model.

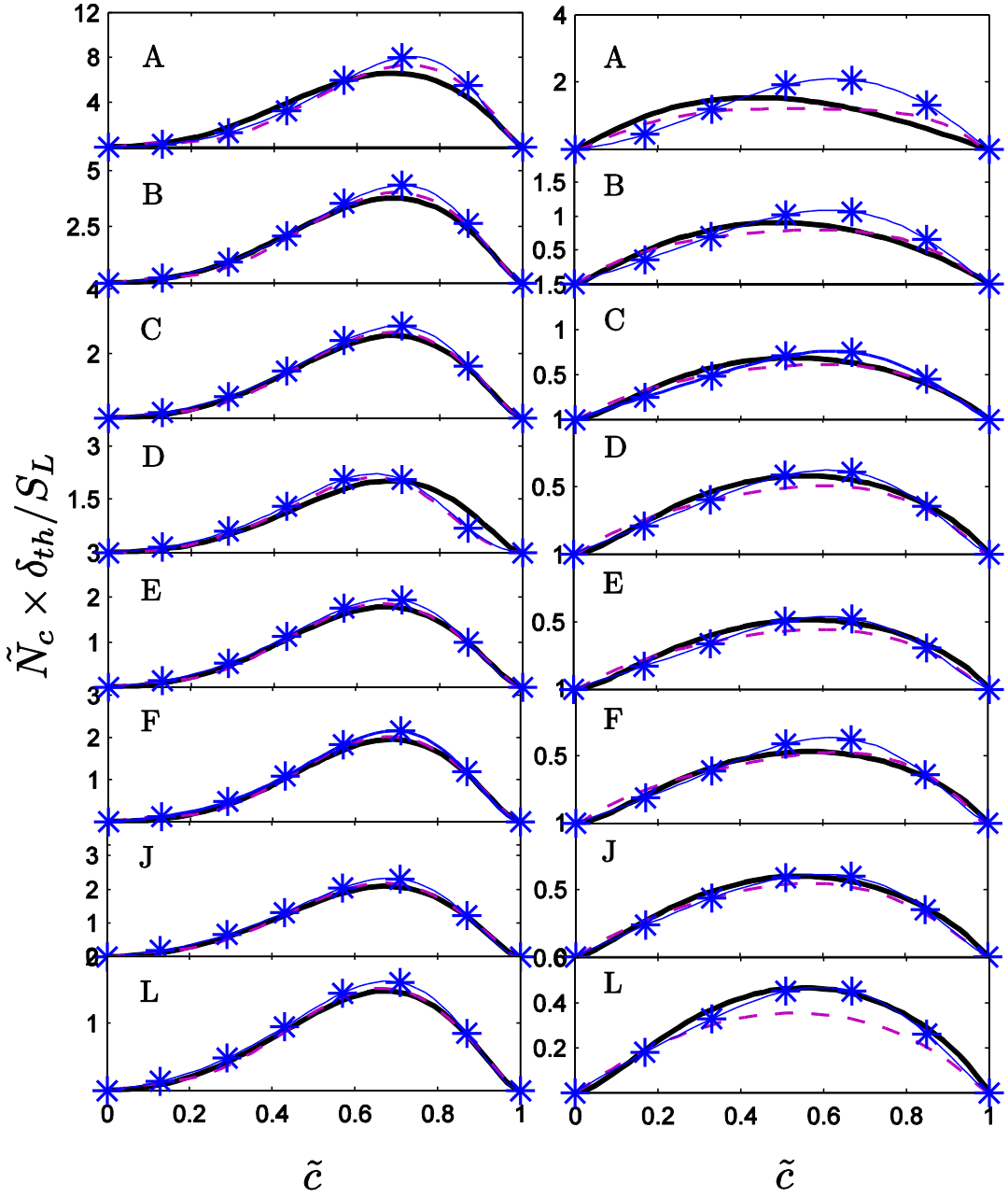

Figure 6.23: Variations of $\tilde{N}_c \times \delta_{th} / S_L$ (——) conditionally averaged in bins of $\tilde{c}$ along with the predictions of static SDR-RE model (eq. (6.66) with β_c according to eq. (6.69)) (—✱—) and dynamic SDR-RE model (eq. (6.66) with β_c according to eq. (6.81)) (- - - -) for $\Delta \approx 0.4\delta_{th}$ (left column) and $\Delta \approx 2.8\delta_{th}$ (right column) in cases A-G and K.

The predictions of the SDR-RE model (i.e. eq. (6.66)) with dynamic evaluation of β_c (according to eq. (6.81)) are compared to the same model prediction with static β_c (according to eq. (6.69)) and mean value of $\tilde{N}_c$ conditional on $\tilde{c}$ obtained from DNS in Fig. 6.23 for cases A-F, J and L at $\Delta \approx 0.4\delta_{th}$ and $\Delta \approx 2.8\delta_{th}$. The variations of the mean values of β_c conditional on $\tilde{c}$ for cases A-F, J and L at $\Delta \approx 0.4\delta_{th}$ and $\Delta \approx 2.8\delta_{th}$ are

shown in Fig. 6.24. The predictions of Ξ_D^V according to eq. (6.66) with dynamic β_c evaluation are also shown in Fig. 6.20. It is evident from Fig. 6.24 that eq. (6.81) predicts appreciable local variation of β_c within the flame brush. Moreover, Fig. 6.24 also suggests an increasing trend of β_c with increasing τ, as suggested by the empirical parameterization given by eq. (6.69). It is evident from Fig. 6.24 that the SDR-RE model with dynamic evaluation of β_c captures the behaviour of mean value of $\widetilde{N}_c$ conditional on $\widetilde{c}$ obtained from DNS data either comparably or better than the static version of the SDR-RE model with β_c parameterisation according to eq. (6.69). The advantages of dynamic model are particularly prominent for small values of Re_t and for flames with small Le (e.g. cases A, F and J) where the dynamic model satisfactorily captures $\widetilde{N}_c$ variation with $\widetilde{c}$, whereas the static version of the model overpredicts the mean value of $\widetilde{N}_c$ conditional on $\widetilde{c}$ for a major portion of the flame brush for $\Delta >> \delta_{th}$ (i.e. $\Delta \approx 2.8\delta_{th}$). Moreover, Fig. 6.20 suggests that the prediction of Ξ_D^V according to eq. (6.66) with dynamic β_c evaluation (i.e. eq. (6.81)) remains satisfactory and comparable to the prediction of the model with static β_c parameterization (i.e. eq. (6.69)). However, the dynamic version of the SDR-RE model (i.e. eq. (6.66)) does not depend on any empirical parametersation of β_c similar to eq. (6.69) but inherently accounts for Re_t, Le and τ dependences of $\widetilde{N}_c$ for a range of different filter widths Δ. A comparison between Figs. 6.21 and 6.23 further reveals that eq. (6.69) with dynamic β_c evaluation is more successful in capturing the local behaviour of $\widetilde{N}_c$ than the power-law model (i.e. eq. (6.71)) with dynamic evaluation of α_D. Moreover, Fig. 6.20 suggests that Ξ_D^V according to eq. (6.66) with dynamic β_c evaluation remains better than the prediction of eq. (6.71) with dynamic evaluation of α_D. This suggests that the power-law models, though widely used for the purpose of algebraic closure of Σ_{gen} (Charlette et al., 2002), may not be suitable for SDR $\widetilde{N}_c$ modelling and this behaviour perhaps arises due to multi-fractal nature of SDR, which was observed previously for passive scalar mixing (Sreenivasan, 1991, 2004; Sreenivasan et al, 1989; Prasad and Sreenivasan, 1990; Shivamoggi, 1995). By contrast, both static and dynamic versions of the SDR-RE model (i.e. eq. (6.66)) are more successful in predicting SDR accurately than the power-law based models for a range of different values of Re_t, Le and τ.

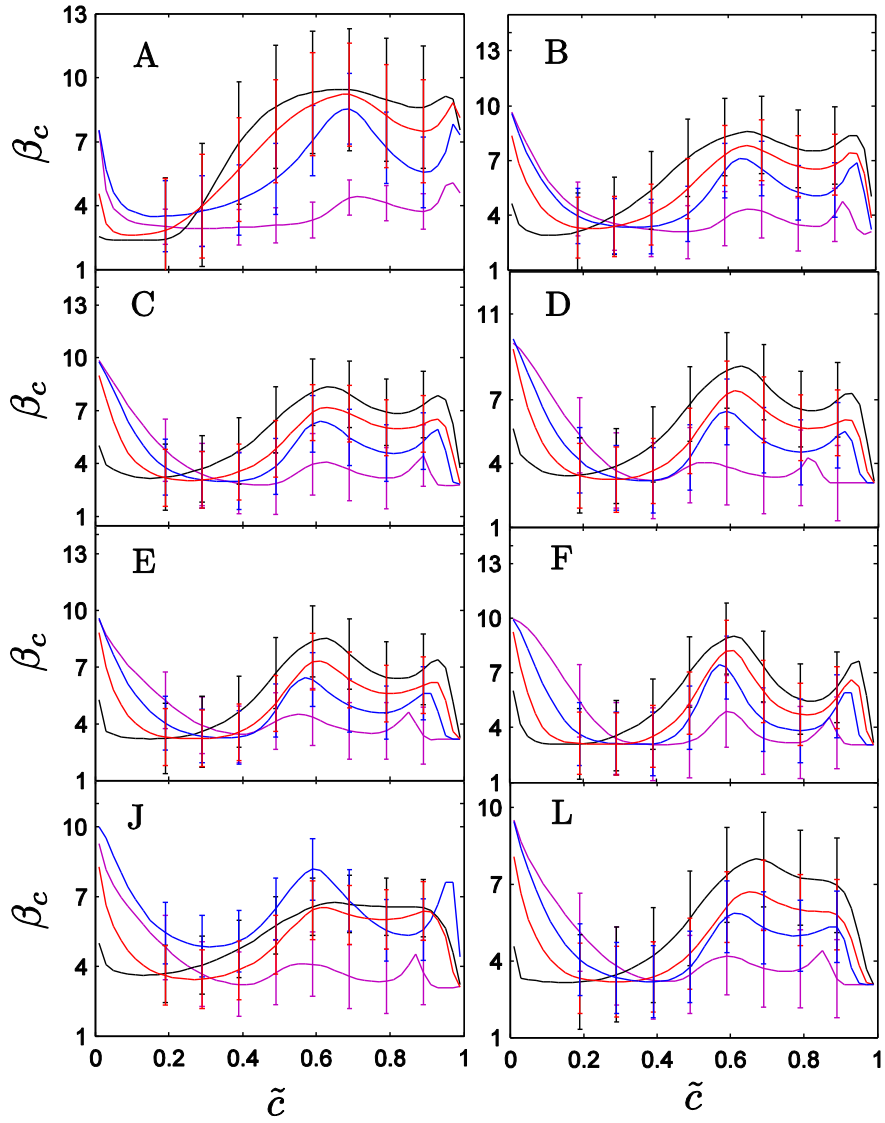

Figure 6.24: Variations of dynamically evaluated β_c conditionally averaged in bins of $\tilde{c}$ for $\Delta \approx 0.4\delta_{th}$ (———), $\Delta \approx 1.2\delta_{th}$ (———), $\Delta \approx 2.0\delta_{th}$ (———) and $\Delta \approx 2.8\delta_{th}$ (———) with the bars indicating one standard deviation variation over the mean in cases A-F, J and L.

6.5 Summary

A simple chemistry DNS database of statistically planar turbulent premixed flames has been used here to investigate the modelling of SDR for LES over a range of different heat release parameter τ, Lewis number *Le* and turbulent Reynolds number Re_t values. The performance of an existing SDR closure for passive scalar mixing (i.e. SDR-C model) has been assessed with respect to $\tilde{N}_c$ extracted from DNS data alongside a model based on a power-law expression (i.e. SDR-PL model) and an existing algebraic RANS-SDR

model, which has been extended here for the purpose of LES (i.e. SDR-RE model). It has been found that the SDR-PL model significantly overpredicts and fails to capture the qualitative variation of the mean values of $\widetilde{N}_c$ conditional on $\widetilde{c}$ for $\Delta > \delta_{th}$, even for the optimum parameters for which this model accurately predicts the volume averaged values of SDR. The SDR-C model with the theoretical value of Smagorinsky constant has been found to underpredict the mean values of $\widetilde{N}_c$ conditional on $\widetilde{c}$ and also the volume averaged values of SDR for all cases considered here. The newly developed SDR-RE model has been found to capture both local and volume-averaged statistics of $\widetilde{N}_c$ for both $\Delta < \delta_{th}$ and $\Delta > \delta_{th}$ in a better manner than the other alternative models for all cases considered here. The performance of the SDR-RE model has been found to improve with increasing Re_t and the SDR-RE model has been demonstrated to satisfactorily predict both local and volume-averaged statistics of $\widetilde{N}_c$ for high values of Re_t in flames with $Le \approx 1.0$ Moreover, it has been found that the modelling of the sub-grid turbulent velocity fluctuation (i.e. u'_Δ) based on Smagorinsky model of the eddy viscosity does not significantly affect the performance of the SDR-RE model. The model parameters proposed originally in the context of RANS have been used for the SDR-RE model except for the model parameter β_c, which is expressed here as a function of heat release parameter τ, as β_c remains a weak function of Re_t and independent of global Lewis number Le.

It is worth noting that the assumption of scale independent functional form is indeed questionable for modelling the quantities related to scalar gradient in premixed flames. However, this concept was successfully used for modelling the generalised FSD Σ_{gen} (Charlette *et al*., 2002) in the past using a power-law approach. However, previous findings (Dunstan *et al*., 2013) and current analysis indicate that the concept of scale-similarity may not be suitable for SDR modelling in the context of LES using a power-law approach. Although the assumption of scale independent functional form is invoked for dynamic evaluation of β_c but this assumption is applied to the function f_1 which is dependent on u'_Δ / S_L and Δ / δ_{th} (see eqs. (6.71) and (6.72)). As the assumption of scale independent functional form has been demonstrated to be successful in capturing the quantities associated with turbulence (e.g. u'_Δ) (Bardina et al., 1980; Zang et al., 1993;

Vreman et al., 1997), this assumption works better for dynamic evaluation of β_c than the dynamic evaluation of power-law exponent.

Chapter 7. Scalar dissipation rate transport and its modelling

As discussed in Chapters 5 and 6, it is possible to model the chemical reaction rate of turbulent premixed combustion based on properly modelled scalar dissipation rate. In turbulent premixed combustion, the transport equation of SDR can be closed if all unclosed terms in SDR transport equation are properly modelled in the context of both RANS and LES. Under the condition that equilibrium is maintained for the generation and destruction of scalar gradient, it is possible to algebraic closure filtered/averaged SDR in both RANS and LES, which was introduced in detail in Chapter 6. The modelling of SDR transport equation for RANS has been studied extensively in the existing literature (Chakraborty and Swaminathan, 2007a, 2007b, 2010, 2013; Chakraborty *et al*., 2008, 2009, 2010, 2011d; Mantel and Borghi, 1994; Mura and Borghi, 2003; Mura *et al*., 2008, 2009; Swaminathan and Bray, 2005). Interested readers are referred to Chakraborty *et al.* (2011d) for a detailed review of the existing modelling methodologies for SDR transport in the context of RANS simulations. However, relatively limited attention has been given to the modelling of SDR transport in the context of LES (Knudsen *et al*., 2012). In order to solve the transport equation of filtered SDR, it is necessary to model the sub-grid/unresolved components of the unclosed terms. Therefore, it is essential to model the unclosed terms of the SDR transport equation for the purpose of LES, which is yet to be addressed for turbulent premixed flames. The instantaneous behaviours of SDR and its transport equation will be provided firstly in this chapter followed by the statistical analysis of filtered SDR and its transport equation for a wide range of different filter widths. The dependences on local strain rate and curvature will be analysed for both instantaneous SDR and filtered SDR and their respective transport equations. The scaling estimates of SDR and the terms of its transport equation have been utilised to model the unclosed terms of filtered SDR transport equation at the end of this chapter.

7.1 Statistical analysis of instantaneous SDR and its transport equation

For the purpose of convience, the transport equation of instantaneous SDR N_c , which is eqs. (3.50) and (3.51) in Chpater 3, is repeated here as:

$$\frac{\partial(\rho N_c)}{\partial t}+\frac{\partial(\rho u_j N_c)}{\partial x_j}=\overbrace{\frac{\partial}{\partial x_j}\left(\rho D\frac{\partial N_c}{\partial x_j}\right)}^{\text{Molecular diffusion: } D_{1I}}\overbrace{-\frac{2D}{\rho}\frac{\partial\rho}{\partial x_j}\frac{\partial c}{\partial x_j}[\dot{w}+\nabla.(\rho D\nabla c)]}^{\text{Density variation: } T_{1I}}$$
$$\underbrace{-2\rho D\frac{\partial c}{\partial x_i}\frac{\partial u_i}{\partial x_j}\frac{\partial c}{\partial x_j}}_{\text{Scalar turbulence interaction: } T_{2I}} \tag{7.1}$$
$$+\underbrace{2D\frac{\partial\dot{w}}{\partial x_j}\frac{\partial c}{\partial x_j}}_{\text{Chemical reaction: } T_{3I}}\underbrace{-2\rho D^2\frac{\partial^2 c}{\partial x_i\partial x_j}\frac{\partial^2 c}{\partial x_i\partial x_j}}_{\text{Molecular dissipation: } (-D_{2I})}+\underbrace{F(D)}_{\text{Diffusivity variation}}$$

where

$$F(D)=\underbrace{2D\frac{\partial c}{\partial x_k}\frac{\partial(\rho D)}{\partial x_k}\frac{\partial^2 c}{\partial x_j\partial x_j}}_{T_{D1}}+\underbrace{2D\frac{\partial c}{\partial x_k}\frac{\partial^2(\rho D)}{\partial x_j\partial x_k}\frac{\partial c}{\partial x_j}}_{T_{D2}}\underbrace{-\frac{\partial}{\partial x_j}\left(\rho N_c\frac{\partial D}{\partial x_j}\right)}_{T_{D3}} \tag{7.2}$$
$$\underbrace{-2\rho D\frac{\partial D}{\partial x_j}\frac{\partial(\nabla c.\nabla c)}{\partial x_j}}_{T_{D4}}+\underbrace{\rho\nabla c.\nabla c\left[\frac{\partial D}{\partial t}+u_j\frac{\partial D}{\partial x_j}\right]}_{T_{D5}}$$

In the above transport equation, density variation term T_{1I}, turbulence scalar interaction term T_{2I}, reaction rate term T_{3I}, molecular dissipation term $(-D_{2I})$ and diffusivity gradient term $F(D)$ lead to unclosed terms of eqn. (3.58), (i.e. $T_2, T_3, T_4, (-D_2)$ and *f*(*D*)), which require modelling in both RANS and LES. Therefore the statistical behaviours of the above instantaneous terms evaluated based on DNS database will provide an accurate picture of their behaviours when the flow is fully resolved, which is of fundamental importance for modelling the unclosed terms of the SDR transport equation in a physically consistent manner as premixed combustion is mainly a sub-grid phononmenon as the flame thickness is only resolved in DNS but not RANS or LES.

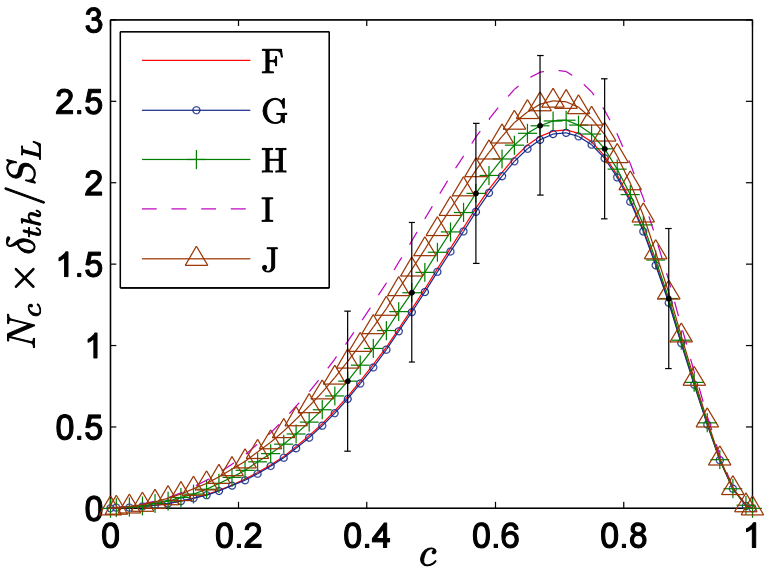

Figure 7.1: Variation of the mean value of $N_c \times \delta_{th} / S_L$ conditional on c values across the flame front for cases F-J with the bar indicating the standard deviation.

The variation of normalised instantaneous SDR $N_c \times \delta_{th} / S_L$ with c for unity Lewis number flames are shown in Fig. 7.1, which is obtained by ensemble averaging the quantity in question on a given c isosurface in the manner often used by previous studies (Boger *et al.*, 1998; Chakraborty and Cant, 2004, 2005; Chakraborty and Klein, 2008, 2008a). It is worth noting that this ensemble averging should not be confused with either Reynolds averaging or conventional conditional averaging operation in the context of RANS simulations because $N_c \times \delta_{th} / S_L$ is evaluated using all the samples for a given c value over the whole domain. Figure 7.1 shows that the maximum value of $N_c \times \delta_{th} / S_L$ is skewed slightly towards the burned gas side of the flame (i.e. $c \approx 0.7$). The peak magnitude of $N_c \times \delta_{th} / S_L$ does not change significantly in response to u'/S_L as the standard deviation for the case in the middle of the parameter range is found to exceed the difference in $N_c \times \delta_{th} / S_L$ values for the cases considered here. In order to understand this behaviour, the variations of the mean values of the terms T_{1I}, T_{2I}, T_{3I}, $(-D_{2I})$ and $F(D)$ conditional on c for cases F and J are shown in Fig. 7.2. The variations of the mean values of the terms in cases G, H and I are qualitatively similar to those in cases F and J and thus are not explicitly shown here. In all cases T_{1I} remains positive throughout the flame. By contrast, $(-D_{2I})$ assumes negative values throughout the flame in all cases as dictated by eq. (7.1). Expressing $\rho = \rho_0 / (1+\tau c)$ for low Mach number unity Lewis

number flames gives rise to an alternative expression for T_1 (Swaminathan and Bray, 2005;Chakraborty et al., 2008, 2010; Chakraborty and Swaminathan, 2010):

$$T_{1I} = 2\rho \frac{\partial u_j}{\partial x_j} N_c \tag{7.3}$$

As dilatation rate $\partial u_i / \partial x_i$ is predominantly positive in premixed flames, T_{1I} for all values of c is positive across the flame and vanishes on both ends of the flame.

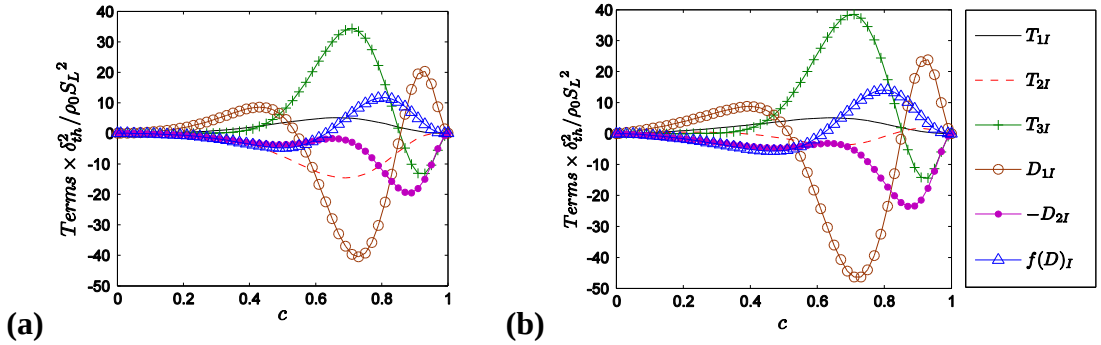

(a) **(b)**

Figure 7.2: Variation of the mean values of $T_{1I}, T_{2I}, T_{3I}, (-D_{2I})$ and $F(D)$ conditional on c values across the flame for cases F (a) and J(b). All the terms of the transport equation of N_c are normalised with respect to the respective values of $\rho_0 S_L^2 / \delta_{th}^2$.

The quantity T_{2I} assumes negative values throughout the flame front for cases F, although T_{2I} remains negative for the major portion of the flame, small positive values can be discerned in cases J. In order to understand this behaviour, the term T_2 can be expressed in the following manner (Swaminathan and Grout, 2006; Chakraborty and Swaminathan, 2007, 2007a; Chakraborty et al., 2008, 2009):

$$T_{2I} = -2\rho N_c (e_\alpha \cos^2\alpha + e_\beta \cos^2\beta + e_\gamma \cos^2\gamma) \tag{7.4}$$

where e_α, e_β and e_γ are the most extensive, intermediate and most compressive principal strain rates and α, β and γ are the angles of the eigenvectors associated with these principal strain rates with ∇c. Equation 7.4 demonstrates that the predominant alignment of e_α with ∇c leads to a negative contribution to T_{2I} whereas a predominant alignment of e_γ with ∇c leads to a positive contribution to T_{2I}.

It has been discussed in the previous analyses (Chakraborty and Swaminathan, 2007, 2007a; Chakraborty *et al*., 2008, 2009) that the alignment of ∇c with e_α and e_γ is determined by relative strengths of strain rate induced by flame normal acceleration a_{chem} and turbulent straining a_{turb}. It has been demonstrated earlier that ∇c preferentially aligns with e_α when a_{chem} dominates over a_{turb}, but tends to aligns with e_γ when a_{turb} dominates over a_{chem}. The strain rate induced by flame normal acceleration due to chemical heat release can be scaled as:

$$a_{chem} \sim \tau\, f(Ka) \frac{S_L}{\delta_{th}} \tag{7.5}$$

where $f(Ka)$ is expected to decrease with increasing (Chakraborty and Swaminathan, 2013). Following Meneveau and Poinsot (1991) a_{turb} can be scaled as:

$$a_{turb} \sim \frac{u'}{l} \tag{7.6}$$

which gives rise to:

$$\frac{a_{chem}}{a_{turb}} \sim \tau\, f(Ka) \frac{S_L l}{u' \delta_{th}} \sim \tau\, f(Ka) Da \sim \tau\, f\left(\frac{\mathrm{Re}_t^{1/2}}{Da} \right) Da \tag{7.7}$$

Alternatively, turbulent straining can be scaled as (Tennekes and Lumley, 1972):

$$a_{turb} \sim \frac{u'}{\lambda} \tag{7.8}$$

where λ is the Taylor micro-scale, which yields

$$\frac{a_{chem}}{a_{turb}} \sim \tau\, f(Ka) \frac{S_L \lambda}{u' \delta_{th}} \sim \tau\, f(Ka) \frac{Da}{\mathrm{Re}_t^{1/2}} \sim \tau\, f\left(\frac{\mathrm{Re}_t^{1/2}}{Da} \right) \frac{Da}{\mathrm{Re}_t^{1/2}} \sim \tau \frac{f(Ka)}{Ka} \tag{7.9}$$

The above scaling relations suggest that a_{chem} strengthens with respect to a_{turb} with increasing Da for a given value of Re_t. Previous analyses (Chakraborty and

Swaminathan, 2007, 2007a; Chakraborty *et al*., 2008, 2009) demonstrated that ∇c predominantly aligns with e_α for $Da >> 1$ flames, whereas ∇c aligns with e_γ in $Da < 1$ flames for comparable value of Re_t. Both eqs. (7.7) and (7.9) indicate that an increase in $Ka \sim \mathrm{Re}_t^{1/2} / Da$ for a given value of Da (e.g. cases F, H and J) gives rise to weakening of a_{chem} in comparison to a_{turb}. This increases the extent of ∇c alignment with e_γ with increasing Ka when Da is held constant as in cases F, H and J. In cases F and H ∇c predominantly aligns with e_α however the extent of this alignment decreases from F to H. This predominant alignment of ∇c with e_α in cases F and H leads to a negative contribution of T_{2I} in these cases. In case J, ∇c predominantly aligns with e_γ in the unburned and fully burned gases but a_{chem} overcomes a_{turb} in the regions of intense heat release close to the middle of the flame and as a result ∇c aligns with e_α in the reaction zone. Thus the mean value of T_{2I} in case J assumes positive values towards both the unburned and burned gas sides, whereas the mean contribution of T_{2I} remains negative close to the middle of the flame. The relation $a_{chem} / a_{turb} \sim \tau\, f(Ka) Da / \mathrm{Re}_t^{1/2}$ indicates that a_{chem} weakens in comparison to a_{turb} with decreasing $\tau Da / \mathrm{Re}_t^{1/2}$. The quantity $\tau Da / \mathrm{Re}_t^{1/2}$ assumes values equal to 0.96, 0.55 and 0.49 for cases G, H and I respectively when the statistics were extracted. This leads to larger extent of ∇c aligning with e_γ in case I (case H) than in case H (case G). This leads to predominantly negative contribution of T_{2I} in cases G and H, whereas T_{2I} assumes positive values towards the unburned and burned gas sides of the flame in case I. However, a_{chem} overcomes a_{turb} in the regions of intense heat release at the middle of the flame and ∇c starts to align with e_α in the reaction zone giving rise to negative values of T_{2I} in case I.

The contribution of T_{3I} remains positive (negative) towards the unburned (burned) gas side of the flame with the transition from positive to negative value taking place close to $c \approx 0.85$. In order to explain this behaviour T_{3I} can be rewritten as:

$$T_{3I} = -2Dn_i \frac{\partial \dot{w}}{\partial x_i} |\nabla c| = -2D \frac{\partial \dot{w}}{\partial n} |\nabla c| \tag{7.10}$$

where n is the spatial coordinate in the local flame normal direction and the flame normal vector $\vec{n}$ points towards the unburned gas side of the flame. For single step chemistry considered here the maximum $\dot{w}$ occurs close to $c \approx 0.85$ (Chakraborty and Cant, 2004; Chakraborty et al., 2008d). This suggests that the probability of finding negative values of $\partial \dot{w}/\partial n$ is significant for $c < 0.85$, which gives rise to positive value of T_{3I} towards the unburned gas side of the flame. For $c > 0.85$, it is of high probability to find $\partial \dot{w}/\partial n > 0$ resulting in negative value of T_{3I} towards the burned gas side of the flame.

Figure 7.2 shows that $F(D)$ is weakly negative towards the unburned gas side before becoming positive towards the burned gas side in all the cases. The magnitude of the mean contribution of $F(D)$ remains comparable to that of T_{1I} in all cases indicating that $F(D)$ cannot be neglected even for flames where ρD is considered to be constant. As for globally adiabatic $Le = 1.0$ flames as cases F-J:

$$\rho = \frac{\rho_0}{1+\tau c} \tag{7.11}$$

such that $\rho N_c \left(\frac{\partial D}{\partial t} + u_i \frac{\partial D}{\partial x_i} \right)$ can be expressed as:

$$\rho N_c \left(\frac{\partial D}{\partial t} + u_j \frac{\partial D}{\partial x_j} \right) = \rho D N_c \left(\frac{\partial u_j}{\partial x_j} \right) = \frac{T_{1I}}{2} \tag{7.12}$$

and the first two terms on the right hand side of eq. (7.2) vanish for constant values of ρD. The contributions of $(T_{D3} + T_{D4})$ are responsible for the change in sign of $F(D)$ in cases F-J.

7.1.1 Local behaviours of N_c and its strain rate and curvature dependence

The marginal probability density functions (pdfs) of normalised N_c^+ (i.e. $N_c \times \delta_{th} / S_L$) for different c isosurfaces across the flame are shown in Fig. 7.3 in log-log scale for case H. The pdfs of N_c in cases F, G, I and J are qualitatively similar to those in cases H and thus are not explicitly shown here. The pdfs for $c < 0.5$ are not shown in Fig. 7.3, as N_c assumes small values in the preheat zone of the flame due to small magnitude of scalar gradient ∇c. It is evident from Fig. 7.3 that the probability of finding high values of N_c

is most prevalent in the middle of the flame with slight skewness towards the burned gas side (i.e. $c \approx 0.7$) and the probability of finding high values of N_c decreases on both unburned and burned gas sides of the flame front. This is consistent with the observed behaviour of the mean values of N_c conditional on c shown in Fig. 7.1. It can be seen in Fig. 7.3 that a log-normal distribution captures the qualitative behaviour of the pdf of N_c although there are some disagreement in the pdf tails. This is consistent with several previous experimental (Sreenivasan and Antonia, 1997; Antonia and Sreenivasan, 1977; Mi *et al*., 1995; Su and Clemens, 2003; Karpetis and Barlow, 2002; Geyer *et al*., 2005; Markides and Mastorakos, 2006) and numerical (Jones and Musonge, 1988; Yeung *et al*., 1990; Hawkes *et al*., 2007) studies investigating the scalar dissipation rate pdf of a passive scalar. An approximate log-normal distribution of SDR in turbulent premixed flames has also been reported in a previous analysis (Swaminathan and Bilger, 2001).

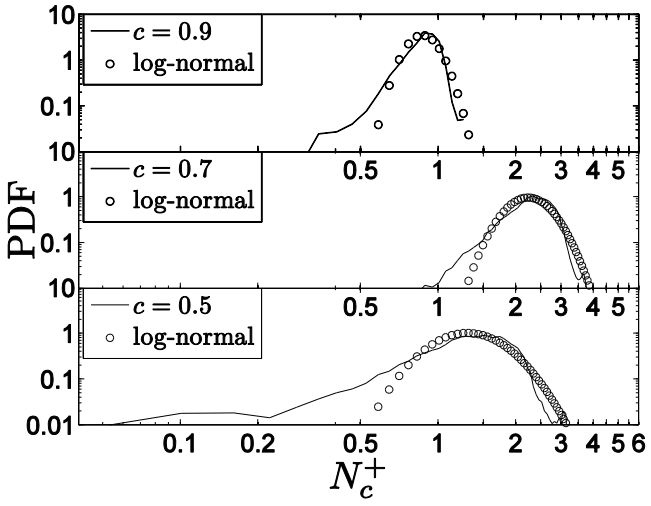

Figure 7.3: The marginal pdf of normalised N_c^+ (i.e. $N_c \times \delta_{th} / S_L$) and the log-normal distribution in log-log scale for $c = 0.5$, 0.7 and 0.9 across the flame for cases H.

The joint pdfs of N_c and tangential strain rate a_T for cases F anf J are shown in Fig. 7.4a respectively for $c = 0.8$ isosurface, which is close to the most reactive region for the present thermo-chemistry. It can be seen from Fig. 7.4a that N_c and a_T are positively correlated on $c = 0.8$ isosurface for cases F and J and similar qualitative behaviour has been observed also for other C isosurfaces in all cases considered here. This positive correlation between N_c and a_T can be explained in the following manner.

- The dilatation rate $\nabla.\vec{u}$ can be devided into tangential component and normal component as:

$$\nabla.\vec{u} = a_T + a_n \text{ where } a_n = n_i n_j \frac{\partial u_i}{\partial x_j} \text{ is the normal strain rate.} \quad (7.13)$$

For unity Lewis number flames $\nabla.\vec{u}$ can be scaled as:

$$\nabla.\vec{u} \sim a_{chem} \sim \tau\, f(Ka) \frac{S_L}{\delta_{th}} \quad (7.14)$$

whereas a_T can be taken to scale with turbulent strain rate as:

$$a_T \sim a_{turb} \sim \frac{u'}{l}, \text{ with integral length scale (Meneveau and Poinsot, 1991) or} \quad (7.15)$$

$$a_T \sim a_{turb} \sim \frac{u'}{\lambda}, \text{ with Taylor's length scale (Tennekes and Lumley, 1972)} \quad (7.16)$$

- Above scalings indicate that $\frac{\nabla.\vec{u}}{a_T}$ scales as:

$$\frac{\nabla.\vec{u}}{a_T} \sim \tau\, f\left(\frac{\mathrm{Re}_t^{1/2}}{Da}\right) Da \text{ or} \quad (7.17)$$

$$\frac{\nabla.\vec{u}}{a_T} \sim \tau\, f\left(\frac{\mathrm{Re}_t^{1/2}}{Da}\right) \frac{Da}{\mathrm{Re}_t^{1/2}} \sim \tau \frac{f(Ka)}{Ka} \quad (7.18)$$

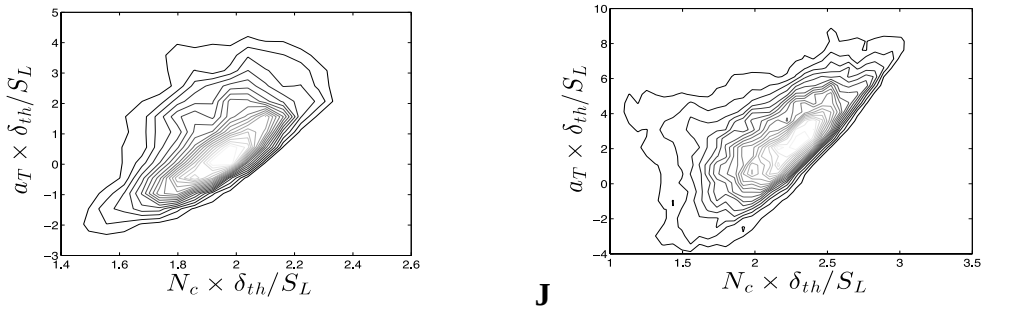

(a)

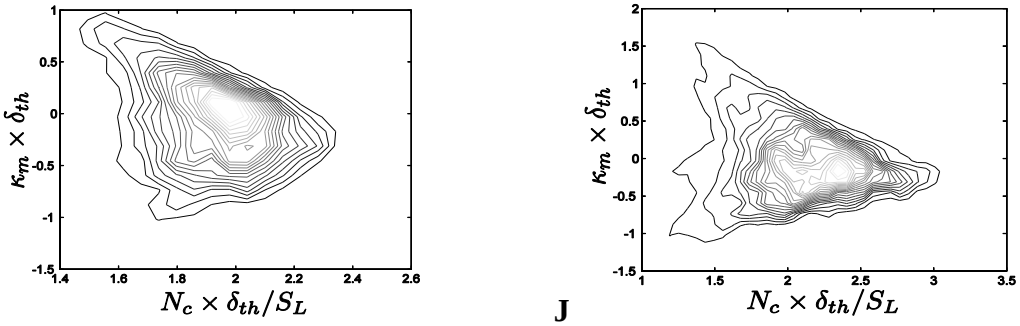

(b)

Figure 7.4: (a) Joint pdfs between $N_c \times \delta_{th} / S_L$ and normalised tangential strain rate $a_T \times \delta_{th} / S_L$ on $c = 0.8$ isosurface for cases F and J. (b) Joint pdf between $N_c \times \delta_{th} / S_L$ and normalised curvature $\kappa_m \times \delta_{th}$ on $c = 0.8$ isosurface for cases F and J.

Both eqs. (7.17) and (7.18) suggest that the magnitude of a_T is likely to supersede the magnitude of $\nabla.\vec{u}$ in most locations within the flame for small values of Da and high values of Ka.

- It has been shown in several previous analyses (Chakraborty and Cant, 2004; Chakraborty *et al.*, 2009) that both $\nabla.\vec{u}$ and a_T assume predominantly positive values and thus a higher magnitude of a_T than $\nabla.\vec{u}$ induces a negative (i.e. compressive) normal strain rate a_n. Thus an increase in a_T often leads to a decrease in $a_n = \nabla.\vec{u} - a_T$ for small (high) values of Da (Ka). Thus, the isoscalar lines come close to each other under the action of decreasing a_n, which leads to increase in the magnitude of scalar gradient ∇c. This is reflected in the positive correlation between N_c and a_T.

The joint pdfs between N_c and curvature κ_m for cases F and J are shown in Fig. 7.4b respectively for $c = 0.8$ isosurface. Cases G, H and I are not explicitly shown here due to their similarity to cases F and J. It can be seen from Fig. 7.4b that the joint pdf between N_c and κ_m exhibits both positive and negative correlating branches on $c = 0.8$ isosurface for cases J, and as a result of this, the net correlation between N_c and κ_m remains weak. The positive correlation branch between N_c and κ_m remains weak for small values of u'/S_L (see Fig. 7.4b for case F). Similar behaviour is observed for other c isosurfaces in all cases considered here and the correlation between N_c and κ_m is weak throughout the flame for high values of u'/S_L (e.g. case J). The observed behaviour can be explained based on the following physical mechanisms:

- It has been shown earlier that both a_T and $\nabla.\vec{u}$ are negatively correlated with κ_m for the flames considered here (Chakraborty *et al.*, 2011) and thus the behaviour of a_n at locations with large positive curvature are principally determined by a_T since $\nabla.\vec{u}$ is small in these zones due to defocusing of heat. Small values of a_T are associated with high values of κ_m at these locations, which lead to small values of N_c at high values of positive κ_m due to positive correlation between N_c and a_T. This leads to a negative correlating branch between N_c and κ_m at the positively curved zones.

- The dilatation rate $\nabla.\vec{u}$ is large in the negatively curved locations due to strong focussing of heat and the magnitude of $\nabla.\vec{u}$ can locally be high enough to supersede the magnitude of a_T, which leads to a positive value of a_n. This tendency strengthens with decreasing κ_m especially in the zones with large negative curvature, which gives rise to an increase in a_n with decreasing curvature. As the distance between the isoscalar lines increases with increasing a_n, the magnitude of scalar gradient ∇c decreases with decreasing κ_m in the negatively curved zones. This leads to the positive correlating branch in the joint pdf of N_c and κ_m (see Figs. 7.4b for case J).
- The relative strengths of the positive and negative correlating branches ultimately determine the net correlation between N_c and κ_m in the high u'/S_L cases. The probability of finding high negative curvature remains small for small values of u'/S_L and as a result the probability of finding high values of $\nabla.\vec{u}$, which locally overcomes a_T, to induce a positive value of a_n, becomes rare (e.g. case F). Thus the combination of positive correlations between N_c and a_T, and negative correlations between a_T and κ_m leads to a predominantly negative correlating branch between N_c and κ_m in the low u'/S_L cases (e.g. case F, see Fig. 7.4b).

The strain rate and curvature dependences of N_c discussed above, in turn affect the local statistical behaviours of T_{1I}, T_{2I}, T_{3I}, $(-D_{2I})$ and $F(D)$ in response to a_T and κ_m. The curvature and strain rate dependences of T_{1I}, T_{2I}, T_{3I}, $(-D_{2I})$ and $F(D)$ are discussed next.

7.1.2 Local Behaviours of T_{1I} and its strain rate and curvature dependence

The marginal pdfs of T_{1I} for different c isosurfaces across the flame are shown in Fig. 7.5a for case H. The pdfs of T_{1I} in cases F, G, I and J are qualitatively similar to those in case H, and thus are not explicitly shown here. It is evident from Figs. 7.5a that the pdfs of T_{1I} suggest $T_{1I} = 2(\nabla.\vec{u})N_c$ assumes predominantly positive values throughout the flame. As dilatation rate $\nabla.\vec{u}$ is principally positive due to thermal expansion in premixed flames (Chakraborty and Cant, 2004; Chakraborty *et al.*, 2009), the contribution of $T_{1I} = 2(\nabla.\vec{u})N_c$ is predominantly positive throughout the flame. Moreover, Fig. 7.5a

demonstrates that the probability of finding high values of T_{1I} is most prevalent in the middle of the flame with slight skewness towards the burned gas side (i.e. $c \approx 0.7$) and the probability of finding high values of T_{1I} decreases on both unburned and burned gas sides of the flame. This is consistent with the observed behaviour of the mean values of N_c conditional on c shown in Fig. 7.2. The probability of finding large magnitudes of $\nabla.\vec{u}$ is the highest at a location which is slightly skewed towards the burned gas side of the flame (Chakraborty *et al.*, 2009). As the distributions of N_c and $\nabla.\vec{u}$ are slightly skewed towards the burned gas side of the flame, the probability of finding large values of $T_{1I} = 2(\nabla.\vec{u})N_c$ becomes high around $c \approx 0.7$.

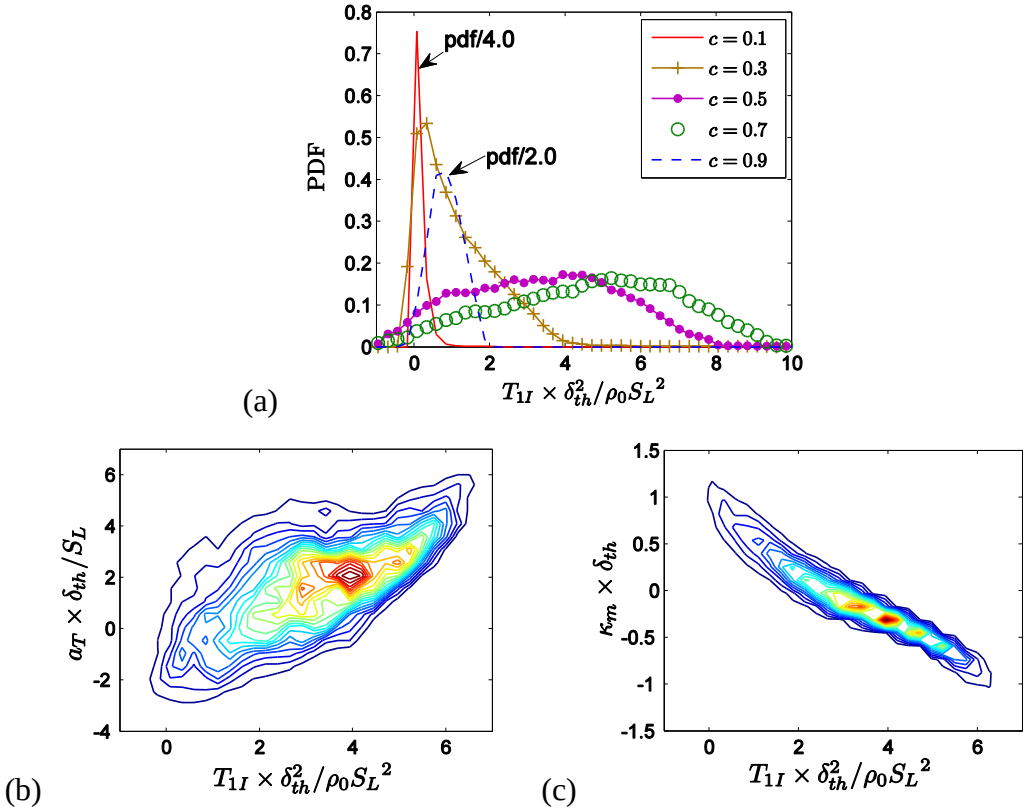

Figure 7.5: (a) The marginal pdfs of $T_{1I} \times \delta_{th}^2 / \rho_0 S_L^2$ for $c = 0.1$, 0.3, 0.5, 0.7 and 0.9 for case H. (b) Joint pdf between $T_{1I} \times \delta_{th}^2 / \rho_0 S_L^2$ and normalised tangential strain rate $a_T \times \delta_{th} / S_L$ on $c = 0.8$ isosurface for case H. (c) Joint pdf between $T_{1I} \times \delta_{th}^2 / \rho_0 S_L^2$ and normalised curvature $\kappa_m \times \delta_{th}$ on $c = 0.8$ isosurface for case H.

The joint pdf between T_{1I} and a_T for case H is shown in Fig. 7.5b for $c = 0.8$ isosurface. It can be seen from Fig. 7.5b that T_{1I} and a_T are positively correlated on $c = 0.8$ isosurface for case H and similar qualitative behaviours have been observed for other C

isosurfaces in all cases considered here. Both $\nabla.\vec{u}$ and a_T are positively correlated for all flames considered here, which along with positive correlation between N_c and a_T (see Fig. 7.4) gives rise to a positive correlation between $T_{1I} = 2(\nabla.\vec{u})N_c$ and a_T.

The joint pdf between T_{1I} and κ_m for case H is shown in Fig. 7.5c for $c = 0.8$ isosurface. It can be seen from Fig. 7.5c that the joint pdf between T_{1I} and κ_m exhibits negative correlation on $c = 0.8$ isosurface for case H and similar qualitative behaviour has been observed for other c isosurfaces in all cases considered here. In all cases the net correlation between N_c and κ_m is weak (see Fig. 7.4) but $\nabla.\vec{u}$ assumes high (small) values at negatively curved locations because of focussing of heat, whereas at convex location $\nabla.\vec{u}$ tends to small values due to heat defocusing. This leads to a predominantly negative correlation between $\nabla.\vec{u}$ and κ_m (Chakraborty et al., 2011). The negative correlation between $\nabla.\vec{u}$ and κ_m is principally responsible for the negative correlation between $T_{1I} = 2(\nabla.\vec{u})N_c$ and κ_m.

7.1.3 Local Behaviours of T_2 and its strain rate and curvature dependence

The marginal pdfs of T_{2I} for different C isosurfaces across the flame are shown in Fig. 7.6a for case H. The pdfs of T_{2I} in cases F, G, I and J are qualitatively similar to those in case H and thus are not explicitly shown here. Figure 7.6a shows that the probability of finding negative values of T_{2I} supersedes the probability of finding positive values. The probability of finding negative values of T_{2I} increases as the heat releasing zone (see the pdfs for $c = 0.7$ isosurface) is approached. It has been discussed earlier that the effects of a_{chem} overcome the effects of a_{turb} in the heat releasing zone to result in a preferential alignment of ∇c with e_α even for small values of Da. This preferential alignment of ∇c with e_α in these zones gives rise to negative values of T_{2I} according to eq. (7.4). The extent of ∇c alignment with e_α (e_γ) decreases (increases) towards both unburned and burned gas sides of the flame due to diminishing effects of a_{chem}.

The contours of joint pdfs between T_{2I} and a_T for $c = 0.8$ are shown Fig. 7.6b for case H and the correlation coefficients between T_{2I} and a_T for different c isosurfaces across

the flame for all cases F-J are shown in Table 7.1. It is evident from Figs. 7.6b and Table 2 that T_{2I} and a_T are positively correlated for high u'/S_L cases (e.g. cases H-J) although the strength of the correlation changes through the flame. However, T_{2I} and a_T are weakly correlated with each other within the flame where the effects of heat release are significant for the cases with small and moderate values of u'/S_L (see Table 7.1). In order to explain this behaviour it is useful to rewrite T_{2I} in the following manner:

$$T_{2I} = -2\rho a_n N_c \tag{7.19}$$

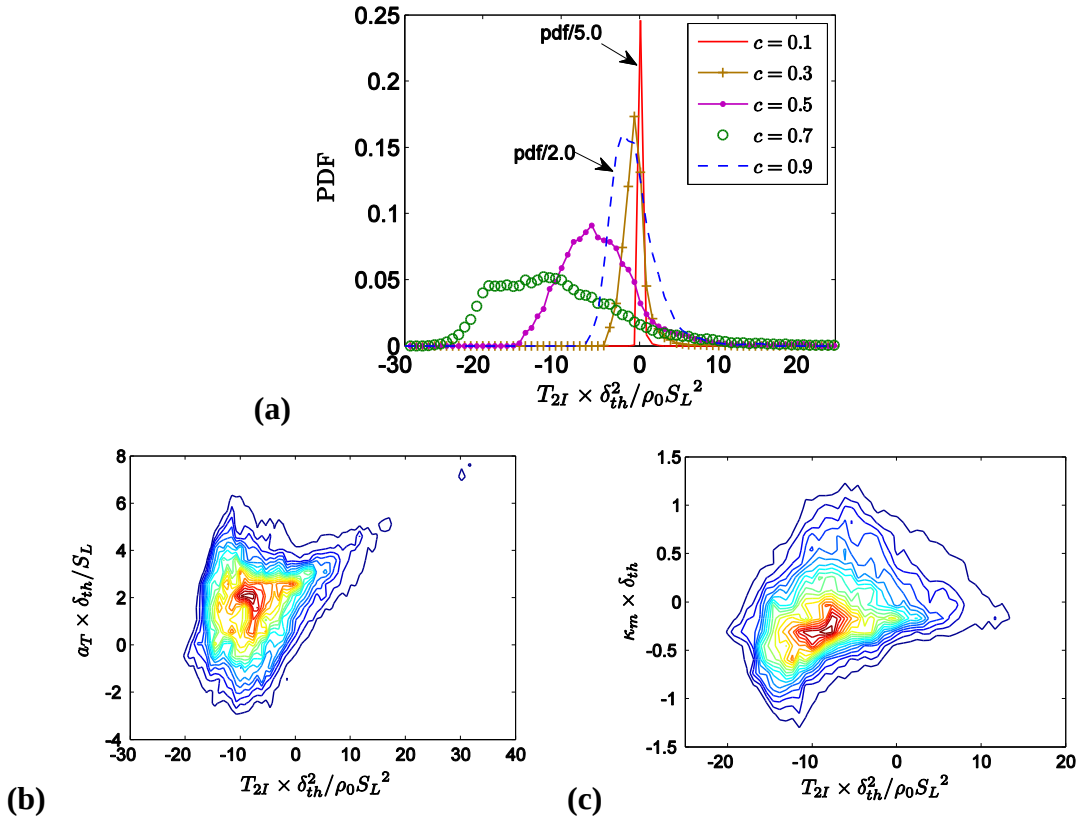

Fig. 7.6: (a) The marginal pdfs of $T_{2I} \times \delta_{th}^2 / \rho_0 S_L^2$ for $c = 0.1$, 0.3, 0.5, 0.7 and 0.9 for case H. (b) Joint pdf between $T_{2I} \times \delta_{th}^2 / \rho_0 S_L^2$ and normalised tangential strain rate $a_T \times \delta_{th} / S_L$ on $c = 0.8$ isosurface for case H. (c) Joint pdf between $T_{2I} \times \delta_{th}^2 / \rho_0 S_L^2$ and normalised curvature $\kappa_m \times \delta_{th}$ on $c = 0.8$ isosurface for cases H.

Based on eq. (7.19) the strain rate dependences of T_{2I} can be explained in the following manner:

- It has already been demonstrated that N_c and a_T are positively correlated with each other (see Fig. 7.4). The quantity $(-a_n) = a_T - \nabla.\vec{u}$ tends to increase with

increasing a_T in the regions where the effects of $\nabla.\vec{u}$ are weak. This along with positive correlation between N_c and a_T leads to a positive correlation between T_{2I} and a_T for both unburned and burned gas sides of the flame for all cases.

- The magnitudes of $\nabla.\vec{u}$ and a_T increase with decreasing κ_m, and thus $(-a_n) = a_T - \nabla.\vec{u}$ might not increase (even decrease) with increasing a_T in the heat releasing zone of the flame where the effects of $\nabla.\vec{u}$ are strong. The a_T dependences of $(-a_n)$ and N_c ultimately determine the nature of the correlation between T_{2I} and a_T. The strain rate and curvature dependences of $\nabla.\vec{u}$ weaken with increasing u'/S_L (Hartung et al., 2008) so $(-a_n) = a_T - \nabla.\vec{u}$ increases with increasing a_T, which leads to a positive correlation between T_{2I} and a_T for the major portion of the flame for cases with high values of u'/S_L (see Table 7.2).

Case	$T_{2I} - a_T$					$T_{2I} - \kappa_m$				
	c =0.1	c = 0.3	c = 0.5	c =0.7	c =0.9	c =0.1	c = 0.3	c = 0.5	c =0.7	c =0.9
F	0.642	-0.098	-0.217	-0.092	0.685	0.141	0.509	0.720	0.614	-0.250
G	0.673	-0.090	-0.208	-0.084	0.676	0.116	0.506	0.719	0.616	-0.227
H	0.751	0.376	0.263	0.263	0.648	0.544	0.252	0.412	0.423	-0.065
I	0.802	0.593	0.616	0.689	0.827	0.052	0.196	0.235	0.198	-0.027
J	0.783	0.662	0.614	0.616	0.787	0.028	0.137	0.223	0.242	-0.014

Table 7.1: Correlation coefficients between T_{2I} and a_T, and between T_{2I} and κ_m on C=0.1, 0.3, 0.5, 0.7 and 0.9 isosurfaces.

The joint pdf between T_{2I} and κ_m for case H is shown in Figure 7.6c respectively for $c = 0.8$ isosurface and the correlation coefficients between T_{2I} and κ_m for different C isosurfaces across the flame are shown in Table 7.1 for all cases considered here. It is evident from Fig. 7.6c and Table 7.1 that T_{2I} and κ_m remain weakly positively correlated except the burned gas side of the flame. The observed curvature dependence of T_{2I} could be explained based on following physical mechanisms:

- The effects of dilatation rate $\nabla.\vec{u}$ and thermal expansion are particularly strong in the negatively curved regions due to focussing of heat. By the same token, the effects of

heat release are weak in the positively curved zones due to defocusing of heat. Thus the effects of a_{chem} are more likely to dominate over the effects of a_{turb} in the negatively curved zones and thus increases the extent of ∇c alignment with e_α as demonstrated earlier by Hartung *et al.* (2008). Weakening of the heat release effects at positively curved zones due to defocusing of heat leads to a greater (lesser) extent of ∇c alignment with e_γ (e_α) in the positively curved zones. The extent of ∇c alignment with e_α increases in the negatively curved zones, which in turn makes T_{2I} increasingly negative (see eq. (7.4)) and the magnitude of the negative contribution of T_{2I} decreases for positive curvature locations. This gives rise to a positive correlation between T_{2I} and κ_m, as observed from Figs. 7.6c and Table 7.1.

- However, the effects of a_{turb} are more likely to dominate over the effects of a_{chem} towards the burned gas side and thus the extent of ∇c alignment with e_γ is determined by local turbulent flow conditions. The effects of flame-generated turbulence become stronger at the negatively curved zones due to stronger thermal expansion effects resulting from focussing of heat especially in the heat releasing zone. The straining induced by flame-generated turbulence may overcome relatively weak effects of $\nabla.\vec{u}$ towards the burned gas side, which can give rise to an increasing extent of ∇c alignment with e_γ increases in the negative curved zones. This in turn gives rise to an increase in T_{2I} (see eq. (7.4)) with decreasing κ_m towards the burned gas side and leads to a negative correlation between T_{2I} and κ_m (see Table 7.1).

7.1.4 Local Behaviours of T_{3I} and its strain rate and curvature dependence

The marginal pdfs of normalised T_{3I} for different c isosurfaces across the flame are shown in Fig. 7.7 for cases H. The pdfs of T_{3I} in cases F, G, I and J are qualitatively similar to those in case H and thus are not explicitly shown here. The pdfs for $c < 0.5$ are not shown in Fig. 7.7 because T_{3I} assumes negligible value in the preheat zone of the flame due to negligible magnitude of the reaction rate $\dot{w}$. It is evident that T_{3I} assumes positive values for the major portion of the flame and the probability of finding high positive values increases towards the most reactive zone (e.g. $c = 0.7$) of the flame front. However, T_{3I} assumes negative values only towards the burned gas side (e.g. $c = 0.9$) of the flame front. This is consistent with the behaviour of T_{3I} shown in Fig. 7.16. The

physical mechanism behind the transition from positive to negative values of the mean contribution of T_{3I} (see eq. (7.10)) is also responsible for obtaining negative (positive) values of T_{3I} towards the burned (unburned) gas side of the flame.

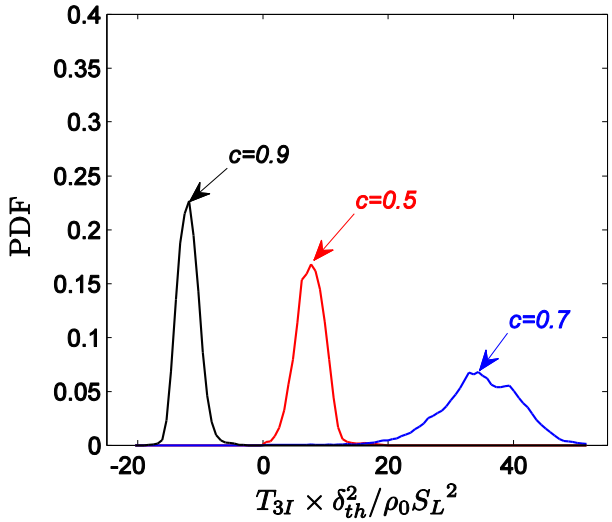

Fig. 7.7: The marginal pdfs of $T_{3I} \times \delta_{th}^2 / \rho_0 S_L^2$ for $c = 0.5$, 0.7 and 0.9 for case H.

The contours of joint pdfs between T_{3I} and a_T for $c = 0.5$, 0.7 and 0.9 isosurfaces are shown Figs. 7.8a-7.8c for case H and similar qualitative behaviour has been observed for other cases considered here. It is evident from Figs. 7.8a-7.8c that T_{3I} and a_T remain positively correlated for the part of the flame where finding positive values of T_{3I} is prevalent. On the other hand T_{3I} and a_T are negatively correlated with each other towards the burned gas side of the flame where T_{3I} is predominantly negative. The observed a_T dependence of T_{3I} can be explained in the following manner:

- It has been demonstrated earlier that N_c and a_T are positively correlated with each other which suggests that $|\nabla c| = |\partial c / \partial n|$ increases with increasing a_T. For low Mach number unity Lewis number flames $\dot{w}$ depends only on c and thus high values of $|\partial \dot{w} / \partial n|$ are associated with high values of $|\nabla c| = |\partial c / \partial n|$ and N_c.
- As N_c and a_T are positively correlated with each other, the magnitude of reaction rate contribution $|T_{3I}| = |2D(\partial \dot{w} / \partial n)|\nabla c||$ is positively correlated with tangential strain rate a_T. Thus T_{3I} is positively (negative) correlated with a_T where T_{3I} assumes positive (negative) values.

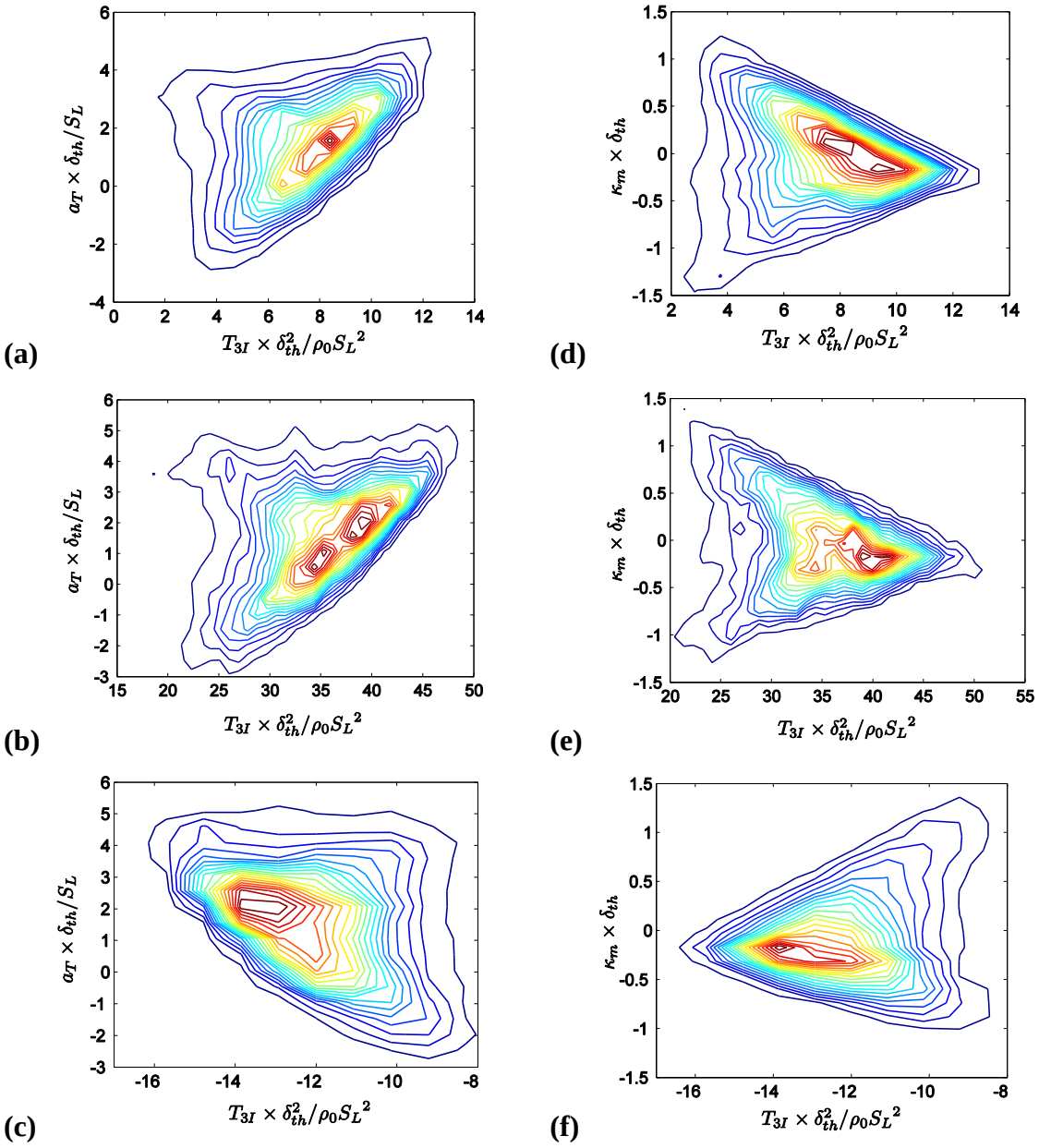

Fig. 7.8: Joint pdfs between $T_{3I} \times \delta_{th}^2 / \rho_0 S_L^2$ and normalised tangential strain rate $a_T \times \delta_{th} / S_L$ on (a) $c = 0.5$, (b) 0.7 and (c) 0.9 isosurfaces for case H . Joint pdfs between $T_{3I} \times \delta_{th}^2 / \rho_0 S_L^2$ and normalised curvature $\kappa_m \times \delta_{th}$ on the (d) $c = 0.5$, (e) 0.7 and (f) 0.9 isosurfaces for case H.

The joint pdfs between T_{3I} and κ_m for case H are shown in Figs. 7.8d-7.8f for $c = 0.5$, 0.7 and 0.9 isosurfaces and similar qualitative behaviour has been observed for other cases considered here. It is evident from Figs. 7.8d-7.8f that the joint pdf of T_{3I} and κ_m exhibit both positive and negative correlating branches and the net correlation is weak throughout the flame.

The physical explanations for the observed κ_m dependence of T_{3I} can be summarised in the following manner:

- The term $|T_{3I}| = |2D(\partial \dot{w}/\partial n)|\nabla c||$ is expected to be positively (negatively) correlated with curvature κ_m at negatively (positively) curved locations for high values of u'/S_L, as in the case of N_c (see case H in Fig. 7.4b), because high values of $|\partial \dot{w}/\partial n|$ are associated with high values of N_c and $|\nabla c| = |\partial c/\partial n|$.
- As a result of the aforementioned physical mechanisms the term T_{3I} and κ_m remain positively (negatively) correlated with curvature κ_m at negatively (positively) curved locations in the planar flames where T_{3I} assumes positive values. By contrast, the joint pdfs of T_{3I} and κ_m exhibit negative (positive) correlation with curvature κ_m at negatively (positively) curved locations within the flame where T_{3I} assumes negative values for the planar flames considered here (see Fig. 7.8f).

Case	$(-D_{2I})-a_T$					$(-D_{2I})-\kappa_m$				
	c =0.1	c = 0.3	c = 0.5	c =0.7	c =0.9	c =0.1	c = 0.3	c = 0.5	c =0.7	c =0.9
F	-0.598	-0.809	-0.368	-0.183	-0.522	0.280	0.577	0.582	-0.020	0.261
G	-0.581	-0.806	-0.389	-0.218	-0.488	0.272	0.554	0.600	0.023	0.225
H	-0.546	-0.699	-0.028	0.050	-0.296	0.283	0.422	0.364	-0.234	-0.001
I	-0.513	-0.652	0.221	-0.078	-0.483	0.231	0.338	-0.074	-0.412	-0.100
J	-0.472	-0.581	0.111	-0.031	-0.378	0.205	0.288	0.174	-0.317	-0.107
V1	-0.712	-0.695	-0.069	-0.616	-0.679	0.700	0.825	-0.176	0.619	0.766
V2	-0.628	-0.525	0.089	-0.445	-0.703	0.475	0.696	0.033	0.159	0.633
V3	-0.452	-0.355	0.130	-0.312	-0.697	0.289	0.481	0.049	-0.104	0.260

Table 7.2: Correlation coefficients between $(-D_{2I})$ and a_T, and between $(-D_{2I})$ and κ_m on $c = 0.1$, 0.3, 0.5, 0.7 and 0.9 isosurfaces.

7.1.5 Local Behaviours of ($-D_{2I}$) and its strain rate and curvature dependence

The marginal pdfs of $(-D_{2I})$ for c isosurfaces representative of leading edge, reaction zone and trailing edge of the flame (e.g. $c = 0.3$, 0.7 and 0.9 isosurfaces) are shown in Fig. 7.9 for case H. The pdfs of $(-D_{2I})$ in cases F, G, I and J are qualitatively similar to that in case H and thus are not explicitly shown here. Figure 7.9 shows that $(-D_{2I})$ assumes negative values throughout the flame and the probability of finding high magnitude of $(-D_{2I})$ increases from unburned gas side towards a region of the flame

which is severely skewed towards the burned gas side (e.g. c = 0.9 isosurface). This behaviour is found to be consistent with the mean behaviour of $(-D_{2I})$ shown in Fig. 7.2. The contours of joint pdfs between $(-D_{2I})$ and a_T for $c = 0.8$ isosurface are shown Fig. 7.9b for case H and the correlation coefficients between $(-D_{2I})$ and a_T for different c isosurfaces across the flame for all cases considered here are shown in Table 7.2. Figures 7.9b and Table 7.2 show that $(-D_{2I})$ and a_T are predominantly negatively correlated throughout the flame but the strength of this negative correlation weakens with increasing u'/S_L and the correlation becomes weakly positive at the middle of the flame for high values of u'/S_L (e.g. cases I and J). This behaviour can be explained in the following manner:

- The instantaneous SDR N_c and the molecular dissipation term $(-D_{2I})$ can be taken to scale as $N_c \sim D/\delta^2$ and $(-D_{2I}) \sim (-\rho D^2/\delta^4) \sim (-\rho N_c^2)$ (where δ is the typical local flame thickness) because in premixed flame the gradients of progress variable are only existent within the flame thickness. Alternatively, $(-D_{2I})$ can be considered to be governed by small-scale eddies and thus the characteristic length scale can be taken to be the Kolmogorov length scale η. However, $\delta/\eta \sim Ka^{1/2}$ remains of the order of unity for all cases considered here (see Table 4.1) and thus one obtains $(-D_{2I}) \sim (-\rho D^2/\delta^4) \sim (-\rho N_c^2)$ when dissipation processes are taken to be governed by η. Both scalings of $(-D_{2I})$ (i.e. $(-D_{2I}) \sim (-\rho D^2/\delta^4) \sim (-\rho N_c^2)$ and $(-D_{2I}) \sim (-\rho D^2/\eta^4) \sim (-\rho N_c^2)Ka^2$) suggest that high magnitudes of the dissipation term $|-D_{2I}|$ are associated with high values of a_T due to positive correlation between N_c and a_T (see Fig. 7.4a).

- As $(-D_{2I})$ assumes negative values, the quantities $(-D_{2I})$ and a_T is predominantly negatively correlated throughout the flame due to positive correlation between $|-D_2|$ and a_T. However, the negative correlation between $(-D_{2I})$ and a_T weakens with increasing u'/S_L due to weakening of positive correlation between N_c and a_T. Thus the correlation between $(-D_{2I})$ and a_T becomes weakly positive at the middle of the flame for high values of u'/S_L (e.g. cases I and J).

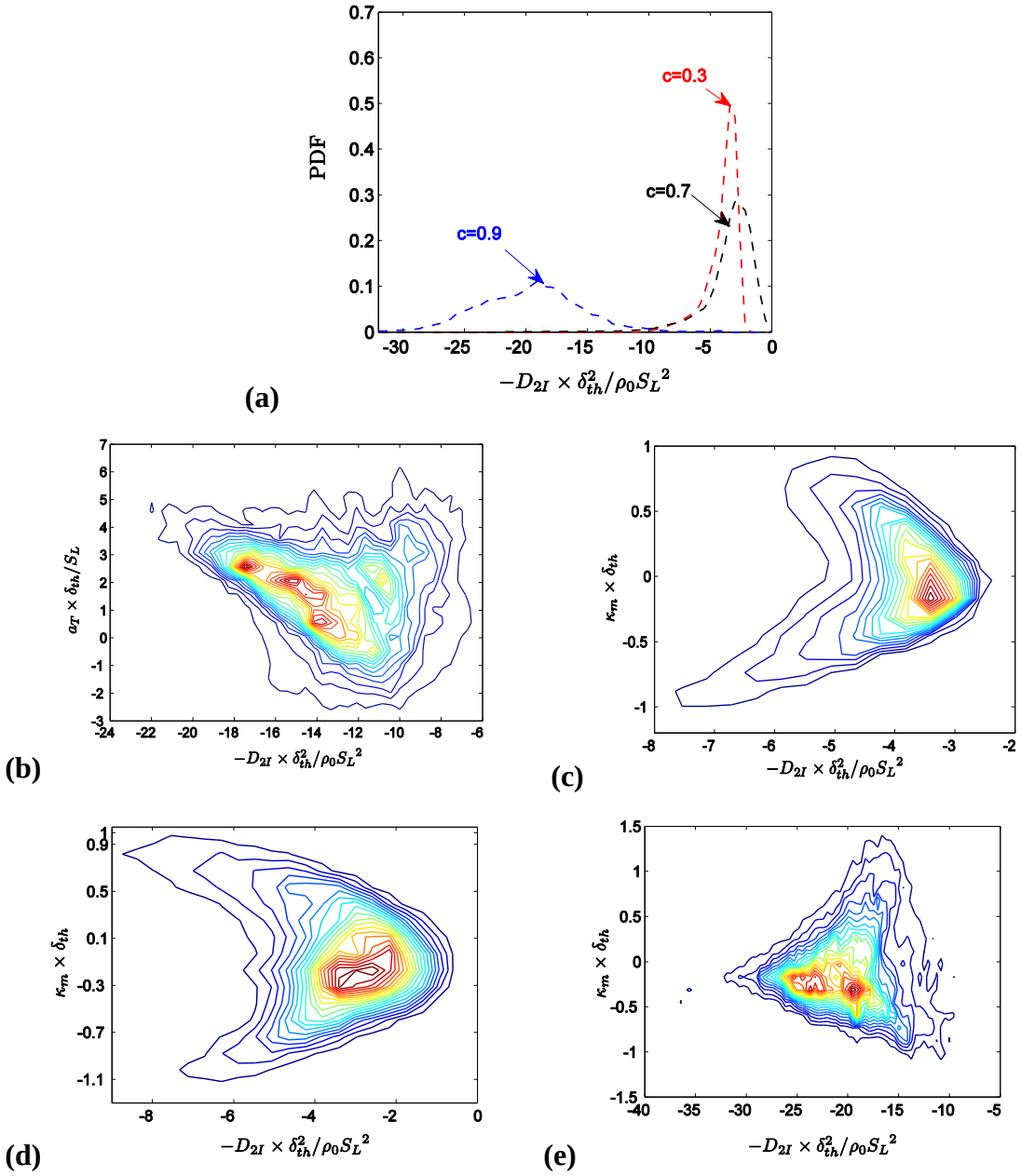

Fig. 7.9: (a) The marginal pdfs of $(-D_{2I}) \times \delta_{th}^2 / \rho_0 S_L^2$ for $c = 0.3$, 0.7 and 0.9 for case H. (b) Joint pdfs between $(-D_{2I}) \times \delta_{th}^2 / \rho_0 S_L^2$ and normalised tangential strain rate $a_T \times \delta_{th} / S_L$ on $c = 0.8$ isosurface for case H. Joint pdfs between $(-D_{2I}) \times \delta_{th}^2 / \rho_0 S_L^2$ and normalised curvature $\kappa_m \times \delta_{th}$ on (c) $c = 0.3$, (d) 0.7 and (e) 0.9 isosurfaces for case H.

The joint pdfs of $(-D_{2I})$ and curvature κ_m for case H are shown in Fig. 7.9 for $c = 0.3$, 0.7 and 0.9 isosurfaces and the correlation coefficients between $(-D_{2I})$ and κ_m for different c isosurfaces across the flame are shown in Table 7.2 for all cases considered here. The joint pdfs of $(-D_{2I})$ and κ_m in cases F,G, I and J are qualitatively similar to those in case H and thus are not shown here. It can be seen from Fig. 7.9 that the quantities

$(-D_{2I})$ and κ_m are non-linearly related to one another. The physical explanations behind the observed behaviour is provided below:

- The molecular dissipation term $(-D_{2I})$ can alternatively be expressed as:

$$(-D_{2I}) = -2\rho D^2 \left\{ \begin{array}{l} \left[\frac{\partial|\nabla c|}{\partial n}\right]^2 + 4\kappa_m|\nabla c|\frac{\partial|\nabla c|}{\partial n} + 4\kappa_m^2|\nabla c|^2 + 2\left[\frac{\partial^2 c}{\partial x_1\partial x_2}\frac{\partial^2 c}{\partial x_1\partial x_2} - \frac{\partial^2 c}{\partial x_1\partial x_1}\frac{\partial^2 c}{\partial x_2\partial x_2}\right] \\ +2\left[\frac{\partial^2 c}{\partial x_1\partial x_3}\frac{\partial^2 c}{\partial x_1\partial x_3} - \frac{\partial^2 c}{\partial x_1\partial x_1}\frac{\partial^2 c}{\partial x_3\partial x_3}\right] + 2\left[\frac{\partial^2 c}{\partial x_2\partial x_3}\frac{\partial^2 c}{\partial x_2\partial x_3} - \frac{\partial^2 c}{\partial x_2\partial x_2}\frac{\partial^2 c}{\partial x_3\partial x_3}\right] \end{array} \right\} \quad (7.20)$$

  The above expression clearly indicates that the third term on the right hand side of eq. 7.20 (i.e. $-8\rho D^2\kappa_m^2|\nabla c|^2$) induces non-linear curvature dependence of the molecular dissipation term $(-D_{2I})$.

- The quantity $\partial|\nabla c|/\partial n$ remains negative (positive) towards the unburned (burned) gas side of the flame (Chakraborty and Cant, 2004; Jerkins et al., 2006; Klein et al., 2006) thus the second term on the right hand side is positively (negatively) correlated with κ_m towards the unburned (burned) gas side of the flame. The first term on the right hand side of eq. 7.20 can be taken to scale as $-2\rho D^2(\partial|\nabla c|/\partial n)^2 \sim -2\rho N_c^2$. It has already been shown that the joint pdf of N_c and κ_m exhibit both positive and negative correlating branches for high values of u'/S_L (see case J in Fig. 7.4b) and thus the joint pdf of $-2\rho D^2(\partial|\nabla c|/\partial n)^2$ and κ_m is also expected to show branches with both positive and negative correlations in these cases. The weak negative correlation between N_c and κ_m for small values of u'/S_L (see case F in Fig. 7.4b) leads to weak positive correlation between $-2\rho D^2(\partial|\nabla c|/\partial n)^2 \sim -2\rho N_c^2$ and κ_m. The last three terms on the right hand side vanish in the limit of small scale isotropy and for the present cases they remain weakly correlated with curvature.

The relative strengths of the above mechanisms determine the net curvature dependence of $(-D_{2I})$. Thus positive and negative correlations between $(-D_{2I})$ and κ_m have been observed within the flame front in all cases considered here.

7.1.6 Local Behaviours of *f(D)* and its strain rate and curvature dependence

The marginal pdfs of $F(D)$ for $c = 0.1$, 0.3, 0.5, 0.7 and 0.9 isosurfaces across the flame front are shown in Fig. 7.10 for case H. The pdfs of $F(D)$ in cases F, G, I and J are qualitatively similar to those in case H and thus are not explicitly shown here. It is evident from Fig. 7.10a that $F(D)$ predominantly assumes negative (positive) values towards the unburned (burned) gas side of the flame (see Fig. 7.2). The density-weighted diffusivity ρD is considered to be constant in cases F-J and thus T_{D1} and T_{D2} are identically zero in these cases. The marginal pdfs of T_{D3} and T_{D4} for case H are shown in Figs. 7.10b and 7.10c, which show that both T_{D3} and T_{D4} predominantly assume positive (negative) values towards burned (unburned) gas side of the flame. As $T_{D5} = T_1 / 2$ in cases F-J, the pdfs of T_{D5} are qualitatively similar to those of T_1 and thus are not shown here. This indicates that T_{D5} shows predominant probability of finding positive values throughout the flame (see Fig. 7.5).

The contours of joint pdfs between $F(D)$ and a_T and between $F(D)$ and κ_m for $c = 0.1$, 0.5 and 0.7 isosurfaces are shown Fig. 7.11 for case H, and the correlation coefficients between $F(D)$ and a_T and $F(D)$ and κ_m for different $\boldsymbol{C}$ isosurfaces across the flame for case H are shown in Figs. 7.12a and 7.12b respectively. Both Figs. 7.11 and 7.12 indicate that $F(D)$ and a_T are negatively (positively) correlated with each other towards the unburned (burned) gas side of the flame brush (i.e. case H).

In order to explain the observed strain rate dependence of $F(D)$ the correlation coefficients between T_{D3}, T_{D4} and T_{D5} with a_T for $c = 0.1$, 0.3, 0.5, 0.7 and 0.9 isosurfaces are also shown Fig. 7.12 for case H. It is evident from Figs. 7.12a and 7.12b that both T_{D3} and T_{D4} remain negatively (positively) correlated with a_T towards the unburned (burned) gas side of the flame.

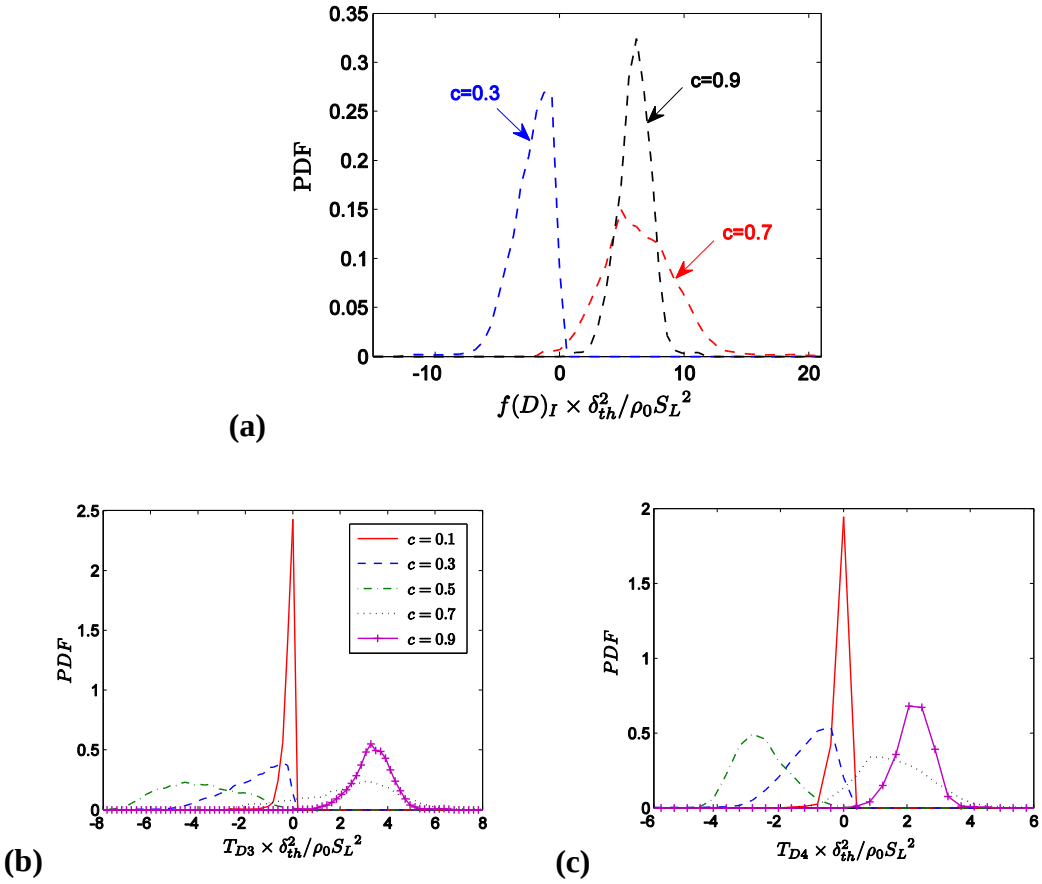

Fig. 7.10: (a) The marginal pdfs of $F(D)\times\delta_{th}^2/\rho_0 S_L^2$ for C=0.1, 0.3, 0.5, 0.7 and 0.9 for case H. The marginal pdfs of (b) $T_{D3}\times\delta_{th}^2/\rho_0 S_L^2$ and (c) $T_{D4}\times\delta_{th}^2/\rho_0 S_L^2$ for C=0.1, 0.3, 0.5, 0.7 and 0.9 across the flame for case H.

The strain rate dependences of T_{D3}, T_{D4} and T_{D5} can be explained in the following manner:

- The magnitudes of T_{D3} and T_{D4} can be taken to scale as: $|T_{D3}| \sim \rho D N_c/\delta^2 \sim \rho N_c^2$ and $|T_{D4}| \sim \rho D N_c/\delta^2 \sim \rho N_c^2$, which indicates that $|T_{D3}| \sim \rho N_c^2$ and $|T_{D4}| \sim \rho N_c^2$ remain positively correlated with a_T due to positive correlation between N_c and a_T (see Fig. 7.4). This suggests that the negative (positive) values of T_{D3} and T_{D4} (see Figs. 7.11 and 7.12) lead to negative (positive) correlations of these terms with a_T due to positive correlations between N_c and a_T (also due to positive correlation between $|T_{D3}| \sim \rho N_c^2$ ($|T_{D4}| \sim \rho N_c^2$) and a_T).

- The term T_{D5} remains positively correlated with a_T throughout the flame, which is consistent with the positive correlation between T_{1I} and a_T shown in Fig. 7.5, as $T_{D5} = 0.5T_{1I}$ in cases F-J considered here (see Fig. 7.12).

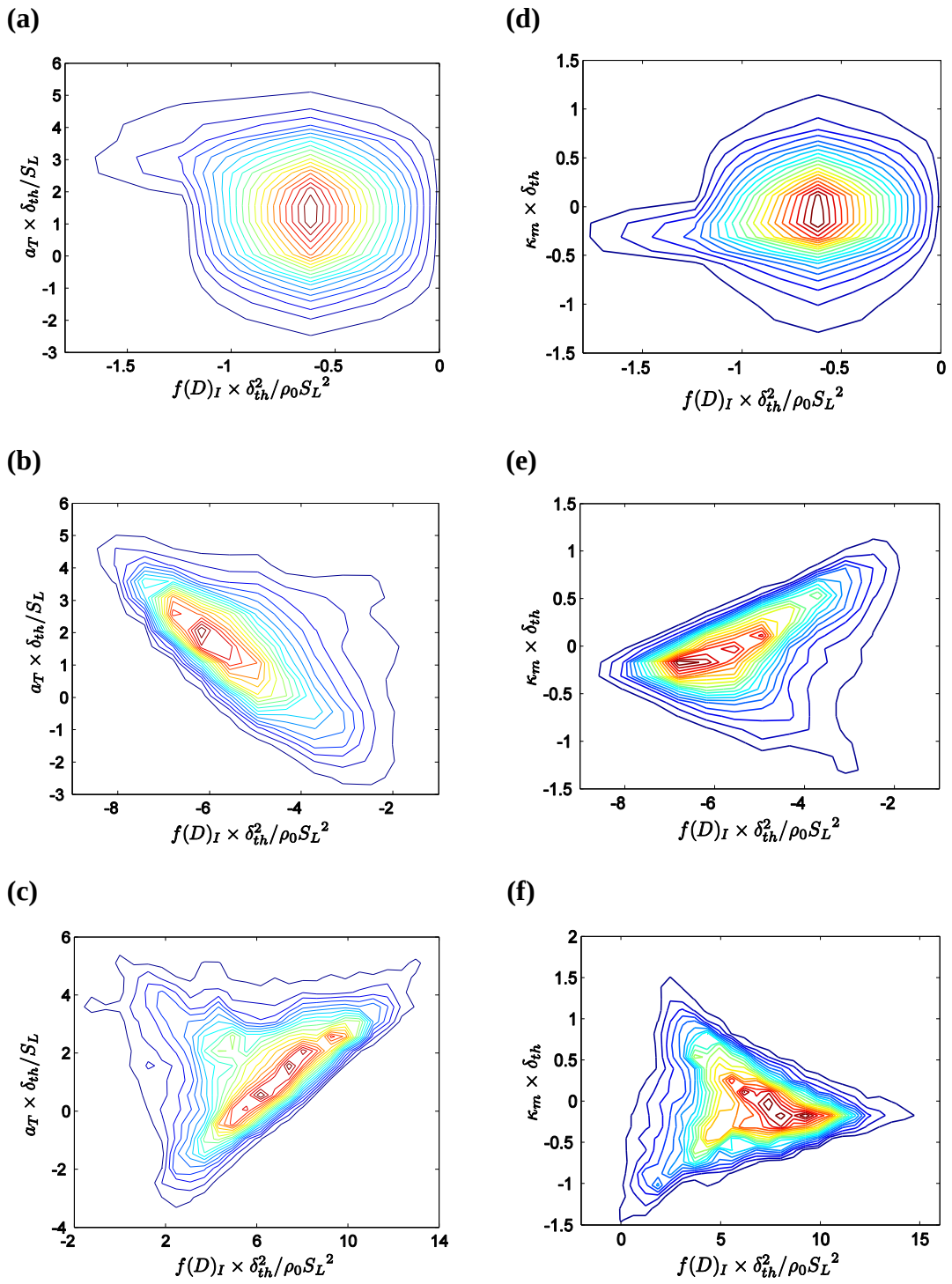

Figure 7.11: Joint pdfs between $F(D)\times\delta_{th}^2/\rho_0 S_L^2$ and normalised tangential strain rate $a_T\times\delta_{th}/S_L$ for case H on (a) c=0.1, (b) 0.5 and (c) 0.7 isosurfaces. Joint pdfs between $F(D)\times\delta_{th}^2/\rho_0 S_L^2$ and normalised curvature $\kappa_m\times\delta_{th}$ on (d) c = 0.1, (e) 0.5 and (f) 0.7 isosurfaces for case H.

- The terms T_{D3}, T_{D4} and T_{D5} remain positively correlated with a_T towards the burned gas side of the flame (see Fig. 7.12a) and these positive correlations result in a net positive correlation between $F(D)$ and a_T towards the burned gas side of the flame. On the other hand, T_{D3} and T_{D4} remain negatively correlated with a_T towards the unburned gas side of the flame (see Fig. 7.12a) and these correlations dominate over the positive correlation between T_{D5} and a_T to result in a net negative correlation between $F(D)$ and a_T towards the unburned gas side of the flame.

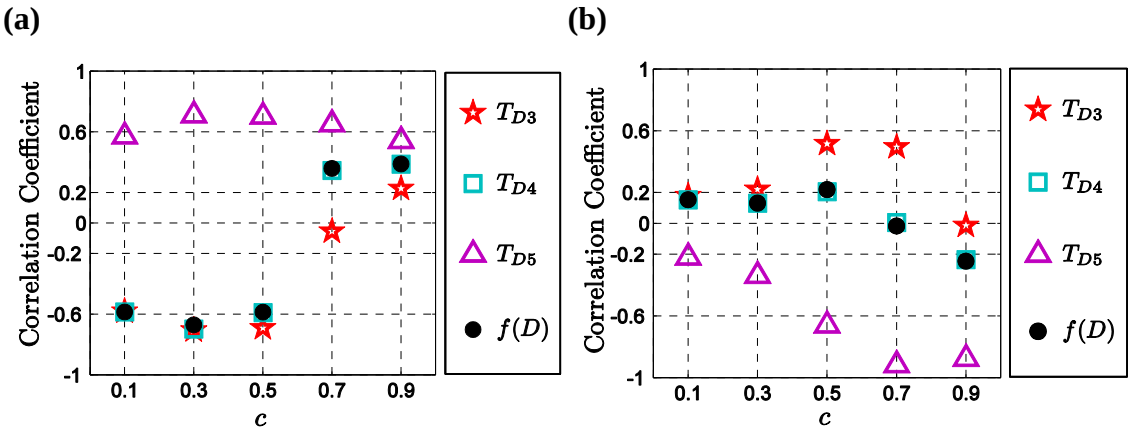

Figure 7.12: (a) Correlation coefficients for the $T_{D3}-a_T$, $T_{D4}-a_T$, $T_{D5}-a_T$ and $F(D)-a_T$ correlations on $c=0.1$, 0.3, 0.5, 0.7 and 0.9 isosurfaces for case H; (b) Correlation coefficients for the $T_{D3}-\kappa_m$, $T_{D4}-\kappa_m$, $T_{D5}-\kappa_m$ and $F(D)-\kappa_m$ correlations on $c=0.1$, 0.3, 0.5, 0.7 and 0.9 isosurfaces for case H.

The correlation coefficients between T_{D3}, T_{D4} and T_{D5} with κ_m for $c=0.1$, 0.3, 0.5, 0.7 and 0.9 isosurfaces are also shown Fig. 7.12b for case H. It is evident from Figs. 7.12b that $F(D)$ and κ_m is weakly correlated throughout the flame. The curvature κ_m dependences of T_{D3}, T_{D4}, T_{D5} and $F(D)$ can be explained in the following manner:

- Both T_{D3} and T_{D4} remain negatively (positively) correlated with a_T towards the unburned (burned) gas side of the flame (see Figs. 7.12a), whereas a_T and κ_m are negatively correlated throughout the flame. Thus, high (low) values of T_{D3} and T_{D4} are associated with high positive values of κ_m towards the unburned (burned) gas side

of the flame, which gives rise to positive (negative) correlations of T_{D3} and T_{D4} with κ_m towards the unburned (burned) gas side.

- As $T_{D5} = 0.5T_{1I}$ for cases F-J), a strong negative correlation between T_{D5} and κ_m has been observed near c = 0.7 isosurface, which is consistent with the negative correlation between T_{1I} and κ_m shown in Fig. 7.5.

7.1.7 Modelling significance

A modelled transport equation of $\widetilde{N}_c$ needs to be solved alongside other modelled conservation equations in LES simulations, when the generation of scalar gradients do not remain in equilibrium with its destruction. In order to solve the transport equation of $\widetilde{N}_c$, models are required for the sub-grid part of each unclosed terms in the $\widetilde{N}_c$ transport equation. It has been reported that the local strain rate and curvature dependence of N_c and the terms of its transport equation for V-flames are found to be qualitatively similar to the behaviour observed for the statistically planar flame case. As the SDR statistics are principally governed by the small-scale molecular processes, the local statistics of N_c and the terms of its transport equation are largely independent of the flow configuration. Thus, the models for $\widetilde{N}_c$ transport developed based on data extracted from canonical configurations might broadly be applicable to different geometries.

7.2 Statistical analysis of filtered SDR and its transport equation

As $\widetilde{N}_c$ approaches to N_c with decreasing filter width Δ (i.e. $\lim_{\Delta\to 0} \widetilde{N}_c = N_c$), the local resolved-scale strain rate and curvature dependences of $\widetilde{N}_c$ and the terms of its transport equation (i.e. $T_1, T_2, T_3, T_4, (-D_2)$ and $f(D)$ in eq. (3.58)) are likely to be qualitatively similar to the local strain rate and curvature dependences of N_c and the terms of its transport equation respectively. It worth noting that T_1 only exists in the filtered SDR transport equation such that the corresponding relations between the instantaneous terms and filtered terms are as:

$$\overline{T_{1I}} = T_2;\ \overline{T_{2I}} = T_3;\ \overline{T_{3I}} = T_4;\ \overline{(-D_{2I})} = (-D_2) \text{ and } \overline{F(D)} = f(D) \qquad (7.21)$$

However, the resolved scale curvature and strain rate dependences of the sub-grid SDR $(\tilde{N}_c - \tilde{D}\nabla\tilde{c}.\nabla\tilde{c})$ and the sub-grid componnents of the unclosed terms of its transport equation (i.e. $T_{2sg} = T_2 - T_{2R}$, $T_{3sg} = T_3 - T_{3R}$, $T_{4sg} = T_4 - T_{4R}$ and $f(D)_{sg} = f(D) - f(D)_R$) are expected to be smeared due to the convolution process of LES filtering, which is yet to be addressed here

For the purpose of convience, the transport equation of filtered SDR (eq. (3.58) is repeated below here following the numbering of this chapter:

$$\frac{\partial(\overline{\rho}\tilde{N}_c)}{\partial t} + \frac{\partial(\overline{\rho}\tilde{u}_j\tilde{N}_c)}{\partial x_j} = \underbrace{\overline{\frac{\partial}{\partial x_j}\left(\rho D\frac{\partial N_c}{\partial x_j}\right)}}_{D_1} + T_1 + T_2 + T_3 + T_4 - D_2 + f(D) \tag{7.22}$$

where the terms on the left hand side denote the transient effects and the resolved advection of $\tilde{N}_c$ respectively. The term D_1 represents the molecular diffusion of $\tilde{N}_c$ and the other terms $T_1, T_2, T_3, T_4, (-D_2)$ and $f(D)$ are all unclosed and given by:

$$T_1 = -\frac{\partial}{\partial x_j}\left(\overline{\rho u_j N_c} - \overline{\rho}\tilde{u}_j\tilde{N}_c\right) \tag{7.23}$$

$$T_2 = \overline{-2\frac{D}{\rho}\left[\dot{w} + \frac{\partial}{\partial x_i}\left(\rho D\frac{\partial c}{\partial x_i}\right)\right]\frac{\partial c}{\partial x_j}\frac{\partial \rho}{\partial x_j}} \tag{7.24}$$

$$T_3 = \overline{-2\rho D\frac{\partial c}{\partial x_i}\frac{\partial u_i}{\partial x_j}\frac{\partial c}{\partial x_j}} \tag{7.25}$$

$$T_4 = \overline{2D\frac{\partial \dot{w}}{\partial x_i}\frac{\partial c}{\partial x_i}} \tag{7.26}$$

$$(-D_2) = \overline{-2\rho D^2\frac{\partial^2 c}{\partial x_i \partial x_j}\frac{\partial^2 c}{\partial x_i \partial x_j}} \tag{7.27}$$

$$\begin{aligned} f(D) = \overline{f_1(D)} = &\underbrace{\overline{2D\frac{\partial c}{\partial x_k}\frac{\partial(\rho D)}{\partial x_k}\frac{\partial^2 c}{\partial x_j \partial x_j}}}_{FD1} + \underbrace{\overline{2D\frac{\partial c}{\partial x_k}\frac{\partial^2(\rho D)}{\partial x_j \partial x_k}\frac{\partial c}{\partial x_j}}}_{FD2} - \underbrace{\overline{\frac{\partial}{\partial x_j}\left(\rho N_c\frac{\partial D}{\partial x_j}\right)}}_{FD3} \\ &\underbrace{-\overline{2\rho D\frac{\partial D}{\partial x_j}\frac{\partial}{\partial x_j}\left(\frac{\partial c}{\partial x_k}\frac{\partial c}{\partial x_k}\right)}}_{FD4} + \underbrace{\overline{\rho\left(\frac{\partial c}{\partial x_k}\frac{\partial c}{\partial x_k}\right)\left[\frac{\partial D}{\partial t} + u_j\frac{\partial D}{\partial x_j}\right]}}_{FD5} \end{aligned} \tag{7.28}$$

The term T_1 represents the effects of sub-grid convection, whereas T_2 denotes the effects of density-variation due to heat release. The term T_3 is determined by the alignment of ∇c with local strain rates $e_{ij} = 0.5(\partial u_i / \partial x_j + \partial u_j / \partial x_i)$, and this term is commonly referred to as the scalar-turbulence interaction term. The term T_4 arises due to reaction rate gradient while $(-D_2)$ denotes the molecular dissipation of SDR and these terms will henceforth be referred to as the reaction rate term and dissipation term respectively. The term $f(D)$, as in eq. (3.63), indicates the effects of variation of mass diffusivity, D, and its interaction with scalar gradients. The transport equation of the resolved components of $\tilde{N}_c$, $\tilde{D}\nabla\tilde{c}.\nabla\tilde{c}$, is repeated here as well for presenting purpose below:

$$\begin{aligned}
&\frac{\partial}{\partial t}\left(\bar{\rho}\tilde{D}\nabla\tilde{c}.\nabla\tilde{c}\right)+\frac{\partial}{\partial x_j}\left(\bar{\rho}\tilde{u}_j\tilde{D}\nabla\tilde{c}.\nabla\tilde{c}\right)\\
&\qquad\overbrace{\approx -2\tilde{D}\frac{\partial\tilde{c}}{\partial x_i}\frac{\partial^2}{\partial x_j\partial x_i}\left(\overline{\rho u_j c}-\bar{\rho}\tilde{u}_j\tilde{c}\right)}^{T_{1R}}\\
&\qquad\overbrace{-\frac{2\tilde{D}}{\bar{\rho}}\frac{\partial\bar{\rho}}{\partial x_i}\frac{\partial\tilde{c}}{\partial x_i}\left[\bar{\dot{w}}+\nabla.\left(\overline{\rho D\nabla c}\right)-\frac{\partial}{\partial x_j}\left(\overline{\rho u_j c}-\bar{\rho}\tilde{u}_j\tilde{c}\right)\right]}^{T_{2R}}\\
&\qquad\underbrace{-2\bar{\rho}\tilde{D}\frac{\partial\tilde{c}}{\partial x_i}\frac{\partial\tilde{u}_j}{\partial x_i}\frac{\partial\tilde{c}}{\partial x_j}}_{T_{3R}}\underbrace{+2\tilde{D}\frac{\partial\tilde{c}}{\partial x_i}\frac{\partial\bar{\dot{w}}}{\partial x_i}}_{T_{4R}}\\
&\qquad\underbrace{+\frac{\partial}{\partial x_j}\left(\bar{\rho}\tilde{D}\frac{\partial}{\partial x_j}\left[\tilde{D}\nabla\tilde{c}.\nabla\tilde{c}\right]\right)}_{D_{1R}}\underbrace{-2\bar{\rho}\tilde{D}\frac{\partial^2\tilde{c}}{\partial x_i\partial x_j}\frac{\partial^2\tilde{c}}{\partial x_i\partial x_j}}_{-D_{2R}}+f(D)_R
\end{aligned} \tag{7.29}$$

where

$$\begin{aligned}
f(D)_R=&-\frac{\partial\tilde{D}}{\partial x_j}\frac{\partial(\bar{\rho}\tilde{D})}{\partial x_j}\frac{\partial\tilde{c}}{\partial x_k}\frac{\partial\tilde{c}}{\partial x_k}-4\bar{\rho}\tilde{D}\frac{\partial\tilde{D}}{\partial x_j}\frac{\partial\tilde{c}}{\partial x_k}\frac{\partial^2\tilde{c}}{\partial x_k\partial x_j}-\bar{\rho}\tilde{D}\nabla\tilde{c}.\nabla\tilde{c}\frac{\partial^2\tilde{D}}{\partial x_j\partial x_j}\\
&+2\tilde{D}\frac{\partial\tilde{c}}{\partial x_k}\frac{\partial\tilde{c}}{\partial x_j}\frac{\partial^2(\bar{\rho}\tilde{D})}{\partial x_k\partial x_j}+2\tilde{D}\frac{\partial\tilde{c}}{\partial x_k}\frac{\partial(\bar{\rho}\tilde{D})}{\partial x_j}\frac{\partial^2\tilde{c}}{\partial x_k\partial x_j}\\
&+\tilde{D}\nabla\tilde{c}.\nabla\tilde{c}(\frac{\partial\bar{\rho}}{\partial t}+\tilde{u}_j\frac{\partial\bar{\rho}}{\partial x_j})+\bar{\rho}\nabla\tilde{c}.\nabla\tilde{c}(\frac{\partial\tilde{D}}{\partial t}+\tilde{u}_j\frac{\partial\tilde{D}}{\partial x_j})+\bar{\rho}\tilde{D}\nabla\tilde{c}.\nabla\tilde{c}\frac{\partial\tilde{u}_j}{\partial x_j}
\end{aligned} \tag{7.30}$$

Based on eqs. (7.22) - (7.30), the resolved strain rate and resolved curvature dependences of the sub-grid conponents of $\tilde{N}_c$, T_2, T_3, T_4, $(-D_2)$ and $f(D)$ will be assessed for turbulent premixed flames datasets of different turbulent intensities.

7.2.1 Sub-grid component of $\tilde{N}_c$ and its strain rate and curvature dependence

The correlation between the sub-grid components of $\tilde{N}_c$ for different filter widths is shown below for a sample case (case F).

$\Delta \approx 0.4\delta_{th}$

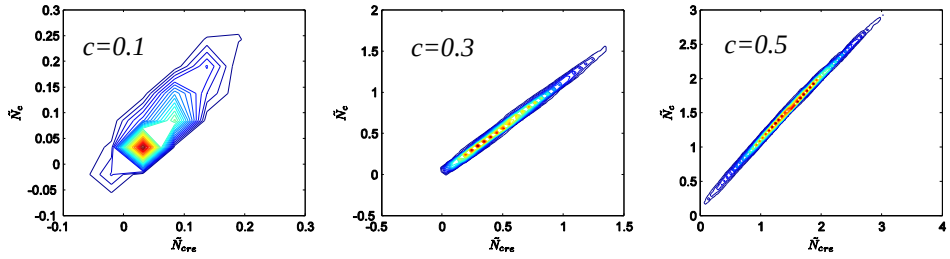

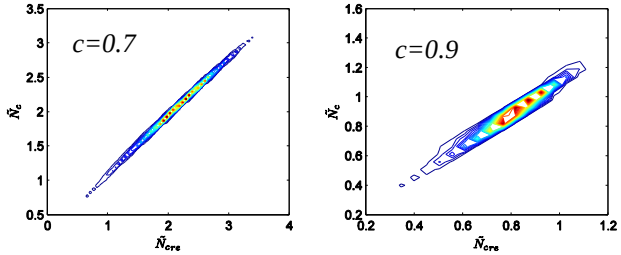

$\Delta \approx 1.2\delta_{th}$

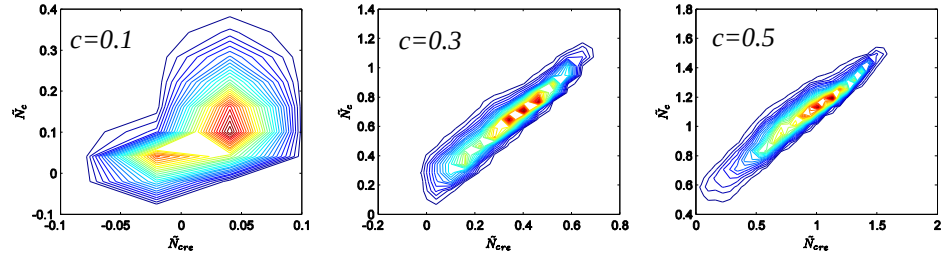

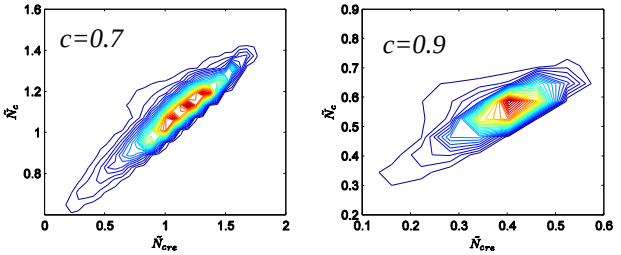

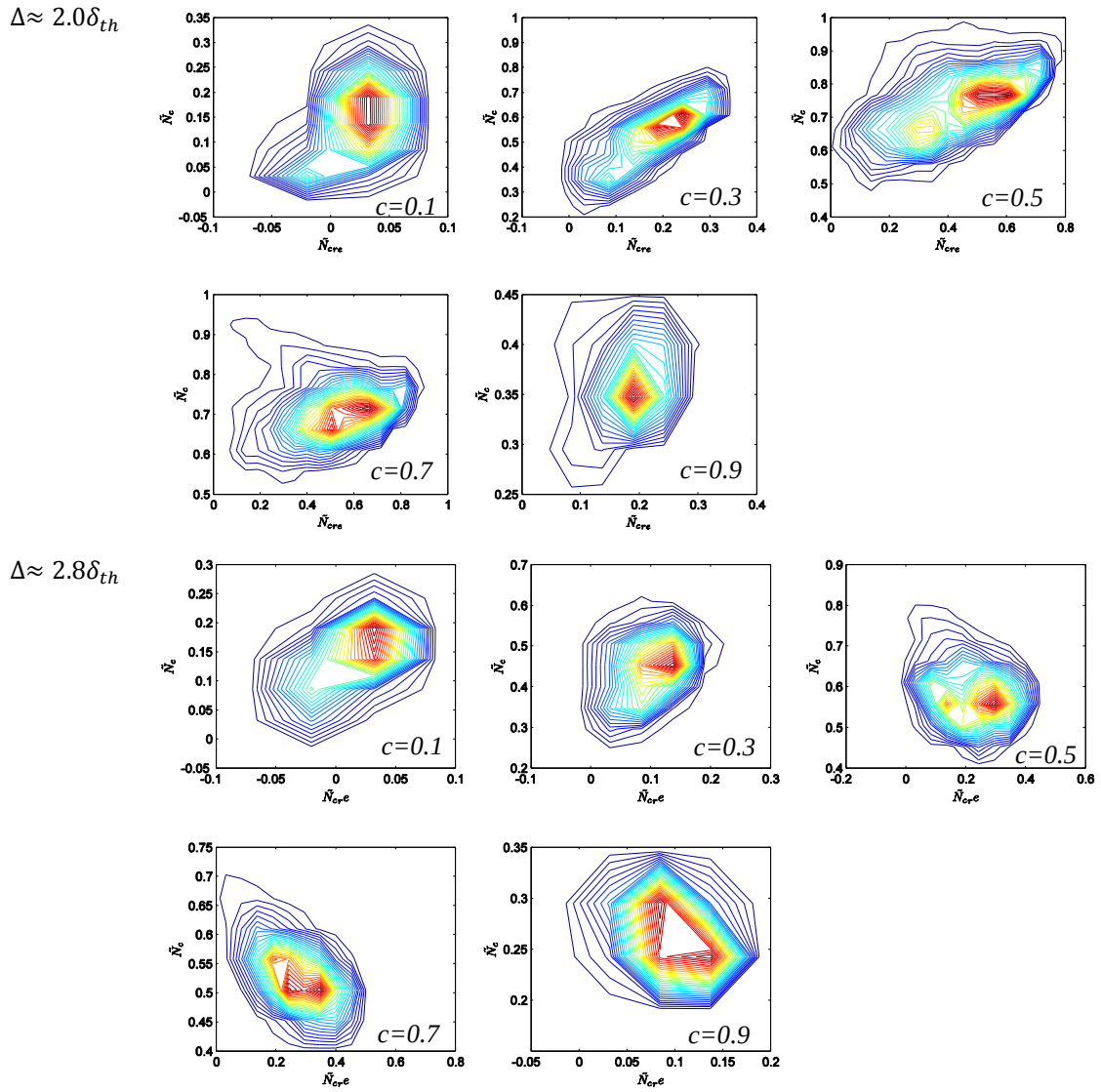

Figure 7.13: Joint pdfs between $\tilde{N}_c \times \delta_{th}/S_L$ and $\tilde{N}_{cre} \times \delta_{th}/S_L$ for case F on c=0.1, 0.3, 0.5, 0.7 and 0.9 isosurface for filter widths $\Delta \approx 0.4\delta_{th}$, $\Delta \approx 1.2\delta_{th}$, $\Delta \approx 2.0\delta_{th}$ and $\Delta \approx 2.8\delta_{th}$.

Figure 7.13 showed that for small filter width (i.e. $\Delta \approx 0.4\delta_{th}$), $\tilde{N}_c \times \delta_{th}/S_L$ and its resolved component are strongly positive correlated. This positive correlation weakens with increasing filter width. For large filter widths (i.e. $\Delta >> \delta_{th}$), $\tilde{N}_c \times \delta_{th}/S_L$ and its resolved component becomes uncorrelated, indicating that it is possible to model $\tilde{N}_c \times \delta_{th}/S_L$ algebraically for $\Delta >> \delta_{th}$ which is often the case in real LES.

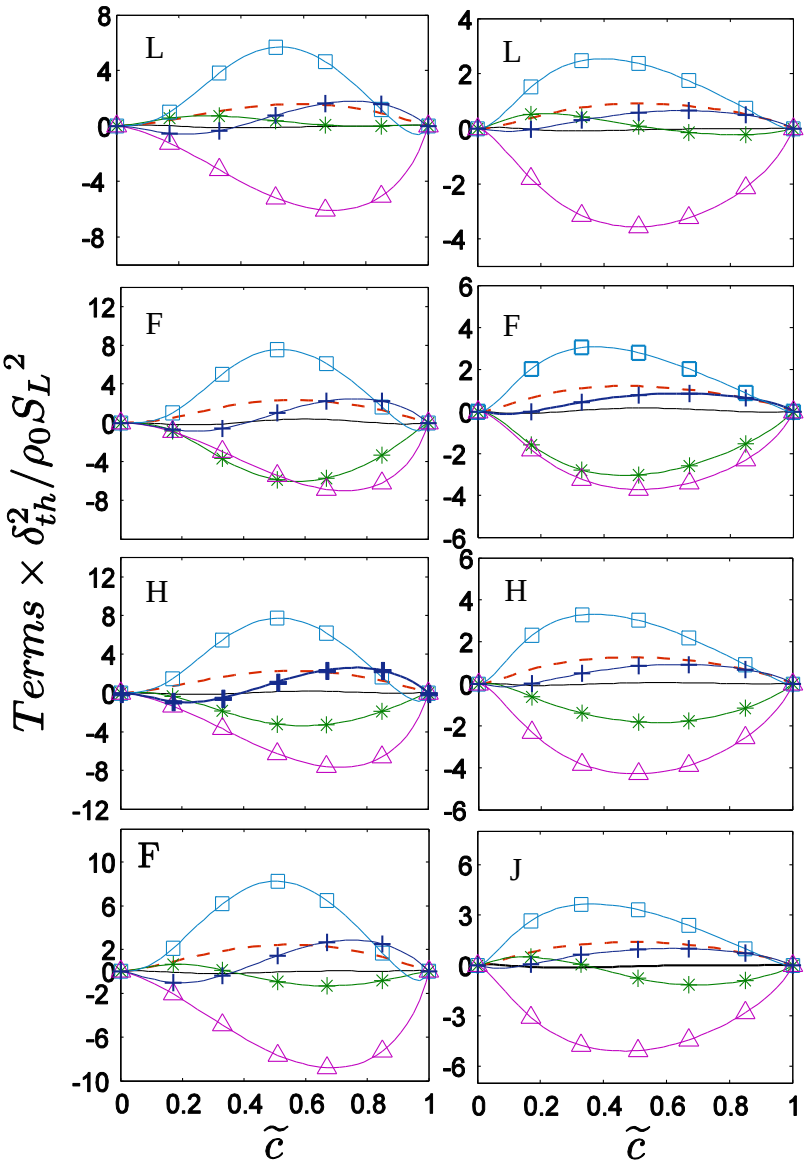

Figure 7.14: Variations of T_1 (——), T_2 (- - - -), T_3 (—✱—), T_4 (—□—), $(-D_2)$ (—△—) and $f(D)$ (—+—) conditionally averaged in bins of $\widetilde{c}$ for $\Delta \approx \delta_{th}$ (1st column) and $\Delta \approx 3.0\delta_{th}$ (2nd column) in cases L, F, H and J.

7.3 Modelling of unclosed terms of SDR transport equation

7.3.1. Modelling of the turbulent transport term T_1

It is evident from eq. 3a that the variation of the turbulent transport term T_1 within the flame brush depends on the sub-grid flux of SDR (i.e. $\overline{\rho u_i N_c} - \overline{\rho}\widetilde{u}_i \widetilde{N}_c$) and its modelling is essential for the closure of T_1. One obtains $(\overline{\rho u_i N_c} - \overline{\rho}\widetilde{u}_i \widetilde{N}_c) \sim \rho_0 S_L^2 / \delta_{th}$ when S_L is used to scale the sub-grid velocity fluctuations associated with sub-grid scalar gradients, and the sub-grid fluctuations of SDR are taken to scale with S_L / δ_{th} (Swaminathan and

Bray, 2005). Using $\rho_0 S_L^2/\delta_{th}$ and Δ to scale $(\overline{\rho u_i N_c} - \overline{\rho}\tilde{u}_i\tilde{N}_c)$ and resolved gradients respectively yields:

$$T_1 \sim \frac{\rho_0 S_L^2}{\Delta\delta_{th}} \sim \frac{\rho_0 S_L^2}{\delta_{th}^2} \times Da_\Delta^{-0.5}\,\mathrm{Re}_\Delta^{-0.5} \text{ for } \Delta >> \delta_{th} \tag{7.31}$$

where $Da_\Delta = \Delta S_L/u'_\Delta\delta_{th}$ and $\mathrm{Re}_\Delta = \rho_0 u'_\Delta\Delta/\mu_0$ are sub-grid Damköhler and turbulent Reynolds number respectively with $u'_\Delta = \sqrt{2k_{sgs}/3}$ and $k_{sgs} = (\overline{\rho u_i u_i} - \overline{\rho}\tilde{u}_i\tilde{u}_i)/2\overline{\rho}$ being the sub-grid turbulent velocity fluctuation and sub-grid kinetic energy respectively. One obtains $Da_\Delta\,\mathrm{Re}_\Delta \sim (\Delta/\delta_{th})^2$ using $D \sim S_L\delta_{th}$ (Swaminathan and Bray, 2005), which indicates that $Da_\Delta\,\mathrm{Re}_\Delta$ increases with increasing Δ. Thus, the magnitude of the turbulent transport term T_1 is expected to decrease in comparison to $\rho_0 S_L^2/\delta_{th}^2$ with increasing Δ according to eq. (7.31). One obtains an alternative scaling estimate of T_1 when the sub-grid fluctuations of velocity and SDR are scaled with respect to u'_Δ and S_L/δ_{th} respectively, which yields:

$$T_1 \sim \frac{\rho_0 S_L u'_\Delta}{\Delta\delta_{th}} \sim \frac{\rho_0 S_L^2}{\delta_{th}^2} \times Da_\Delta^{-1} \text{ for } \Delta >> \delta_{th} \tag{7.32}$$

Equation (7.32) also suggests that the magnitude of the turbulent transport term T_1 is expected to decrease in comparison to $\rho_0 S_L^2/\delta_{th}^2$ with increasing Δ, as Da_Δ increases with increasing Δ (Dunstan *et al*., 2013).

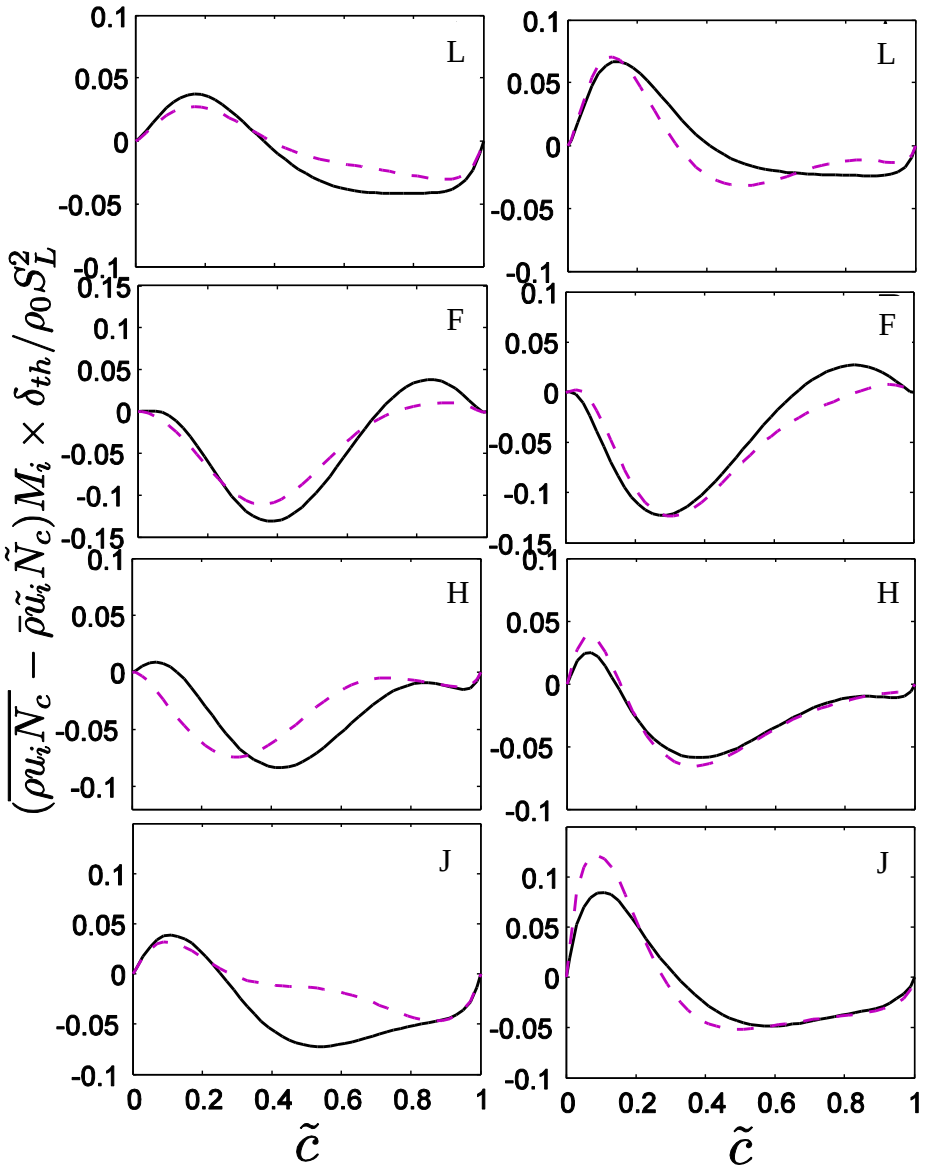

Figure 7.15: Variations of $(\overline{\rho u_i N_c} - \overline{\rho}\tilde{u}_i\tilde{N}_c)M_i \times \delta_{th}/\rho_0 S_L^2$ (——) conditionally averaged in bins of $\tilde{c}$ along with the predictions of eq. (7.43) (- - - -) for $\Delta \approx \delta_{th}$ (1st column) and $\Delta \approx 3.0\delta_{th}$ (2nd column) in cases L, F, H and J.

Sub-grid flux of SDR $(\overline{\rho u_i N_c} - \overline{\rho}\tilde{u}_i\tilde{N}_c)$ is often modelled using a gradient hypothesis as (Chakraborty *et al*., 2011a):

$$(\overline{\rho u_i N_c} - \overline{\rho}\tilde{u}_i\tilde{N}_c) = -\overline{\rho}D_t \frac{\partial \tilde{N}_c}{\partial x_i} \tag{7.33}$$

where D_t is the eddy diffusivity. It has been demonstrated earlier that the turbulent scalar flux of scalar gradients (e.g. FSD and SDR) may exhibit counter-gradient transport for

the flames when counter-gradient transport is observed for $(\overline{\rho u_i c} - \overline{\rho}\widetilde{u}_i\widetilde{c})$ (Chakraborty and Swaminathan, 2010, 2013; Chakraborty *et al*., 2011d; Veynante *et al*., 1997; Chakraborty and Cant, 2009). Recently, Chakraborty and Swaminathan (2013) proposed a RANS model for turbulent flux of SDR which is capable of predicting both gradient and counter-gradient transport of SDR in the following manner:

$$\left\langle \rho u_i'' \varepsilon_c \right\rangle = \lambda_c (\Phi - \widetilde{c}) \frac{[\left\langle \rho u_i'' c'' \right\rangle - \alpha_1 \left\langle \rho \right\rangle \hat{c}(1-\hat{c})\sqrt{2\hat{k}/3} M_i^R]\hat{\varepsilon}_c}{[\left\langle \rho c''^2 \right\rangle / \left\langle \rho \right\rangle + \hat{c}(1-\hat{c})]} - \alpha_2 \mu_t \frac{\partial \hat{\varepsilon}_c}{\partial x_i} \tag{7.34}$$

where $\left\langle Q \right\rangle$, $\hat{Q} = \left\langle \rho Q \right\rangle / \left\langle \rho \right\rangle$ and $Q'' = Q - \hat{Q}$ are Reynolds average and Favre average, and Favre fluctuation of Q and μ_t, $\hat{\varepsilon}_c$, $\hat{k}$ and $\hat{\varepsilon}$ are the eddy viscosity, Favre-mean SDR, turbulent kinetic energy and its dissipation rate respectively in the context of RANS, which are defined as:

$$\mu_t = 0.09\left\langle \rho \right\rangle \frac{\hat{k}^2}{\hat{\varepsilon}};\ \hat{k} = 0.5\frac{\left\langle \rho u_i'' u_i'' \right\rangle}{\left\langle \rho \right\rangle} \text{ and } \hat{\varepsilon} = \frac{1}{\left\langle \rho \right\rangle}\left\langle \mu \frac{\partial u_i''}{\partial x_j}\frac{\partial u_i''}{\partial x_j} \right\rangle \tag{7.35}$$

In eq. (7.34) $\lambda_c = 2$ and $\Phi = 0.5$ are the model parameters and $M_i^R = -(\partial \hat{c}/\partial x_i)/|\nabla \hat{c}|$ is the i^{th} component of the resolved flame normal vector. According to Bray *et al.* (1985), $\left\langle \rho u_i'' c'' \right\rangle$ can be expressed in the following manner:

$$\left\langle \rho u_i'' c'' \right\rangle = \left\langle \rho \right\rangle [\left\langle u_i \right\rangle_P - \left\langle u_i \right\rangle_R]\hat{c}(1-\hat{c}) + O(\gamma_c) \tag{7.36}$$

where $\left\langle u_i \right\rangle_P$ and $\left\langle u_i \right\rangle_R$ are the conditional mean velocities in x_i-direction in products and reactants respectively and the contribution $O(\gamma_c)$ arises from burning mixture which scales with $1/Da$ (i.e. $O(\gamma_c) \sim O(1/Da)$). Thus the contribution of $O(\gamma_c)$ is expected to be negligible for $Da >> 1$ flames. Veynante *et al.* (1997) demonstrated that the slip velocity $[\left\langle u_i \right\rangle_P - \left\langle u_i \right\rangle_R]$ can be expressed as:

$$[\left\langle u_i \right\rangle_P - \left\langle u_i \right\rangle_R] = -(-\alpha_E \sqrt{2\hat{k}/3} + \tau S_L) M_i^R \tag{7.37}$$

where α_E is an appropriate efficiency function. Equation (7.37) leads to the following expression for $\left\langle \rho u_i'' c'' \right\rangle$:

$$\left\langle \rho u_i'' c'' \right\rangle = \left\langle \rho \right\rangle (\alpha_E \sqrt{2\hat{k}/3} - \tau S_L) M_i^R \hat{c}(1-\hat{c}) + O(\gamma_c) \tag{7.38}$$

Thus, the quantity $(\alpha_E \sqrt{2\hat{k}/3})\langle \rho \rangle \hat{c}(1-\tilde{c}) M_i^R$ in eq. (7.38) can be taken to represent the effects of turbulent velocity fluctuation on turbulent scalar flux $\left\langle \rho u_i'' c'' \right\rangle$. Thus, the heat release and turbulent velocity fluctuation effects in eq. (7.34) can be identified as:

Heat release effects

$$\lambda_c (\Phi - \tilde{c}) \frac{[\left\langle \rho u_i'' c'' \right\rangle - \alpha_E \langle \rho \rangle \hat{c}(1-\hat{c}) \sqrt{2\hat{k}/3} M_i^R] \hat{\varepsilon}_c}{[\left\langle \rho c''^2 \right\rangle / \langle \rho \rangle + \hat{c}(1-\hat{c})]} \tag{7.39}$$

Turbulent velocity fluctuation effects

$$\lambda_c (\Phi - \tilde{c}) \frac{[-(\alpha_1 M_i^R - \alpha_E M_i^R) \langle \rho \rangle \hat{c}(1-\hat{c}) \sqrt{2\hat{k}/3}] \hat{\varepsilon}_c}{[\left\langle \rho c''^2 \right\rangle / \langle \rho \rangle + \hat{c}(1-\hat{c})]} - \alpha_2 \mu_t \frac{\partial \hat{\varepsilon}_c}{\partial x_i} \tag{7.40}$$

Chakraborty and Swaminathan (2013) proposed the following expressions for α_1, α_2 and Φ:

$$\alpha_1 = 0.22;\ \alpha_2 = 4.0[1 - 0.5 erf(\mathrm{Re}_L/6)] \text{ and } \Phi = 1 - 0.5 erf(\mathrm{Re}_L/3) \tag{7.41}$$

where $\mathrm{Re}_L = \rho_0 \tilde{k}^2 / \mu_0 \tilde{\varepsilon}$ is the local turbulent Reynolds number, ensuring the model parameters reach asymptotic limit for large values of Re_L (i.e. $\mathrm{Re}_L \to \infty$) (Chakraborty and Swaminathan, 2013). It is worth noting that eq. (7.34) is not only valid for high Damköhler number (i.e. $Da >> 1$) flames but also for low Damköhler number (i.e. $Da < 1$) flamelet combustion in the thin reaction zones regime (Peters, 2000). For $Da >> 1$ one obtains $\left\langle \rho c''^2 \right\rangle \approx \langle \rho \rangle \hat{c}(1-\hat{c})$ due to bimodal pdf of c (Bray, 1980) and under that condition eq. (7.34) for $\lambda_c = 2.0$ reduces to an expression proposed by Veynante *et al.* (1997) which is strictly valid only for high values of Damköhler number (i.e. $Da >> 1$) in the context of FSD transport. For $Da < 1$ combustion $\left\langle \rho c''^2 \right\rangle / \langle \rho \rangle < \hat{c}(1-\hat{c})$, and thus the involvement of $\left\langle \rho c''^2 \right\rangle$ in eqs. (7.34), (7.39) and (7.40) inherently accounts for $O(\gamma_c)$ contributions in eqs. (7.36) and (7.38). The contribution of $O(\gamma_c)$ is expected to weaken

with increasing Da as $\left\langle \rho c''^2 \right\rangle$ approaches $\hat{c}(1-\hat{c})$. It was demonstrated by Chakraborty and Swaminathan (2010, 2013) and Chakraborty *et al.* (2011d) that eq. (7.34) not only predicts $\left\langle \rho u_i'' \varepsilon_c \right\rangle$ for $Da >> 1$ flames but also for $Da < 1$ thin reaction zones regime combustion.

The RANS modelling of turbulent scalar flux can be extended for LES as (Rymer, 2001):

$$[\overline{\rho u_i c} - \overline{\rho}\tilde{u}_i\tilde{c}] = \overline{\rho}[\overline{(u_i)}_P - \overline{(u_i)}_R]\tilde{c}(1-\tilde{c}) = -\overline{\rho}[-\alpha_E' u_\Delta' + \tau S_L]\tilde{c}(1-\tilde{c})M_i \qquad (7.42)$$

where α_E' is an appropriate efficiency function and $M_i = -(\partial\tilde{c}/\partial x_i)/|\nabla\tilde{c}|$ is the i^{th} component of the resolved flame normal vector for LES. Using eq. (7.42) and extending the aforementioned RANS modelling argument given by eqs. (7.34-7.41) for the purpose of LES allows one to model $(\overline{\rho u_i N_c} - \overline{\rho}\tilde{u}_i\tilde{N}_c)$ in the following manner:

$$\overline{\rho u_i N_c} - \overline{\rho}\tilde{u}_i\tilde{N}_c = \left\{(\Phi' - \tilde{c})\frac{\gamma_1[\overline{\rho u_i c} - \overline{\rho}\tilde{u}_i\tilde{c}] - \gamma_2\overline{\rho}\tilde{c}(1-\tilde{c})u_\Delta' M_i}{\tilde{c}(1-\tilde{c})}\tilde{N}_c - \overline{\rho}(C_F\Delta)u_\Delta'\frac{\partial\tilde{N}_c}{\partial x_i}\right\} \qquad (7.43)$$

where $\gamma_1, \gamma_2, \Phi'$ and C_F are the model parameters and the following values have been suggested based on the current *a-priori* DNS assessment:

$$\gamma_1 = 1.8,\ \gamma_2 = 4.9 - 3.2erf(0.15\,\mathrm{Re}_\Delta),\ \Phi' = 0.7 \text{ and } C_F = 0.11 \qquad (7.44)$$

Equation (7.44) ensures that γ_2 reaches an asymptotic limit for large values of Re_Δ (i.e. $\mathrm{Re}_\Delta \to \infty$). The predictions of $(\overline{\rho u_i N_c} - \overline{\rho}\tilde{u}_i\tilde{N}_c)M_i \times \delta_{th}/\rho_0 S_L^2$ according to eq. (7.43) are compared to the corresponding quantity extracted from DNS data for $\Delta \approx \delta_{th}$ and $\Delta \approx 3\delta_{th}$ in Fig. 7.15 for cases L, F, H and J. Figure 7.15 shows that eq. 9a satisfactorily predicts $(\overline{\rho u_i N_c} - \overline{\rho}\tilde{u}_i\tilde{N}_c)M_i \times \delta_{th}/\rho_0 S_L^2$ for both $\Delta \approx \delta_{th}$ and $\Delta >> \delta_{th}$ (e.g. $\Delta \approx 3.0\delta_{th}$) in turbulent flames with different values of τ and Re_t when the model parameters according to eq. 9b are used. However, the agreement between the predictions of eq. 9a and DNS data improves with increasing Δ (see Fig. 7.15). It can be seen from Fig. 7.14 that the magnitude of T_1 remains negligible in comparison to the magnitudes of $T_2, T_3, T_4, (-D_2)$ and $f(D)$ in all cases for all values of Δ. Thus, the uncertainties

associated with the modelling of $(\overline{\rho u_i N_c} - \overline{\rho}\tilde{u}_i \tilde{N}_c)$ do not have major implications in the closure of SDR $\tilde{N}_c$ transport.

7.3.2 Reaction rate gradient terms T_2

For low Mach number globally adiabatic $Le = 1.0$ flames ρ can be expressed as $\rho = \rho_0 /(1+\tau c)$ (Bray *et al*., 1985), which gives rise to an alternative expression of T_2 as:

$$T_2 = 2\overline{\left(\rho \frac{\partial u_i}{\partial x_i} N_c\right)} \tag{7.45}$$

The resolved part of T_2 can be taken as:

$$(T_2)_{res} = 2\overline{\rho}\tilde{D}\nabla\tilde{c}.\nabla\tilde{c}\frac{\partial \tilde{u}_i}{\partial x_i} \tag{7.46}$$

As the dilatation rate $(\partial u_i / \partial x_i)$ is predominantly positive in turbulent premixed flames, the contribution of T_2 remains positive in all cases irrespective of the filter width Δ. The dilatation rate can be taken to scale as $(\partial u_i / \partial x_i) \sim \tau S_L / \delta_{th}$ (Chakraborty and Swaminathan, 2007a,b; Chakraborty *et al*., 2009) . Thus, T_2 can be scaled as:

$$T_2 \sim \frac{\rho_0 \tau S_L^2}{\delta_{th}^2} \tag{7.46}$$

whereas the resolved component $(T_2)_{res}$ can be taken to scale as:

$$(T_2)_{res} \sim \frac{\rho_0 S_L^2}{\delta_{th}^2} \times \frac{U_{ref}}{S_L} \times \left(\frac{\delta_{th}}{\Delta}\right)^3 \sim \frac{\rho_0 S_L^2}{\delta_{th}^2} \times \frac{U_{ref}}{S_L} \times \mathrm{Re}_\Delta^{-1.5}\, Da_\Delta^{-1.5} \text{ for } \Delta >> \delta_{th} \tag{7.47}$$

where U_{ref} is a velocity scale representing the Favre-filtered velocity components $\tilde{u}_i$. The above scaling estimates demonstrate that T_2 remains of the order of $\rho_0 \tau S_L^2 / \delta_{th}^2$ irrespective of Δ. By contrast, the magnitude of $(T_2)_{res}$ remains comparable to $\rho_0 S_L^2 / \delta_{th}^2$ for $U_{ref} \sim S_L$ and $\Delta \approx \delta_{th}$, but the magnitude of $(T_2)_{res}$ is expected to decrease with increasing Δ. This suggests that the sub-grid component $(T_2)_{sg} = T_2 - (T_2)_{res}$ plays an

increasingly important role with increasing Δ, which can be substantiated from Fig. 7.16 where the variations of the mean values of T_2 and $(T_2)_{sg} = T_2 - (T_2)_{res}$ conditional on $\tilde{c}$ are shown for cases L, F, H and J for $\Delta \approx \delta_{th}$ and $\Delta \approx 3.0\delta_{th}$.

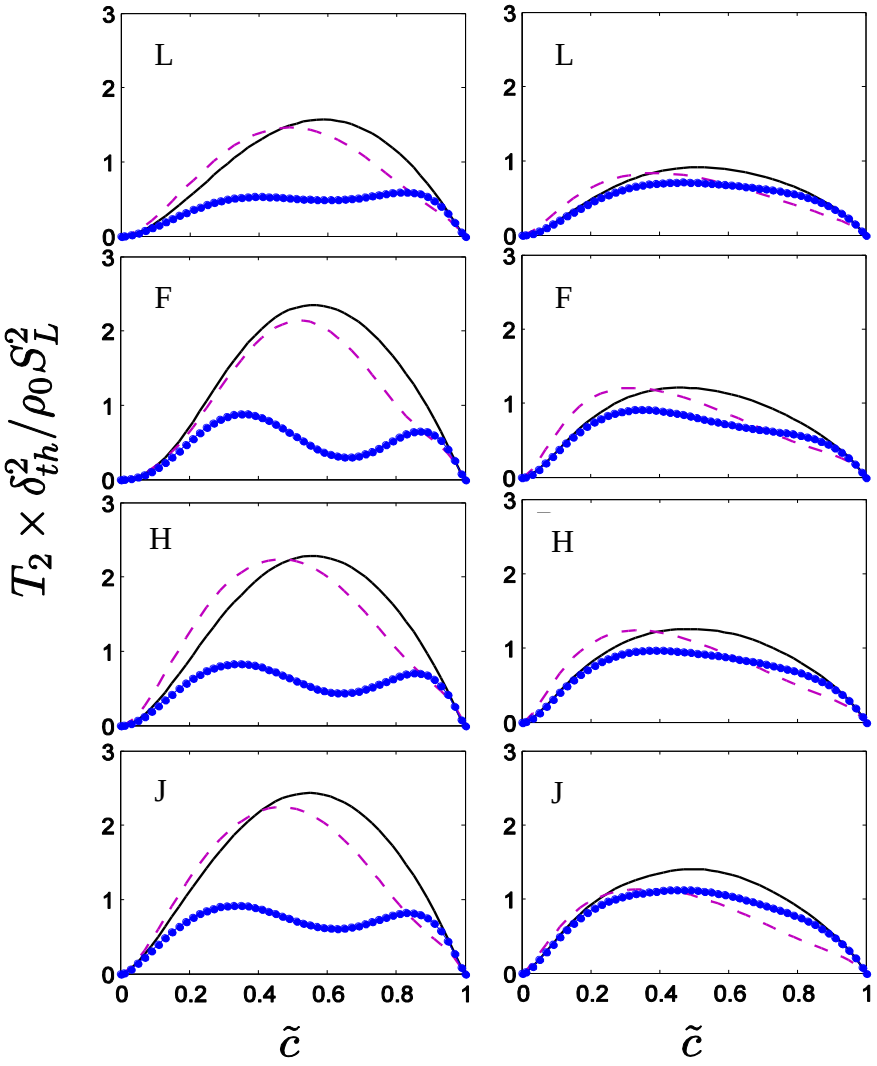

Figure 7.16: Variations of T_2 (——) and $(T_2)_{sg}$ (—●—) conditionally averaged in bins of $\tilde{c}$ along with the predictions of eq. (7.49) (- - - -) for $\Delta \approx \delta_{th}$ (1st column) and $\Delta \approx 3.0\delta_{th}$ (2nd column) in cases L, F, H and J.

Scaling $(\partial u_i / \partial x_i)$ and N_c with respect to $\tau S_L / \delta_{th}$ and S_L / δ_{th} respectively leads to the following model for $\langle 2D(\partial u_i / \partial x_i)\nabla c''.\nabla c'' \rangle$ in the context of RANS (Chakraborty *et al*., 2008, 2010; Chakraborty *et al*., 2011d; Chakraborty and Swaminathan, 2010, 2013):

$$\langle 2D(\partial u_i / \partial x_i)\nabla c''.\nabla c'' \rangle = 2B_{T_2}\tau S_L \frac{\langle \rho \rangle \hat{\varepsilon}_c}{\delta_{th}(1+Ka_L)^{1/2}} \tag{7.48}$$

where B_{T_2} is a model parameter of the order of unity which depends on the thermo-chemistry and $Ka_L \approx (S_L)^{-3/2}(\hat{\varepsilon}\delta_{th})^{1/2}$ is the local Karlovitz number. As $(T_2)_{sg} = T_2 - (T_2)_{res}$ is expected to behave similar to $\left\langle 2D(\partial u_i / \partial x_i)\nabla c''.\nabla c'' \right\rangle$ for $\Delta >> \delta_{th}$ and both of these quantities scale with $\rho_0 \tau S_L^2 / \delta_{th}^2$, the existing RANS modelling methodology for $\left\langle 2D(\partial u_i / \partial x_i)\nabla c''.\nabla c'' \right\rangle$ has been extended here for the modelling T_2 in the following manner:

$$T_2 = 2\bar{\rho}\tilde{D}\nabla\tilde{c}.\nabla\tilde{c}\frac{\partial\tilde{u}_i}{\partial x_i} + \beta_{T_2}\tau S_L \frac{[\bar{\rho}\tilde{N}_c - \bar{\rho}\tilde{D}\nabla\tilde{c}.\nabla\tilde{c}]}{\delta_{th}(1.0 + Ka_\Delta)^{1/2}} \tag{7.49}$$

where $Ka_\Delta = (u'_\Delta / S_L)^{3/2}(\Delta / \delta_{th})^{-1/2}$ is local sub-grid Karlovitz number and β_{T_2} is a model parameter, which is taken to be 2.7 based on the current analysis. The first term on right hand side of eq. (7.49) accounts for $(T_2)_{res}$ whereas the second term accounts for the sub-grid component. According to eq. (7.49) the term T_2 approaches to $(T_2)_{res}$ when the flow is completely resolved in the following manner:

$$\lim_{\Delta\to 0} T_2 = \lim_{\Delta\to 0} 2\bar{\rho}\tilde{D}\nabla\tilde{c}\cdot\nabla\tilde{c}\frac{\partial\tilde{u}_i}{\partial x_i} = 2\rho D\nabla c.\nabla c\frac{\partial u_i}{\partial x_i} \tag{7.50}$$

$$\lim_{\Delta\to 0} \tilde{N}_c = \lim_{\Delta\to 0} \tilde{D}\nabla\tilde{c}.\nabla\tilde{c} = D\nabla c.\nabla c \tag{7.51}$$

The local Karlovitz number Ka_Δ dependence of $(T_2)_{sg}$ ensures that the effects of $(\partial u_i / \partial x_i)$ diminish as combustion approaches the broken reaction zones regime (Chakraborty *et al.*, 2008, 2010; Chakraborty *et al.* 2011d; Chakraborty and Swaminathan, 2010, 2013). However, the local Ka_Δ dependence of $(T_2)_{sg}$ suggested in eq. (7.49) is one of the several possible options, which suggests a diminishing strength of $(T_2)_{sg}$ with increasing Ka_Δ. Thus, any other parameterisation, which predicts weakening of $(T_2)_{sg}$ with increasing Ka_Δ, can also be used for the modelling of T_2. The predictions of eq. (7.49) with $\beta_{T2} = 2.7$ are compared to T_2 extracted from DNS data in Fig. 7.16, which shows that eq. (7.49) satisfactorily predicts the quantitative behaviour of T_2 for a range of different values of Δ for turbulent premixed flames with different values of Re_t and τ.

7.3.3 Scalar turbulence interaction term T_3

The term T_3 can be expressed as (Chakraborty and Swaminathan, 2007a,b; Chakraborty *et al*., 2009; Chakraborty *et al*., 2010):

$$T_3 = -2\overline{\rho(e_\alpha \cos^2\alpha + e_\beta \cos^2\beta + e_\gamma \cos^2\gamma)N_c} \quad (7.52)$$

where e_α, e_β and e_γ are the most extensive, intermediate and the most compressive principal strain rates and their angles with ∇c are given by α, β and γ respectively, which suggests that a preferential collinear alignment of ∇c with e_α and e_γ leads to a negative contribution and positive contribution respectively of T_3. It has been demonstrated earlier (Chakraborty and Swaminathan, 2007a,b; Chakraborty *et al*., 2009; Chakraborty *et al*., 2010) that ∇c aligns with e_γ (i.e. $|\cos\gamma| = 1.0$) when turbulent fluid-dynamic straining a_{turb} overcomes the strain rate a_{chem} induced by flame normal acceleration and *vice versa.* The variations of the mean values of T_3 conditional on $\tilde{c}$ are shown in Fig. 7.14 for cases L, F, H and J at $\Delta \approx \delta_{th}$ and $\Delta \approx 3.0\delta_{th}$. Figure 7.14 shows that T_3 is negative throughout the flame brush for cases F and H but assumes positive values towards unburned gas side of the flame brush and negative values towards burnt gas side of the flame brush respectively in cases L and J. In cases F and H, the reaction progress variable gradient ∇c predominantly aligns with e_α, however, the extent of this alignment decreases from case F to case H. This predominant alignment of ∇c with e_α in cases F and H leads to negative contributions of T_3 in these cases. In case F, the reaction progress variable gradient ∇c predominantly aligns with e_γ in the unburned gas region but the effects of a_{chem} overcome the effects of a_{turb} in the regions of intense heat release and ∇c starts to align with e_α in the reaction zone. Thus, positive value of T_3 can be discerned towards the unburned gas side in case F, whereas T_3 assumes negative values for the rest of the flame brush. When the statistics were extracted, $\tau Da/\mathrm{Re}_t^{1/2}$ is equal to $0.96, 0.55, 0.49$ for cases H, I and J respectively, which gives rise to greater extent of ∇c alignment with e_γ in case J (case I) than in case I (case H). Therefore T_3 assumes predominantly negative values in cases H and I, whereas positive

contribution towards the unburned gas sides of the flame brush is observed for T_3 in case J (not shown here) as a_{chem} overcomes a_{turb} in the regions of intense heat release and ∇c starts to align with e_α in the reaction zone. The effects of a_{chem} are weaker in case L than in cases F-J due to smaller value of τ and thus a_{turb} dominates over a_{chem} for a major portion of the flame brush in case L than in case I, although turbulent flow conditions are similar in these cases. This leads to greater extent of positive contribution of T_3 in case L than in case I but in both cases T_3 assumes negative values towards the burned gas side of the flame brush as a_{chem} dominates over a_{turb} in the regions of intense heat release.

Scaling the strain rate associated with sub-grid fluctuations of velocity using S_L and δ_{th} (Swaminathan and Bray, 2005) gives:

$$T_3 \sim \frac{\rho_0 S_L^2}{\delta_{th}^2} \tag{7.53}$$

whereas the resolved part of T_3 can be scaled as:

$$(T_3)_{res} = -2\overline{\rho}\widetilde{D}\frac{\partial\widetilde{c}}{\partial x_i}\frac{\partial\widetilde{u}_i}{\partial x_j}\frac{\partial\widetilde{c}}{\partial x_j} \sim \frac{\rho_0 S_L^2}{\delta_{th}^2}\times\frac{U_{ref}}{S_L}\times\left(\frac{\delta_{th}}{\Delta}\right)^3 \sim \frac{\rho_0 S_L^2}{\delta_{th}^2}\times\frac{U_{ref}}{S_L}\times \mathrm{Re}_\Delta^{-1.5} Da_\Delta^{-1.5} \text{ for } \Delta >> \delta_{th} \tag{7.54}$$

An alternative scaling of T_3 can be obtained when the sub-grid turbulent straining is taken to scale with (u'_Δ / Δ):

$$T_3 \sim \frac{\rho_0 \widetilde{N}_c u'_\Delta}{\Delta} \sim \frac{\rho_0 S_L^2}{\delta_{th}^2}\times Da_\Delta^{-1} \quad \text{for} \quad \Delta >> \delta_{th} \tag{7.55}$$

Equations (7.53-7.55) suggest that the contribution of $(T_3)_{res}$ to T_3 is expected to be negligible for $\Delta >> \delta_{th}$. This can be substantiated from Fig. 7.17, where the variations of the mean values of $(T_3)_{sg} = T_3 - (T_3)_{res}$ conditional on $\widetilde{c}$ are also shown for cases L, F, H and J.

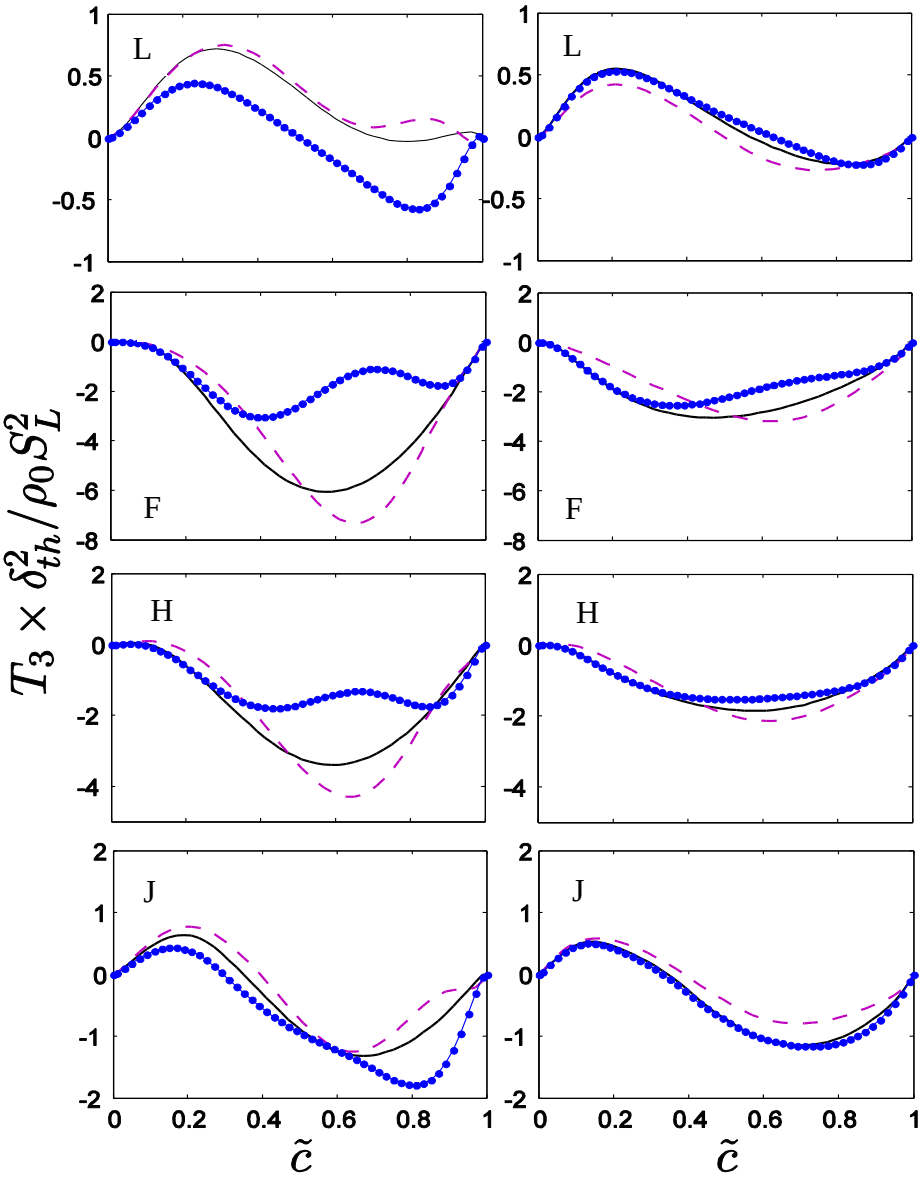

Figure 7.17: Variations of T_3 (——) and $(T_3)_{sg}$ (—●—) conditionally averaged in bins of $\tilde{c}$ along with the predictions of eq. (7.56) (- - - -) for $\Delta \approx \delta_{th}$ (1st column) and $\Delta \approx 3.0\delta_{th}$ (2nd column) in cases L, F, H and J.

The above scaling arguments are used here to propose a model for T_3 as:

$$T_3 = -2\overline{\rho D}\frac{\partial \tilde{c}}{\partial x_i}\frac{\partial \tilde{u}_i}{\partial x_j}\frac{\partial \tilde{c}}{\partial x_j} + (1 - f_{T_3})(C_3 - C_4 \tau . Da_\Delta^*)\frac{u'_\Delta}{\Delta}\overline{\rho}\tilde{N}_c \qquad (7.56)$$

where C_3 and C_4 are the model parameters and $Da_L^* = S_L \rho_0 \Delta / u'_\Delta \overline{\rho} \delta_{th}$ is the density-weighted local sub-grid Damköhler number. The first (second) term on the right hand side of eq. (7.56) denotes $res(T_3)$ ($(T_3)_{sg} = T_3 - (T_3)_{res}$) and f_{T_3} is a bridging function in

terms of Δ/δ_z, which ensures that $(T_3)_{sg} \approx T_3$ for $\Delta >> \delta_{th}$ and T_3 approaches to $(T_3)_{res}$ when the flow is fully resolved:

$$\lim_{\Delta\to 0} T_3 = -\lim_{\Delta\to 0} 2\overline{\rho D}\frac{\partial\widetilde{c}}{\partial x_i}\frac{\partial\widetilde{u}_i}{\partial x_j}\frac{\partial\widetilde{c}}{\partial x_j} = -2\rho D\frac{\partial c}{\partial x_i}\frac{\partial u_i}{\partial x_j}\frac{\partial c}{\partial x_j} \tag{7.57}$$

The term $C_3\overline{\rho}\widetilde{N}_c(u'_\Delta/\Delta)$ in eq. (7.56) is consistent with the scaling estimate given by eq. 15c, which accounts for the alignment of ∇c with e_γ. By contrast, $-\tau C_4 Da^*_\Delta\overline{\rho}\widetilde{N}_c(u'_\Delta/\Delta) = -\tau C_4\rho_0\widetilde{N}_c(S_L/\delta_{th})$ accounts for the alignment of ∇c with e_α, and is consistent with scaling estimate given by eq. (7.55). The effects of a_{chem} weaken with increasing Karlovitz number and thus the model parameter C_4 is expected to have local sub-grid Karlovitz number Ka_Δ dependence. Based on the current *a-priori* analysis the following expressions for C_3, C_4 and f_{T_3} have been proposed here:

$$C_3 = 7.5\ ;\ C_4 = 0.75(1.0+Ka_\Delta)^{-0.4} \text{ and } f_{T_3} = \exp[-1.05(\Delta/\delta_z)^2] \tag{7.58}$$

The above values have been chosen based on a least-squares analysis. An alternative set of functional relations for C_4 and f_{T_3}, which will satisfy the expected asymptotic trends in terms of Ka_Δ and (Δ/δ_z) respectively, can also be used for the modelling of T_3.

The predictions of eq. (7.56) with the model parameters given by eq. (7.58) are compared with DNS data in Fig. 7.17. It can be seen from Fig. 7.17 that the model given by eq. (7.56) provides satisfactory prediction of T_3 for a range of different values of Δ, and for flames with different values of Re_t and τ when the model parameters listed in eq. (7.58) are used.

7.3.4. Modelling of the combined reaction, dissipation and diffusivity gradient contribution [T_4-D_2+$f(D)$]

The variations of the mean values of $[T_4 - D_2 + f(D)]$ conditional on $\widetilde{c}$ are shown in Fig. 7.18 for A, B, D and F for $\Delta \approx \delta_{th}$ and $\Delta \approx 3.0\delta_{th}$, showing that $[T_4 - D_2 + f(D)]$ acts as a sink (source) term towards the burned (unburned) gas side of the flame brush for $\Delta \approx \delta_{th}$ (also for $\Delta < \delta_{th}$ not shown here). However, the mean value of

$[T_4 - D_2 + f(D)]$ conditional on $\tilde{c}$ is predominantly negative for $\Delta >> \delta_{th}$ (e.g. $\Delta \approx 3.0\delta_{th}$).

The term T_4 can be expressed as: $T_4 = -\overline{2D(\partial \dot{w}/\partial n)|\nabla c|}$ where n is the direction of the local flame normal which points towards the unburned gas. For the present thermo-chemistry the maximum value of reaction rate $\dot{w}$ occurs close to $c \approx 0.85$ (Chakraborty and Cant, 2004). This suggests that the probability of finding negative (positive) values of $\partial \dot{w}/\partial n$ is significant for $c < 0.85$ ($c > 0.85$) leading to positive (negative) mean value of T_4 towards the unburned (burned) gas side of the flame brush. The molecular dissipation term $(-D_2)$ is negative according to eq. 3e. It is often assumed that ρD is a constant (Peters, 2000), which allows one to express $\overline{\rho \nabla c \cdot \nabla c[\partial D/\partial t + \vec{u} \cdot \nabla D]}$ as:

$$\overline{\rho \frac{\partial c}{\partial x_k}\frac{\partial c}{\partial x_k}\left[\frac{\partial D}{\partial t} + u_j \frac{\partial D}{\partial x_j}\right]} = \overline{\rho N_c \frac{\partial u_j}{\partial x_j}} = \frac{T_2}{2} \tag{7.59}$$

Thus, $\overline{\rho \nabla c \cdot \nabla c[\partial D/\partial t + \vec{u} \cdot \nabla D]}$ assumes positive values throughout the flame brush, whereas the contributions of third and fourth terms on the right hand side of eq. 3f are responsible for the change in sign of $f(D)$ from negative in the unburned gas side to positive in the burned gas side. As $\overline{\rho \nabla c \cdot \nabla c[\partial D/\partial t + \vec{u} \cdot \nabla D]}$ is one of the major components of $f(D)$ and it scales with $(T_2/2)$, the net contribution of $f(D)$ can be scaled as $f(D) \sim T_2 \sim \rho_0 S_L^2/\delta_{th}^2$, whereas the resolved component, $\{f(D)\}_{res}$, can be taken to scale as:

$$\begin{aligned}\{f(D)\}_{res} &= 2\tilde{D}\frac{\partial \tilde{c}}{\partial x_k}\frac{\partial(\bar{\rho}\tilde{D})}{\partial x_k}\frac{\partial^2 \tilde{c}}{\partial x_j \partial x_j} + 2\tilde{D}\frac{\partial \tilde{c}}{\partial x_k}\frac{\partial^2(\bar{\rho}\tilde{D})}{\partial x_j \partial x_k}\frac{\partial \tilde{c}}{\partial x_j} - \frac{\partial}{\partial x_j}\left[\overline{\rho}\tilde{D}\left(\frac{\partial \tilde{c}}{\partial x_k}\frac{\partial \tilde{c}}{\partial x_k}\right)\frac{\partial \tilde{D}}{\partial x_j}\right] \\ &- 2\overline{\rho}\tilde{D}\frac{\partial \tilde{D}}{\partial x_j}\frac{\partial}{\partial x_j}\left(\frac{\partial \tilde{c}}{\partial x_k}\frac{\partial \tilde{c}}{\partial x_k}\right) + \overline{\rho}\left(\frac{\partial \tilde{c}}{\partial x_k}\frac{\partial \tilde{c}}{\partial x_k}\right)\left[\frac{\partial \tilde{D}}{\partial t} + \tilde{u}_j\frac{\partial \tilde{D}}{\partial x_j}\right] \sim \frac{\rho_0 S_L^2}{\delta_{th}^2} \times \left(\frac{\delta_{th}}{\Delta}\right)^4 \sim \frac{\rho_0 S_L^2}{\delta_{th}^2} \times \mathrm{Re}_\Delta^{-2}\, Da_\Delta^{-2}\end{aligned} \tag{7.60}$$

Equation (7.60) indicates that the contribution of $\{f(D)\}_{res}$ to $f(D)$ weakens with increasing $\Delta/\delta_{th} \sim \mathrm{Re}_\Delta^{1/2}\, Da_\Delta^{1/2}$. Scaling $\dot{w}$ and $(\partial \dot{w}/\partial n)$ using $\rho_0 S_L/\delta_{th}$ and $\rho_0 S_L/\delta_{th}^2$ respectively yields:

$$T_4 \sim \frac{\rho_0 S_L^2}{\delta_{th}^2} \tag{7.61}$$

whereas scaling $\nabla^2 c$ using $1/\delta_{th}^2$ (Swaminathan and Bray, 2005) provides:

$$(-D_2) \sim \frac{\rho_0 S_L^2}{\delta_{th}^2} \tag{7.62}$$

The resolved terms $(T_4)_{res}$ and $(-D_2)_{res}$ can in turn be scaled as:

$$(T_4)_{res} = 2\widetilde{D}\nabla\overline{\dot{w}}.\nabla\widetilde{c} \sim \frac{\rho_0 S_L^2}{\delta_{th}^2} \times \left(\frac{\delta_{th}}{\Delta}\right)^2 \sim \frac{\rho_0 S_L^2}{\delta_{th}^2} \times \mathrm{Re}_\Delta^{-1} Da_\Delta^{-1} \tag{7.63}$$

$$(-D_2)_{res} = -2\overline{\rho}\widetilde{D}^2\left(\frac{\partial^2\widetilde{c}}{\partial x_i \partial x_j}\right)\left(\frac{\partial^2\widetilde{c}}{\partial x_i \partial x_j}\right) \sim \frac{\rho_0 S_L^2}{\delta_{th}^2} \times \left(\frac{\delta_{th}}{\Delta}\right)^4 \sim \frac{\rho_0 S_L^2}{\delta_{th}^2} \times \mathrm{Re}_\Delta^{-2} Da_\Delta^{-2} \tag{7.64}$$

These estimates suggest that the magnitudes of $(T_4)_{res}$, $(-D_2)_{res}$ and $\{f(D)\}_{res}$ decrease with increasing Δ. Thus, the magnitudes of $(T_4)_{sg} = T_4 - (T_4)_{res}$, $(-D_2)_{sg} = -D_2 + (D_2)_{res}$ and $\{f(D)\}_{sg} = f(D) - \{f(D)\}_{res}$ remain of the order of $\rho_0 S_L^2/\delta_{th}^2 \sim \overline{\rho}\widetilde{N}_c^2$ for $\Delta >> \delta_{th}$.

The net contribution of $2\langle D\nabla\dot{w}\nabla c''\rangle$, $\langle\phi(D)\rangle$ and $(-2\langle\rho D^2(\nabla^2 c''\cdot\nabla^2 c'')\rangle)$ in the context of RANS scales as $\rho_0 S_L^2/\delta_{th}^2$ (Swaminathan and Bray, 2005), and is usually modelled collectively (Mantel and Borghi, 1994; Mura and Borghi, 2003; Chakraborty *et al*., 2018, 2010; Chakraborty *et al*., 2011d; Chakraborty and Swaminathan, 2010, 2013) as:

$$2\left\langle D\frac{\partial\dot{w}}{\partial x_i}\cdot\frac{\partial\dot{w}}{\partial x_i}\right\rangle + \langle\phi(D)\rangle - 2\left\langle\rho D^2\frac{\partial^2 c''}{\partial x_i\partial x_j}\frac{\partial^2 c''}{\partial x_i\partial x_j}\right\rangle = -\frac{\beta_2 < \rho > \hat{\varepsilon}^2}{[\hat{c}(1-\hat{c})]} \tag{7.65}$$

where $\beta_2 = 6.7$ is a model parameter (Chakraborty *et al*., 2008, 2010; Chakraborty and Swaminathan, 2010, 2013). As $(T_4)_{sg} - (D_2)_{sg} + \{f(D)\}_{sg}$ is expected to behave similar to $2\langle D\nabla\dot{w}\nabla c''\rangle + \langle\phi(D)\rangle - 2\langle\rho D^2(\nabla^2 c''\cdot\nabla^2 c'')\rangle$ for $\Delta >> \delta_{th}$ and these quantities scale as $\rho_0 S_L^2/\delta_{th}^2 \sim \overline{\rho}\widetilde{N}_c^2$, the existing RANS closure has been extended here for the modelling of $[T_4 + f(D) - D_2]$ as:

$$T_4 - D_2 + f(D) = (T_4)_{res} - (D_2)_{res} + \{f(D)\}_{res} - (1 - f_{TD})\beta_3(\tilde{c} - c^*)\overline{\rho}\frac{[\tilde{N}_c - \tilde{D}\nabla\tilde{c}.\nabla\tilde{c}]^2}{\tilde{c}(1-\tilde{c})} \quad (7.66)$$

where the last term on the right hand side of eq. (7.66) accounts for $(T_4)_{sg} - (D_2)_{sg} + \{f(D)\}_{sg}$, β_3 and c^* are the model parameters, and the term $(\tilde{c} - c^*)/[\tilde{c}(1-\tilde{c})]$ has been used to capture the correct qualitative behaviour of $[T_4 - D_2 + f(D)]$ across the flame brush. In eq. (7.66) $f_{TD} = \exp[-0.27(\Delta/\delta_z)^{1.7}]$ is a bridging function in terms of Δ/δ_z, which ensures:

$$\lim_{\Delta\to 0}[T_4 - D_2 + f(D)] = \lim_{\Delta\to 0}[(T_4)_{res} - (D_2)_{res} + \{f(D)\}_{res}]$$
$$= 2D\frac{\partial\dot{w}}{\partial x_i}\frac{\partial c}{\partial x_i} + \phi(D) - 2\rho D^2\frac{\partial^2 c}{\partial x_i \partial x_j}\frac{\partial^2 c}{\partial x_i \partial x_j} \quad \text{when } (1 - f_{TD}) \to 0.0 \quad (7.67)$$

A least squares method yielded the following optimum values of β_3, f_{TD} and c^* based on the current *a-priori* analysis:

$$\beta_3 = 5.7;\ f_{TD} = \exp[-0.27(\Delta/\delta_z)^{1.7}];\ \text{and}\ c^* = 1.0 - 0.83erf(0.5\Delta/\delta_z - 2.3) \quad (7.68)$$

The parameterisation of c^* ensures that the transition from positive to negative contribution of $[T_4 + f(D) - D_2]$ has been captured accurately for both $\Delta \le \delta_{th}$ and $\Delta > \delta_{th}$. The predictions of eq. (7.66) for the model parameters given by eq. (7.68) are shown in Fig. (7.18), which demonstrates that this model captures both the qualitative and quantitative behaviours of $[T_4 + f(D) - D_2]$ for both $\Delta \approx \delta_{th}$ (also for $\Delta < \delta_{th}$ but not shown here) and $\Delta >> \delta_{th}$ (e.g. $\Delta \approx 3.0\delta_{th}$) for different values of Re_t and τ.

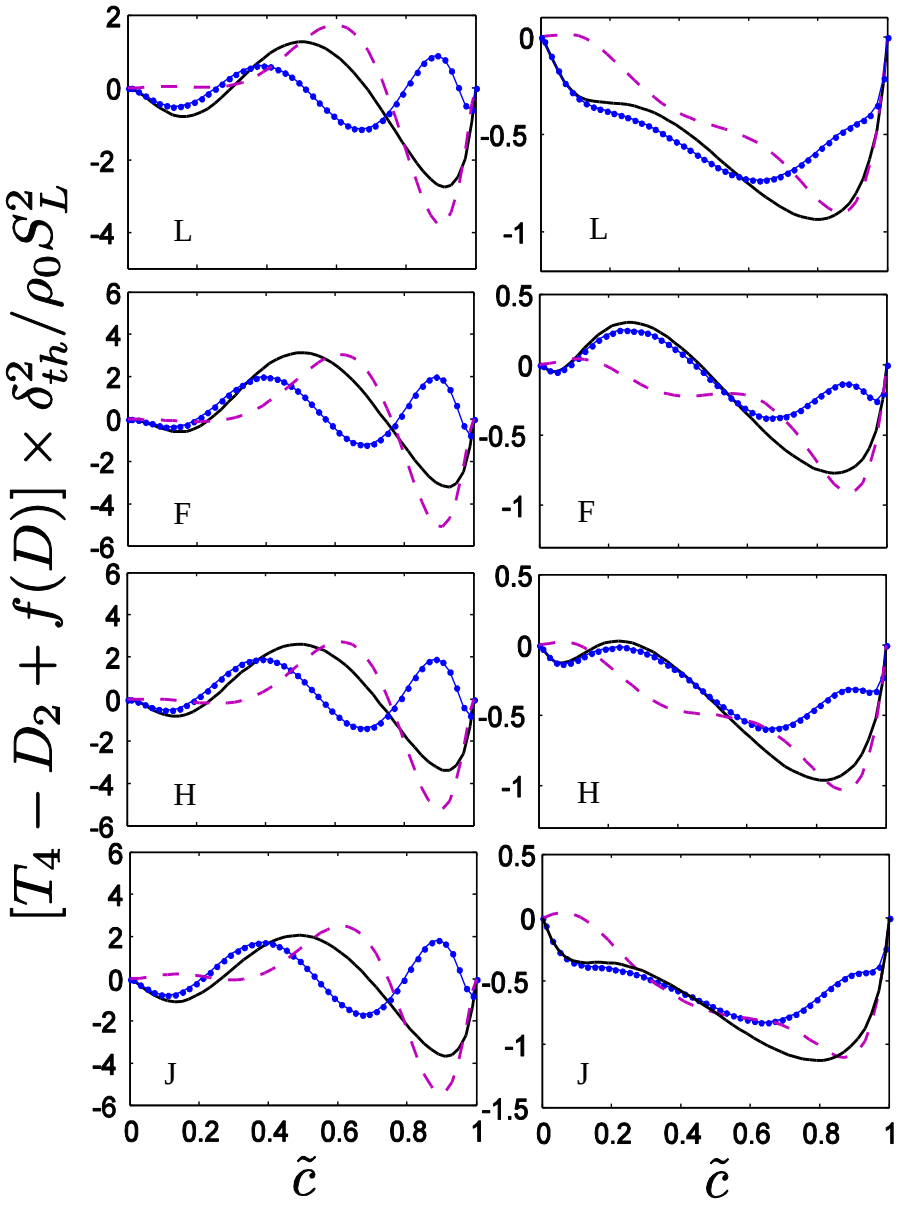

Figure 7.18: Variations of $[T_4 + f(D) - D_2]$ (——) and $[(T_4)_{sg} - (D_2)_{sg} + \{f(D)\}_{sg}]$ (—●—) conditionally averaged in bins of $\tilde{c}$ along with the predictions of eq. (7.66) (- - - -) for $\Delta \approx \delta_{th}$ (1st column) and $\Delta \approx 3.0\delta_{th}$ (2nd column) in cases L, F, H and J.

The combined contribution of the terms D_1, T_4, $f(D)$ and $(-D_2)$ can be expressed as (Chakraborty *et al*., 2008; Chakraborty *et al*., 2011d):

$$D_1 + T_4 - D_2 + f(D) \approx -2\overline{D\nabla.(\rho S_d \vec{n}|\nabla c|)|\nabla c|} + 2\overline{D\rho S_d \nabla.\vec{n}|\nabla c|^2} \qquad (7.69)$$

where $S_d = [\dot{w} + \nabla.(\rho D \nabla c)]/(\rho|\nabla c|)$ and $\vec{n} = -\nabla c/|\nabla c|$ are the flame displacement speed and local flame normal vector respectively.

It is evident from eq. (7.69) that the terms T_4, $f(D)$ and $(-D_2)$ scale with $\rho_0 S_L^2/\delta_{th}^2$, whereas D_1 scales as $D_1 \sim \rho_0 S_L^2/\delta_{th}^2 \times Da_\Delta^{-1} Ra_\Delta^{-1}$. This along with eq. (7.69) suggests that the net contribution of $[T_4 - D_2 + f(D)]$ originates due to flame normal propagation and flame curvature. This justifies modelling these terms together (Mantel and Borghi, 1994; Chakraborty *et al*., 2018, 2010; Chakraborty *et al*., 2011d; Chakraborty and Swaminathan, 2010, 2013). Although eq. (7.66) reasonably satisfactorily predicts $[T_4 + f(D) - D_2]$ for all cases considered here, modelling of the terms T_4, $f(D)$ and $(-D_2)$ collectively may lead to loss of their individual significances. As this is the very first attempt to model the SDR transport equation terms in the context of premixed combustion LES, there is a scope for further improvement in the future.

7.4 SDR transport modelling for non-unity Lewis turbulent premixed flames

7.4.1 Modelling of the turbulent transport term T_1

The unclosed term T_1 can be scaled in the following manner:

$$T_1 \sim \frac{\rho_0 \overline{\tau} g(Le) S_L \widetilde{N}_c}{\Delta} \sim \frac{\rho_0 \overline{\tau} g(Le) S_L^2}{\delta_{th}^2} \times Le \times Da_\Delta^{-0.5} \mathrm{Re}_\Delta^{-0.5} \text{ for } \Delta >> \delta_{th} \tag{7.70}$$

where $g(Le)$ is a function increasing with decreasing *Le*, which accounts for flame normal acceleration, S_L is used to scale the sub-grid velocity fluctuations associated with sub-grid scalar gradients, and the sub-grid fluctuations of SDR are taken to scale with S_L/δ_L. Alternatively, one obtains the following expression when the sub-grid velocity fluctuations are taken to scale with u'_Δ:

$$T_1 \sim \frac{\rho_0 u'_\Delta \widetilde{N}_c}{\Delta} \sim \frac{\rho_0 S_L^2}{\delta_{th}^2} \times Le \times Da_\Delta^{-1} \quad \text{for } \Delta >> \delta_{th} \tag{7.71}$$

It is worth noting that the scaling estimate given by eq. (7.70) (eq. (7.71)) is more appropriate for counter-gradient (gradient) transport. Equations (7.70) and (7.71) can be combined to suggest the following scaling estimate, which is valid for both gradient and counter-gradient transport:

$$T_1 \sim \frac{\overline{(\rho u_i N_c} - \overline{\rho}\widetilde{u}_i \widetilde{N}_c)}{\Delta} \sim \frac{\overline{(\rho u_i c} - \overline{\rho}\widetilde{u}_i \widetilde{c})\widetilde{N}_c}{\Delta} \quad \text{and}$$

$$\overline{(\rho u_i N_c} - \overline{\rho}\widetilde{u}_i \widetilde{N}_c) \sim \overline{(\rho u_i c} - \overline{\rho}\widetilde{u}_i \widetilde{c})\widetilde{N}_c \text{ for } \Delta >> \delta_{th} \tag{7.72}$$

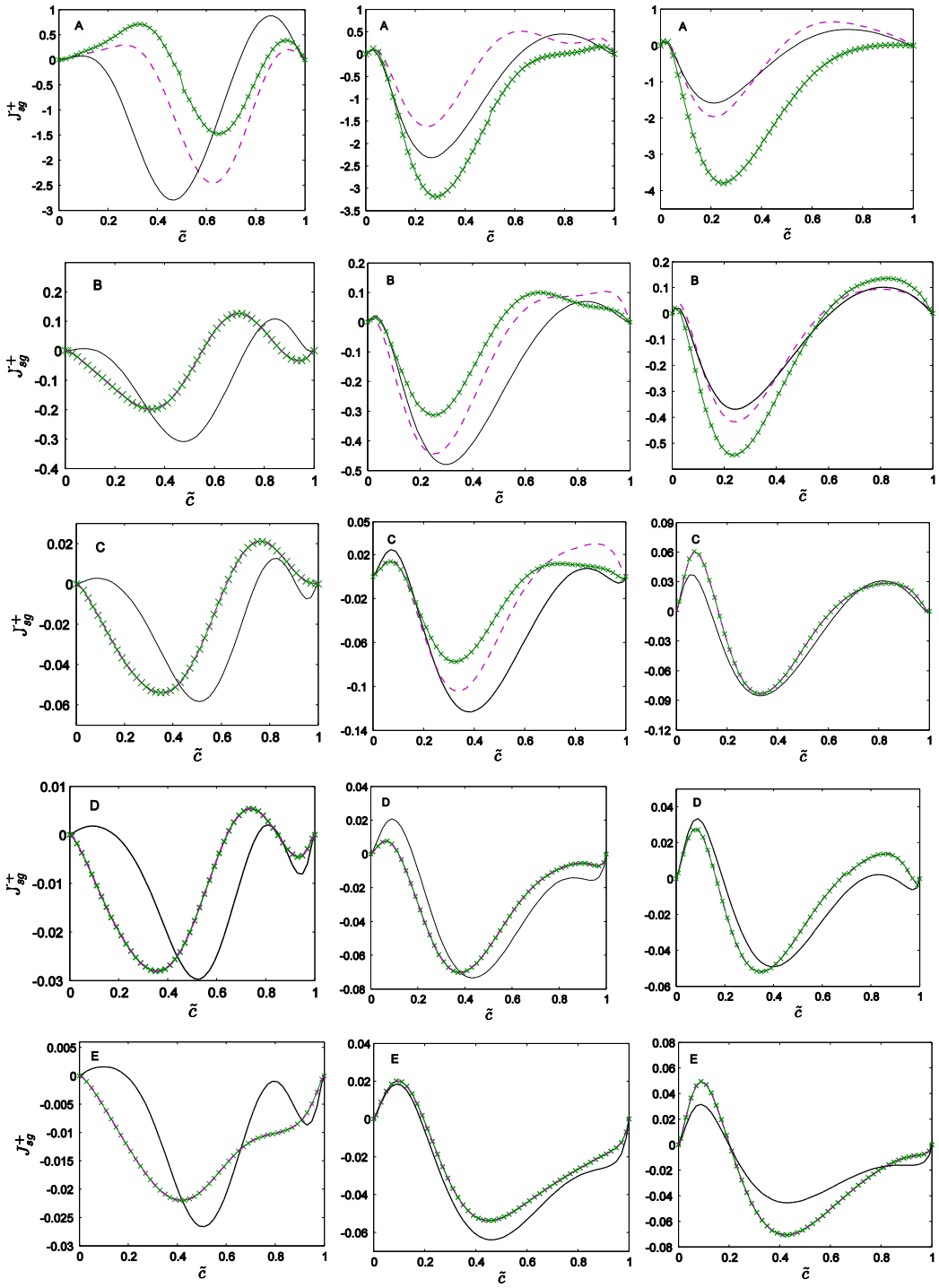

Figure 7.19: Variations of $J_{sg}^{+} = (\overline{\rho u_i N_c} - \overline{\rho}\tilde{u}_i \tilde{N}_c) M_i \times \delta_{th} / \rho_0 S_L^2$ (——) conditionally averaged in bins of $\tilde{c}$ along with the predictions of eqs. (7.43) and (7.44) with $\Phi' = 0.7$ (—×—) and eq. 6a and 6b with Φ' according to eq. (7.73) (- - - -) for $\Delta \approx 0.4\delta_{th}$ (1st column), $1.6\delta_{th}$ (2nd column) and $2.8\delta_{th}$ (3rd column) in cases A-E (1st-5th row).

The predictions of $J_{sg}^{+} = (\overline{\rho u_i N_c} - \overline{\rho}\tilde{u}_i \tilde{N}_c) M_i \times \delta_{th} / \rho_0 S_L^2$ according to the model in previous section, i.e. eq. (7.43), with $\Phi' = 0.7$ are compared to the corresponding quantity extracted from DNS data for $\Delta \approx 0.4\delta_{th}$, $1.6\delta_{th}$ and $2.8\delta_{th}$ in Fig. 7.19 for cases A-E.

Figure 7.19 shows that even though eq. (7.43) predicts J_{sg}^{+} in a reasonable manner in the cases with $Le \approx 1.0$ (e.g. cases C-E), this model does not adequately capture the correct qualitative and quantitative behaviours of J_{sg}^{+} for the flames with $Le << 1.0$ (i.e. cases A and B). The model given by eqs. (7.43) and (7.44) does not explicitly account for non-unity Lewis number effects, so it is not surprising that this model does not adequately capture the behaviour of $(\overline{\rho u_i N_c} - \overline{\rho}\widetilde{u}_i \widetilde{N}_c)$ for $Le << 1.0$ flames where the non-dimensional temperature $T^{+} = (T - T_0)/(T_{ad} - T_0)$ field is significantly different from c field, which alters the distribution of heat release and thermal expansion effects within the flame brush in comparison to the $Le \approx 1.0$ flames. This behaviour is mimicked here by introducing Le dependence of the model parameter Φ' in the following manner:

$$\Phi' = 0.3(1 - Le) + 0.7 \tag{7.73}$$

The predictions of the model given by eq. (7.73) with Φ' according to eq. (7.73) are also shown for in Fig.7.19, which shows that the model with new parameterisation $\Phi' = 0.3(1 - Le) + 0.7$ predicts J_{sg}^{+} satisfactorily for all filter widths in all cases considered here and the agreement between the predictions of eq. (7.43) and DNS data improves with increasing Δ (see Fig. 7.19). It worth noting that the sub-grid flux of scalar (i.e. $\overline{\rho u_i c} - \overline{\rho}\widetilde{u}_i \widetilde{c}$) itself requires modelling in LES, and the performance of the models for $(\overline{\rho u_i N_c} - \overline{\rho}\widetilde{u}_i \widetilde{N}_c)$ and the turbulent transport term T_1 depend on the modelling of $(\overline{\rho u_i c} - \overline{\rho}\widetilde{u}_i \widetilde{c})$. The modelling of $(\overline{\rho u_i c} - \overline{\rho}\widetilde{u}_i \widetilde{c})$ is beyond the scope of current analysis and interested readers are referred to Appendix for further discussion on the modelling of $(\overline{\rho u_i c} - \overline{\rho}\widetilde{u}_i \widetilde{c})$ for non-unity Lewis number flames.

7.4.2 Modelling of the density variation term T_2

According to previous analyses, T_2 can be scaled for flames with low Mach number globally adiabatic $Le \neq 1.0$ flames as:

$$T_2 \sim 2\overline{\left(\rho \frac{\partial u_i}{\partial x_i} N_c\right)} \sim \frac{\rho_0 \tau S_L^2}{Le^{m-1}\delta_{th}^2} \tag{7.74}$$

where m is a positive number greater than unity (i.e. $m > 1$).

Term	**Model expression**
$[\overline{\rho u_i N_c} - \overline{\rho}\tilde{u}_i\tilde{N}_c]$	$[\overline{\rho u_i N_c} - \overline{\rho}\tilde{u}_i\tilde{N}_c] = (\Phi - \tilde{c})\frac{\gamma_1[\overline{\rho u_i c} - \overline{\rho}\tilde{u}_i\tilde{c}] - \gamma_2\overline{\rho}\tilde{c}(1-\tilde{c})u'_\Delta M_i}{\tilde{c}(1-\tilde{c})}\tilde{N}_c$ $- \overline{\rho}(C_F\Delta)u'_\Delta\frac{\partial\tilde{N}_c}{\partial x_i}$ where $\gamma_1 = 1.8$, $\gamma_2 = 4.9 - 3.2erf(0.15\mathrm{Re}_{t\Delta})$, $\mathrm{Re}_{t\Delta} = \rho_0 u'_\Delta\Delta/\mu_0$, $\Phi = 0.3(Le-1)+0.7$ and $C_F = 0.11$
T_2	$T_2 = \overline{\rho}\tilde{D}\nabla\tilde{c}.\nabla\tilde{c}\frac{\partial\tilde{u}_i}{\partial x_i} + \frac{K_c^* f_{T_2}(Le)S_L}{(1.0+Ka_\Delta)^{1/2}\delta_{th}}[\overline{\rho}\tilde{N}_c - \overline{\rho}\tilde{D}\nabla\tilde{c}.\nabla\tilde{c}]$ where $Ka_\Delta = (u'_\Delta/S_L)^{3/2}(\Delta/\delta_{th})^{-1/2}$ is local sub-grid Karlovitz number and $f_{T_2}(Le) = \frac{3.3}{Le^{2.57}erf[4(1.0-Le)+1.4]}$.
T_3	$T_3 = -2\overline{\rho D}\frac{\partial\tilde{c}}{\partial x_i}\frac{\partial\tilde{u}_i}{\partial x_j}\frac{\partial\tilde{c}}{\partial x_j} + (1-f_{T_3})[C_3 - C_4\Gamma(Le)\tau.Da^*_\Delta]\frac{u'_\Delta}{\Delta}\overline{\rho}\tilde{N}_c$ where $C_3 = 7.5$, $C_4 = 0.75(1.0+Ka_\Delta)^{-0.4}$, $f_{T_3} = \exp[-1.05(\Delta S_L/\alpha_{T0})^2]$ and $Da^*_\mathrm{L} = S_L\rho_0\Delta/u'_\Delta\overline{\rho}\delta_{th}$ $\Gamma(Le) = \frac{1.7(1-\tilde{c})^p}{Le^{2.57}}\left(\frac{\delta_L}{\delta_{th}}\right)^{1.3}$ with $p = 0.2+1.5(1-Le)$
$[T_4 - D_2 + f(D)]$	$T_4 - D_2 + f(D) = (T_4)_{res} - (D_2)_{res} + \{f(D)\}_{res}$ $-(1-f_{TD})\beta'_3\overline{\rho}(\tilde{c}-c^*)\frac{[\tilde{N}_c - \tilde{D}\nabla\tilde{c}.\nabla\tilde{c}]^2}{\tilde{c}(1-\tilde{c})}$ where $(T_4)_{res} = 2\tilde{D}\frac{\partial\overline{\dot{w}}}{\partial x_i}\frac{\partial\tilde{c}}{\partial x_i}$, $(-D_2)_{res} = -2\overline{\rho}\tilde{D}^2\frac{\partial^2\tilde{c}}{\partial x_i\partial x_j}\frac{\partial^2\tilde{c}}{\partial x_i\partial x_j}$, $\{f(D)\}_{res} = 2\tilde{D}\frac{\partial\tilde{c}}{\partial x_k}\frac{\partial(\overline{\rho}\tilde{D})}{\partial x_k}\frac{\partial^2\tilde{c}}{\partial x_j\partial x_j}$ $+2\tilde{D}\frac{\partial\tilde{c}}{\partial x_k}\frac{\partial^2(\overline{\rho}\tilde{D})}{\partial x_j\partial x_k}\frac{\partial\tilde{c}}{\partial x_j} - \frac{\partial}{\partial x_j}\left[\overline{\rho}\tilde{D}\nabla\tilde{c}.\nabla\tilde{c}\frac{\partial\tilde{D}}{\partial x_j}\right]$, $-2\overline{\rho}\tilde{D}\frac{\partial\tilde{D}}{\partial x_j}\frac{\partial(\nabla\tilde{c}.\nabla\tilde{c})}{\partial x_j} + \overline{\rho}\nabla\tilde{c}.\nabla\tilde{c}\left[\frac{\partial\tilde{D}}{\partial t} + \tilde{u}_j\frac{\partial\tilde{D}}{\partial x_j}\right]$ $f_{TD} = \exp[-0.27(S_L\Delta/\alpha_{T0})^{1.7}]$, $c^* = 1.0 - 0.83erf[0.5(\Delta S_L/\alpha_{t0}) - 2.3]$ and $\beta'_3 = 5.7/Le^{0.2}$

Table 7.3: Summary of the proposed models for the unclosed terms of the SDR $\tilde{N}_c$ transport equation for non-unity Lewis flames.

The resolved part of T_2 can be taken as:

$$(T_2)_{res} = \overline{\rho}\widetilde{D}\nabla\widetilde{c}.\nabla\widetilde{c}\,\frac{\partial\widetilde{u}_i}{\partial x_i} \sim \frac{\rho_0 S_L^2}{\delta_{th}^2} \times \frac{U_{ref}}{S_L} \times Le^{-1}\,\mathrm{Re}_\Delta^{-1.5}\,Da_\Delta^{-1.5} \tag{7.75}$$

where U_{ref} is a velocity scale representing the Favre-filtered velocity components $\widetilde{u}_i$. The above scaling estimates demonstrate that T_2 remains of the order of $\rho_0 S_L^2/\delta_{th}^2$ irrespective of Δ. By contrast, the magnitude of $(T_2)_{res}$ remains comparable to $\rho_0 S_L^2/\delta_{th}^2$ for $U_{ref} \sim S_L$ and $\Delta \approx \delta_{th}$, but the magnitude of $(T_2)_{res}$ is expected to decrease with increasing Δ.

This suggests that the sub-grid component $(T_2)_{sg} = T_2 - (T_2)_{res}$ plays an increasingly important role with increasing Δ, which can be substantiated from Fig. 7.20 where the variations of the mean values of T_2 and $(T_2)_{sg} = T_2 - (T_2)_{res}$ conditional on $\widetilde{c}$ are shown for cases A-E for $\Delta \approx 0.4\delta_{th}$, $1.6\delta_{th}$ and $2.8\delta_{th}$.

The prediction of eq.(7.49) is also shown in Fig. 7.20 for cases A-E for $\Delta \approx 0.4\delta_{th}$, $1.6\delta_{th}$ and $2.8\delta_{th}$. A comparison between the predictions of eq. (7.49) and the normalised T_2 extracted from explicitly filtered DNS data reveals that eq. (7.49) satisfactorily predicts T_2 for a range of different filter widths for flames with $Le \approx 1.0$ (e.g. cases C-E) but this model significantly under-predicts the magnitude of T_2 for the $Le << 1.0$ cases (e.g. cases A and B). The magnitude of T_2 is expected to increase with decreasing Le due to the strengthening of heat release effects as a result of enhanced burning rate for small values of Lewis number (see Table 6.1). As this effect is missing in eq. (7.49), this model under-predicts the magnitude of T_2 for the $Le << 1.0$ cases (e.g. cases A and B) where the effects of enhanced heat release due to differential diffusion of heat and mass are particularly strong.

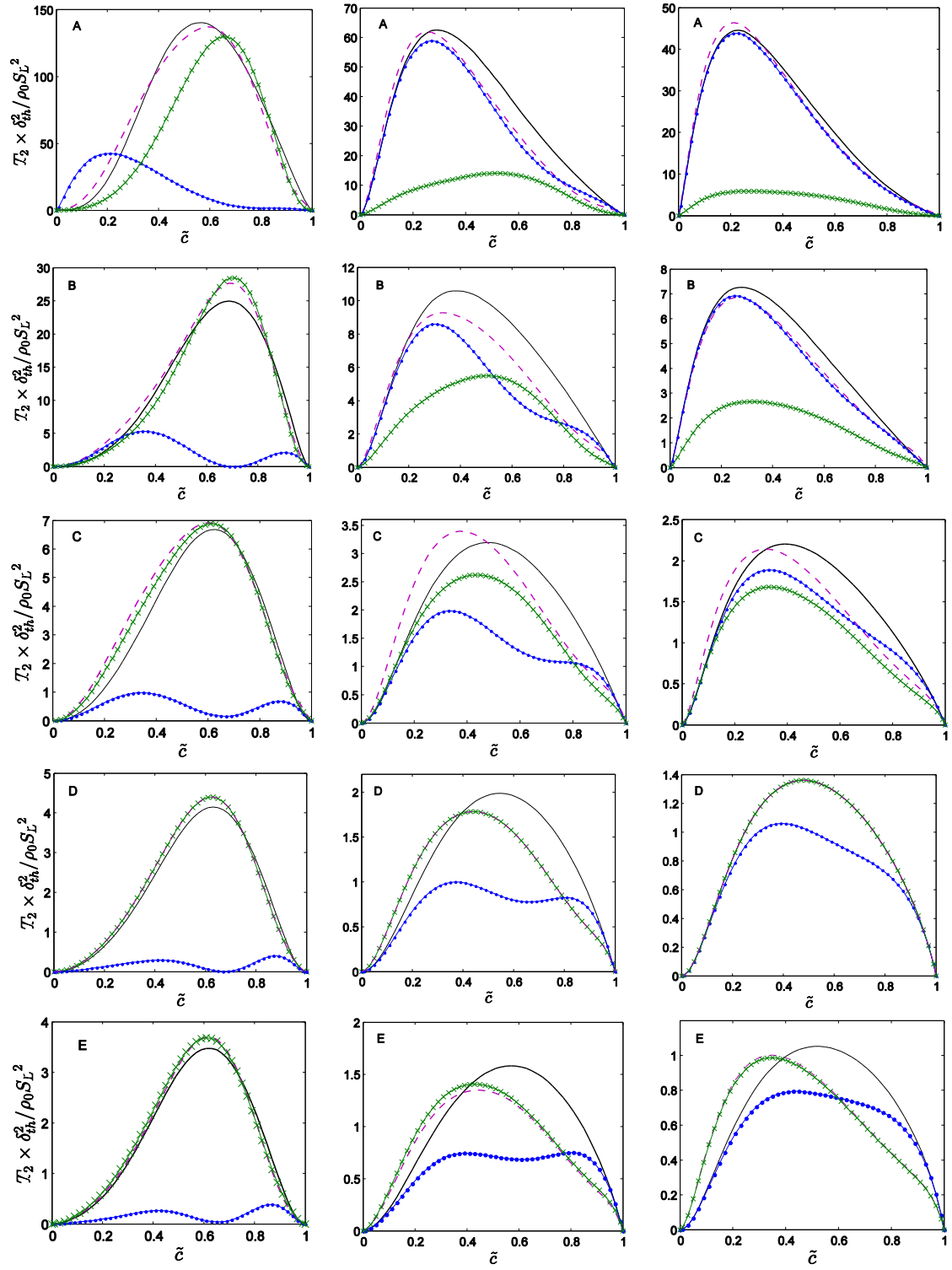

Figure 7.20: Variations of T_2 (——) and $(T_2)_{sg}$ (—●—) conditionally averaged in bins of $\tilde{c}$ along with the predictions of eq.(7.49) (—×—) and eq. (7.76) (- - - -) for $\Delta \approx 0.4\delta_{th}$ (1st column), $1.6\delta_{th}$ (2nd column) and $2.8\delta_{th}$ (3rd column) in cases A-E (1st-5th row). All the terms are normalised with respect to $\rho_0 S_L^2 / \delta_{th}^2$.

Here the model given by eq. (7.49) has been extended in order to account for the effects of *Le* in the following manner:

$$T_2 = \overline{\rho}\widetilde{D}\nabla\widetilde{c}.\nabla\widetilde{c}\,\frac{\partial\widetilde{u}_i}{\partial x_i} + f_{T_2}(Le)\frac{K_c^* S_L}{\delta_{th}(1.0+Ka_\Delta)^{1/2}}[\overline{\rho}\widetilde{N}_c - \overline{\rho}\widetilde{D}\nabla\widetilde{c}.\nabla\widetilde{c}] \qquad (7.76)$$

$$\text{where } f_{T_2}(Le) = \frac{3.3}{Le^{2.57}erf[4(1.0-Le)+1.4]} \text{ and } K_c^* = \frac{\delta_{th}}{S_L}\frac{\int_0^1[\rho N_c\nabla\cdot\vec{u}f(c)]_L\,dc}{\int_0^1[\rho N_c f(c)]_L\,dc} \qquad (7.77)$$

In eq. (7.77) $f_{T_2}(Le)$ accounts for the strengthening of heat release effects with decreasing Le. The parameter K_c^* is a thermo-chemical parameter, which provides information regarding the SDR-weighted dilatation rate $\nabla\cdot\vec{u}$.

The thermo-chemical parameter K_c^* accounts for the correlation between $\nabla\cdot\vec{u}$ and ρN_c within the flame front. It is possible to approximate $f(c)$ as: $f(c)=1/|\nabla c|_L$, which enables one to evaluate K_c^* from laminar flame data. The thermo-chemical parameter K_c^*/τ is also affected by Le and it is equal to 0.52, 0.67, 0.71, 0.78 and 0.79 for the $Le=0.34$, 0.6, 0.8, 1.0 and 1.2 flames considered here. The predictions of eq. (7.76) are compared with respect to the predictions from eq. (7.49) and T_2 extracted from DNS data in Fig. 7.20, which shows that eq. (7.76) satisfactorily predicts the quantitative behaviour of T_2 for a range of different values of Δ for flames with *Le* ranging from 0.34 to 1.2.

7.4.3 Modelling of the scalar turbulence interaction term T_3

The variations of the mean values of T_3 conditional on $\widetilde{c}$ are shown in Fig. 7.21 for cases A-E at $\Delta\approx 0.4\delta_{th}$, $1.6\delta_{th}$ and $2.8\delta_{th}$. Figure 7.21 shows that T_3 assumes predominantly negative values throughout the flame brush for cases A-C but assumes positive (negative) values towards the unburned (burned) gas side of the flame brush in cases D and E. Equation (7.52) suggests that a predominant collinear alignment of ∇c with e_α (e_γ) leads to a negative (positive) value of T_3. The flame normal acceleration strengthens with decreasing Le, and thus ∇c predominantly aligns with e_α for the $Le<<1$ flames (e.g. cases A and B) which leads to negative values of T_3. By contrast, turbulent straining overcomes the flame normal acceleration on both ends of the flame brush for the $Le\approx 1.0$ cases considered here (e.g. cases C-E), which leads to positive values of T_3 both on

unburned and burned gas sides of the flame brush. However, the flame normal acceleration dominates over turbulent straining in the middle of the flame brush where the effects of heat release are strong even in the $Le \approx 1.0$ cases considered here (e.g. cases C-E), which leads to negative values of T_3 for the major portion of the flame brush in these cases.

The effects of ∇c alignment with e_α on T_3 can be scaled in the following manner:

$$T_3 \sim \frac{\rho_0 \tau S_L \tilde{N}_c}{Le^n \delta_{th}} \sim \frac{\rho_0 \tau S_L^2}{Le^{n-1} \delta_{th}^2} \tag{7.78}$$

whereas the contribution of ∇c alignment with e_γ on T_3 can be scaled as:

$$T_3 \sim \frac{\rho_0 u'_\Delta \tilde{N}_c}{\Delta} \sim \frac{\rho_0 S_L^2}{\delta_{th}^2} \times Le \times \mathrm{Pr}^{-1/2} \times Ka_\Delta \quad \text{for } \Delta >> \delta_{th} \tag{7.79}$$

The Lewis number Le dependence in eq. 11a (with $n > 1$) accounts for greater extent of ∇c alignment with e_α for the flames with $Le << 1.0$. A comparison of eqs. (7.54) and (7.79) reveals that the contribution of $(T_3)_{res}$ to T_3 is expected to weaken with increasing Δ, and this behaviour can indeed be seen from Fig. 7.21, which shows that the magnitude of $(T_3)_{res}$ decreases with increasing Δ.

The modelling of T_3 for unity *Le* cases, i.e. eq. (7.56) with the model parameters given by eq. (7.58) are compared with T_3 extracted from DNS data in Fig. 7.21, which shows that eq. (7.56) adequately captures the qualitative and quantitative behaviours of T_3 for the $Le \approx 1.0$ cases considered here (e.g. cases C-E) but this model has been found to under-predict the magnitude of the negative contribution of T_3 in the $Le << 1.0$ cases (e.g. cases A and B) for $\Delta > \delta_{th}$. It has already been noted that the increased extent of scalar gradient destruction in the $Le << 1.0$ flames due to preferential ∇c alignment with e_α under strong action of flame normal acceleration is not addressed in the model given by eq. (7.56). Thus, this model underpredicts the negative contribution of T_3 for the flames with $Le << 1.0$.

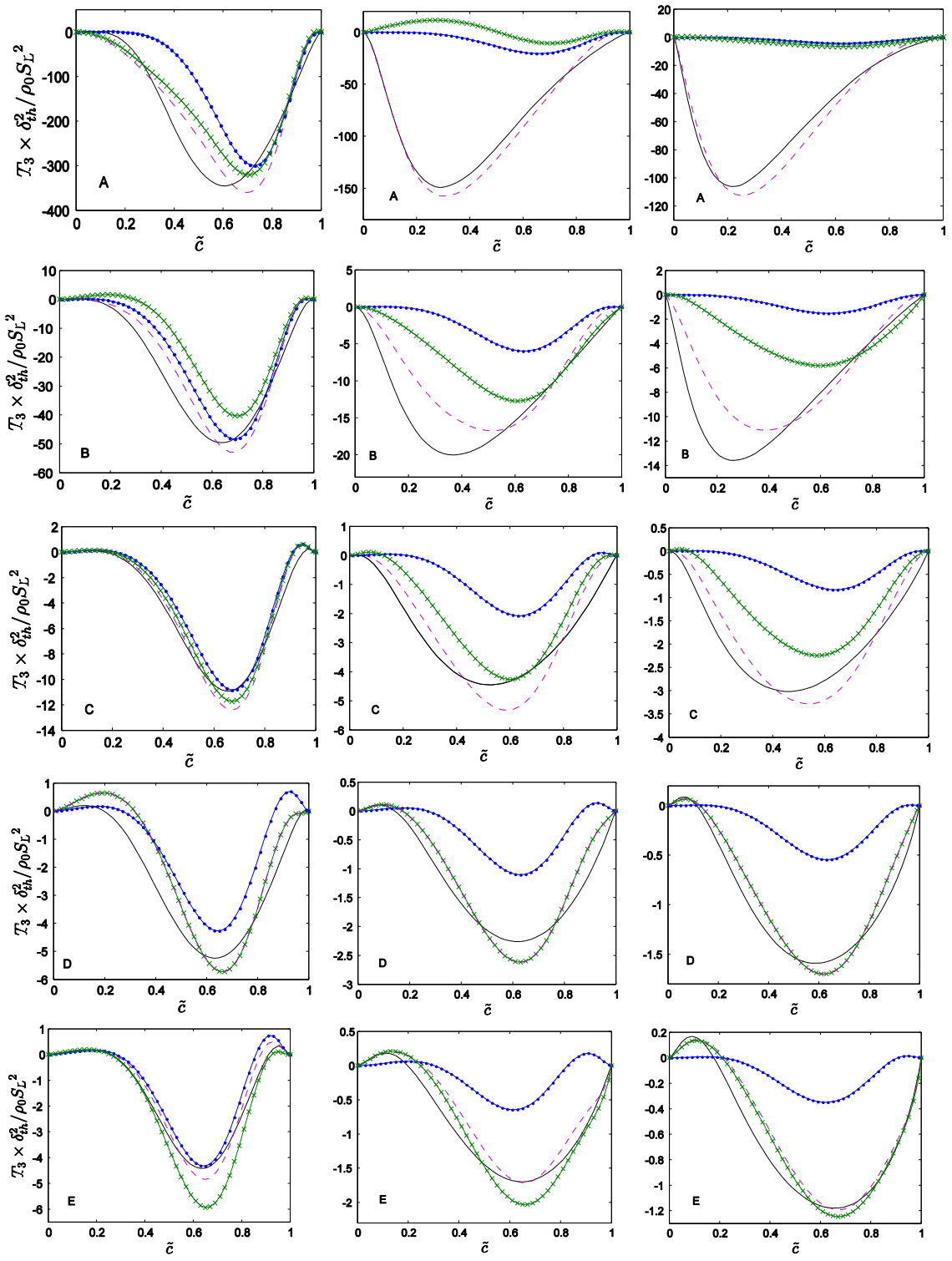

Figure 7.21: Variations of T_3 (——) and $(T_3)_{res}$ (—●—) conditionally averaged in bins of $\tilde{c}$ along with the predictions of eqs.(7.56) and (7.58) (—×—) and eqs. (7.80) and (7.81) (- - - -) for $\Delta \approx 0.4\delta_{th}$ (1st column), $\Delta \approx 1.6\delta_{th}$ (2nd column) and $\Delta \approx 2.8\delta_{th}$ (3rd column) in cases A-E (1st-5th row).

Here eq. (7.56) has been modified in the following manner to account for non-unity Lewis number effects:

$$T_3 = -2\overline{\rho D}\frac{\partial \tilde{c}}{\partial x_i}\frac{\partial \tilde{u}_i}{\partial x_j}\frac{\partial \tilde{c}}{\partial x_j} + (1 - f_{T_3})[C_3 - C_4\Gamma(Le)\tau.Da^*_\Delta]\frac{u'_\Delta}{\Delta}\overline{\rho}\tilde{N}_c \qquad (7.80)$$

$$\text{where} \qquad \Gamma(Le) = \frac{1.7(1-\tilde{c})^p}{Le^{2.57}}\left(\frac{\delta_L}{\delta_{th}}\right)^{1.3} \quad \text{and} \quad p = 0.2 + 1.5(1.0 - Le) \qquad (7.81)$$

The involvement of the function $\Gamma(Le)$ in eq. (7.81) account for the strengthening of ∇c alignment with e_α under strong actions of flame normal acceleration in flames with small values of Lewis number. The presence of $(1-\tilde{c})^p$ helps eq. (7.81) to capture the qualitative behaviour of T_3 across the flame brush. It can be seen from Fig. 7.21 that the model given by eq. (7.81) provides satisfactory qualitative and quantitative predictions of T_3 for all the flames with different values of *Le* for a range of different values of Δ.

7.4.4 Modelling of the combined reaction, dissipation and diffusivity gradient contribution [T_4-D_2+$f(D)$]

The variations of the mean values of $[T_4 - D_2 + f(D)]$ conditional on $\tilde{c}$ are shown in Fig.7.22 for A-E for $\Delta \approx 0.4\delta_{th}$, $1.6\delta_{th}$ and $2.8\delta_{th}$. It can be seen from Fig. 7.22 that $[T_4 - D_2 + f(D)]$ acts as a sink (source) term towards the burned (unburned) gas side of the flame brush for $\Delta \approx 0.4\delta_{th}$ and $\Delta \approx 1.6\delta_{th}$, but the mean value of $[T_4 - D_2 + f(D)]$ conditional on $\tilde{c}$ assumes predominantly negative values for $\Delta \approx 2.8\delta_{th}$. It can be seen from Table 7.3 that the order of magnitudes of T_4, $(-D_2)$ and $f(D)$ remain comparable according to the scaling estimates and their magnitudes are expected to increase with decreasing Le. Furthermore, the scaling estimates of $(T_4)_{res}$, $(-D_2)_{res}$ and $\{f(D)\}_{res}$ in Table 6.1 suggest that their contributions are expected to weaken with increasing Δ. Thus, the sub-grid components $(T_4)_{sg} = T_4 - (T_4)_{res}$, $(-D_2)_{sg} = -D_2 + (D_2)_{res}$ and $\{f(D)\}_{sg} = f(D) - \{f(D)\}_{res}$ are expected to play major roles for $\Delta >> \delta_{th}$. The aforementioned behaviours of the resolved and sub-grid components of T_4, $(-D_2)$ and $f(D)$ can be confirmed from Fig. 7.22. It can be seen from Table 6.1 that the magnitudes of $(T_4)_{sg}$, $(-D_2)_{sg}$ and $\{f(D)\}_{sg}$ remain of the order of $\rho_0 S_L^2/\delta_{th}^2 \sim \overline{\rho}\tilde{N}_c^2$ for $\Delta >> \delta_{th}$

but their magnitudes are expected to increase with decreasing *Le*, which can indeed be substantiated from Fig. 7.22.

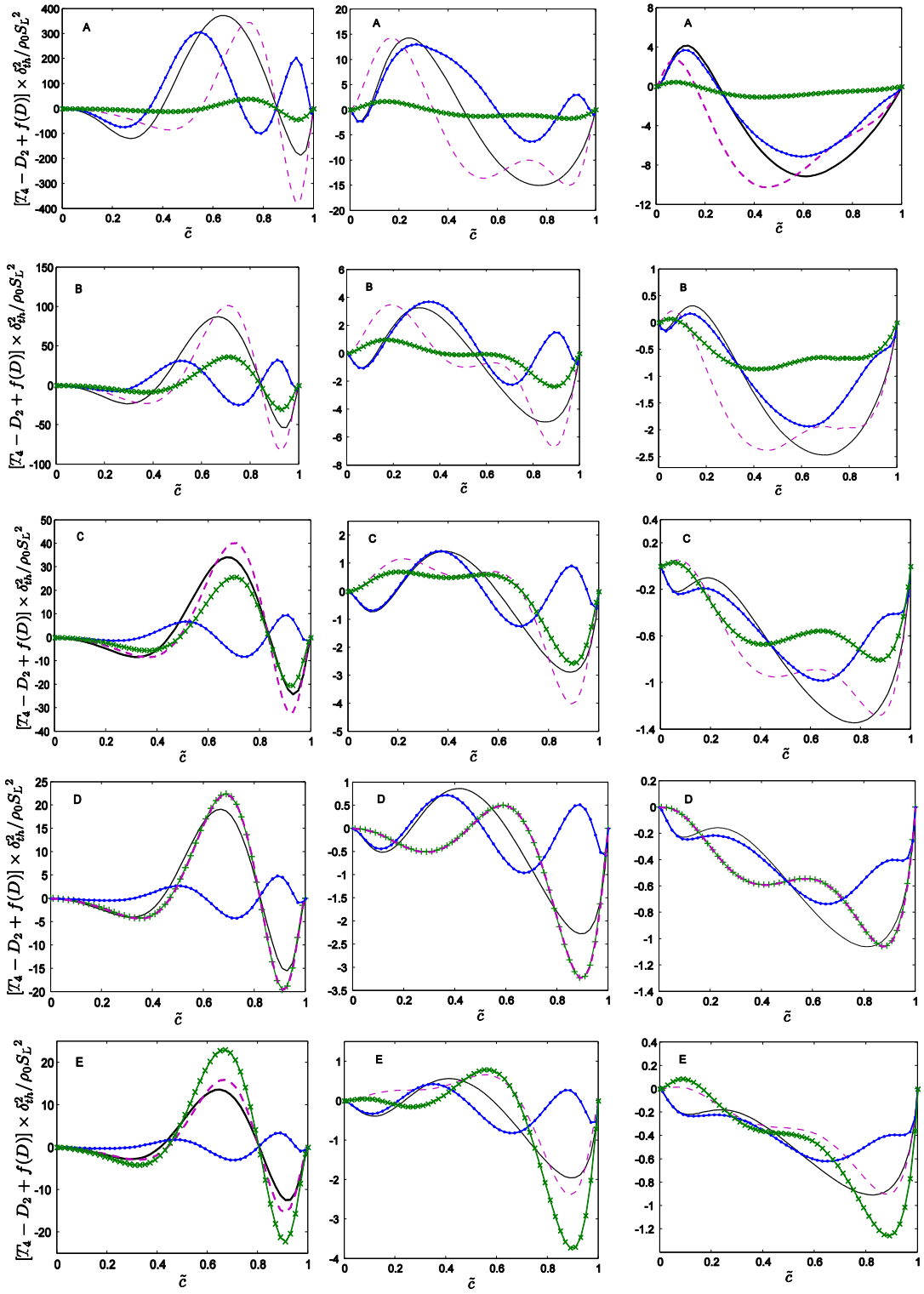

Figure 7.22: Variations of $[T_4 + f(D) - D_2]$ (——) and $[(T_4)_{sg} - (D_2)_{sg} + \{f(D)\}_{sg}]$ (—●—) conditionally averaged in bins of $\tilde{c}$ along with the predictions of eqs.15i and 15ii (—×—) and eq. 16 (- - - -) for $\Delta \approx 0.4\delta_{th}$ (1st column), $1.6\delta_{th}$ (2nd column) and $2.8\delta_{th}$ (3rd column) in cases A-E (1st-5th row). All the terms are normalised with respect to $\rho_0 S_L^2/\delta_{th}^2$.

The predictions of eq. (7.66) are shown in Fig. 7.22, which show that this model captures both the qualitative and quantitative behaviours of $[T_4 + f(D) - D_2]$ for the $Le \approx 1.0$ cases considered here (e.g. case C-E) but this model under-predicts the magnitude of $[T_4 + f(D) - D_2]$ significantly for the $Le << 1.0$ cases (e.g. cases A and B). It is worth noting that the model given by eq. 15a does not account for the increased magnitude of $\{T_4 - D_2 + f(D)\}_{sg}$ for small values of Le (see Table 7.3) so perhaps it is not surprising that this model under-predicts the magnitude of $[T_4 + f(D) - D_2]$ for the flames with $Le << 1.0$ (e.g. cases A and B). The increased magnitude of $[T_4 + f(D) - D_2]$ for small values of Le is accounted for by modifying eq. 15a in the following manner:

$$T_4 - D_2 + f(D) = (T_4)_{res} - (D_2)_{res} + \{f(D)\}_{res} - (1 - f_{TD})\beta_3'(\tilde{c} - c^*)\overline{\rho}\frac{[\tilde{\dot{N}}_c - \tilde{D}\nabla\tilde{c}.\nabla\tilde{c}]^2}{\tilde{c}(1-\tilde{c})} \text{ with } \quad \beta_3' = 5.7Le^{-0.2} \tag{7.82}$$

where c^* and f_{TD} are kept the same as in eq. (7.68). The predictions of eq. (7.68) are shown in Fig. 7.22, which demonstrates that eq. (7.68) captures both the qualitative and quantitative behaviours of $[T_4 + f(D) - D_2]$ for a range of different filter widths for all the different *Le* cases considered here.

7.5 Summary

This chapter has disccuessed the models of the unclosed terms of SDR transport equation based on a-priori analysis of a simple chemistry DNS databse. It is worth noting that the flamelet assumption is invoked while deriving these models so they are expected to remain valid in the corrugated flamelets and thin reaction zones regimes (Peters, 2000) of turbulent premixed combustion.

The scaling estimates and the newly proposed models for the aforementioned unclosed terms of the SDR $\tilde{\dot{N}}_c$ transport equation are summarised in Table 7.3 for quick reference for the readers and future potential users of these models. The scaling estimates in Table 6.1 suggest that the terms $T_2, T_3, T_4, (-D_2)$ and $f(D)$ remain leading order contributors to the SDR $\tilde{\dot{N}}_c$ transport and the magnitude of T_1 remains negligible in comparison to the

terms $T_2, T_3, T_4, (-D_2)$ and $f(D)$ irrespective of Damköhler and turbulent Reynolds numbers. It is worth noting that some of the unresolved components of T_1 and T_3 can be neglected in the context of RANS simulations for high values of turbulent Reynolds number Re_t. The components, which do not play an important role in RANS, may not be negligible in the context of LES because of partial resolution of the flow field. Thus, the terms T_1 and T_3 are modelled on their own in the context of LES without splitting them into their components. It is also worth noting that although Table 6.1 suggests that the magnitude of T_1 is negligible compared to $T_2, T_3, T_4, (-D_2)$ for all Δ in all cases, the turbulent transport term T_1 still need to be modelled and included in the model implementation for LES for numerical stability.

The newly proposed models for the unclosed terms of the SDR $\tilde{N}_c$ transport equation are summarised in Table 7.3 for quick reference for the readers and future potential users of these models. The scaling estimates in Table 6.1 indicate that the terms $T_2, T_3, T_4, (-D_2)$ and $f(D)$ remain leading order contributors to the SDR $\tilde{N}_c$ transport and the magnitude of T_1 remains negligible in comparison to the terms $T_2, T_3, T_4, (-D_2)$ and $f(D)$ irrespective of Damköhler and turbulent Reynolds numbers. This is consistent with the observations made from Fig. 7.15. However, the turbulent transport term T_1 still need to be modelled and included in the model implementation for LES for numerical stability.

Chapter 8. Assessment of SDR closures for detailed chemistry cases

The algebraic SDR closure and the closures of unclosed terms of the SDR transport equation discussed in Chapters 6 and 7 are assessed in this chapter using a three-dimensional detailed chemistry based V-flame DNS database of stoichiometric hydrogen-air turbulent premixed flames, where the assessments of models are based on reaction progress variable defined based on the mass fractions of two species H_2O (major product) and H_2 (reactant). The reaction progress variable (RPV) based on mass fractions of H_2O and H_2 are denoted as c_{H_2O} and c_{H_2} respectively, which are defined in the following manner:

$$c_{H_2} = \frac{(Y_{H_2})_0 - (Y_{H_2})}{(Y_{H_2})_0 - (Y_{H_2})_\infty} \text{ and } c_{H_2O} = \frac{(Y_{H_2O}) - (Y_{H_2O})_0}{(Y_{H_2O})_\infty - (Y_{H_2})_0} \tag{8.1}$$

where $(Y_{H_2})_0 = 0.028$, $(Y_{H_2O})_0 = 0.0$, $(Y_{H_2})_\infty = 0.0$ and $(Y_{H_2O})_\infty = 0.255$ for stoichiometric H_2-air premixed flame. The assessment of the SDR algebraic closure will be provided in the following section, which will be followed by the assessment of the modelled unclosed terms of filtered SDR transport equation. A brief conclusion will be provided by the end of this chapter.

8.1 Assessment of algebraic closure

8.1.1 The statistical behaviour of SDR with PRV based on different species

The SDRs for reaction progress variable based on hydrogen (i.e. c_{H_2}) and water (i.e. c_{H_2O}) mass fraction are denoted as $\widetilde{N}_{c_{H_2}}$ and $\widetilde{N}_{c_{H_2O}}$ respectively.

It can be observed from Fig. 8.1 that the magnitude of $\tilde{N}_c$ conditional on bins of $\tilde{c}$ are decreasing with increasing filter width Δ, consistent with the findings in previous chapters. The above scaling arguments suggest the resolved components of $\tilde{N}_c$ decreases with increasing Δ, leading to lower magnitude of $\tilde{N}_c = \tilde{D}\nabla\tilde{c}\cdot\nabla\tilde{c} + (\tilde{N}_c)_{sg}$ for larger filter width. The diminishing peak value of $\tilde{N}_c$ conditional on bins of $\tilde{c}$ resulting from the averaging process involved in LES filtering is also observable from Fig. 8.1. Note that

the magnitudes of the peak values of $\widetilde{N}_{c_{H_2}}$ is generally greater than $\widetilde{N}_{c_{H_2O}}$ which can be explained by the differential diffusion of effects as $Le_{H_2} < Le_{H_2O}$.

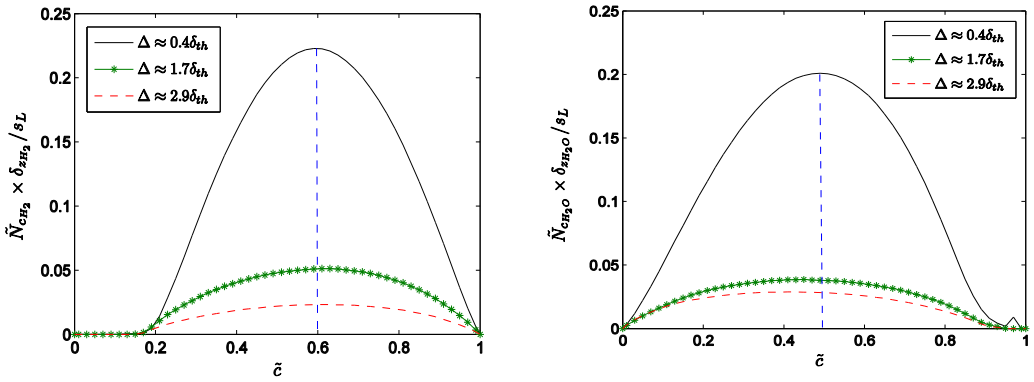

Figure 8.1: Variation of $\widetilde{N}_{c_{H_2}}$ and $\widetilde{N}_{c_{H_2O}}$ with $\tilde{c}$ at $\Delta \approx 0.4\delta_{th}$, $\Delta \approx 1.7\delta_{th}$ and $\Delta \approx 2.8\delta_{th}$ for v-flame case.

The values of $\tilde{c}$ where the conditional mean value of SDR attains its peak values convey some physical meaning. It can be seen from Fig. 8.1 that the peak value of $\widetilde{N}_{c_{H_2}}$ skews slightly towards the burnt side, coinciding with the peak value of the chemical reaction, while the one of $\widetilde{N}_{c_{H_2O}}$ shows a more symmetric distribution with $\tilde{c}_{H_2O}$. Moreover, Fig. 8.2 shows the wrinkling factor Ξ_V of c_{H_2O} and c_{H_2} for a range of LES filter widths. The power-law exponent parameter of the wrinkling factor are found to follow the relation as $\alpha_{H_2} > \alpha_{H_2O}$, which can be attributed to the differential diffusion effects of different species as $Le_{H_2} < Le_{H_2O}$, which is consistent with the findings with simple chemistry DNS database in Chapter 6. It can be seen from Fig. 8. 2 that Ξ_D increases with increasing Δ/δ_{th} indicating that the sub-grid contribution to SDR increases with an increase in LES filter width. It can further be seen Fig 8.2 that Ξ_D for the SDR based on c_{H_2} assumes greater values than the SDR of c_{H_2O}. Figure 8.2 also shows that the algebraic SDR model satisfactorily captures the behaviour of the wrinkling factor Ξ_D for both choices of reaction progress variable.

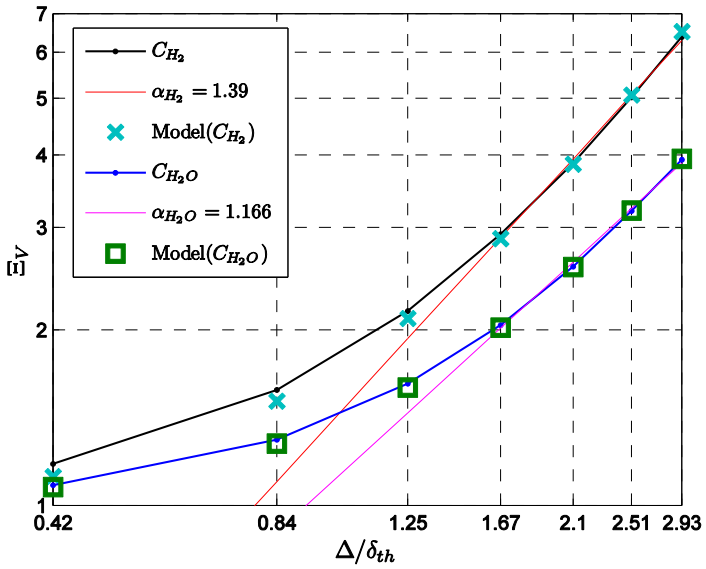

Figure 8.2: The volume averaged behaviour of the wrinkling factor Ξ_V of c_{H_2O}, c_{H_2} with the algebraic predictions of the volume averaged values.

8.1.2. Filtered transport equation behaviours

The statistical behaviours of the normalised unclosed terms of SDR transport equation are shown in Fig. 8.3 for different filter widths for both c_{H_2O} and c_{H_2}.

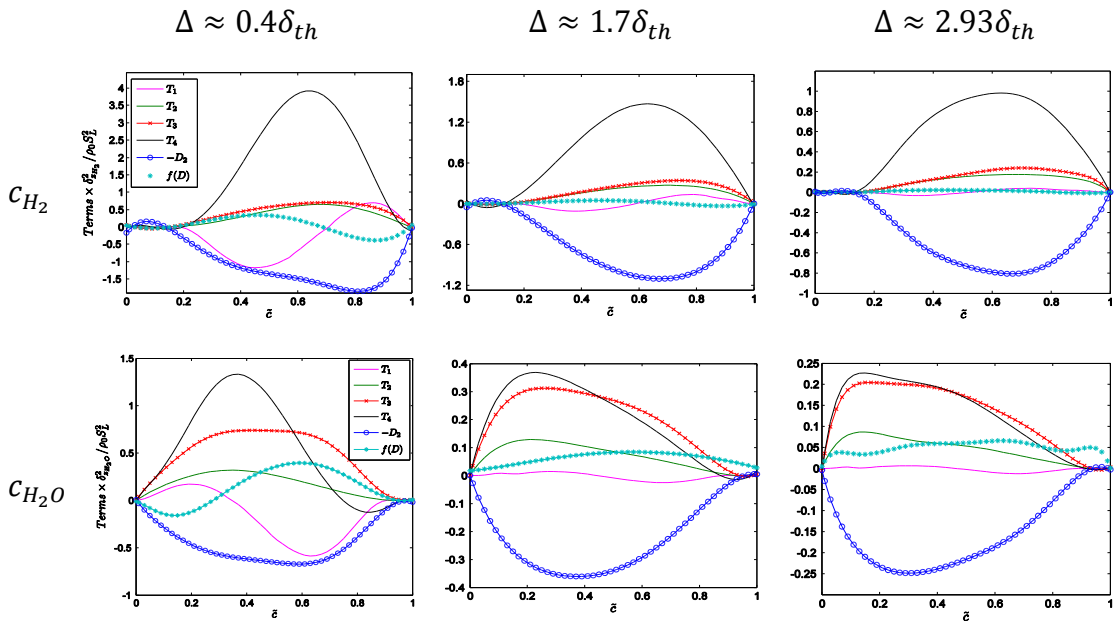

Figure 8.3: Statistical behaviours of unclosed terms of SDR transport equation based on c_{H_2O}, c_{H_2} for filter widths $\Delta \approx 0.4\delta_{th}, 1.7\delta_{th}$ and $2.9\delta_{th}$ respectively.

It can be observed from Fig. 8.3 that T_2 and $(-D_2)$ act as source and sink respectively for all filter widths for both $\widetilde{N}_{c_{H_2}}$ and $\widetilde{N}_{c_{H_2O}}$, which is consistent with previous findings. The

contribution of T_4 is positive for major portion of the flame brush before becoming negative towards the burned gas side for $\Delta \leq \delta_{th}$ (e.g. $\Delta \approx 0.4\delta_{th}$) but for $\Delta > \delta_{th}$ (e.g. $\Delta \approx 2.8\delta_{th}$) the contribution of T_4 remains a leading-order source throughout the flame brush. The term T_3 assumes mainly positive values for both $\widetilde{N}_{c_{H_2}}$ and $\widetilde{N}_{c_{H_2O}}$ for all filter widths whereas in simple chemical cases T_3 show predominantly negative contributions. As shown in Chapter 6, the contributions of T_3 can be expressed as $T_3 = -2\overline{\rho(e_\alpha \cos^2\alpha + e_\beta \cos^2\beta + e_\gamma \cos^2\gamma)N_c}$ where e_α, e_β and e_γ are the most extensive, intermediate and the most compressive principal strain rates and their angles with ∇c are given by α, β and γ respectively. The scalar gradient ∇c aligns with e_α when the effects of strain rate induced by flame normal acceleration a_{chem} overcome the effects of turbulent straining a_{turb} and *vice versa*. The strain rate a_{chem} scales as $a_{chem} \sim \tau f(Ka) S_L / \delta_{th}$ where $f(Ka)$ is expected to decrease with increasing Ka where the effects of heat release are expected to be weak. Scaling a_{turb} as: $a_{turb} \sim u'/l$ yields $a_{chem} / a_{turb} \sim \tau f(Ka) Da$. The effects of a_{turb} dominate over the effects of a_{chem} throughout the flame brush due to smaller values of τ than in simple chemistry cases, which leads to a predominant alignment of ∇c with e_γ leading to positive values of T_3 throughout the flame brush for both c_{H_2} and c_{H_2O}. It can be seen from Fig. 8.3 that the relative magnitude of T_3 is greater in the case of c_{H_2O} than in the case of c_{H_2}. The magnitude of conditional mean value of T_3 is comparable to that of $(-D_2)$ for c_{H_2O}, whereas conditional mean value of T_3 is smaller than that of $(-D_2)$ for c_{H_2}. As $Le_{H_2} < Le_{H_2O}$, the extent of alignment of ∇c with e_γ is stronger for c_{H_2O} than in the case of c_{H_2}. This leads to a stronger positive contribution of T_3 in the case of c_{H_2O} than in the case of c_{H_2}. The term $f(D)$ consists of both positive and negative contribution for small filter width but assumes mainly positive contribution with larger filter width, which is consistent with previous findings for simple chemistry case. It can be seen from Fig. 8.3 that the magnitude of the all the terms decrease with increasing Δ, which is consistent with previous finding based on simple DNS data.

8.1.3. Algebraic SDR closure behaviour

Figure 8.3 demonstrates that for filter width larger than thermal flame thickness (i.e. $\Delta > \delta_{th}$), the magnitude of T_1 is negligible compared to $T_2, T_3, T_4, (-D_2)$ and $f(D)$. This enables one to write: $T_2+T_3+T_4-D_2+f(D) \approx 0.0$ when equilibrium is maintained between generation and destruction of scalar gradients. Figure 8.4 shows that $[T_2 + T_3 + T_4 + f(D)] \sim \mathrm{O}(-D_2)$ holds for all filter widths, implying the assumption of the newly proposed SDR algebraic model in Chapter 6 generally holds for this detail chemistry case.

The predictions of algebraic closure of Favre-filtered SDR (i.e. eq. (6.66)) along with the parameterisation according to eq. (6.69) for $\widetilde{N}_{c_{H_2}}$ and $\widetilde{N}_{c_{H_2O}}$ are shown in Fig. 8.5 for filter widths $\Delta \approx 0.4\delta_{th}, 1.7\delta_{th}$ and $2.9\delta_{th}$. It is evident from Fig. 8.5 that eq.(6.66) satisfactorily predicts both the qualitative and quantitative behaviours of SDR across the flame brush for both choices of reaction progress variable, while the local peak values are slightly overestimated for small filter width and the overestimation diminishes with increasing filter width.

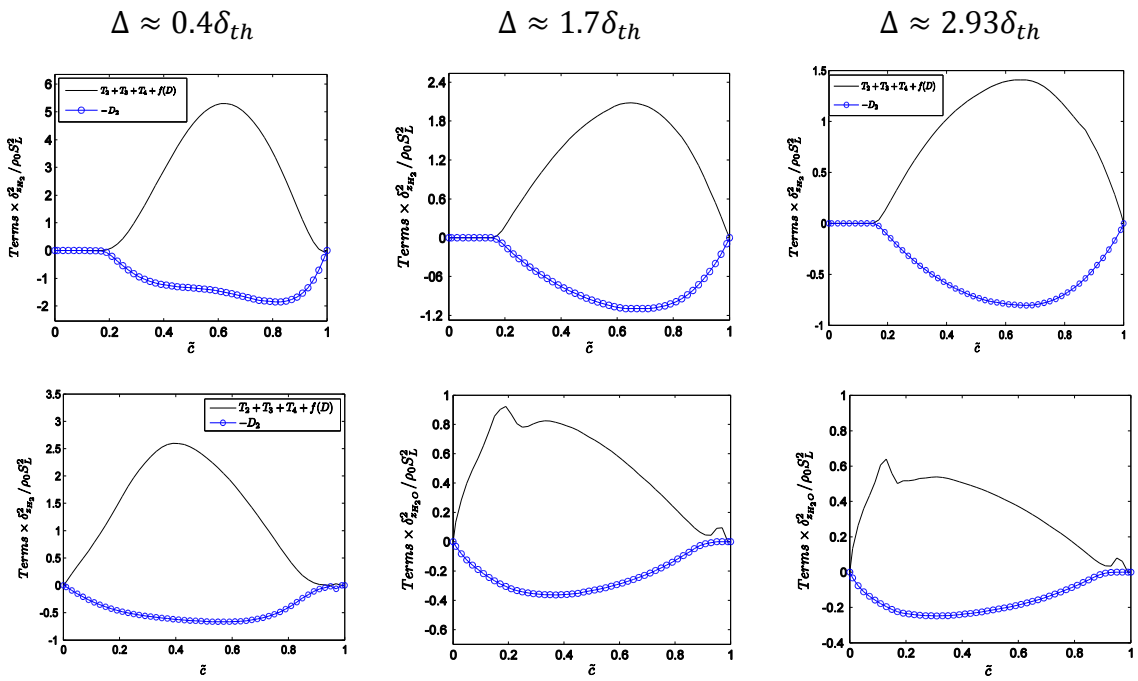

Figure 8.4: The comparison between $[T_1 + T_2 + T_3 + f(D)]$ and $(-D_2)$ for case V60 of c_{H_2} for filter widths $\Delta \approx 0.4\delta_{th}, 1.7\delta_{th}$ and $2.9\delta_{th}$ respectively.

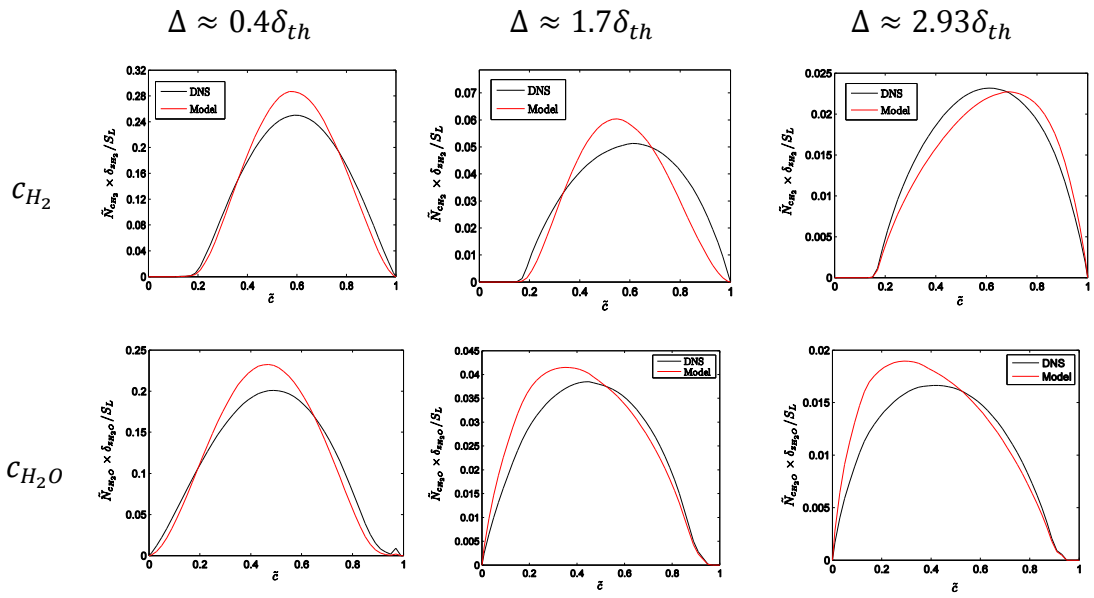

Figure 8.5: The assessment of the algebraic closure behaviour for v-flame case of c_{H_2O}, c_{H_2} for filter widths $\Delta \approx 0.4\delta_{th}$, $1.7\delta_{th}$ and $2.9\delta_{th}$ respectively.

Figure 8.5 also suggested that the magnitude of $\widetilde{N}_{c_{H_2}}$ is greater than that of $\widetilde{N}_{c_{H_2O}}$ after normalisation with the corresponding Zel'dovich flame thickness $\delta_{z_{c_{H_2}}}$ and $\delta_{z_{c_{H_2O}}}$ respectively due to $Le_{c_{H_2}}(\sim 0.3) < Le_{c_{H_2O}}(\sim 0.8)$ (Minamoto et. al., 2011), which is consistent with the conclusion of previous chapter. Thus, the evidence based on *a priori* DNS analysis suggests that the algebraic SDR model provides a robust closure for Favre-filtered SDR $\widetilde{N}_c$ for both simple and detailed chemistry, and this inference was also supported by *a posteriori* assessments based on actual LES simulations (Ma *et al*., 2014; Butz *et al*., 2015).

8.2. Assessment of the modelled SDR transport equation

The models for unclosed terms of the transport equation proposed in Chapter 7 are assessed in this section in the context of the closures of both $\widetilde{N}_{c_{H_2}}$ and $\widetilde{N}_{c_{H_2O}}$ transport equations respectively. All the results are shown as normalised with the corresponding Zel'dovich flame thickness $\delta_{z_{c_{H_2}}} = D_{c_{H_2}}/S_L$ and $\delta_{z_{c_{H_2O}}} = D_{c_{H_2O}}/S_L$.

8.2.1 Assessment of the modelling of the density variation term T_1

Figure 8.3 demonstrates that T_1 exhibits both positive and negative contribution across the flame brush, where both gradient and counter-gradient transport of the sub-grid flux of SDR are observed, consistent with the results of simple chemistry database. It is worth

noting that for $\tilde{c}_{H_2}$, T_1 shows positive contribution towards the burnt gas side while acts as a consumption near the unburnt gas side. The maximum value of $T_1(H_2)$ occurs near $\tilde{c}_{H_2} \approx 0.7$ towards burnt gas side while the peak value of $T_1(H_2O)$ are obtained close to the unburnt gas side. As the expression of term $T_1 = -\nabla.(\overline{\rho u N_c} - \bar{\rho}\tilde{u}\tilde{N}_c)$ indicates, the modelling of T_1 directly relies on the model of the sub-grid flux of SDR, denoted as $(\overline{\rho u_i N_c} - \bar{\rho}\tilde{u}_i\tilde{N}_c)_{Model}$. The modelling of sub-grid flux (i.e. eq. (7.43) and (eq. 7.44)) is assessed by implemented into T_1 as:

$$\text{Model}(T_1) = -\frac{\partial}{\partial x_i}(\overline{\rho u_i N_c} - \bar{\rho}\tilde{u}_i\tilde{N}_c)_{Model} \tag{8.1}$$

The variation of normalized T_1 and the predictions of eq. (8.1) are shown in Fig. 8.6 for both both $\widetilde{N}_{c_{H_2}}$ and $\widetilde{N}_{c_{H_2O}}$ for filter widths $\Delta \approx 0.4\delta_{th}, 1.7\delta_{th}$ and $2.9\delta_{th}$. The model under predicts the magnitude for $\Delta \approx 0.4\delta_{th}$, but roughly captures the qualitative variation of T_1. However, the performance of the model improves with increasing filter width where both quantitative and qualitative behaviours are reasonably well captured.

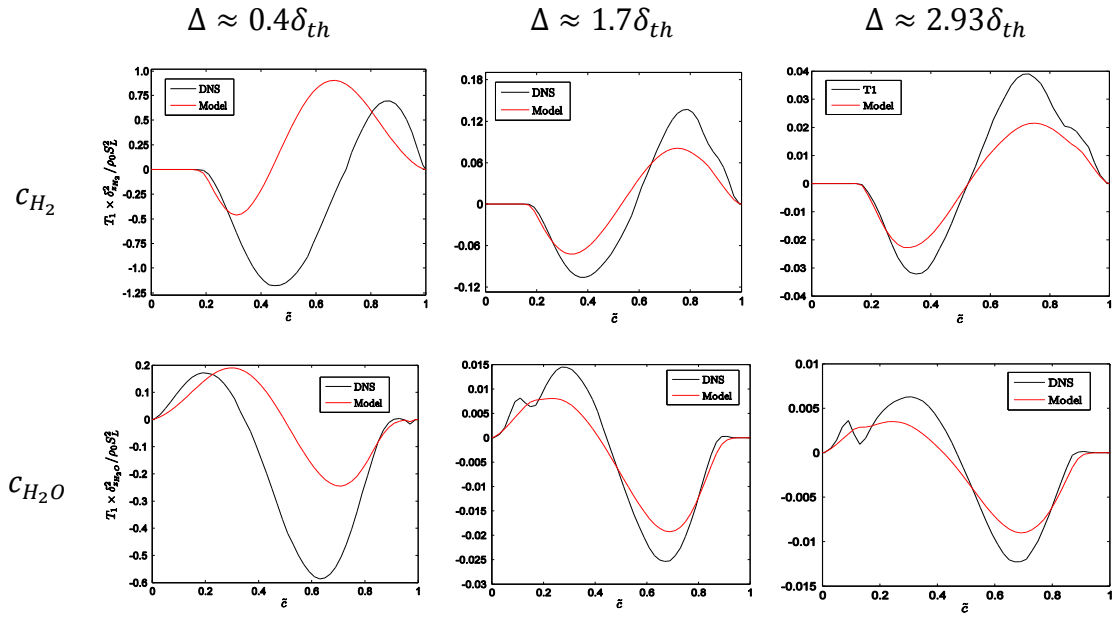

Figure 8.6: The assessment of the modelling of normalised T_1 of c_{H_2O}, c_{H_2} for filter widths $\Delta \approx 0.4\delta_{th}, 1.7\delta_{th}$ and $2.9\delta_{th}$ respectively.

8.2.2 Assessment of the modelling of the density variation term T_2

Figure 8.3 demonstrates that the term T_2 exhibits positive contribution for both $\widetilde{N}_{c_{H_2}}$ and $\widetilde{N}_{c_{H_2O}}$ for all filter widths, with the magnitude decreasing with increasing filter width. The variation of T_2 shifts towards burnt gas side for $\widetilde{N}_{c_{H_2}}$ while T_2 skews towards unburnt gas side for RPV based on water. The scaling analysis of $T_2 \sim 2\,\overline{\rho \nabla . \vec{u} N_c}$ suggests the local value of T_2 is affected by correlation between the dilatation rate $\nabla . \vec{u}$ and the instantaneous SDR.

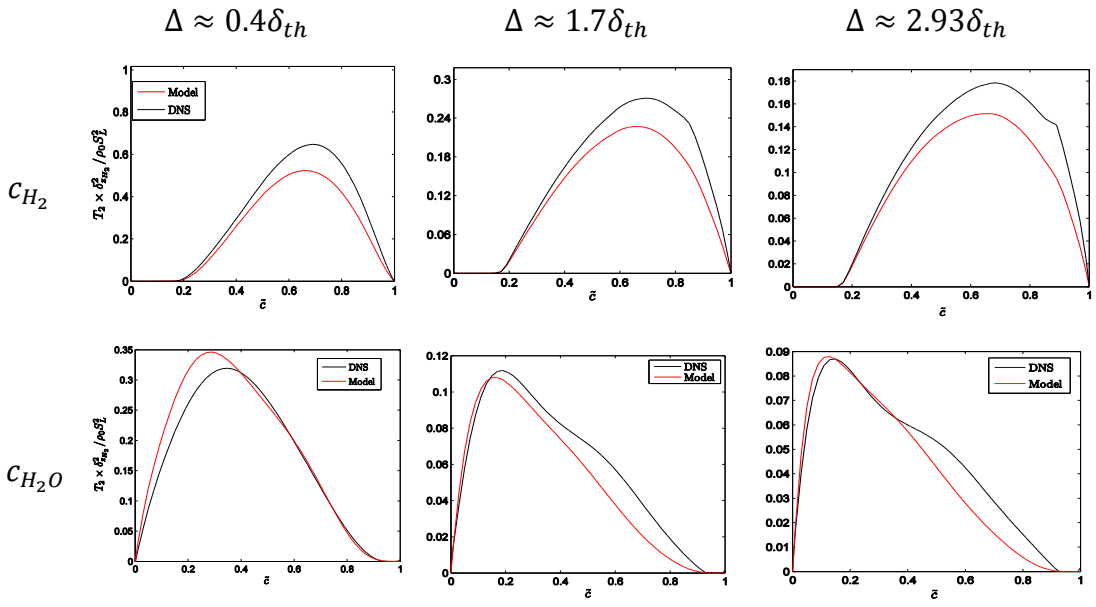

Figure 8.7: The assessment of the modelling of normalised T_2 for filter widths $\Delta \approx 0.4\delta_{th}, 1.7\delta_{th}$ and $2.9\delta_{th}$ for c_{H_2O}, c_{H_2} respectively.

The Lewis number *Le* of hydrogen is close to 0.3 while the *Le* of the water is 0.83, such that the magnitude of T_2 of water for different filter width is smaller than the corresponding one of hydrogen, which is consistent with previous finding. In order to take the differential diffusion effects into consideration, eq. (7.76) and eq. (7.77) are compared with the filtered T_2 for both $\widetilde{N}_{c_{H_2}}$ and $\widetilde{N}_{c_{H_2O}}$ for filter widths $\Delta \approx 0.4\delta_{th}, 1.7\delta_{th}$ and $2.9\delta_{th}$ respectively in Figure 8.7. The results from Fig. 8.7 indicate $T_2(H_2)$ are captured qualitatively but slightly over-predicted for the peak values, whereas $T_2(H_2O)$ has been reasonable well captured for quantitative and qualitative behaviours for all filter widths.

8.2.3 Assessment of the modelling of the scalar turbulence interaction term T_3

Figures 8.3 and 8.8 both demonstrate that T_3 acts as a predominant positive term for both $\widetilde{N}_{c_{H_2}}$ and $\widetilde{N}_{c_{H_2O}}$ except assuming small negative values close to the unburnt (burnt) gas side for $\widetilde{N}_{c_{H_2}}$ ($\widetilde{N}_{c_{H_2O}}$). Comparing the magnitude of T_3 with other leading order unclosed terms for both $\widetilde{N}_{c_{H_2}}$ and $\widetilde{N}_{c_{H_2O}}$, the contribution of T_3 is more prominent for $\widetilde{N}_{c_{H_2O}}$ transport than the relative contribution to $\widetilde{N}_{c_{H_2}}$ transport, which can be explained by scaling T_3 for this v-flame case with $a_{turb}{\sim}u'/\lambda$ as:

$$T_3{\sim}\overline{\rho a_{turb} N_c}{\sim}\frac{\rho_0 S_L^2}{\delta_{th}^2}\times\frac{Le}{Pr^{0.5}}\times Ka_\Delta \tag{8.2}$$

The relative contribution of T_3 is expected to be higher for the species of higher Le. The scaling analysis of T_3 eqs. (8.2) also demonstrates the sensitivity of T_3 with Le, thereforethe predictions of eqs. (7.80) and (7.81) are compared with the normalised T_3 with respect to $\tilde{c}_{H_2O}$, $\tilde{c}_{H_2}$ for filter widths $\Delta \approx 0.4\delta_{th}, 1.7\delta_{th}$ and $2.9\delta_{th}$ respectively.

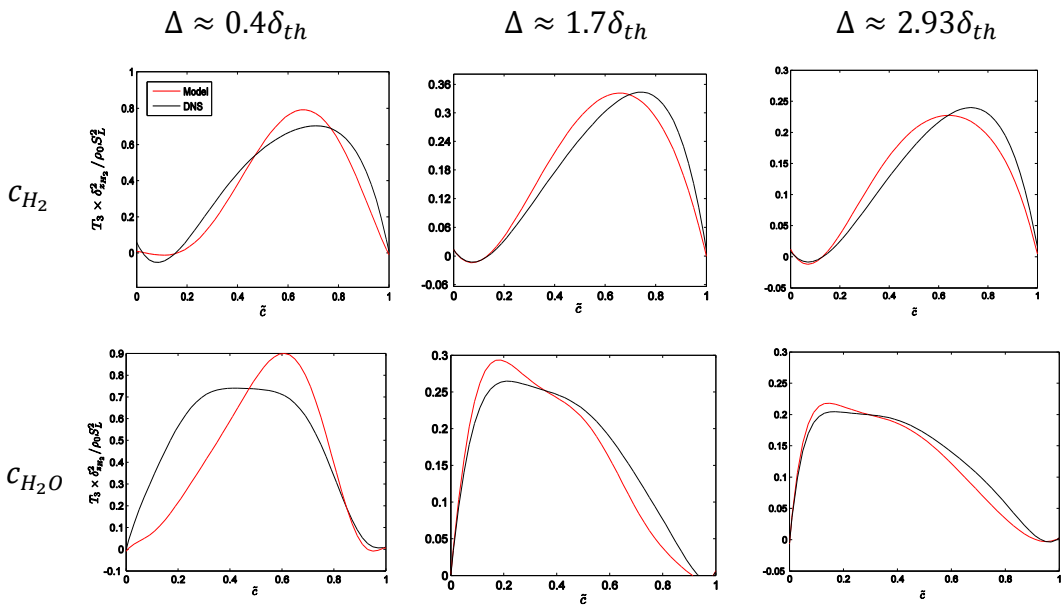

Figure 8.8: The assessment of the modelling of normalised T_3 of c_{H_2O}, c_{H_2} for filter widths $\Delta \approx 0.4\delta_{th}, 1.7\delta_{th}$ and $2.9\delta_{th}$ respectively.

It can be observed that the model captures both quantitative and qualitative behaviour of T_3 for $\Delta \gg \delta_{th}$. However, the peak value of T_3 is shown to be over-predicted by eqs. (7.80) and (7.81) for small filter widths (e.g. $\Delta \approx 0.4\delta_{th}$) for c_{H_2O}. As the contribution of the unresolved $T_{3_{sg}}$ is negligible for $\Delta \ll \delta_{th}$, this under-prediction hardly affects the

model behaviour for practical LES where the grid size is usually much larger than thermal flame thickness (i.e. $\Delta \gg \delta_{th}$).

8.2.4. Assessment of the modelling of [T_4-D_2+$f(D)$]

Figure 8.3 shows that the order of magnitude of T_4, $(-D_2)$ and $f(D)$ remain comparable for this detail chemistry DNS database.It can further be seen from Fig. 8.3 that T_4 assumes predominantly positive values while $(-D_2)$ assumes negative contribution throughout the flame, and $f(D)$ assumes both positive and negative contribution, which is consistent with the behaviours observed from simple chemistry DNS database.

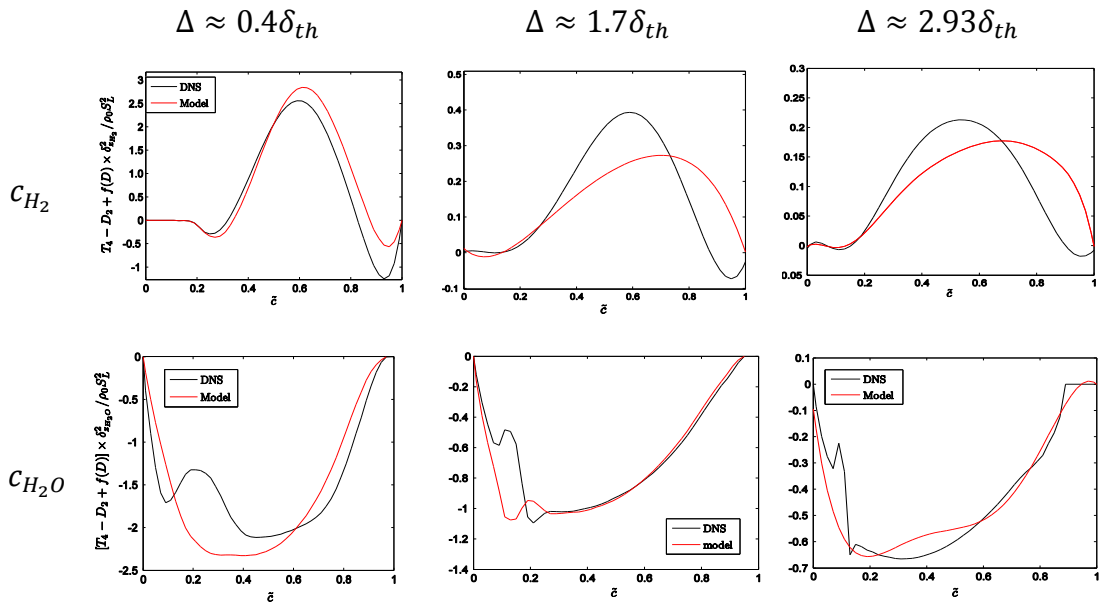

Figure 8.9: The assessment of the modelling of normalised $[T_4 - D_2 + f(D)]$ of c_{H_2O}, c_{H_2} for filter widths $\Delta \approx 0.4\delta_{th}, 1.7\delta_{th}$ and $2.9\delta_{th}$ respectively.

The magnitude of T_4 for c_{H_2} assumes much higher contribution in comparison to that forc_{H_2O}. As $T_4 = 2\overline{D\nabla\dot{w}\cdot\nabla c} \approx -\int_0^\infty \int_0^1 [2D(\partial\dot{w}/\partial n)|\nabla c|]_L \, p(c,|\nabla c|;\vec{x};\Delta) dc d|\nabla c|$ subject to the flamelet assumption where p is the sub-filter probability density function. Therefore negative (positive) values of $(\partial\dot{w}/\partial n)$ lead to positive (negative) values of T_4 when the flame is partially resolved. When the flame is completely unresolved, the sub-filter volume includes more positive samples with high magnitudes of $(-2D(\partial\dot{w}/\partial n)|\nabla c|)$ than the negative samples which are confined only in a small region within the flame front. This leads to predominantly positive values of T_4 throughout the flame brush for $\Delta > \delta_{th}$.

Moreover, the magnitude of T_4 is dependent on the choice of c, and on the behaviour of $(\partial \dot{w}/\partial n)|\nabla c|$.

The model given by eq. (7.82) is compared to $[T_4 - D_2 + f(D)]$ extracted from DNS data for both c_{H_2O} and c_{H_2} for filter widths $\Delta \approx 0.4\delta_{th}, 1.7\delta_{th}$ and $2.9\delta_{th}$ in Fig. 8.9. It can be seen from Fig. 8.9 that $[T_4 - D_2 + f(D)]$ assumes both positive and negative values, which has been captured qualitatively for all filter widths. By contrast, $[T_4 - D_2 + f(D)]$ for $\widetilde{N}_{c_{H_2O}}$ is found to demonstrate negative contribution throughout the flame brush, which is qualitatively captured by eq. (7.82). The order of magnitude of the $[T_4 - D_2 + f(D)]$ is captured by the model for all filter widths for both c_{H_2O} and c_{H_2} but there is a scope for improvement for quantitative predictions.

8.3. Comments

The developed closures of SDR and the unclosed terms of its transport equation based on simple chemistry DNS data have been further assessed in this chapter by comparing the model predictions with the filtered DNS results of a detail chemistry DNS database for a stoichiometric turbulent hydrogen-air V-flame. The algebraic closure is found to capture the local SDR both quantitatively and qualitatively for all filter widths with the robust performance irrespective of the choice of the reaction progress variables based on major reactant and product mass fractions.

A model for the sub-grid flux of $\widetilde{N}_c$ which was proposed and validated based on simple chemistry DNS data, has been found to yield reasonable agreement between the modelled turbulent transport term T_1 and the filter DNS results for $\Delta > \delta_{th}$ with no significant sensitivity to the choice of the reaction progress variable. The maximum values of the density variation term T_2 and scalar turbulence interaction term T_3 are found to be affected by the choice of the definition of the reaction progress variable. However, the models of T_2 and T_3 have been found to capture the DNS results both qualitatively and quantitatively for all filter widths for both $\widetilde{N}_{c_{H_2O}}$ and $\widetilde{N}_{c_{H_2}}$. The combined contribution of reaction dissipation and diffusive gradient terms $[T_4 - D_2 + f(D)]$ exhibits distinctively different behaviours for $\widetilde{N}_{c_{H_2O}}$ and $\widetilde{N}_{c_{H_2}}$ and the model proposed for $[T_4 - D_2 + f(D)]$ based on simple chemistry database only captures the qualitative behaviours for $\widetilde{N}_{c_{H_2}}$ transport equation, but shows quantitative agreement with DNS results only for

$\widetilde{N}_{c_{H_2O}}$ transport equation. Thus, further assessment and improvement of the modelling of $T_4, (-D_2)$ and $f(D)$ is necessary.

Chapter 9. Conclusions and future work

9.1 Conclusions

Here Direct Numerical Simulation (DNS) databases of turbulent premixed flames for a range of different values of heat release parameter τ, global Lewis number *Le* and turbulent Reynolds number Re_t has been investigated in detail for the purpose of the reaction rate closure of turbulent premixed combustion in the context of Large Eddy Simulations (LES). The reaction rate closure based on scalar dissipation rate (SDR) is well-established for Reynolds Averaged Navier-Stokes (RANS) simulations (Borghi, 1990; Borghi and Dutoya, 1978; Chakraborty and Swaminathan, 2007a, 2007b, 2010, 2011, 2013; Chakraborty et al., 2008, 2010, 2011a; Kolla et al., 2009; Mantel and Borghi, 1994; Mura and Borghi, 2003; Mura et al., 2008, 2009; Swaminathan and Bray, 2005; Swaminathan and Grout, 2006), while this modelling approach for LES, which is a promising simulation tool for industrial combustors design, is yet to be investigated. The current thesis aims at proposing a generalized SDR based reaction rate closure for turbulent premixed combustion in the context of LES.

A closure for the filtered reaction rate $\overline{\dot{w}}$ using the Favre-filtered Scalar Dissipation Rate (SDR) $\widetilde{N}_c$ for LES of turbulent premixed combustion has been proposed by extending an existing SDR based reaction rate closure for RANS simulations, where a satisfactory performance of this LES closure is observed for a range of different values of heat release parameter τ, global Lewis number *Le* and turbulent Reynolds number Re_t.

A-priori DNS assessment of the SDR closures based on a model used for passive scalar mixing and a power-law closure has been conducted but they have been found unsuitable for the reactive turbulent flows in premixed flames. Subsequently, an existing algebraic model of Favre-averaged SDR for RANS has been extended here for LES. The performances of the algebraic closures of $\widetilde{N}_c$ have been assessed with respect to Favre-filtered SDR extracted from the DNS data. It has been found that the newly proposed model of $\widetilde{N}_c$ for LES predicts both local and volume-averaged behaviours of SDR satisfactorily for a range of filter widths for turbulent premixed flames with different

values of τ, *Le* and Re_t. The satisfactory performance of this newly developed SDR closure has been justified by analysing the statistical behaviour of Favre-filtered SDR transport using DNS data of freely propagating statistically planar turbulent premixed flames. The DNS data has been explicitly filtered using a Gaussian filter to obtain the unclosed terms of the Favre-filtered SDR transport equation, arising from sub-grid transport (T_1), density variation due to heat release (T_2), strain rate contribution due to the alignment of scalar and velocity gradients (T_3), correlation between the gradients of reaction rate and reaction progress variable (T_4), molecular dissipation of SDR ($-D_2$) and diffusivity gradients $f(D)$. It has been found that $T_2, T_3, T_4, (-D_2)$ and $f(D)$ are the leading order contributors to the SDR transport and the magnitude of T_1 remains smaller than the magnitudes of $T_2, T_3, T_4, (-D_2)$ and $f(D)$ irrespective of the filter width. A detailed scaling analysis has been carried out to justify the behaviour of the SDR transport equation terms in relation to the variation of the filter width. The scaling relation has been utilised to propose models for the unclosed terms of SDR transport equation in the context of Large Eddy Simulation (LES) and their performances have been assessed with respect to their corresponding quantities obtained from explicitly filtered DNS data. These newly proposed models have been found to satisfactorily predict both the qualitative and quantitative behaviours of these unclosed terms for a range of different values of filter widths Δ, heat release parameter τ, Lewis number *Le* and turbulent Reynolds number Re_t.

The closures which have been developed using simple chemistry DNS database have been subsequently assessed using a three dimensional detailed chemistry database of H_2-air V-flame. The algebraic model for SDR is found to capture both qualitative and quantitative behaviours of SDR obtained from DNS data with reaction progress variable *c* defined based on different species. The sub models of the terms of SDR transport equation have been found to satisfactorily capture qualitative behaviours of the explicitly filtered terms of the detailed chemistry DNS database.

9.1.1 Remarks on algebraic closure of SDR

The SDR based reaction rate closure for LES has been investigated over a range of different values of heat release parameter τ, Lewis number *Le* and turbulent Reynolds number Re_t values. The DNS data has been explicitly filtered using a Gaussian filter

kernel to assess the validity of an existing SDR based mean reaction rate closure for RANS in the context of LES. The existing SDR based reaction rate closure in the context of RANS has been extended here for LES using *a-priori* DNS analysis and the newly proposed model has been demonstrated to predict $\overline{\dot{w}}$ satisfactorily for a range of different values of τ, Le and Re_t provided the Favre filtered SDR $\widetilde{N}_c$ is appropriately modelled. The performance of an existing SDR closure for passive scalar mixing (i.e. SDR-C model) has been assessed with respect to $\widetilde{N}_c$ extracted from DNS data alongside a model based on a power-law expression (i.e. SDR-PL model) and an existing algebraic RANS-SDR model, which has been extended here for the purpose of LES (i.e. SDR-RE model). It has been found that the SDR-PL model significantly over-predicts and fails to capture the qualitative variation of the mean values of $\widetilde{N}_c$ conditional on $\widetilde{c}$ for $\Delta > \delta_{th}$, even for the optimum parameters for which this model accurately predicts the volume averaged values of SDR. The SDR-C model with the theoretical value of Smagorinsky constant has been found to underpredict the mean values of $\widetilde{N}_c$ conditional on $\widetilde{c}$ and also the volume averaged values of SDR for all cases considered here. The newly developed SDR-RE model has been found to capture both local and volume-averaged statistics of $\widetilde{N}_c$ for both $\Delta < \delta_{th}$ and $\Delta > \delta_{th}$ in a better manner than the other alternative models for all cases considered here. The performance of the SDR-RE model has been found to improve increasing value of Re_t and the SDR-RE model has been demonstrated to predict both local and volume-averaged statistics of $\widetilde{N}_c$ for high values of Re_t in flames with $Le \approx 1.0$ Moreover, it has been found that the modelling of the sub-grid turbulent velocity fluctuation (i.e. u'_Δ) based on Smagorinsky-Lily model of the eddy viscosity does not significantly affect the performance of the SDR-RE model. The model parameters proposed originally in the context of RANS have been used for the SDR-RE model except for the model parameter β_c, which is expressed here as a function of heat release parameter τ, as β_c remains a weak function of Re_t and independent of global Lewis number Le. This SDR-RE model has been subsequently assessed with respect to a three dimensional filtered detail chemistry DNS database, where satisfactory behaviors have been observed that both quantitative and qualitative behaviors are captured for different filter widths.

The SDR-PL and SDR-RE models later have been investigated further by dynamic evaluation of model parameters. The possibility of SDR closure using a power-law model based on dynamic evaluation of the model parameter has been assessed and is found to capture the local variation of N_c both qualitatively and quantitatively for small filter width for $Le \approx 1$ flames, but under-predicts N_c for $Le << 1$ flames. The prediction of volume-averaged SDR also suffers especially for $Le << 1$ flames. The under-predictions of volume-averaged behaviour of density-weighted SDR increase with increasing filter width. The empirical parameterisation of β_c in the SDR-RE model can be avoided by using a dynamic formulation which captures the local behaviour of SDR either comparably or better than the static formulation for a range of different values of Δ, τ, Le and Re_t, whereas the volume-averaged SDR is also adequately predicted. Thus, the dynamic formulation based on the SDR-RE model seems to be a viable option for algebraic N_c closure for turbulent premixed flames. However, this newly proposed model has been assessed here based on simple chemistry DNS for moderate values of Re_t with decaying turbulence and thus needs to be assessed further based on detailed chemistry based DNS data for higher values of Re_t. Although the static version of the SDR-RE model has already been implemented in actual LES simulations and satisfactory agreement with experimental findings has been obtained (Butz *et al*., 2015; Ma *et al*., 2014) the proposed dynamic model also needs to be implemented in actual LES simulations in a configuration for which experimental data is available for the purpose of *a-posteriori* assessment.

9.1.2 Remarks on modelled generalised SDR transport equation

As the scaling analysis of turbulent transport term T_1 indicated, both gradient transport and counter-gradient transport are observed, the modelling of T_1 has been proposed based on model of sub-grid flux $(\overline{\rho u_i N_c} - \overline{\rho}\widetilde{u}_i \widetilde{N}_c)$, where effects of the heat release parameter, Lewis number, Karlovitz number and Damköhler number have been accounted for. However, the flux of SDR $(\overline{\rho u_i N_c} - \overline{\rho}\widetilde{u}_i \widetilde{N}_c)$ itself requires modelling in the context of LES as well, and the performances of the models for $(\overline{\rho u_i N_c} - \overline{\rho}\widetilde{u}_i \widetilde{N}_c)$ and the turbulent transport term T_1 depend on the modelling of $(\overline{\rho u_i c} - \overline{\rho}\widetilde{u}_i \widetilde{c})$. The modelling of

$(\overline{\rho u_i c} - \overline{\rho}\widetilde{u}_i\widetilde{c})$ is beyond the scope of current analysis and interested readers are referred to Gao *et al*., (2015) for further discussion on the modelling of $(\overline{\rho u_i c} - \overline{\rho}\widetilde{u}_i\widetilde{c})$.

Scaling estimates are used for modelling the density variation term T_2, which is a leading order contribution to the SDR transport. This term is highly sensitive to the differential diffusion of heat and mass, characterised by *Le*. The contribution of the unresolved part of T_2, increases with increasing filter width, while the contribution of resolved part is diminishing with increased filter width.

The scalar turbulence interaction term T_3 can assume both negative and positive values depending on the alignment of scalar gradient ∇c with the most extensive , intermediate and the most compressive principal strain rates, denoted as e_α,e_β and e_γ respectively. It has been found that ∇c aligns with e_γ when turbulent fluid-dynamic straining a_{turb} overcomes the strain rate a_{chem} induced by flame normal acceleration and *vice versa.* The modelling of T_3 has been proposed explicitly accounting for the competition between a_{turb} and a_{chem}.

The kinematic form of the SDR transport equation indicates the possibility of modelling the remaining unclosed terms $[T_4 - D_2 + f(D)]$ collectively, which has been adopted in this analysis based on their same scaling estimates.

All the proposed models for the unresolved terms of SDR transport equation have been assessed based on both simple and detailed chemistry DNS database. The model are shown to capture both the qualitative and quantitative behaviours of the unresolved terms of the SDR transport equation for different filter widths. However, the results also indicates the necessity of further work on modelling the combined contribution of the reaction, dissipation and diffusion gradient term $[T_4 - D_2 + f(D)]$ and it is worth considering the individual contributions of these terms. Moreover, these proposed models need to be implemented into LES codes to evaluate their performance for laboratory-scale and practical flames. However, these closure models also interact with other closures for turbulence and scalar mixing in LES simulations. Thus, due care must be taken to the detailed evaluation of these models through *a-posteriori* assessment.

9.2 Future work

Although the newly developed SDR closure has been found to yield promising results, there are scopes for further improvement.

9.2.1 Turbulent Reynolds number

The turbulent Reynolds numbers of the DNS database used in the current study is relatively moderate, however, turbulent Reynolds numbers of real burners are extremely expensive to achieve using DNS. Although useful physical insights can be obtained based on *a-priori* analysis of both simple and detailed chemistry based DNS data for moderate values of Re_t, the models developed based on the analysis of these DNS data need to be validated further for higher values of Re_t based on experiment and DNS data. A couple of LES posteriori assessment for higher values of Re_t have been carried out for the SDR algebraic closure (Butz et al., 2015; Ma et al., 2014), where corresponding experiment measurements are available, further assessment for dynamic algebraic closure and transport equation based closure will be necessary.

9.2.2 Effects of flame-wall interaction

The investigation of the flame-wall interaction is out of the scope of current study, however, this relation is crucial for the design of practical combustors. The flame is likely to be quenched once it propagates towards the walls of combustors and under the condition of flame quenching, the assumption involved during the derivation of algebraic closure (e.g. SDR-RE model) may become invalid. These proposed models in the current analysis require modifications to make them suitable for the flame-wall interaction.

9.2.3 Stratified combustion, equivalence ratio and fuel blending

The current study concentrates on purely premixed turbulent combustion and provides valuable physical insights of the effects of heat release parameter, turbulent Reynolds number, Lewis number on the SDR and its transport statistics. However, the effects of equivalence ratio and the fuel blending on the SDR based reaction rate closure for LES are yet to be addressed along with the elements of SDR and its transport for stratified mixture combustion.

9.2.4 A *posterior* assessment in actual LES and experimental validation

Although the proposed models for SDR and its transport equation have been assessed with both simple and detail DNS databases based on *a-priori* analyses, it remains however necessary to assess the model performance in an actual LES, as in actual LES, the modelling and numerical inaccuracies may interact in a complicated manner that the prediction can be more accurate if these inaccuracies cancel each other or rather erroneous if these inaccuracies augment each other. This necessitates a comprehensive a posteriori assessment of the algebraic SDR closure based on actual LES simulations. A few recent assessments have been carried out on this purpose (Ma *et al*., 2014; Butz *et al*., 2015; Langella *et al*., 2015), interested readers please refer to them. Last but not the least, the models proposed in this thesis are necessary to be validated by real experiments.

References

Abdel-Gayed, R.G., Bradley, D., Hamid, M., and Lawes, M., (1984), Lewis number effects on turbulent burning velocity, *Proc. of Combustion Institute*, **20**, pp.505-512.

Ashurst, W.T, Peters, N., and Smooke, M.D.: Numerical simulation of turbulent flame structure with non-unity Lewis number, *Combust. Sci. Tech.*, 53, 339-375(1987).

Baum, T., Haworth, D., Poinsot, T., and Darabiha, N., (1994), Direct Numerical Simulation of $H_2/O_2/N_2$ flames with complex chemistry in two-dimensional turbulent flows, *J. Fluid Mech.*, 284, 1-32.

Bachelor, G.K., Townsend, A.A., (1948), Decay of turbulence in final period, *Proc. R.Soc. Lond*, **A194**, 527-543.

Bilger, R.W., (1993), Conditional Moment Closure for turbulent reacting flows, *Phys. Fluids A*, **5,** 436-444.

Bilger, R.W. (2004) Some aspects of scalar dissipation, *Flow Turb. Combust.*, **72(2-4),** 93.

Boger, M., Veynante, D., Boughanem, H., and Trouvé, A., (1998), Direct Numerical Simulation analysis of flame surface density concept for Large Eddy Simulation of turbulent premixed combustion, *Proc. of Combustion Institute*, **27**, 917-925.

Boudier, P., Henriot, S., Poinsot, T., and Baritaud, T., (1992), A model for turbulent flame ignition and propagation in spark ignition engines, *Proc. of Combustion Institute*, **24**,503-510.

Bray, K.N.C. (1979). The interaction between turbulence and combustion. *Proc. Combust. Inst*., **17**, 223–233. 59, 91, 99, 101

Bray, K.N.C., (1980), Turbulent flows with premixed reactants, in *Turbulent Reacting Flows*, Springer Verlag, Berlin Heidelburg, New York, eds. Libby, P.A., and Williams, F.A., pp. 115-183.

Bray, K.N.C., Libby, P.A. & Moss, J.B. (1985). Unified modelling approach for premixed turbulent combustion–Part I: General formulation. *Combust. Flame*, **61**, 87–102. 11

Bray, K.N.C., (1990), Studies of turbulent burning velocity, *Proc. R.Soc. Lond*, **A 431**, 315-335.

Bray, K.N.C., and Peters, N., (1994), Laminar flamelets in turbulent flames, in *Turbulent Reacting Flows*, Academic Press Limited, London, eds. Libby, P.A., and Williams, F.A., pp. 63-113.

Bray, K.N.C., and Swaminathan, N. (2011) Fundamentals and challenges, Turbulent premixed flame, (Eds. N. Swaminathan, K.N.C. Bray), Cambridge University Press, 1st Edition, Cambridge, UK, pp. 1-40.

Bruneaux, G., Poinsot, T., and Ferziger, J.H., (1997), Premixed flame-wall interaction in turbulent channel flow: budget for the flame surface area density evolution equation and modelling, *J.Fluid Mechanics*, **349**, 191-219.

Butler, T.D., and O'Rourke, P.J., (1976), A numerical method for two-dimensional unsteady reacting flows, *Proc. of Combustion Institute*, **16**, 1503-1515.

Butz D, Gao Y, Kempf AM, Chakraborty N. (2015), Large Eddy Simulations of a turbulent premixed swirl flame using an algebraic Scalar Dissipation Rate closure, *Combustion and Flame*, **162** (9), 3180-3196.

Cant, R.S. (1999). Direct numerical simulation of premixed turbulent flames. *Phil. Trans. R. Soc. Lond. A.*, **357**, 3583–3604. 13, 14.

Cant, R.S., (2001), Initial conditions for Direct Numerical Simulation of turbulence, *Report number CUED-THERMO-2001/01*, Cambridge University Engineering Department, Cambridge.

Cant, R.S., and Bray, K.N.C., (1988), Strained laminar flamelet calculations of premixed turbulent combustion in a closed vessel, *Proc. of Combustion Institute*, **22**, pp. 791-799.

Cant, R.S., Pope, S.B., and Bray, K.N.C., (1990), Modelling of flamelet surface to volume ratio in turbulent premixed combustion, *Proc. of Combustion Institute*, **23**, 809-815.

Cant, R.S., Rutland, C.J., and Trouvé, A., (1990) Statistics for laminar flamelet modelling, *Proceeding of the Summer Program 1990*, Center for Turbulence Research, Stanford, pp. 271-279.

Cant, R.S. SENGA2 User Guide in: Technical Report CUED/A–THERMO/TR67, Cambridge University Engineering Department, 2012.

Chakraborty, N., and Cant, R.S., (2003), Tangential strain rate and curvature effects on the displacement speed of an unsteady turbulent premixed flame in a quasi-stationary configuration, European Combustion Meeting 2003, Orléans, France.

Chakraborty, N., and Cant, R.S., (2004), Unsteady effects of strain rate and curvature on turbulent premixed flames in an inflow-outflow configuration, *Combust. Flame*, **137**, 129-147.

Chakraborty, N. and Cant, R.S.: Influence of Lewis number on curvature effects in turbulent premixed flame propagation in the thin reaction zones regime. *Phys. Fluids*, 17, 105105 (2005).

Chakraborty, N. and Cant, R. S. (2007) A priori analysis of the curvature and propagation terms of the flame surface density transport equation for large eddy simulation. *Phys. Fluids*, **19**, 105101.

Chakraborty, N., and Swaminathan, N. (2007a) Influence of Damköhler number on Turbulence-Scalar interaction in Premixed Flames, Part I: Physical Insight, *Phys. Fluids*, **19,** 045103.

Chakraborty, N., and Swaminathan, N. (2007b) Influence of Damköhler number on Turbulence-Scalar interaction in Premixed Flames, Part II: Model Development., *Phys. Fluids*., **19**, 045104.

Chakraborty, N. and Klein, M.:Influence of Lewis number on the Surface Density Function transport in the thin reaction zones regime for turbulent premixed flames. *Phys. Fluids*, 20, 065102 (2008).

Chakraborty, N., Rogerson, J.W., and Swaminathan, N. (2008) *A Priori* assessment of closures for scalar dissipation rate transport in turbulent premixed flames using direct numerical simulation, *Phys. Fluids*., **20**,045106.

Chakraborty, N., Klein, M., Swaminathan, N.: Effects of Lewis number on reactive scalar gradient alignment with local strain rate in turbulent premixed flames. Proc. Combust. Inst., 32, 1409–1417 (2009).

Chakraborty, N., Cant, R.S. (2009a) Effects of Lewis number on scalar transport in turbulent premixed flames, *Phys. Fluids*, **21**, 035110.

Chakraborty, N., Cant, R.S. (2009b) Effects of Lewis number on turbulent scalar transport and its modelling in turbulent premixed flames.,*Combust. Flame*, **156**, 1427.

Chakraborty, N., Cant, R.S. (2009c) Physical insight and modelling for Lewis number effects on turbulent heat and mass transport in turbulent premixed flames, *Numer. Heat Trans. A*, **55**,8,762.

Chakraborty, N., Klein, M., Swaminathan, N. (2009) Effects of Lewis number on reactive scalar gradient alignment with local strain rate in turbulent premixed flames, *Proc. Combust. Inst.,* 32, 1409.

Chakraborty, N., Rogerson, J.W, and Swaminathan, N. (2010) The scalar gradient alignment statistics of flame kernels and its modelling implications for turbulent premixed combustion, *Flow Turb. Combust.*, **85**,1, 25.

Chakraborty, N., and Swaminathan, N. (2010) Effects of Lewis number on scalar dissipation transport and its modelling implications for turbulent premixed combustion, *Combust. Sci. Technol.*,**182**, 1201.

Chakraborty, N., and Cant, R.S. (2011) Effects of Lewis number on Flame Surface Density transport in turbulent premixed combustion, *Combust. Flame*, **158**, 1768.

Chakraborty, N., and Swaminathan, N. (2011) Effects of Lewis Number on Scalar Variance Transport in Premixed Flames, *Flow Turb. Combust*., **87**, 261.

Chakraborty, N., Champion, M., Mura, A., and Swaminathan, N. (2011a) Scalar dissipation rate approach to reaction rate closure, Turbulent premixed flame, (Eds. N. Swaminathan, K.N.C. Bray), Cambridge University Press, 1st Edition, Cambridge, UK, pp. 76-102.

Chakraborty, N., Katragadda, M., Cant, R.S. (2011b) Effects of Lewis number on turbulent kinetic energy transport in turbulent premixed combustion, *Phys. Fluids*, **23**, 075109.

Chakraborty, N., Katragadda, M., Cant, R.S. (2011c) Statistics and modelling of turbulent kinetic energy transport in different regimes of premixed combustion" *Flow Turb. Combust.*, **87**,205.

Chakraborty, N., Hartung, G., Katragadda, M., Kaminski, C. F. (2011d) A numerical comparison of 2D and 3D density-weighted displacement speed statistics and implications for laser based measurements of flame displacement speed, *Combust. Flame*, **158,** 1372.

Chakraborty, N., Cant, R.S. (2013) Turbulent Reynolds number dependence of Flame Surface Density transport in the context of Reynolds Averaged Navier Stokes Simulations, *Proc. Combust. Inst.*, **34**, 1347.

Chakraborty, N., and Swaminathan, N. (2013) Reynolds number effects on scalar dissipation rate transport and its modelling in turbulent premixed combustion, *Combust. Sci. Technol.*, **185**, 676.

Chakraborty, N., Lipatnikov, A. (2013) Conditional velocity statistics for high and low Damköhler number turbulent premixed combustion in the context of Reynolds Averaged Navier Stokes simulations, *Proc. Combust. Inst.* ,**34**, 1333.

Chakraborty, N., Lipatnikov, A.N. (2013) Effects of Lewis number on the statistics of conditional fluid velocity in turbulent premixed combustion in the context of Reynolds Averaged Navier Stokes simulations, *Phys. Fluids*, **25**, 045101.

Charlette, F., Meneveau, C., Veynante, D., (2002), A power law wrinkling model for LES of premixed turbulent combustion, Part I: Non dynamic formulation and initial tests, *Combust. Flame*, **131**, 159-180.

Charlette, F., Meneveau, C., Veynante, D., (2002), A power law wrinkling model for LES of premixed turbulent combustion, Part II: Dynamic formulation, *Combust. Flame*, **131**, 181-197.

Chen, J., H., and Im, H.G., (1998), Correlation of flame speed with stretch in turbulent premixed Methane/Air flames, *Proceedings of Combustion Institute*, Pittsburgh, **27**, 819-826.

Chen, J., H., and Im, H.G., (2000), Stretch effects on the burning velocity of turbulent premixed Hydrogen/Air flames, *Proceedings of Combustion Institute*, **28**, 211-218.

Chen, J.H., Choudhary, A., de Supinski, B., DeVries, M., Hawkes, E. R., Klasky, S., Liao, W. K., Ma, K., L., Mellor-Crummey, J., Podhorski, N., Sankaran, R., Shende, S. and Yoo, C. S.: Terascale direct numerical simulations of turbulent combustion using S3D. Computational Science & Discovery, **2**, 015001(2009).

Cheng, R.K., Shepherd, I.G., and Talbot, L., (1988), Reaction rates in premixed turbulent flames and their relevance to turbulent burning speed, *Proceedings of Combustion Institute*, **28**, 771-780.

Cheng, W.K., and Diringer, J.A., (1991), Numerical modelling of SI engine combustion with a flame sheet model, *SAE Technical Paper 910268.*

Chew, T.C., Bray, K.N.C., and Britter, R.E., (1990), Spatially resolved flamelet statistics for reaction rate modelling, *Combust. Flame*, **80**, 65-82.

Clavin, P., and Williams, F.A. (1981), Effects of Lewis number on propagation of wrinkled flames in turbulent flow, *Prog. Aeronaut. Astronaut*., **86**,403-442.

Clavin P., and Williams, F.A., (1982), Effects of molecular diffusion and thermal expansion on the structure and dynamics of turbulent premixed flames in turbulent flows of large scale and small intensity, *J.Fluid Mech*., **128**,251-282.

Colin, O., Ducros, F., Veynante, D., and Poinsot, T., (2000), A thickened flame model for large eddy simulations of turbulent premixed combustion, *Phys. Fluids A*, **12,** 7, 1843-1863.

Colucci, P.J., Jaberi, A., and Givi, P., (1998), Filtered density function for Large Eddy Simulation of turbulent reacting flows, *Phys. Fluids A*, **10**, 2,499-515.

Comte-Bellot, G., and Corrsin, S., (1966), The use of contraction to improve the isotropy of grid turbulence, *J.Fluid Mech.*, **26**,657-682.

Cook, A.W., and Riley, J.J., (1994), A subgrid model for equilibrium chemistry in turbulent flows, *Phys. Fluids A*, **6**, 8, 2868-2870.

Cook, A.W., and Riley, J.J., (1998), Subgrid scale modelling for turbulent reacting flows, *Combust. Flame*, **112**, 593-606.

Cook, A.W., Riley, J.J., and Kosály, G., (1997), A laminar flamelet approach to subgrid scale chemistry in turbulent flows, *Combust. Flame*, **109**, 332-341.

Driscoll, J.F., and Gulati, A., (1988), Measurement of various terms in turbulent kinetic balance within a flame and comparison with theory, *Combust. Flame*, **72** 131-152.

Duclos, J.M., Veynante, D., and Poinsot, T., (1993), A comparison of flamelet models for turbulent premixed combustion, *Combust. Flame*, **95,**101-107.

Dunstan, T., Minamoto, Y., Chakraborty, N., Swaminathan, N.: Scalar dissipation rate modelling for Large Eddy Simulation of turbulent premixed flames, Proc. Combust. Inst. 34, 1193-1201 (2013).

Dutt, P., (1988), Stable boundary conditions and difference schemes for Navier Stokes equations, *J. Numer. Analysis*, **25**, 245-267.

Echekki, T., and Mungal, M.G, (1990), Flame speed measurement at the tip of a slot burner: Effects of flame curvature and hydrodynamic stretch,*Proc. of Combustion Institute*, **23**, 455-461.

Echekki, T., and Chen, J.H., (1996), Unsteady strain rate and curvature effects in turbulent premixed methane-air flames, *Combust. Flame*, **106**, 184-202.

Echekki, T., and Chen, J.H., (1999), Analysis of the Contribution of Curvature to Premixed Flame Propagation, *Combust. Flame*, **118**, 303-311.

Echekki, T., and Mastorakos, E., (2010) Turbulent Combustion Modelling: Advances, New Trends and Perspectives, Springer, New York.

Fureby, C., and Löfstörm, C., (1994), Large Eddy Simulation of reacting flows applied to bluff body stabilised flames, *Proc. of Combustion Institute*, **25**,1257-1264.

Gao.F., and O'Brien, E., (1993), A Large Eddy Simulation scheme for turbulent reacting flows, *Phys.Fluids* A, 5, **6**, 1282-1284.

Gao Y, Klein M, and Chakraborty N. (2015), Assessment of sub-grid scalar flux modelling in premixed flames for Large Eddy Simulations: A-*priori* Direct Numerical Simulation analysis. *European Journal of Mechanics - B/Fluids*, **52**, 97–108.

Gavrilakius, S., Tsai, H.M., Voke, P., and Leslie, D.C., (1985), Large Eddy Simulation of low Reynolds number channel flow by spectral and finite difference methods, in *Direct and Large Eddy Simulations of Turbul*ence, eds., Schumann, U., and Friedrich, R., Friedr. Viewg & Sohn, Braunschweig/Wiesbaden, pp. 105-118.

Germano, M., Maffio, A., Sello, S., and Mariotti, G., (1997), On the extension of the dynamic modelling procedure to turbulent reacting flows, in *Direct and Large Eddy simulation II*, eds., Chollet, J., Voke, P., and Kleiser, L., Kluwer Academic Publishers, Amsterdam, pp.291-300.

Germano, M., Piomelli, U., Moin, P., and Cabot, W.H., (1991), A dynamic sub-grid scale eddy viscosity model, *Phys. Fluids A*, **3**, 7, 1760-1765.

Givi, P., (1989), Model free simulations of turbulent reacting flows, *Prog. Energy and Combustion Sci*., **15**, 1-107.

Gouldin, F.C., Bray, K.N.C., and Chen, J.Y., (1989), Chemical closure for fractal flamelets, *Combust. Flame*, **77**, 241-259.

Gran, I.R., Echekki, T., and Chen, J.H., (1996), Negative flame speed in an unsteady 2-D premixed flame: A computational study, *Proc. of Combustion Institute*, **26**, 211-218.

Girimaji, S.S., and Zhou, Y. (1996) Analysis and modeling of subgrid scalar mixing using numerical data, *Phys. Fluids*, **8**(5), 1224.

Grout, R.: An age extended progress variable for conditioned reaction rates. *Phys. Fluids*, 19, 105107 (2007).

Han, I. and Huh, K.H.: Roles of displacement speed on evolution of flame surface density for different turbulent intensities and Lewis numbers for turbulent premixed combustion. *Combust. Flame*, 152, 194-205 (2008).

Haworth, D.C., and Poinsot, T.J., (1992), Numerical simulations of Lewis number effects in turbulent premixed flames, *J. Fluid Mech.*, **244**, 405-436.

Haworth, D.C., Cuenot, B., Blint, R.J., and Poinsot, T.J., (2000), Numerical simulations of turbulent Propane-Air combustion with non homogeneous reactants, *Combust. Flame*, **121**, 395-417.

Hélie, J. and Trouvé, A., (1998), Turbulent flame propagation in partially premixed combustion, *Proc. Combust. Inst.* **27**, 891-898.

Im, H.G., Lund, T.S., and Ferziger, J.H., (1997), Large Eddy Simulation of turbulent front propagation with dynamic subgrid models, *Phys. Fluids A*, **9**, 12, 3826-3833.

Im, H.G., and Chen, J.H., (2002), Preferential diffusion effects on the burning rate of interacting turbulent premixed Hydrogen-Air flames, *Combust. Flame*, **126**, 246-258.

Jaberi, F.A., and James, S., (1998), A dynamic similarity model for large eddy simulation of turbulent combustion, *Phys. Fluids A*, **10**,7, 1775-177.

Jaberi, F.A., Colucci, P.J., James, S., Givi, P., and Pope, S.B., (1999), Filtered mass density function for Large Eddy Simulation of turbulent reacting flows, *J. Fluid Mech.*, **401**, 85-121.

Jenkins, K.W., and Cant, R.S. (1999), DNS of turbulent flame kernels, *Proc. Second AFOSR Conf. on DNS and LES*, eds. (Knight and Sakell), Rutgers University, *Kluwer Academic Publishers*, pp. 192-202.

Jenkins, K.W., and Cant, R.S., (2002), Curvature effects on flame kernels in a turbulent environment, *Proc. Combustion Institute,* **29**, 2023-2029.

Jiménez, C., Haworth, D.C., Cuenot, B., Poinsot, T.J., (2002), Direct Numerical Simulation and modelling for lean stratified Propane-Air flames, *Combust. Flame*, **128**, 1-21.

Kim, W.W., and Menon, S., (1995), A new dynamic one equation sub grid scale model for Large Eddy Simulations, *AIAA Paper No. 95-0356.*

Kim, W.W., Menon, S., and Mongia, H.C., (1999), Large Eddy Simulation of a gas turbine combustor flow, *Combust. Sci. Tech*., **143**,25-62.

Klimenko, A.Y., (1990), Multicomponent diffusion of various scalars in turbulent flows, *Fluid Dyn*., **25**, 327-334.

Klimenko, A.Y., and Bilger, R.W., (1999), Conditional Moment Closure for turbulent combustion, *Prog. Energy and Combust. Sci*., pp.595-687.

Knudsen, E., Richardson, E.S., Doran, E.M., Pitsch, H. and Chen, J.H. (2012) Modeling scalar dissipation and scalar variance in large eddy simulation: Algebraic and transport equation closures, *Phys. Fluids*, **24**, 055103.

Kobayashi, H., Kawahata, T., Seyama, S., Fujimari, T., Kim, J. (2002) Relationship between the Smallest Scale of Flame Wrinkles and Turbulence Characteristics of High-pressure, High-temperature Turbulent Premixed Flames. *Proc. Combust. Inst.*, **29**, 1793.

Kuo, K.K., (1986), *Principles of Combustion*, J.Wiley and Sons, New York.

Kolla, H., Rogerson, J., Chakraborty, N., and Swaminathan, N.: Prediction of turbulent flame speed using scalar dissipation rate. *Combust. Sci. Tech*. 181, 518-535 (2009).

Lee, M.J., Choi, C.R., Huh, K.Y., (1998), Application of Coherent Flame Model to counterflow turbulent premixed combustion and extinction, *Comb. Sci. Tech*., **138**, 1-25.

Lele, S.K., (1992), Compact finite difference schemes with spectral like resolution, *J.Comp.Phys.*, **103**, pp.16-42.

Libby, P.A., and Williams, F.A., (1980), Turbulent flows with premixed reactants, in *Turbulent Reacting Flows*, Springer Verlag, Berlin Heidelburg, New York, eds. Libby, P.A., and Williams, F.A., pp. 1-43.

Libby, P.A., and Williams, F.A., (1994), Laminar flamelets in turbulent flames, in *Turbulent Reacting Flows*, Academic Press Limited, London, eds. Libby, P.A., and Williams, F.A., pp. 1-61.

Louch, D.S., and Bray, K.N.C. (2001), Vorticity in unsteady premixed flames: Vortex pair-Premixed flame interactions under imposed body forces and various degrees of heat release and laminar flame thickness, *Combust. Flame*, 125, 1279-1309.

Ma T, Gao Y, Kempf AM, Chakraborty N. (2014), Validation and Implementation of algebraic LES modelling of Scalar Dissipation Rate for reaction rate closure in turbulent premixed combustion, *Combustion and Flame*, **161**(12), 3134-3153.

Mantel, T. and Borghi, R., (1994), New model of premixed wrinkled flame propagation based on a scalar dissipation equation, *Combust. Flame*, **96**, 4, 443-457.

Meneveau, C., and Poinsot, T., (1991), Stretching and quenching of flamelets in premixed turbulent combustion, *Combust. Flame*, **86**, 311-332.

Minamoto, Y., Fukushima, N., Tanahashi, M., Miyauchi, T., Dunstan, T.D. and Swaminathan, N. (2011) Effect of flow-geometry on turbulence-scalar interaction in premixed flames, *Physics of Fluids*, 23 (12) 125107.

Minamoto, Y, T. D. Dunstan, Swaminathan, N and Cant, R. S. (2013) DNS of EGR-type turbulent flame in MILD condition, *Proc. Combust. Inst*, 34 (2) 3231-3238.

Minamoto, Y, Swaminathan, N, Cant R. S. and Leung, T. (2014) Reaction zones and their structure in MILD combustion, Combustion Science and Technology, 186 (8) 1075-1096.

Minamoto, Y and Swaminathan, N, (2014) Scalar gradient behaviour in MILD combustion, *Combustion and Flame*, 161 (4) 1063-1075.

Mizomoto, M., Asaka, S., Ikai, S., Law, C.K., (1984) Effects of preferential diffusion on the burning intensity of curved flames. *Proc. Combust. Inst*., 20: 1933–1940.

Möler, S.I., Lundgren, E., and Fureby, C., (1996), Large Eddy Simulation of turbulent combustion, *Proc. of Combustion Institute*, **26**,241-248.

Mura, A. and Borghi, R. (2003) Towards an extended scalar dissipation equation for turbulent premixed combustion, *Combust. Flame*, **133**,193.

Mura, A., Tsuboi, K., and Hasegawa, T. (2008) Modelling of the correlation between velocity and reactive scalar gradients in turbulent premixed flames based on DNS data. *Combust. Theor. Modell*. **12** 671.

Mura, A., Robin, V, Champion, M., and Hasegawa, T. (2009) Small-scale features of velocity and scalar fields of turbulent premixed flames. *Flow Turb. Combust*., **82**, 339.

Pera, C., Chevillard, S., Reveillon, J.: Effects of residual burnt gas heterogeneity on early flame propagation and on cyclic variability in spark-ignited engines. Combust. Flame, 160, 1020-1032 (2013).

Peters, N., (2000), Turbulent Combustion, *Cambridge Monograph on Mechanics*, Cambridge University Press, Cambridge.

Pitsch, H., and Duchamp, L.G., (2002), Large-Eddy Simulation of Turbulent Premixed Combustion using Level-Set Approach, *Proc. of Combustion Institute*, **29**,2001-2004.

Poinsot, T., Veynante, D., and Candel, S., (1990), Diagrams of premixed turbulent combustion based on direct simulation, *Proc. of Combustion Institute*, **23**,613-619.

Poinsot, T., Veynante, D., and Candel, S., (1991), Quenching processes and premixed turbulent combustion diagrams, *J. Fluid Mech.*, **228**, 561-606.

Poinsot, T., Lele, S.K., (1992), Boundary conditions for direct simulation of compressible viscous flows, *J. Comp. Phys*., **101**, 104-129.

Poinsot, T., Echekki, T., Mungal, M., (1992), A study of the laminar flame tip and implications for turbulent premixed combustion, *Combust. Sci. Tech*., 81(1-3): 45-73.

Poinsot, T., Haworth, D.C., and Brauneaux, G., (1993), Direct simulation and modelling of flame-wall interaction for premixed turbulent combustion, *Combust. Flame*, **95**, 118-132.

Poinsot, T., Candel, S., and Trouvé, A., (1996), Applications of Direct Numerical Simulation to premixed turbulent combustion, *Prog. Energy Combust. Sci*., **21**, 531-576.

Poinsot, T. and Veynante, D., (2001), *Theoretical and numerical combustion*, R.T.Edwards Inc., Philadelphia, USA.

Poinsot, T. and Veynante, D., (2004), *Combustion*, in Encyclopedia of Computational Mechanics. Edited by Erwin Stein, Ren´e de Borst and Thomas J.R. Hughes.

Pope, S.B., (1985), Pdf methods for turbulent reacting flows, *Prog. Energy Combust. Sci*., **11**, 119-192.

Pope, S.B., (1988), The evolution of surfaces in turbulence, *Int J. Engng. Sci*., **26**, 5, 445-469.

Pope, S.B., (1990), Computation of turbulent combustion: progress and challenges, *Proc. of Combustion Institute*, **23**, 591-612.

Pope, S.B., (2000), *Turbulent Flows*, Cambridge University Press, Cambridge.

Pope, S.B., and Cheng, W.K., (1988), The stochastic flamelet model of turbuilent premixed combustion, *Proc. of Combustion Institute*, **22**, 781-789.

Pope, S.B., Yeung, P.K., and Girimaji, S.S., (1989), The curvature of material surfaces in isotropic turbulence, *Phys. Fluids A*, **1**, 12,2010-2018.

Prosser, R., (2002), Toward improving boundary conditions for reactive flow simulations I: acoustically transparent inflow boundary conditions (submitted to *J. Comp. Phys.*)

Reddy, H. and Abraham, J. (2012) Two-Dimensional Direct Numerical Simulation Evaluation of the Flame Surface Density Model for Flames Developing from an Ignition Kernel in Lean Methane/Air Mixtures Under Engine Conditions, *Phys. Fluids*, **24**,105108.

Rogallo, R.S., (1981), Numerical experiments in homogeneous turbulence, *NASA Technical Memorandum 81315*, NASA Ames Research Center, California.

Rutland, C.J.and Ferziger, H. (1991). Simulations of flame-vortex interactions. *Combust. Flame*, **84**, 343–360. 13.

Rutland, C.J. and Cant, R.S. (1994). Turbulent transport in premixed flames. *Proceedings of the Summer Program, Centre for Turbulence Research*, Stanford University/NASA-Ames, 75–94. 13.

Rutland, C., and Trouvé, A., (1993), Direct Simulations of premixed turbulent flames with nonunity Lewis numbers, *Combust. Flame*, **94**, 41-57.

Rymer, G. (2001) Analysis and modeling of the mean reaction rate and transport terms in turbulent premixed combustion, *PhD thesis*, E´cole Centrale Paris.

Sivashinsky, G.I., (1977), Diffusional-thermal theory of cellular flames, *Combust. Sci. Tech.*, **16**,137-146.

Sivashinsky, G.I., (1983), Instabilities, Pattern Formation and Turbulence in Flames, *Annu. Rev. Fluid Mech.*, **15**,179-199.

Smiljanovski,V., Moser, V., and Klein,R., (1997), A Capturing Tracking hybrid scheme for deflagaration discontinuities, *Combust. Theory Modelling*, **1**(2), 183-215.

Smith, T., and Menon, S., (1996), Model simulations of freely propagating turbulent premixed flames, *Proc. of Combustion Institute*, 26, 229-306.

Smith, T., and Menon, S., (1996), One dimensional simulations of freely propagating turbulent premixed flames, *Combust. Sci. Tech*., **128**,99-130.

Smooke, M.D., Giovangigli, V., in: Smooke M.D. (Ed.), *Reduced Kinetic Mechanisms and Asymptotic Approximations for Methane-Air Flames*, vol. 384, Springer Verlag, New York, 1991, pp. 1–28.

Spalding, D.B., (1970), Mixing and chemical reaction in steady, confined turbulent flames, *Proc. of Combustion Institute*, **13**, 649-657.

Sivashinsky, G.I.: Diffusional-thermal theory of cellular flames. Combust. Sci. Tech., 16, 137-146 (1977).

Swaminathan, N. & Bilger, R.W. (1997). Direct numerical simulation of turbulent nonpremixed hydrocarbon reaction zones using a two-step mechanism. *Comb. Sci. Technol*., **127**, 167–196. 13, 14

Swaminathan, N., and Bilger, R.W., (1998), Conditional variance equation and its analysis, *Proc. of Combustion Institute*, **25**, 1191-1198.

Swaminathan, N., and Bilger, R.W., (1998), Assessment of combustion submodels for non-premixed hydrocarbon flames, *Combust. Flame*, **116**, 519-545.

Swaminathan, N., and Bilger, R.W., (2001), Analyses of conditional moment closure for turbulent premixed flames, *Combust. Theory Modelling*, **5**, 1-20.

Swaminathan, N., Bilger, R.W., and Cuenot, B., (2001), Relationship between turbulent scalar flux and conditional dilatation in premixed flames with complex chemistry, *Combust. Flame*, **126**, 1764-1779.

Swaminathan, N. and Bray, K.N.C. : Effects of dilatation on scalar dissipation in turbulent premixed flames. *Combust. Flame*, 143, 549-565 (2005).

Swaminathan, N., and Grout, R. (2006) Interaction of turbulence and scalar fields in premixed flames, *Phys. Fluids.* **18**, 045102.

Tennekes, H. and Lumley, J. L.: A first course in turbulence, MIT press, Massachusetts, USA, (1972).

Treurniet, T.C., Nieuwstadt, F.T.M., Boersma, B.J.: Direct Numerical Simulation of homogeneous turbulence in combination with premixed combustion at low Mach number modeled by the G-equation, *J. Fluid Mech*., 565, 25-62(2006).

Trouvé, A., (1994), The production of premixed flame surface area in turbulent shear flow, *Combust. Flame*, **99**, 687-696.

Trouvé, A., and Poinsot, T., (1994), The evolution equation for flame surface density in turbulent premixed combustion, *J. Fluid Mech.*, **278**, 1-31.

Tullis, S. and Cant, R.S., (2002), Scalar Transport Modeling in Large Eddy Simulation of Turbulent premixed Flames, *Proc. of Combust. Institute*, **29**, 2097-2104.

U. S. Energy Information Administration, International Energy Outlook 2013 With Projections to 2040, DOE/EIA-0484 .

Vervisch, L., Bidaux, E., Bray, K.N.C., and Kollmann, W., (1995), Surface density function in premixed turbulent combustion modelling, similarities between probability density function and flame surface approaches, *Phys. Fluids A*, **7**, 10, 2496-2503.

Veynante, D., Duclos, J.M., and Piana, J., (1994), Experimental analysis of flamelet models for premixed turbulent combustion, *Proc. of Combustion Institute*, **25**,1249-1256.

Veynante, D., Piana, J., Duclos, J.M., and Martel, C., (1996), Experimental analysis of flame surface density models for premixed turbulent combustion, *Proc. of Combustion Institute*, **26**, 413-420.

Veynante, D., Trouvé, A., Bray, K.N.C., and Mantel, T., (1997), Gradient and counter-gradient scalar transport in turbulent premixed flames, *J. Fluid Mech.*, **332**, 263-293.

Veynante, D., and Poinsot, T., (1997), Large Eddy Simulations of combustion instabilities in turbulent premixed burners, *Annual Research Briefs 1997*, Centre for Turbulence Research, Stanford University, USA, pp.253-275.

Veynante, D., and Vervisch, L., (2002), Turbulent combustion modelling, *Prog. Energy and Combust. Sci*., **28**, 193-266.

Wray, A.A., (1990), Minimal storage time advancement schemes for spectral methods, unpublished report, NASA Ames Research Center, California.